The Pennsylvania State University

The Graduate School

Department of Energy and Mineral Engineering

AN ARTIFICIAL NEURAL NETWORK BASED TOOL-BOX FOR SCREENING

AND DESIGNING IMPROVED OIL RECOVERY METHODS

A Thesis in

Petroleum and Natural Gas Engineering

by

Claudia Helena Parada Minakowski

Submitted in Partial Fulfillment
of the Requirements
for the Degree of

Doctor of Philosophy

May 2008

The thesis of Claudia Helena Parada Minakowski was reviewed and approved* by the following:

Turgay Ertekin
Program Chair
Professor of Petroleum and Natural Gas Engineering
George E. Trimble Chair in Earth and Mineral Sciences
Thesis Advisor
Chair of Committee

Robert Watson
Associate Professor of Petroleum and Natural Gas Engineering and
Geo-Environmental Engineering

Luis Felipe Ayala
Assistant Professor of Petroleum and Natural Gas Engineering

Mirna Urquidi-Macdonald
Professor of Engineering Science and Mechanics

*Signatures are on file in the Graduate School

ABSTRACT

Typically, improved oil recovery (IOR) methods are applied to oil reservoirs that have been depleted by natural drive mechanism. Descriptive screening criteria for IOR methods are used to select the appropriate recovery technique according to the fluid and rock properties. The existing screening guidelines neither provide information about the expected reservoir performance nor suggest a set of project design parameters that can be used towards the optimization of the process.

In this study, artificial neural networks are used to build two neuro-simulation tools for screening and designing miscible injection, waterflooding and steam injection processes. The tools are intended to narrow the ranges of possible scenarios to be modeled using conventional simulation, reducing the potentially extensive time and energy spent in modeling studies and analysis.

A commercial reservoir simulator is used to generate the data supplied to train and validate the artificial neural networks. The proxy models are built considering four different well patterns with different well operating conditions as the design parameters. Different expert systems are developed for each well pattern. The screening networks, or forward application, predict oil production rate and cumulative oil production profiles for a given set of rock and fluid properties, and design parameters. The inverse application provides the necessary design parameters for a given set of reservoir characteristics and for the specified (desired) process performance indicators.

The results of this study show that the networks are able to recognize the strong correlation between the displacement mechanism and the reservoir characteristics as they

effectively forecast hydrocarbon performance for different reservoir types undergoing diverse recovery processes. The inverse proxy models are able to predict the operation conditions at the same time that accurately provide the complete oil production profiles. Both neuro-simulation applications are built within a graphical user interface to facilitate the display of the results.

The project design tool-box helps in the quantitative project assessment if proper combinations of expected project abandonment time and total oil recovery are provided for the same reservoir. Its use, when combined with the screening network application, becomes a powerful tool that facilitates the evaluation and validation of the proposed production scenarios.

The tools proposed in this study have the potential of providing a new means to design a variety of efficient and feasible IOR processes by using artificial intelligence. Appropriate guidelines are provided to the reservoir engineer, which decrease the number of possible scenarios to be studied and reduce the time spent with conventional reservoir simulation methodology.

TABLE OF CONTENTS

LIST OF FIGURES

LIST OF TABLES

NOMENCLATURE

A: area (acres)

AT: Abandonment time (days)

Bo: oil formation volume factor (STB/RB)

Bg: gas formation volume factor (scf/RB)

Bw: water formation volume factor (STB/RB)

BT: breakthrough time (days)

C: Corey's correlation constant (dimensionless)

C_{gas}:   capillary pressure coefficient for the gas-oil system

C_{oil}:   capillary pressure coefficient for the oil-water system

e: error (%)

ET: early time (days)

h: thickness (ft)

H: enthalpy (BTU/lb)

k: absolute permeability (md)

kr: relative permeability (fraction)

M: mobility ration (fraction)

P: pressure (psia)

Pc: capillary pressure (psi)

q_o: oil production rate (STB/d)

q_t: cumulative oil production (STB)

Rs: solution gas-oil ration (scf/STB)

So_r: residual oil saturation (fraction)

Sw_{irr}:   irreducible water saturation (fraction)

T: temperature (^{o}F)

t: time (days)

v: fluid velocity (cm/s)

V: volume (ft^3)

Δ: differential

ϕ: porosity (%)

μ: viscosity (cp)

θ: contact angle between water and rock surface (degrees)

Abbreviations:

ANN: artificial neural network

BHP: bottom hole pressure (psia)

CO_2: carbon dioxide

EOR: enhance oil recovery

EOS: equation of state

FCM: first contact miscibility

GUI: graphical user interface

IFT: interfacial tension

IOR: improved oil recovery

LMS: least mean squared

MCM: multiple-contact miscibility

MMP: minimum miscibility pressure

N_2:   nitrogen

PR: Peng-Robinson (equation of state)

PVT: pressure-volume-temperature

SD: standard deviation

WOR: water-oil ratio

Subscripts:

D: displacing phase

d: displaced phase

nw: non-wetting phase

w: wetting phase

ACKNOWLEDGEMENTS

I express my sincere appreciation and gratitude to my academic advisor and mentor, Dr. Turgay Ertekin, for his constant support, professional guidance, patience and friendship during my studies at Penn State. I also extend my gratitude to Dr. Luis Ayala, Dr. Mirna Urquidi-Macdonald and Dr. Robert Watson for their interest in serving as committee members. Their valuable suggestions, insights, and contributions to this work are greatly appreciated.

I would like to extend my appreciation to my fellow graduate students, friends and family, especially my sister, Rosa Cristina, for her encouragement and support throughout my entire academic life.

This work is dedicated to the memory of my parents, Cristina and Silvestre. Their love and vision guided me throughout this journey.

Chapter 1

INTRODUCTION

The first stage of production of any oil reservoir involves oil displacement by natural drive mechanisms such as solution gas drive, gas cap drive and gravity drainage. Traditionally, recovery methods are applied to oil reservoirs to enhance the ultimate production after reservoirs have been depleted naturally. These methods, in general, involve the injection of a recovery agent with the aim of improving the oil displacement process by reducing the interfacial tension or improving the mobility ratio. Some other methods involve the in situ generation of heat to improve oil displacement by reducing the oil viscosity. In more recent years, to optimize the process, improved oil recovery techniques are applied to reservoirs even before their natural energy drive is exhausted by primary depletion. Then, once again, the study of these methods has become of more special interest in petroleum engineering.

Assessing the most suitable recovery process is an important and critical analysis that establishes the economic success of a field deployment of the process. Recovery methods are expensive techniques that are applied according to the nature of the hydrocarbon fluid and rock properties. Usually, reservoir engineers refer to descriptive screening criteria for improved oil recovery methods for field appraisal purposes. These guidelines are developed from real field data and they allow the engineer to identify the appropriate recovery technique for a candidate reservoir.

Published screening criteria are of useful general reference, but they fail to provide the expected quantification for the reservoir performance. In appraisal stage, the anticipated oil production can be ascertained from laboratory data or from computational modeling. Reservoir simulation is, without a doubt, a preferred evaluation method since it provides flexibility to analyze different production schemes. However, assessment of all possible deployment plans for a specific reservoir is an extremely time-demanding task and also requires high technical expertise. In practice, only few implementation schemes for production plans are effectively evaluated due to time and manpower constraints.

In this study, a neuro-simulation application is developed to provide general screening criteria for the more common hydrocarbon recovery techniques at the same time that introduces some quantification of the anticipated oil production. The estimation of reservoir recovery provides an additional criterion to facilitate the selection of the appropriate recovery technique and provides the basis to assess the economic feasibility of the project.

Screening criteria for oil recovery methods should not be considered as explicit guidelines for every single reservoir prospect and further evaluations are still necessary to complete the appraisal of reservoir deployments of these techniques. Therefore, an inverse application of the expert system is structured to provide recommended field development and design guidelines for a given recovery technique as applied to a reservoir of certain characteristics. This inverse tool aids considerably to reduce the time invested in further reservoir analyses by narrowing down the possible production schemes to be evaluated by hard computing (reservoir simulation).

The proposed tools provide some new avenues to design efficient and feasible recovery projects based on the characteristics of a candidate reservoir by using artificial intelligence. The proxy models are developed using artificial neural networks, a technique that has been expanding rapidly in petroleum engineering applications.

Chapter 2

LITERATURE REVIEW

2.1 Improved Oil Recovery

Oil recovery processes are traditionally divided into three categories: primary, secondary and tertiary. Primary recovery refers to the first stage of oil production where oil is displaced by natural drive mechanisms such as solution gas drive, water influx or gravity drainage. Secondary recovery is usually implemented after primary production starts declining. In general, the aim of this second stage of operations is to maintain pressure by applying techniques such as waterflooding or gas injection. Tertiary recovery is implemented when secondary methods are economically unfeasible. Mechanisms as injection of miscible gases, chemicals or thermal energy are usually applied in this third stage of production [Lake, 1989; Green & Willhite, 2003].

In general, tertiary recovery processes can be classified into three categories: thermal, chemical and solvent methods. Thermal processes consist of injection of thermal energy or generation of heat in-situ in order to improve oil displacement by reducing its viscosity. Injection of steam is the most widely used thermal method nowadays. Chemical processes involve the injection of surfactants or alkaline agents to reduce the inter-facial tension and improve the displacing efficiency. Solvent methods consist of injecting a displacement fluid that improves the mobility ratio, and therefore, the macroscopic displacement. Solvent methods include miscible and immiscible

displacement processes. Typical injection fluids are carbon dioxide and nitrogen [Lake, 1989]. Figure **2-1** shows a schematic classification of the oil recovery methods.

Improved oil recovery (IOR) processes are techniques which are designed to increase oil production. Tertiary recovery processes are commonly known as IOR techniques. However, IOR also comprises other practical endeavors such as reservoir management, reservoir characterization and infill drilling **[**Green & Willhite, 2003**]**.
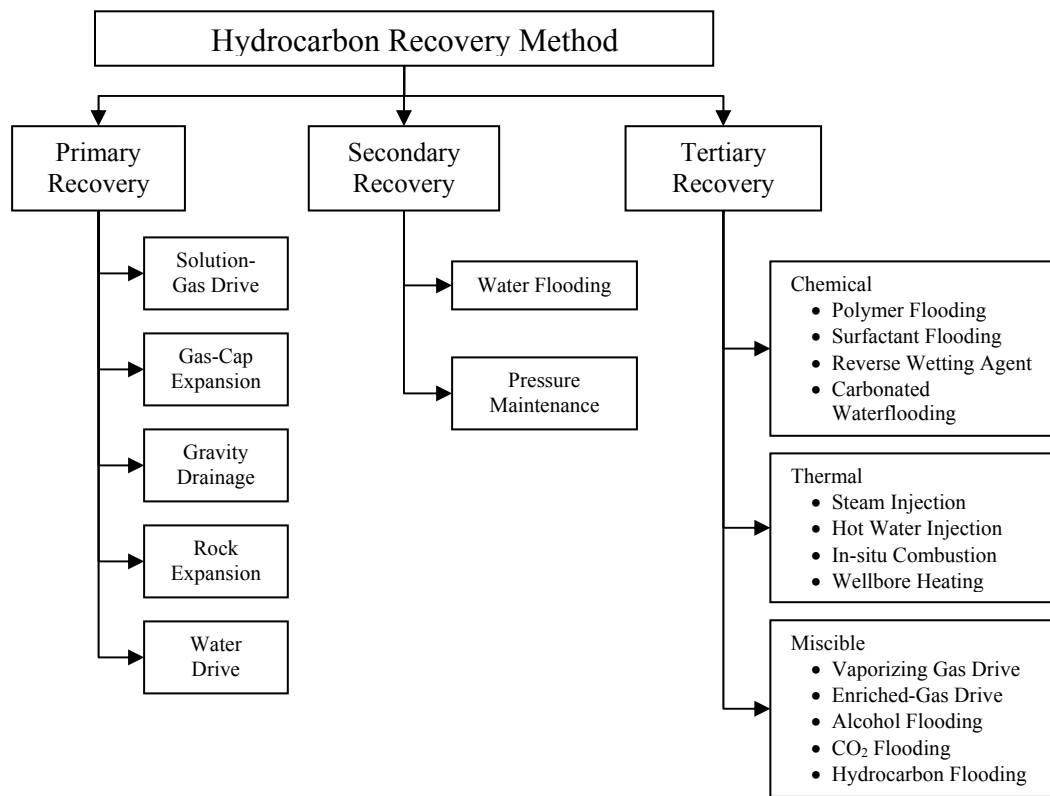
Figure **2-1**: Hydrocarbon Recovery Methods (Adapted from Ertekin et al., 2001)

2.1.1 Miscible Displacement Processes

Miscible displacement processes are those where the injection fluid is mixed with the oil in place and the resulting mixture is a single phase [Stalkup, 1983]. Miscible displacement processes are classified as first contact miscibility (FCM) and multiple-contact miscibility (MCM), depending upon how miscibility conditions are developed. FCM mechanism occurs entirely in one hydrocarbon phase. One example of FCM is a mixture of ethanol and water. Despite of the proportion in which they are mixed, only one phase is formed with no visible interface. Figure **2-2** shows a typical ternary diagram with displacement of a crude oil by a light component solvent. Mixtures of light component and heavy hydrocarbons that are within the two-phase region are not miscible. In addition, any mixture that yields to compositions in the two-phase region is an immiscible mixture. However, any mixture of light components and intermediate hydrocarbons and mixtures of heavy and intermediate hydrocarbons are miscible since they are within the single-phase region. First-contact miscibility is achieved if the straight line that represents the dilution path between the solvent and the reservoir oil does not cross the two-phase region [Lake, 1989; Green & Willhite, 2003].
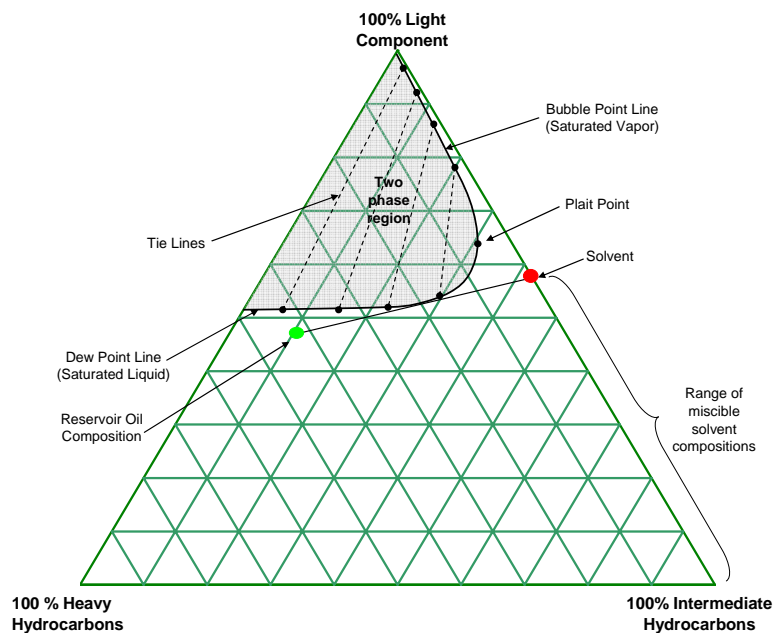
Figure **2-2**: First-Contact Miscibility Process (adapted from Lake, 1989)

Multi-contact miscibility processes take place when two fluids are not miscible at first contact but they require several contacts in order to reach miscibility. The multiple-contact processes are classified as vaporizing gas drive, condensing gas drive and CO_2 displacements.

2.1.1.1 Vaporizing Gas Drive

In vaporizing gas drive, the injected solvent is usually a lean gas whose composition enriches since intermediate components are vaporized from the crude into the injected fluid. The solvent becomes miscible with the original crude as it displaces throughout the reservoir. This process can be easily described using a ternary diagram as

shown in Figure **2-3**. In this example, the solvent consists of 100% light component while the crude composition is a mixture of mainly intermediate components whose composition lies on the right hand side of the limiting tie line. The straight line describing the dilution path crosses the two-phase region. Therefore, the two fluids are not initially miscible and oil is partially displaced immiscibly away from the wellbore while some oil remains undisplaced behind the solvent. The undisplaced oil in contact with the solvent leads to an overall composition M_1. The tie line crossing over M_1 provides the gas G_1 and liquid L_1 compositions in equilibrium. More solvent injection pushes equilibrium gas G1 into the reservoir where it becomes in contact with fresh oil. Equilibrium liquid L_1 remains behind as residual saturation. In this second contact, a second overall composition M_2 is formed with gas G_2 and liquid L_2 in equilibrium. Additional injection of solvent will push equilibrium gas G_2 toward fresh oil and a mixture M_3 will be reached. As the injection continues, the composition of the equilibrium gas will enrich moving along the dew point curve until it reaches the plait point composition. At this point the displacement becomes miscible since all compositions will be on a straight dilution path with the oil reservoir. Even though the vaporizing gas drive has been described as a batch operation, this process is a continuous operation in actual reservoirs. Then, miscible transition zones are generated between reservoir oil and injected solvent [Stalkup, 1983].
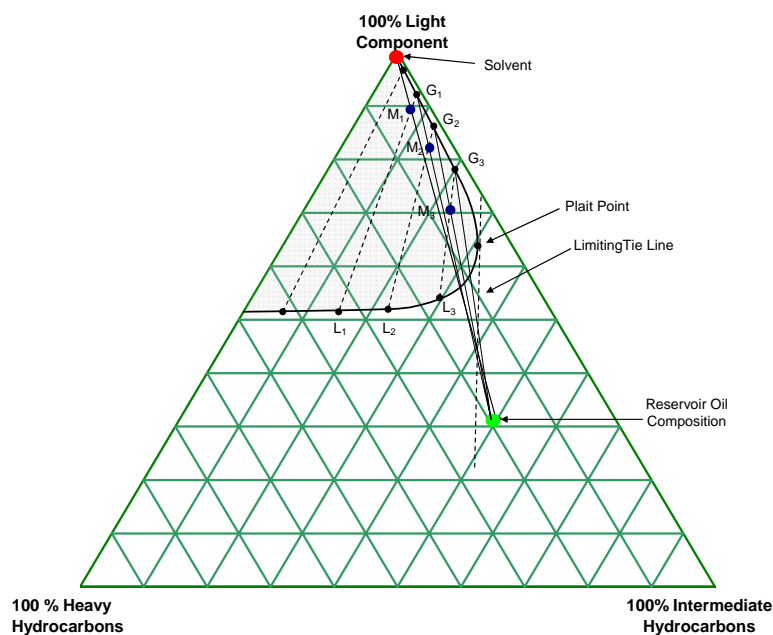
Figure **2-3**: Vaporizing Gas Drive Process (adapted from Lake, 1989)

It should be noted that the limiting tie line determines whether the process is miscible or not. Miscibility develops provided that the reservoir oil and the injected solvent compositions lie on opposite sides of the limiting tie line. Miscibility can be achieved by the vaporizing gas drive process as long as the reservoir composition is on the right of the limiting tie line and the solvent composition is on the left. If both, oil and solvent compositions, lie on the left of the limiting tie line, gas enrichment will occur up to the composition of the equilibrium gas that falls on the extended tie line that passes through the reservoir oil composition as shown in Figure **2-4** [Stalkup, 1983].
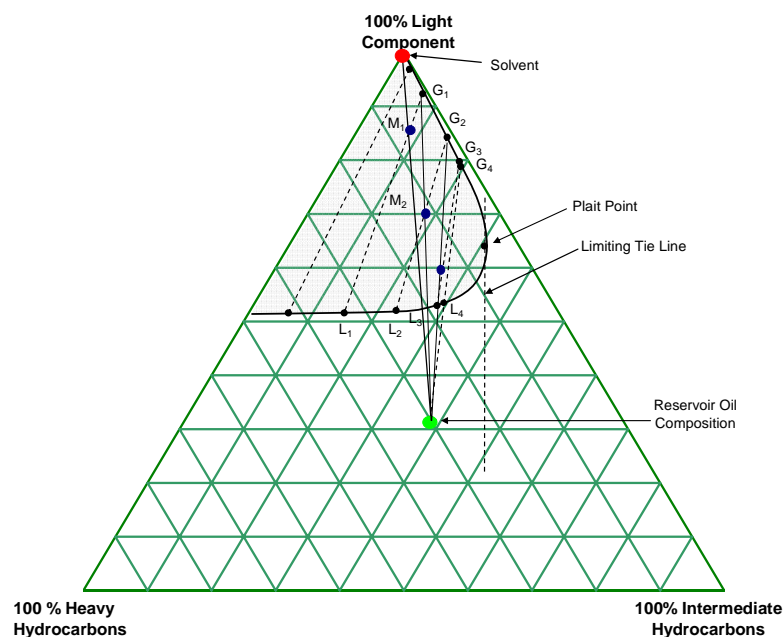
Figure **2-4**: Representation of Immiscible Process (adapted from Lake, 1989)

Reservoir pressure and gas composition are parameters that define whether miscibility conditions will be achieved in a vaporizing gas drive process. For a given injection gas composition, there is a minimum pressure above which dynamic miscibility is achieved. This pressure is called minimum miscibility pressure (MMP). As reservoir pressure increases, the size of the two-phase region reduces. Therefore, a lower concentration of intermediate hydrocarbons in the injection gas will achieve miscibility as pressure increases [Stalkup, 1983]. For a vaporizing gas drive displacement process the MMP is the minimum pressure at which the limiting tie line passes through the reservoir oil composition on a ternary diagram [Green & Willhite, 2003].

2.1.1.2 Condensing Gas Drive

In a condensing gas drive, or enriched-gas process, the injected solvent usually contains significant amount of intermediate molecular weight hydrocarbons. The reservoir oil is enriched by components condensing from the injected solvent. Reservoir oil becomes miscible due to changes in its composition. Condensing gas drive processes normally occur at lower pressures than vaporizing processes [Green & Willhite, 2003].

The minimum solvent composition for miscibility lies on the intersection of limiting tie line and the zero-heavy hydrocarbon composition side of the ternary diagram as shown in Figure **2-5**.
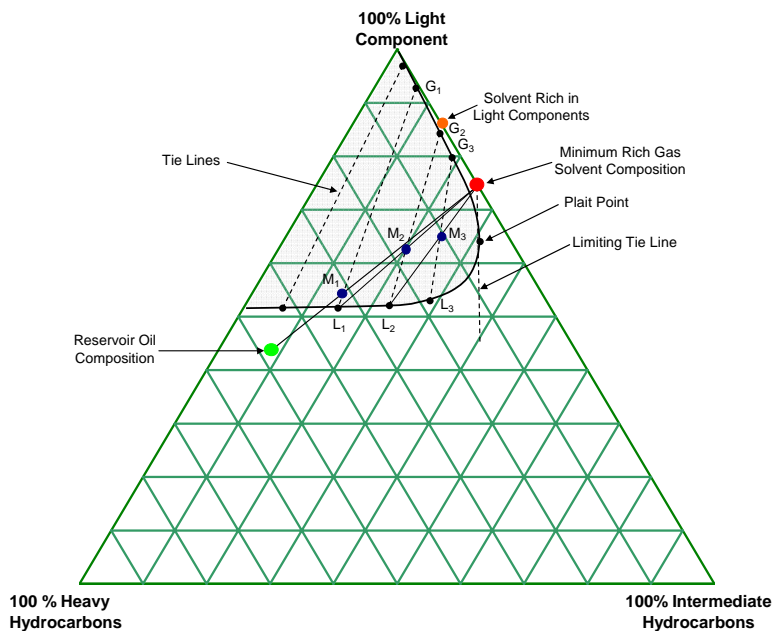
Figure **2-5**: Condensing Gas Drive Process (adapted from Lake, 1989)

It is noted that the minimum solvent composition and the reservoir oil are immiscible at first contact. Mixture M_1 is formed as a result of this first contact. The tie line passing through mixture M_1 gives the composition of the corresponding gas G_1 and liquid L_1 in equilibrium. Additional injection of solvent pushes the equilibrium gas G_1 into the reservoir leaving behind the equilibrium liquid L_1, which is immobile. Then liquid L_1 mixes with the solvent generating mixture M_2. Equilibrium gas G_2 and liquid L_2 result from this second contact. By further injection of solvent, the composition of the liquid is enriched and moves along the bubble point curve until it reaches the plait point. At this stage, the two fluids are completely miscible since the dilution path between then lies on the single-phase region.

If injected solvent contains less intermediate components than the minimum solvent composition, the oil will not be enriched to the point of miscibility. For example, if the solvent composition is given by the intersection of extension of the tie line G_2-L_2 with the right side of the ternary diagram in Figure **2-5**, the reservoir oil will enrich up to L_2 since further injection will always lead to equilibrium gas and liquid G_2 and L_2. Miscibility is achieved by condensing-gas drive processes when the reservoir oil composition is at the left of the limiting tie line and the solvent composition is on the opposite side, on the right [Stalkup, 1983].

For a given solvent injection and oil reservoir compositions, the MMP in a condensing gas drive process is the minimum pressure at which the limiting time line passes through the solvent fluid composition on a ternary diagram [Green & Willhite, 2003].

2.1.1.3 CO$_2$ and N$_2$ Miscible Displacement Process

Carbon dioxide is not miscible at first contact with oil at typical reservoir pressures. However, miscibility can be achieved by multiple contacts within the reservoir where mass transfer between the CO$_2$ and the hydrocarbon components occurs as miscibility is approached. Then, oil and CO$_2$ flow together since the oil-enriched CO$_2$ phase cannot be distinguished from the CO$_2$-enriched oil phase and there is no interfacial tension between these fluids. Miscibility development between CO$_2$ and hydrocarbons is a function of pressure and temperature. However, for an isothermal reservoir, pressure is the main parameter to consider in the design of CO$_2$ displacement.

At high pressures, CO$_2$ develops a phase whose density is close to that of a liquid while its viscosity remains low. The denser CO$_2$ phase has the capacity to extract more hydrocarbon components from oil than when it is in gas phase at lower pressures. Even though the low viscosity of gas with respect to oil is unfavorable for sweep efficiency, CO$_2$ can reduce the oil viscosity which improves recovery.

The pressure necessary to reach miscibility with CO$_2$ is, in general, considerably lower than that to achieve miscibility with a mechanism of displacement that involves natural gas, flue gas or nitrogen [Jarrel et al., 2002].

Nitrogen is widely used in miscible displacement projects because of its easy allocation. Typically, air separation plants are used as sources of nitrogen. However, nitrogen injection projects may be limited to deep reservoirs in order to lead to miscible displacement [Stalkup, 1983]. Firoozabadi and Aziz (1986) found that nitrogen miscibility is mainly a function of the hydrocarbon composition and the reservoir

temperature. Nitrogen MMP decreases at higher temperatures because the solubility of nitrogen increases at temperatures above $100^{o}F$ [Stalkup, 1983].

2.1.2 Prediction of MMP

The condition necessary for a gas to achieve miscibility with oil, FCM or MMP, are usually determined with experimental data in the laboratory using a slim tube test. However, slim tube tests are expensive and time consuming [Jarrel et al, 1996]. When slim tube data are not available, there are two alternatives to determine MMP: phase behavior mathematical models and empirical correlations.

When experimental data are available, MMP is usually predicted from empirical correlations. Empirical correlations are simple to apply but they are limited to the conditions used in their generation. Therefore, predicted values may involve significant errors if the correlation is applied outside of its applicable limits. Empirical correlations are commonly used to determine initial estimates or as a screening tool. On the other hand, mathematical models provide more reliable results but their accuracy depends on the calibration of the EOS using experimental PVT data.

2.1.2.1 EOS Phase Behavior Calculation for MMP

Mathematical models can determine the MMP by vapor-liquid flash equilibrium calculation using an EOS. However, the EOS must be tuned uisng regression. Critical properties of the plus fraction, the binary parameters and the volume shift parameters are

modified in order to match the experimental data. One common approach to determine the miscibility conditions consists of finding the critical tie line, which is a line tangent to the critical locus. Johns and Orr (1996) developed a general analytical approach for calculating the MMP for multicomponent oils. In their work, MMP is determined using a tie line intersection method to determine the critical tie line. Tie lines passing through the gas and oil compositions are extended and intersected with the crossover tie line. When any of these tie lines becomes the critical one, the MMP is found. However, their work concentrated on displacement by a single gas component. Afterward, Wang and Orr (1998) expanded this approach by developing a model applicable to systems with multicomponent injection gas. Further study was presented by Jessen et al. (1998). The algorithm to calculate the tie line intersection point was modified to improve predictions close to the critical region. Yuan and Johns (2005) have presented a more recent study in which the solution is accelerated by reducing the number of equations and unknown parameters. The methodology of intersecting tie lines for MMP calculation is commonly applied in phase behavior commercial software; where the displacement processes are studied using ternary diagrams and pressure-composition diagrams generated using an EOS.

Another common method to mathematically determine the MMP is to use a compositional reservoir simulator. Slim tube experiments can be reproduced using a 1-D model. Recovery is recorded at 1.2 pore volumes of solvent injection at different pressures as shown in Figure **2-6**. The sharp change in the curve denotes the change in the mechanism of displacement, from immiscible to miscible as pressure increases [Stalkup, 1983].
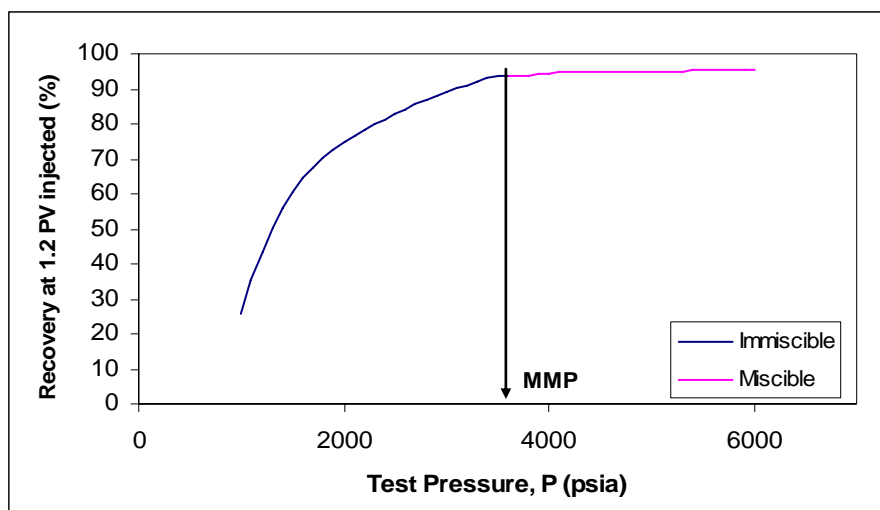
Figure **2-6**: MMP Estimation using a Compositional Reservoir Model

In the present study, WinProp [1] phase behavior software is used to determine the thermodynamic MMP, while miscible displacement process is modeled using GEM[2] compositional reservoir simulator. The EOS selected to perform all phase equilibrium calculations is Peng Robinson (PR), the same equation used by Johns and Orr (1996), Wang and Orr (1998) and Jessen et al. (1998) in their developments. The equation of state as well as the viscosity correlations used in the simulations throughout this study can be found in Appendix 1.

---

[1] WinProp is a phase behavior commercial software developed by CMG, Calgary, Canada.
[2] GEM is commercial compositional reservoir simulator developed by CMG, Calgary, Canada.

2.1.2.2 Empirical Correlations for MMP Prediction

Several empirical correlations have been developed to determine the thermodynamic MMP for different solvents such as CO_2 and N_2. However, the accuracy of these correlations depends upon the limits of their applicability. As a general practice, correlations are used in the absence of a slim tube test data or phase equilibrium data.

Yelling and Metcalfe (1980) developed a mathematical correlation to estimate the MMP for pure CO_2 injection based on experimental results from a slim tube using light West Texas oil. Their correlation is developed for hydrocarbons whose C_5^+ average molecular weight is less than 180. The composition of oil is not given as an input. The thermodynamic MMP is adjusted to the bubble point if the calculated MMP is less than the bubble point pressure. Holm and Josendal (1982) also developed a correlation to predict the MMP for CO_2 injection where the molecular weight is given as an input, as well as reservoir pressure and temperature.

On the other hand, different correlations for N_2-MMP calculation have been published. Firoozababadi and Aziz (1986) developed a correlation for N_2 based on temperature, concentration of intermediates components and volatility. Volatility is represented by the molecular weight of C_7^+ fraction. A further correlation presented by Hudgins et al. (1990) included also the dependency of the MMP on CH_4 contain.

2.1.3 Mobility Effects on Miscible Displacement

The basic mechanics of flow in porous media are described by Darcy's law, where the fluid velocity is proportional to the pressure gradient in the direction of flow as seen in Equation **2.1**:

$$v = -\frac{k * k_r}{\mu}\frac{dp}{dx}$$ **2.1**

where v is the fluid velocity, k is the absolute permeability of the rock, k_r is the relative permeability of the fluid, μ is the fluid viscosity and dp/dx is the pressure gradient in the x-direction. The group $k * k_r / \mu$ is called the mobility group.

In displacement processes, the relationship between the mobility of the displacing fluid to the displaced fluid is called the mobility ratio, M, and is calculated using Eq. **2.2**:

$$M = \frac{\left(k_D / \mu_D\right)}{\left(k_d / \mu_d\right)}$$ **2.2**

where the subscript D denotes the displacing phase and subscript d the displaced phase. The mobility ratio is an important parameter in displacement processes as it affects the volumetric sweep. A value of M greater than 1 leads to unfavorable displacement since the displacing solvent has a preference to move in the reservoir. On the other hand, a value of M less than 1 is indicative of a stable displacement process.

Typically, viscosities of most solvents are less than in-situ oil viscosities. This difference produces a mobility ratio greater than 1 and may reduce significantly the sweep efficiency. Also, effects such as fingering and channeling in high-permeable zones are commonly observed in miscible displacement processes [Willhite, 2003].

2.1.4 Steam Injection Processes

Steam injection is the most commonly used thermal recovery method. The simplest well configuration for a steam drive requires two wells; one steam injector and one oil producer, as shown in Figure **2-7**. At the beginning of the steam injection process, a steam zone is formed around the injection well, where the reservoir is heated to the steam temperature. Ahead of the steam zone, the light oil components are vaporized in the distillation zone. As we move away from the injector, the temperature profile drops to the initial reservoir temperature. As steam injection continues, the steam zone moves towards the producer displacing most of the oil. Typically, oil recovery increases rapidly until steam breakthrough is achieved.
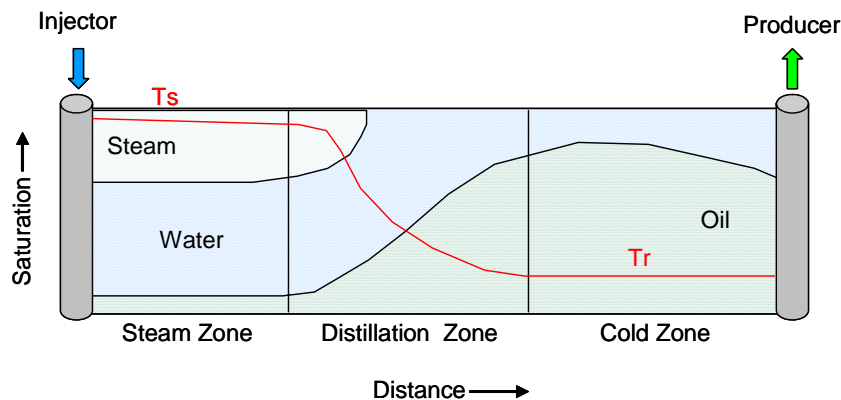
Figure **2-7**: Temperature and Saturation Distribution in a Steam Drive (adapted from Lake, 1989)

In general, steam injection processes are limited to certain reservoir conditions. The main criteria for steam operations are depth, permeability and reservoir pressure.

Steam injection may become economically impractical in reservoirs deeper than 3,000 ft due to wellbore heat losses. Large rock permeabilities are desirable so that steam injection rates are sufficient to allow the heat front to move a substantial distance. Then, the steam injection rates can compensate for the heat losses to the underburden and overburden. In addition, the maximum injection pressure is normally limited to the critical pressure of steam, 3206.2 psia. However, most steam projects are performed at considerable lower injection pressures. High steam injection pressure implies high injection temperatures and densities, resulting in small steam volumes and low oil recovery [Green & Willhite, 2003].

2.1.4.1 Steam-Drive Displacement Mechanisms

Steam injection operations involve several displacement mechanisms. Wilman et al. (1961) studied these mechanisms by injecting steam into different cores saturated with different oil samples. Observations from their results indicate that three main displacement mechanisms take place in a steam drive: oil viscosity reduction, thermal expansion of the oil and steam distillation. Oil viscosity reduction improves the mobility of the oil, while the thermal expansion favors the oil displacement through the reservoir. These two mechanisms are also found in hot water injection operations. Note that steam distillation is the more important displacement mechanism in steam injection operations. In general, hot water drives are not as efficient as steam drives since steam distillation is not present in hot water drive processes.

Steam distillation displaces a large amount of oil by vaporizing the oil that remains behind the cold zone. Volek and Pryor (1972) studied in more detail the steam distillation mechanism in light oil displacement. Their observed that hydrocarbons vaporize because of the reduction in their partial pressure in the presence of steam. The light oil components are distilled from the residual oil and carried beyond the steam front, where they condensate and mix with the oil bank ahead. The entire process leads to higher oil recoveries as the steam zone advances towards the producer.

2.1.4.2 Heat Losses

The steam front condensates as it moves through the reservoir due to heat losses. There are different sources of heat loss in steam injection operations. Heat losses to fluids and reservoir rock are the most significant sources of heat loss in thermal recovery processes. In addition, heat is also lost from surface equipment and wellbores. However, heat losses from surface equipment are minimized by appropriate insulation, while heat losses from wellbores only become significant with large depths, even if insulation is included in the well completion.

Numerical simulation of thermal recovery methods takes into account the diverse sources of heat gain/loss using the energy balance equation. Heat losses to overburden and underburden are usually determined using semi-analytical models. Temperature is assumed to change as a function of time and vertical distance from the reservoir boundaries. The heat loss rate and its derivative with respect to temperature are calculated and incorporated directly in the energy conservation derivatives. The energy lost is

included explicitly in the energy balance equation. These calculations are performed in each grid block facing the upper and lower reservoir boundaries. The only properties necessary to determine heat losses to rock are the thermal conductivity and heat capacity of the adjacent base and cap rock [Vinsome & Westerveld, 1980].

Heat losses to fluids take place by diffusion of energy from a region of high temperature to a region of low temperature. The energy flow in reservoirs occurs mainly by convection. Although conduction may be also present in the reservoir, convection dominates conduction in the main direction of fluid flow. The diffusion of heat is calculated using the thermal conductivity of the fluids and the existing temperature gradients.

2.1.5 Water Injection Processes

Secondary EOR methods include waterflooding, water injection and gas injection. However, secondary EOR processes are usually referred as waterflooding processes [Green & Willhite, 2003]. The displacement mechanism involved in both waterflooding and water injection operations are mostly the same. Accordingly, it is rather difficult to define a boundary that separates both processes. Typically, waterflooding is performed when water injection starts after the economic productive limit of the reservoir is achieved, while pressure maintenance by water injection starts before this limit is achieved [Frick & Taylor, 1962].

The design of a water injection operation includes the evaluation of the rock properties such as permeability, porosity, pore distribution, areal coverage and thickness.

In addition, it is necessary to evaluate the rock-fluid properties as capillary pressure and relative permeability. The results of this evaluation should lead the reservoir engineer to establish the appropriate design of the water injection operation. The design includes the injection pattern, injection rates and pressures, and identification of water sources [Craig, 1993].

2.1.5.1 Displacement of Immiscible Phases

Water and oil are immiscible at most reservoir pressures and temperatures, and also, at surface conditions due to the small solubility between these phases. When immiscible phases are present in a porous medium, the interfacial tension (IFT) between fluids governs the saturation distribution and phase displacement. The IFT is an indicator of miscibility. The lower the IFT, the two phases are more likely to achieve miscibility conditions [Willhite, 1986].

Fluid distribution is not only governed by the forces at fluid-fluid surfaces, but also, by the forces at the fluid-solid interface. When two immiscible fluids are in direct contact with a solid surface, one of the fluids is more strongly attracted to the solid surface than the other fluid. The fluid adhered to the solid is referred as the wetting phase while the other is referred as the non-wetting phase. The rock wettability is determined by the contact angle between the water and the rock surface "θ". If $\theta<90^{o}$, as shown in Figure **2-8**, the system is considered water-wet. On the contrary, if If $\theta>90^{o}$, the system is considered oil-wet. An angle close to 0° suggests a strongly water-wet system, and angle

close to 180° suggests a strongly oil-wet system. An angle close to 90° indicates intermediate wettability [Green & Willhite, 2003].
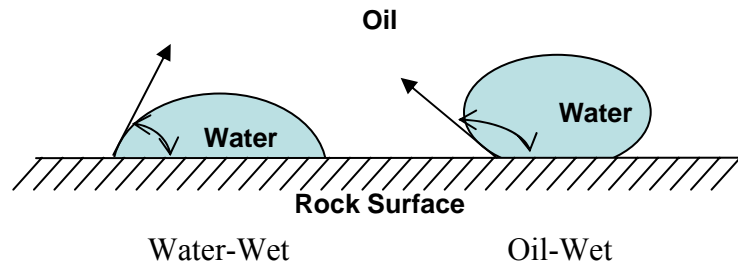
Figure **2-8**: Wettability of Oil-Water-Rock System (Adapted from Willhite, 1986)

Due to the interfacial tension between the fluids, a pressure difference is found across the interface. This difference in pressure is called capillary pressure, "P_c". It is determined as the pressure of non-wetting phase "P_{nw}" minus the pressure of the wetting phase "P_w", as shown in Eq. **2.3**:

$$P_c = P_{nw} - P_w$$ **2.3**

Capillary pressure can be positive or negative depending on the wettability of the system. The fluid that exhibits the lower pressure is the wetting phase. Correlations of pressure difference between two phases at different saturations are provided by capillary pressure curves.

The wettability of the rock also affects the relative permeability of the reservoir. This is clearly demonstrated on the asymmetry of the curves. Typical relative permeability curves for a water-wet rock and oil-wet rock are shown in Figure **2-9**. The saturation where the relative permeability of both phases is the same is greater than 50%

in water wet systems. On the contrary, in an oil-wet rock, the saturation where both relative permeabilities are equal is less than 50%.

Water-Wet System   Oil-Wet System
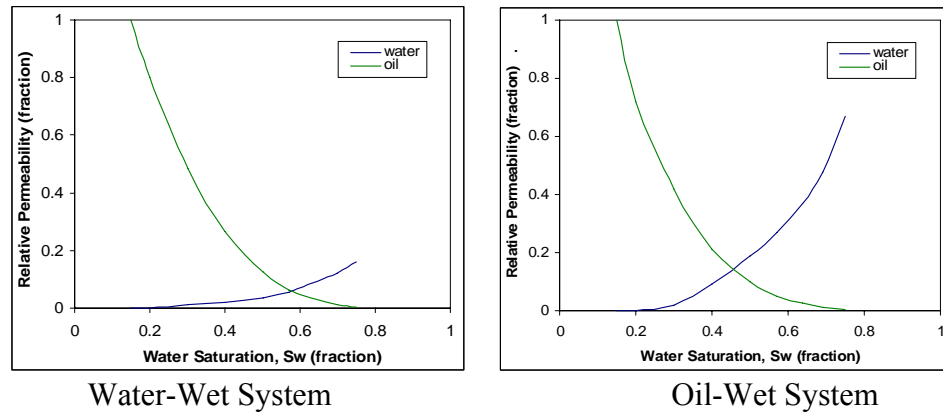
Figure **2-9**: Effect of Wettability on Relative Permeability Curves

The trapping mechanism of the fluids in a reservoir rock depends on the pore structure of the porous medium, fluid-rock interactions and fluid-fluid interactions. Usually, when the non-wetting fluid is displaced by a wetting fluid, the non-wetting phase is trapped as isolated drops. The capillary effects holding the drops cannot overcome the relative small viscous forces. Then, the non-wetting phase is usually resided in the large porous of the rock [Green & Willhite, 2003].

2.2 Hard Computing-Reservoir Simulation

At the present time deterministic and stochastic tools in reservoir simulation are widely used techniques. These hard computing reservoirs simulation protocols combine

the physics of flow in porous media with computer programming to study reservoir performance under different scenarios [Ertekin et al., 2001]. In general, reservoir modeling can be classified under two main categories: black-oil simulation and compositional simulation. In black oil modeling, fluid behavior depends exclusively on the reservoir pressure and the recovery mechanism is not affected by changes in composition. The fluid is represented using there phases of constant composition. The phases are gas, oil and water. Gas can be dissolved in the oil phase and oil can be vaporized into the gas phase. Fluid phase behavior is represented by the formation volume factors (B_g, B_o, B_w) and the solution gas-oil ratios (R_s). Typical applications of black oil simulation involve modeling of primary recovery mechanisms, waterflooding and chemical-flooding processes.

Compositional simulators are applied when the composition of the phases is changing throughout the simulation time, and the recovery mechanism is strongly affected by those changes. The compositional changes are described by a cubic equation of state. Compositional simulation involves longer computational time since vapor-liquid flash calculation is performed at each grid block to determine the phase equilibrium. Some common applications of compositional simulation are multi-contact miscible displacement processes and pressure maintenance operations in volatile and gas condensate reservoirs.

One of the modern applications of reservoir simulation is the modeling of thermal recovery processes such as steam injection and in-situ combustion. Thermal simulators use the compositional approach, where the energy-balance equation and the mass-balance equation are applied simultaneously.

2.3 Overview of Artificial Neural Networks (ANN)

Artificial neural network is an information processing technique that mimics the performance of the biological neural networks using a mathematical model [Fausett, 1994]. The earliest development of an artificial neural network dates from 1943 with the work of Warren McCulloch and Walter Pitts. However, it was until 1980's when ANN started to become popular due to the development of powerful computing systems [Hagan et al., 1996].
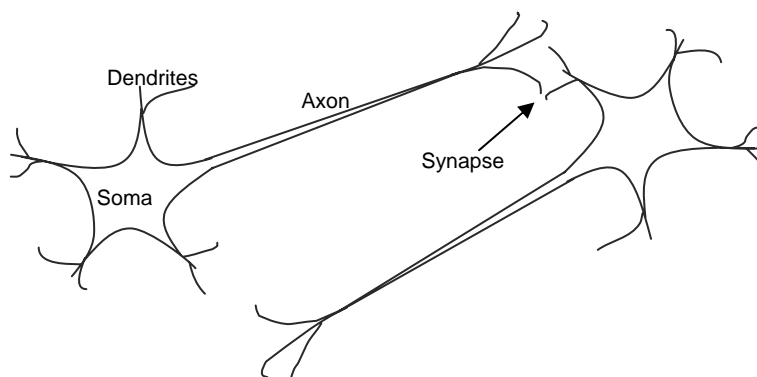
Figure **2-10**: Schematic of Biological Neurons (adapted from Hagan et al., 1996**)**

A biological neuron consists of three main components: dendrites, soma or cell body and axon as shown in Figure **2-10**. Neurons exchange information in the form of electrical signals through the dendrites. The soma sums and thresholds all received signals, and then, releases an electrical impulse through the axon to other neurons. The points where the axon and the dendrites are in contact are called synapses.

Artificial neural networks do not simulate complex biological neural systems, but they present fundamental similarities in their structure to their biological counterpart. A

schematic of a multiple input neuron is shown in Figure **2-11**. Each input P is multiplied

by a weight w. The weight corresponds to the strength of the synapses. The body of the

neuron is represented by the summation of all w*P products and its modification by a

transfer function. The neuron's output "a" represents the electrical impulse carried

through the axon [Hagan et al., 1996].
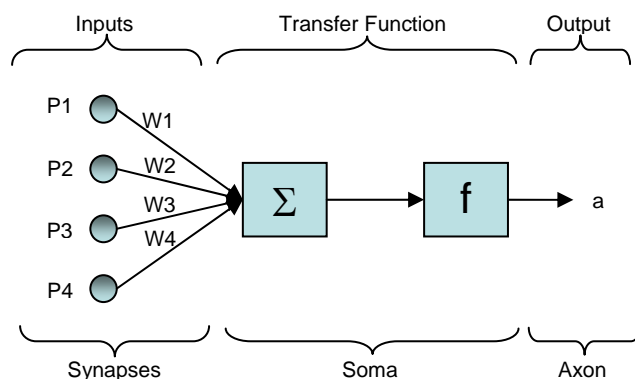
Figure **2-11**: Multiple Input Neuron

2.3.1 Artificial Neural Network Architecture

In most of artificial neural network applications it is common to find neurons

arranged in layers. Neurons belonging to the same layer usually perform in similar way

although their behavior is mainly conditioned to their activation or transfer function and

the connections (weights) with other neurons. The arrangement into layers and the

connections between neurons is what defines the network architecture. In general,

networks are classified into single layer or multilayer. Figure **2-12** shows typical

architectures for single layer and multilayer networks. In a single layer arrangement there

are only one input layer and one output layer connected with one layer of connection weights. In general, the input layer is not counted as a layer since it only provides the input data and no calculations are performed on the input layer.

A) Single Layer Network   B) Multilayer Network
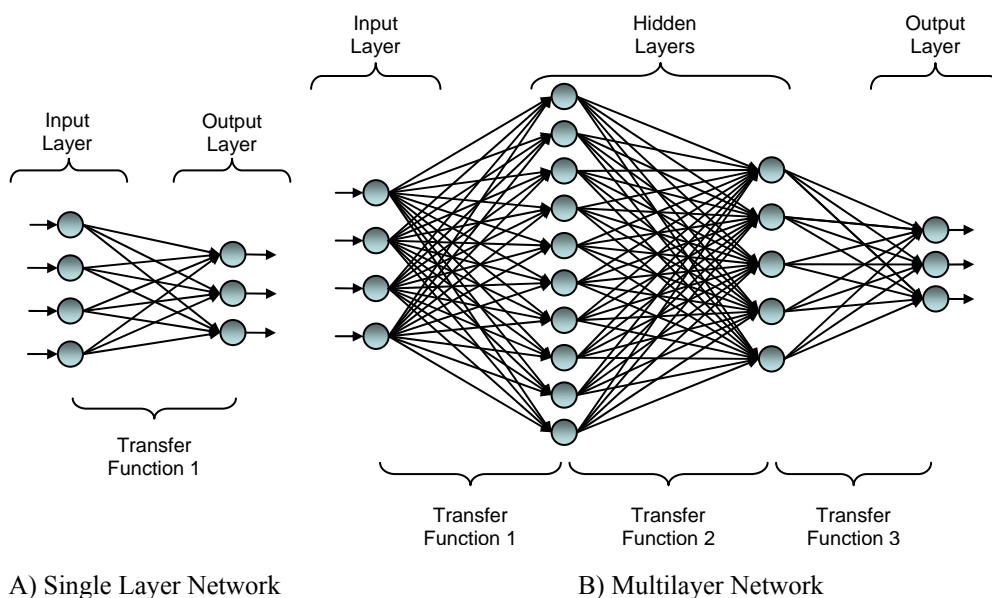
Figure **2-12**: Classification of Network Architectures

The multilayer structure includes internal layers connecting the input and output layers. The internal layers are called hidden layers since they do not interact directly with the external surroundings of the net.   The multilayer network shown in Figure **2-12** consists of three layers; two hidden layers and one output layer connected by three layers of weights. Multilayer networks are typically used to solve very complex problems than those solved by single ones. However, the selection of single or multilayer architectures must be done carefully since multilayer networks involve a challenging training process [Fausett, 1994].

2.3.1.1 Weights and Network Training

The weights are the neural synapse parameters that quantify the influence that an input stimulus has on one neuron. A positive weight represents an excitatory stimulus while a negative weight corresponds to an inhibitory stimulus. A zero weight value indicates no connection or stimulus. The weight connections between layers of neurons are denoted as weight matrices "W". Typically, the matrix element w_{ij}, is used to denote the weight connecting the output of neuron i to the input of neuron j [Patterson, 1996].

Weights are determined during an iterative training process. In general, the training processes can be classified as supervised and unsupervised. In supervised training an input vector or pattern is provided with its associated target or output vector. The weights are initially set to zero or to a small random number. Then, the weights are tuned iteratively according to a learning algorithm until the calculated output target is similar to the given target within some fixed error. In unsupervised training only an input vector pattern is provided. The weights are modified so that similar input patterns are assigned to the same target [Fausett, 1994]. In general, most neural networks are trained using a supervised process.

Besides the training method, another main factor to consider while training a network is the data itself. It is desirable to have extensive training data that cover most of the possible scenarios under study. However, it is common practice to normalize the inputs and outputs in the interval between -1 and 1 to regulate the influence of the data sets.

In the present study all data sets will be normalized between -1 and 1. Also, sets of input pattern – output target are generated using a commercial reservoir simulator in order to train all the networks using a supervised process.

2.3.1.2 Transfer Functions

The transfer function scales the response of an artificial neuron to an external stimulus, and generates the neuron activation [Maren et al., 1990]. Usually, the same activation function is applied to all neurons in one given layer but custom networks may assign different functions in one layer. Networks are typically designed using nonlinear activation functions, especially in multilayer networks since the result of providing a signal through two or more layers with linear elements can be also achieved with only one layer of linear elements [Fausett, 1994 and Maren et al., 1990].

The basic output of a neuron "a" using a linear transfer function is equal to its input "n" as given in Eq. **2.4**:

$$a=n \hspace{6cm} \textbf{2.4}$$

Sometimes, a threshold or bias is also included in the transfer function. The bias "b" is treated as another weight, which adds a constant value to the input of the neuron, scaling it to a practical range [Fausett, 1994]. The basic or pure linear transfer function is shown on the left of Figure **2-13**, while the linear function with bias is shown on the right of the same figure. Frequently, linear functions are applied to the output layer since it allows the network to produce its output within the desired limits without having to denormalize them.

$$a = purelin(n)$$ $$a = purelin(wp + b)$$
Linear Transfer Function   Single-Input *purelin* Neuron
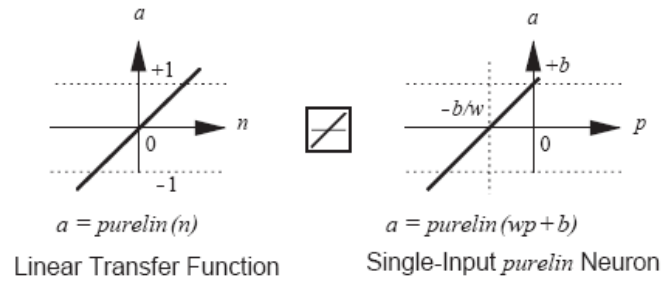
Figure **2-13**: Linear Transfer Function (reproduced from Hagan et al., 1996)

Sigmoid functions are powerful continuous, nonlinear transfer functions. The log-sigmoid and the hyperbolic tangent sigmoid function are the most common ones in neural network applications using back propagation training algorithm because they are differentiable, which reduces the computational requirements during training.

The log-sigmoid function, given in Eq. **2.5**, takes the input signal, which can be anywhere between minus and plus infinity, activates the neuron and scales its output in the interval between 0 and 1. Figure **2-14** shows the log-sigmoid function with and without bias.

$$a = \frac{1}{1 + e^{-n}}$$ **2.5**
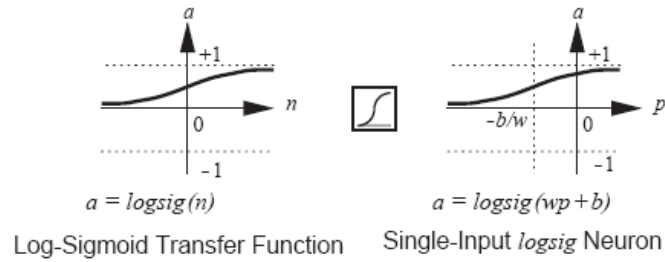
Figure **2-14**: Log-Sigmoid Transfer Function (reproduced from Hagan et al., 1996)

The hyperbolic tangent sigmoid, see Eq. **2.6**, scales the neuron output in the interval between -1 and 1. Figure **2-15** shows the hyperbolic tangent sigmoid.

$$a = \frac{e^n - e^{-n}}{e^n + e^{-n}}$$ **2.6**
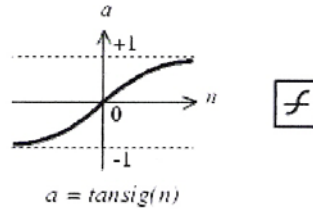
Figure **2-15**: Hyperbolic Tangent Sigmoid Transfer Function (reproduced from Demuth et al., 2007)

Some other widely used transfer functions are the threshold logic and hard limit functions. Table **2-1** shows a list of these other common functions. However, in the present work multilayer networks with sigmoid functions are proved to be more appropriate for our problem. Previous works, as the one presented by Gorucu (2005),

have also shown that these types of architectures are more suitable for applications on similar reservoir engineering problems.

Table **2-1**: Transfer Functions (reproduced from Hagan et al., 1996)

Name	Input/Output Relation	Icon	MATLAB Function
Hard Limit	$a = 0 \quad n < 0$ $a = 1 \quad n \geq 0$		hardlim
Symmetrical Hard Limit	$a = -1 \quad n < 0$ $a = +1 \quad n \geq 0$		hardlims
Linear	$a = n$		purelin
Saturating Linear	$a = 0 \quad n < 0$ $a = n \quad 0 \leq n \leq 1$ $a = 1 \quad n > 1$		satlin
Symmetric Saturating Linear	$a = -1 \quad n < -1$ $a = n \quad -1 \leq n \leq 1$ $a = 1 \quad n > 1$		satlins
Log-Sigmoid	$a = \dfrac{1}{1 + e^{-n}}$		logsig
Hyperbolic Tangent Sigmoid	$a = \dfrac{e^{n} - e^{-n}}{e^{n} + e^{-n}}$		tansig
Positive Linear	$a = 0 \quad n < 0$ $a = n \quad 0 \leq n$		poslin
Competitive	$a = 1 \quad$ neuron with max n $a = 0 \quad$ all other neurons	C	compet

2.3.2 Multilayer Feedforward Networks with Back Propagation

Multilayer feedforward network with back propagation learning process is the most widely used network architecture [Maren et al., 1990 and Patterson, 1995]. The main feature in feedforward nets is their layered structure with forward connections between the neurons. Back propagation is a supervised learning process that can be applied to any multilayer network that undergo supervised learning process with

differentiable transfer functions. In general, back propagation networks are commonly

applied in pattern classification, signal filtering and mapping problems [Fausett, 1994 and

Maren et al., 1990].

The back propagation algorithm consists of three main steps: the feedforward of

the input patterns layer by layer throughout the network, back propagation of the

calculated error and appropriate adjustments of the connection weights.

The learning rule of the back propagation process is the *Generalized Delta Rule*,

which is a generalized form of the *Least Mean Squared* (LMS) rule. The Generalized

Delta Rule allows the modification of the weights and biases of all layers by using the

chain rule, with the aim of reducing the difference between the network output (*a*) and

the desired target (*t*). This difference is calculated using the LMS error, as shown in

Eq. **2.7**:

$$e = \frac{1}{N} \sum_{i=1}^{N} (t(i) - a(i))^2 \qquad \qquad \textbf{2.7}$$

where N is the number of inputs.

The adjustment of the connection weights is performed using the *steepest descent*

rule where the errors are related to the weights using the function *delta* as given in

Eq. **2.8**:

$$w_{i,j}^{new} = w_{i,j}^{old} - \alpha * delta(w_{i,j}^{old}) * a_j \qquad \qquad \textbf{2.8}$$

where $w_{i,j}$ denotes the old and new values of the weight connecting neuron *i* and *j*. α is a

constant, called *learning rate*, that governs how the weights are affected by the delta. The

term $delta(w_{i,j}^{old})$ represents the delta function evaluated at the old value of $w_{i,j}$. In

general, the delta function is calculated as the negative value of the derivative of the error with respect to its corresponding weight as shown in Eq. **2.9** [Maren et al., 1990]:

$$delta(w_{i,j}) = -\frac{\partial e}{\partial w_{i,j}}$$

2.9

The back propagation learning rule requires a bounded activation function that is continuous, differentiable and monotonically non-decreasing. Sigmoid functions are the preferred option since they comply with all these requirements. They are bounded since for the large positive inputs, they become asymptotic to a value of 1 and for large negative inputs, asymptotic to a value of either 0 or -1. The main advantage of bounded functions is that the activated output can be classified basically as high and low, which are considered stable states.

According to Maren (1990), differentiation is important when selecting the transfer function since the adjustments performed to the connection weights are proportional to the derivative of the activation function. Notice that both log-sigmoid and hyperbolic tangent sigmoid functions are positive as shown in Figure **2-16**. For either large positive or large negative values, the derivative of both functions is close to zero, meaning that the weight adjustment will be small. When the activated output is in the middle range, a large adjustment is desired since the output is not close to neither stable state, but the largest derivative is achieved at the middle value, leading to a large change in weight. Notice that the activation of log sigmoid function is not symmetric about zero, which may affect the performance of the network. When it is not possible to rescale the log sigmoid activation, the hyperbolic tangent sigmoid function is highly recommended because of its symmetry about zero.
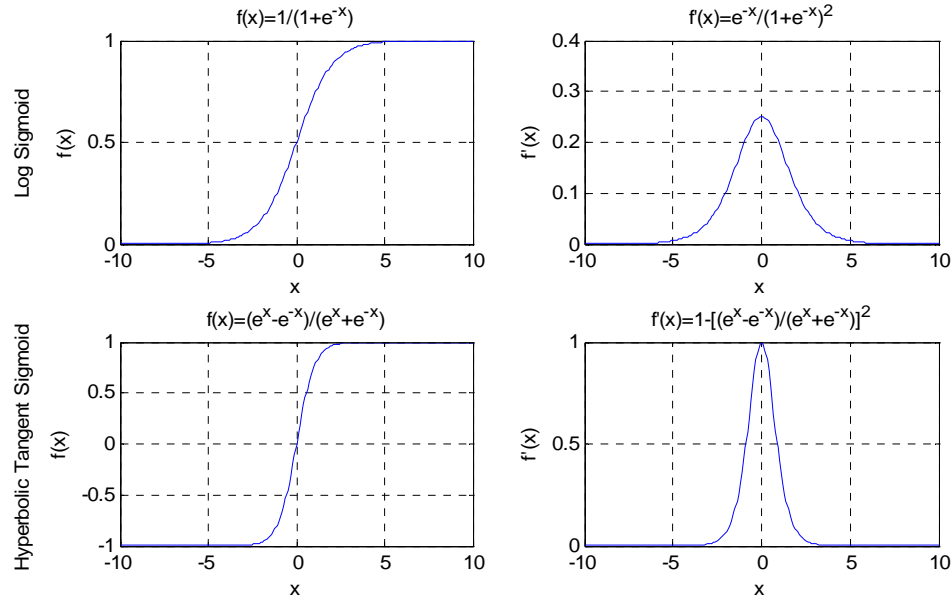
Figure **2-16**: Sigmoid Transfer Functions and their Derivatives

2.3.3 Convergence and Training Efficiency

Convergence problem arises when the network calculates a lower total error than the one in the previous iteration, but it does not lead to a global minimum error. In this case, the network has memorized the training data sets and cannot predict accurately other general cases. A common technique to avoid memorization is early stopping. In this method an extra set of data, called validation, is also fed to the network together with the training data set. The network is trained exclusively with the training data set while the error of the validation set is monitored. Usually both validation and training errors start deceasing during the early stages of training. When the network starts overtraining, the validation error starts increasing while the training error continues decreasing. At this

point, the training process is stopped and the values of connection weights and bias are taken when the validation error is minimum [Demuth et al., 2007 and Maren et al., 1990].

Network convergence can be time consuming if the majority of the output targets are close to either stable state, that is, the asymptotic values of the sigmoid functions. One common approach to improve convergence is to modify the number of neurons in the hidden layers. Also, training may be improved by applying a transformation or *functional link* to the input patterns such as logarithm, square root or Fourier transform. A functional link, if selected appropriately, may help to regulate the influence of weak and strong inputs.

The learning rate can also be used to enhance the training speed and efficiency. Large learning rates lead to faster training but introduce some degree of fluctuation while small learning rates provide more stabilization but delay the learning process, which may direct convergence to local minimum.

Another way to improve the training process is to introduce *momentum* to the steepest descent rule. Momentum acts as a filter that smoothes the oscillation in the descent path due to several local minima since the network moves in the direction of a combination of the current gradient and the previous direction of the weight change [Fausett, 1994]. Eq. **2.10** shows how the back propagation rule is modified when momentum coefficient, γ, is added:

$$w_{i,j}^{new} = \gamma * w_{i,j}^{old} - (1-\gamma) * \alpha * delta(w_{i,j}^{old}) * a_j \qquad \textbf{2.10}$$

The values of momentum coefficient are between 0 and less than 1.

2.3.4 Application of Neuro-Simulation

Neuron-simulation is a technique that couples soft-computing (artificial neural networks) and hard-computing techniques. In the present study, reservoir simulation modeling is employed to generate the network training data. For instance, reservoir characteristics, recovery mechanism and operating performance can be used to create sets of patterns/targets in the network. During the learning process, the network creates an internal mapping that captures the relationship between the inputs and outputs. After training, the net can be used to forecast the reservoir response to conditions different from those used in training. This methodology reduces the computational time necessary to simulate and evaluate a large universe of reservoir conditions.

Neuro-simulation has been widely used in diverse petroleum applications. Some of the recent work includes the proxy model developed by Ayala et al. (2004) for gas-condensate reservoir exploitation. Odusote et al. (2004) presented a screening tool-box for recovery of coalbed methane by CO_2 injection, and Gorucu et al. (2005) characterized carbon dioxide sequestration and coalbed methane projects.

In the present study, neuro-simulation will be used to generate a tool-box for prediction of reservoir behavior undergoing different oil recovery mechanisms. Hard-computing will be used to generate study cases necessary for training and further testing of the network's predictive capabilities. The inverse problem, where the reservoir performance is known, will be implemented to design recommended operating well conditions.

Chapter 3

STATEMENT OF THE PROBLEM

The proper implementation of a set of screening criteria for improved oil recovery methods is essential in assessing the field development plan and the economic evaluation of green and mature oil reservoirs as well. Previous studies have presented descriptive screening guidelines for IOR methods based on fluid and rock properties. However, the existing screening criteria fail to provide information about the expected reservoir performance. Moreover, the published criteria are not strict guidelines applicable to a particular reservoir candidate. Further assessments of sets of field deployment design parameters are crucial to complete the appraisal of reservoir implementations.

In order to combine recommended guidelines for IOR methods along with the expected reservoir performance, the main objective of this study is to create a tool-box for IOR screening criteria that also provides the expected oil production profile for a reservoir of known characteristics. The screening is performed based on the reservoir description parameters such as rock properties, fluid properties and exploitation plan. The tool-box is developed using an artificial neural network algorithm due to its ability to provide immediate results within an acceptable error margin if properly trained.

The proposed screening network includes three of the most common IOR techniques currently applied worldwide: miscible carbon dioxide injection, nitrogen injection and steam injection. In addition, waterflooding processes are also included in

the tool-box as it is a common technique extensively applied for pressure maintenance to speed up the recovery performance.

Typically, screening IOR processes is the first step in the evaluation of the economic feasibility of a reservoir project. In general, available screening guidelines are generated from field data but most of the time they lack details about the production schemes implemented in these projects. Reservoir engineers typically evaluate different field exploitation plans after a recovery technique has been proposed in order to verify if the selection was appropriate, and also, to optimize the hydrocarbon recovery. Evaluation and optimization protocols are usually performed using commercial reservoir simulators. This stage of the reservoir assessment approach requires significant investment of time and skillful professionals. In real projects, time is not always available and not all possible production schemes are tested due to the high computational requirements and time involved.

This study also seeks to overcome the time limitations involved in the optimization stage. Therefore, an inverse use of the screening tool-box is proposed to provide the design parameters for IOR processes. The proposed expert system will provide some guidelines on the appropriate reservoir development plan, which helps to narrow down the possible production scenarios to be evaluated by typical reservoir simulation methodology.

The use of the proposed neuro-simulation application, together with conventional simulation, should become a more efficient designing protocol for oil reservoir operations.

Chapter 4

RESERVOIR MODEL

Reservoir simulation is a tool widely used by petroleum engineers to forecast the performance of hydrocarbon reservoirs under various operating conditions. Simulation plays an important role in assessing the appropriate production development plan for green fields and also optimizing current production schemes for mature fields already under development. In addition, reservoir simulation is a key factor used in assessing the economic deployment of any reservoir project.

The fundamental properties needed to build a reservoir model include the rock properties, fluid properties and formation architecture. These variables are defined by mother-nature and are unique to each reservoir. In addition, it is necessary to define the design parameters, which are under control of the reservoir engineer. The design parameters include drilling and completion techniques, well pattern, well spacing and the recovery mechanism to be implemented to maximize oil recovery.

In order to build an ANN screening tool-box for reservoir applications, it is necessary to have reservoir data for training and validation purposes. Therefore, diverse reservoir models were built and run using CMG©[3] commercial simulator. These models were built according to the process to be incorporated within the artificial intelligent simulator.

---

[3] CMG is a commercial reservoir simulator developed by Computer Modeling Group Ltd. Calgary, Canada.

4.1 Fluid Properties

4.1.1 PVT Data and Initial Reservoir Conditions

Some of the suggested screening criteria for IOR methods include oil gravity, viscosity and composition [Taber, 1997]. In order to compile a good range of oil properties for current IOR methods, four different hydrocarbons compositions are considered throughout the development of this research study: two black oil fluids, one volatile oil fluid and one heavy oil fluid. Table **4-1** shows these four fluids compositions. The first three PVT compositions were taken from the literature. However, PVT#4 corresponds to a sample taken from a real heavy oil field located in Middle East that is currently producing under steam injection.

Table **4-1**: Molar Composition of PVT Data

	PVT 1 Black Oil [Mc Cain, 1990]	PVT 2 Volatile Oil [Papp et al, 1998]	PVT 3 Black Oil [Rathmell, 1971]	PVT 4 Black Oil (Real Sample)
CO_2	0.91	0.51	3.2	0.11
N_2	0.16	1.8	0.03	0.69
C1	36.47	46.8	27.81	10.78
C2	9.67	8.09	8.21	0.12
C3	6.95	10.91	5.99	0.42
iC4	1.44	4.26	0.31	0.30
nC4	3.93	6.86	4.1	0.32
iC5	1.44	3.71	1.3	0.29
nC5	1.41	3.81	2.3	0.26
C6	4.33	4.73	4.62	0.64
C7+	33.29	8.52	42.13	86.09
MW	218	156	223	532
s.g	0.8515	0.782	875	0.925
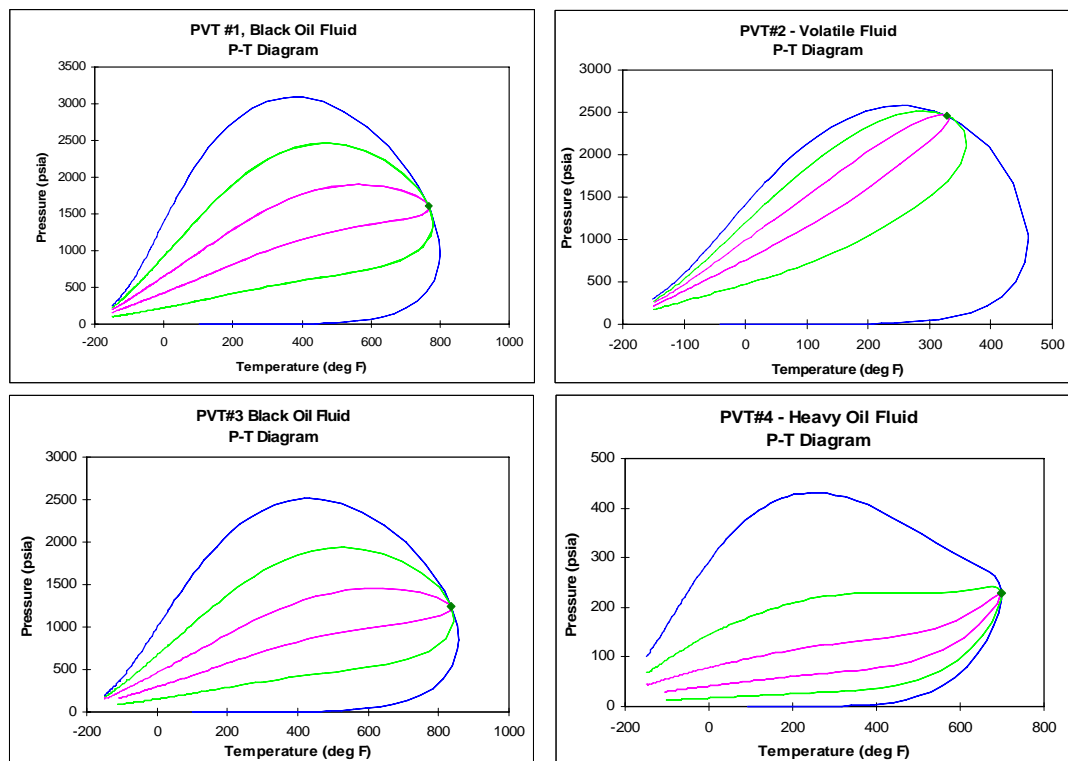
Figure **4-1**: PVT Phase Envelopes

Figure **4-1** shows four two-phase Envelopes generated by WinProp©**4** using Peng-Robinson equation of state. The PVT#1 and PVT#3 exhibit the characteristics of a black-oil reservoir fluid. The quality lines are distributed uniformly within the two-phase region. Also, the critical temperature is higher than typical reservoir temperatures (100-250 ^{o}F). The P-T diagram generated for PVT#2 is typical of volatile oils. The temperature range covered by the two-phase region is smaller. The critical temperature is closer to usual reservoir temperatures and the quality lines are displaced upwards towards the bubble point curve.

4 WinProp is a commercial software for phase behavior developed by CMG, Calgary, Canada

Laboratory data obtained from a differential liberation experiment were used in the construction of the phase envelope for PVT#4. Different parameters were modified in the regression to match the EOS with the experimental data. The bubble point locus curve for PVT#4 in Figure **4-1** shows that this fluid is in liquid phase for pressures above 430 psia. Low bubble point pressures are characteristic of heavy oil compositions.

The initial conditions are very important parameters in the design of the reservoir model. These conditions should be specified within the typical ranges used in the majority of current IOR projects. Taber and Martin (1983) and Taber et al. (1997) indicate that temperature is not a critical factor in the screening of the IOR mechanisms considered in this study. However, miscible displacement projects may require deep reservoirs in order to maintain pressures above the MMP, and deep reservoirs are commonly associated with high temperatures. Then, it would be recommended to set an initial temperature closer to the higher limit of its typical range. Teletzke et al. (2005) published a list of fields that are good candidates for miscible injection in the Malay Basin. The temperatures of the reservoirs in the Malay Basin range from 170°F to 252°F.

Figure **4-2** shows the frequency of reservoir temperatures in the Malay Basin. The normal temperature is around 220°F. Therefore, the reservoir temperature for all reservoir models in the present study is set at 220°F since it falls in the typical range for the IOR process and it can be related to deep reservoirs.
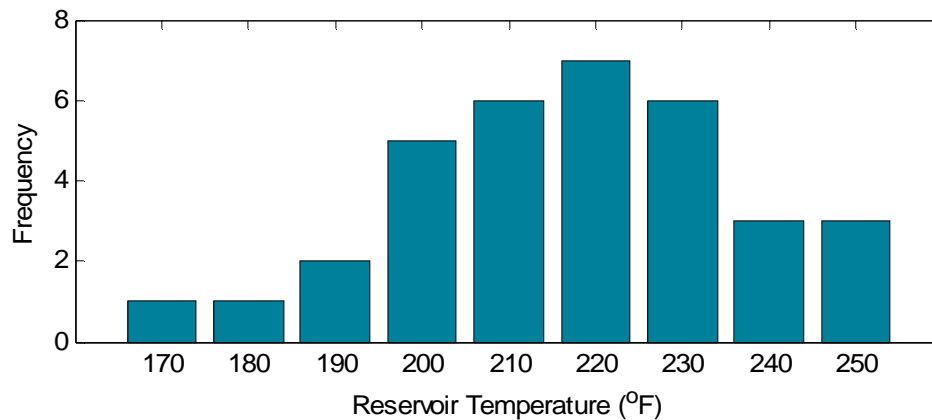
Figure **4-2**: Reservoir Temperatures in the Malay Basin (from Teletzke, et al., 2005)

The initial pressure should facilitate the development of miscible conditions. Then, the MMP is used as a criterion to define that initial condition. The CO_2- and N_2-MMP values were calculated for PVT compositions 1, 2 and 3 at different gas/oil equilibrium fractions. Figure **4-3** shows the calculated MMP using WinProp. The miscibility pressures for PVT#1 are higher than those for PVT#2 and PVT#3. In addition, the calculated MMP is higher for nitrogen injection, as expected.

It is desirable to set the same initial pressure in the reservoirs undergoing CO_2 and N_2 injection in order to generate comparable cases. Then, for PVT#1 the initial pressure is established at 5000 psia, a value below the maximum CO_2- and N_2-MMP values. Miscibility will be achieved in both cases since injection pressures must be above the MMP. For PVT#2 and PVT#3, the initial pressure is fixed at 3000 psia, which is close to the calculated MMP. The initial pressure of PVT#4 was established as 1000 psia since that is the reported initial pressure of the Middle East field.
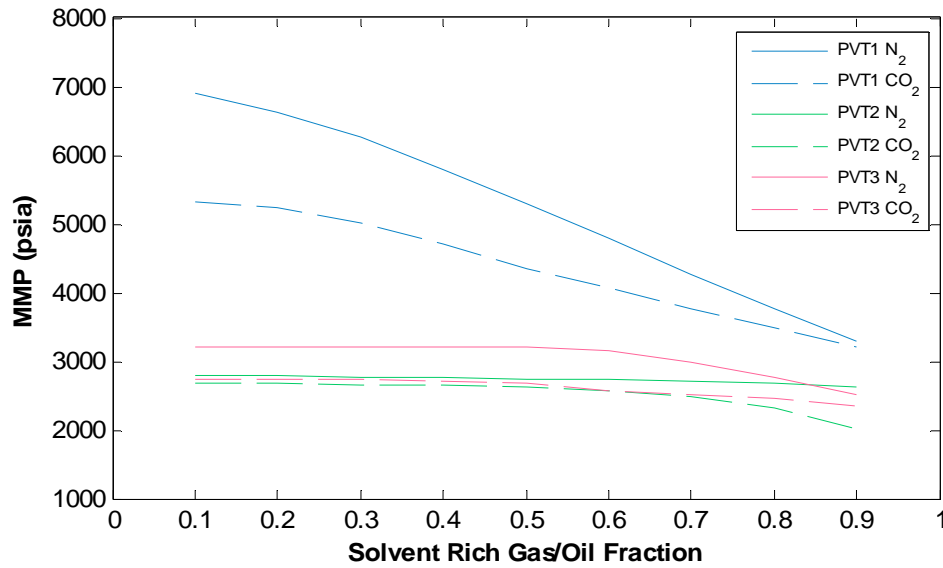
Figure **4-3**: MMP Variation with Solvent Rich Gas/Oil Mol Fraction @ T=220°F

4.2 Well Patterns and Grid Orientation Effects

In general, IOR screening criteria include the reservoir properties. Since the properties are unique characteristics of each reservoir, the screening criteria are based on average properties. Average properties can be represented with a homogeneous and isotropic reservoir model, which simplifies the problem under study without reducing the accuracy of the model representation. Therefore, the reservoir models considered in the present study were built using a homogeneous isotropic grid system.

Four different study cases of well patterns were used in the numerical simulation model. These are normal 4-spot, normal 5-spot, normal 7-spot and normal 9-spot patterns as shown in Figure **4-4**. In order to minimize the computational time, each pattern is modeled using a typical element of symmetry. An element of symmetry is a section of

the reservoir that can be used to generate the entire reservoir development scheme. In a simulation model there should be symmetry with respect to the number of grid blocks (Nx, Ny Nz), grid block dimensions (dx, dy, dz), reservoir rock properties such as permeability (kx, ky, kz) and porosity (ϕ), number of wells, well location, well type (producer, injector), well operating conditions, reservoir structure (boundaries and depth), initial pressure and initial fluid saturations [Abou-Kassem et al., 2006].
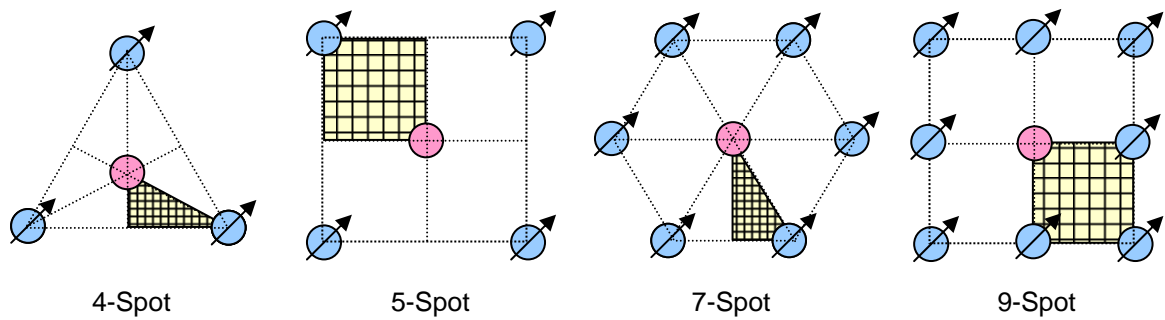
Figure **4-4**: Well Patterns and Element of Symmetry

Figure **4-4** also shows the element of symmetry used in each of the well patterns. Notice that the minimum element of symmetry was selected for the 4-spot ($^1/_6$ of the pattern area) and 7-spot ($^1/_{12}$ of the pattern). For the 5-spot and 9-spot cases, $^1/_4$ of the pattern area was used instead of the minimum element, which is $^1/_8$ of the pattern area. This grid element offers the advantage of having a rectangular model without pinch outs, corner point geometry or an irregular boundary. Nevertheless, a different grid orientation can be also used for the 5-spot pattern, which generates a direct line drive path between the injectors and the producers as shown in Figure **4-5**. Since the breakthrough time will

be different depending on the grid orientation, both grid systems, normal and direct line drive 5-spot, are modeled and the average of production, injection, breakthrough time and abandonment time are calculated to account for the grid orientation effects. A similar approach is not applied to the other well patterns. Different orientation of the grid generates two irregular boundaries in the 4 and 7-spot cases and four irregular boundaries in the 9-spot. Irregular boundaries do not help to provide a better model representation but they tend to increase the numerical dispersion in the simulator results.
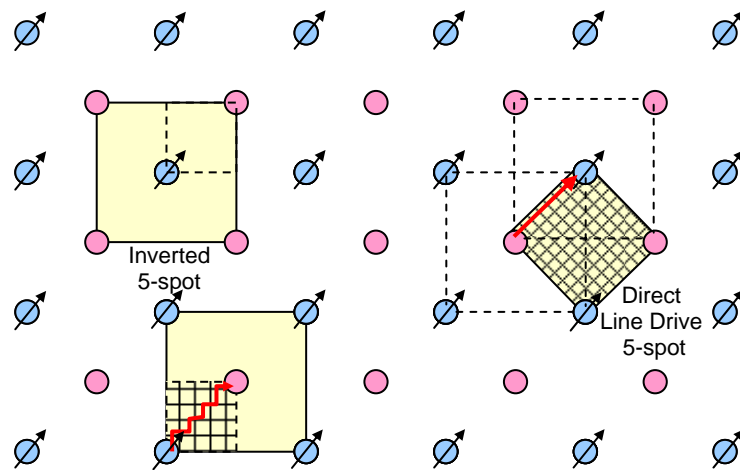
Figure **4-5**: Different 5-Spot Well Arrangements

4.3 Sensitivity of the Numerical Model to the Grid Dimensions

Sensitivity of the numerical model on grid block size was performed in order to minimize the grid effects on the simulation results. A three-dimensional (3D) simulation base case was built using the PVT #1 undergoing CO_2 injection. This base case was built

using 4 horizontal layers of same thickness. No aquifer was incorporated in the model. The wells were completed in all four layers. Different numbers of blocks were tested using pattern areas of 10, 60 and 100 acres. The same number of blocks is specified in the x and y-directions to preserve symmetry in the 5-spot and 9-spot well patterns, which generates square grid blocks. The same criterion is applied to 4-spot and 7-spot patterns, which creates rectangular grid blocks. All patterns conserved homogeneous and isotropic property distributions. The number of blocks tested was 10, 15, 20, 25, 30, 40 and 50. The properties used to generate these models are presented in Table **4-2**.

Table **4-2**: Simulation Properties for Grid Size Sensitivity Analysis

Parameter	Value
Injection BHP	6000 psia
Production BHP	3000 psia
Initial Pressure	5000 psia
Initial Temperature	220°F
Initial Water Saturation	20 %
Horizontal Permeability	100 md
Vertical Permeability	10 md
Thickness	50 ft
Porosity	25 %

Figure **4-6** shows the oil production rate and CO_2 mole fraction in the production stream in a 4-spot arrangement. It is noted that results are slightly sensitive to the number of blocks since oil production and CO_2 fraction curves exhibit similar behavior for all the cases studied. The curves seem to converge when large block numbers are used. Since a considerable number of data sets must be generated to train the ANN tool-box, the grid

dimensions were selected according to the number of runs needed in order to optimize the computational time needed. However, 10x10 grids provide an evident deviation at early times in production. Then, this grid configuration was avoided.

Sensitivities performed for the other well patterns are shown in Appendix 2.
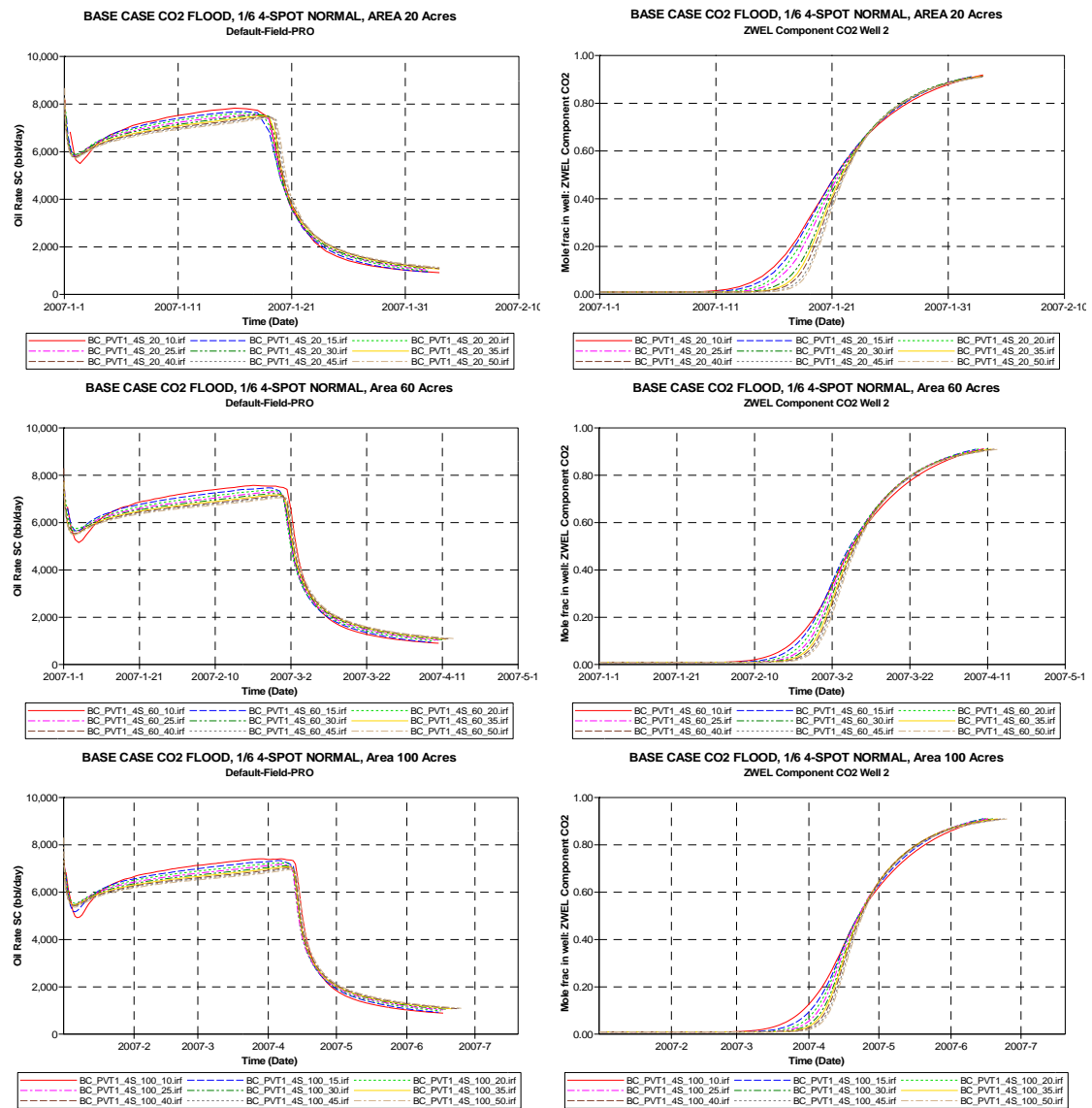
Figure **4-6**: Sensitivity Analysis on Grid Size – Normal 4-Spot Well Pattern

4.4 Reservoir Layering and Well Completion

In the present study, all reservoir simulation models are built using 3D grids to effectively model the gravitational effects. In miscible injection processes, the solvent is injected into the reservoir hydrocarbon zones to achieve miscibility between fluids. By the same token, steam is injected only into the reservoir hydrocarbons zones to minimize heat losses to the adjacent rock. Therefore, the grid models undergoing CO_2, N_2 and steam injection do not include aquifers. The models are built using four layers that represent only the oil zone. Gas zone is not included since the reservoirs are initially saturated. Also, initial water saturation is set as the connate water saturation. For these three processes, the wells are completed in all four layers. Figure **4-7 A** shows a 3D grid model of 4-spot well configuration using PVT#1 fluid undergoing CO_2 injection. The same layering is also used in N_2 and steam injection processes.

In waterflooding processes, water is injected underneath the oil zone to maintain pressure. Therefore, the models representing waterflooding processes are built using five layers. The first four layers correspond to the oil zone while the bottom layer corresponds to the water zone. No gas zone is incorporated into the model since the reservoirs are also initially saturated. The water injector is completed below the oil-water contact, or fifth layer. Figure **4-7 B** shows a 3D grid model of 4-spot well configuration using PVT#1 fluid undergoing water injection.
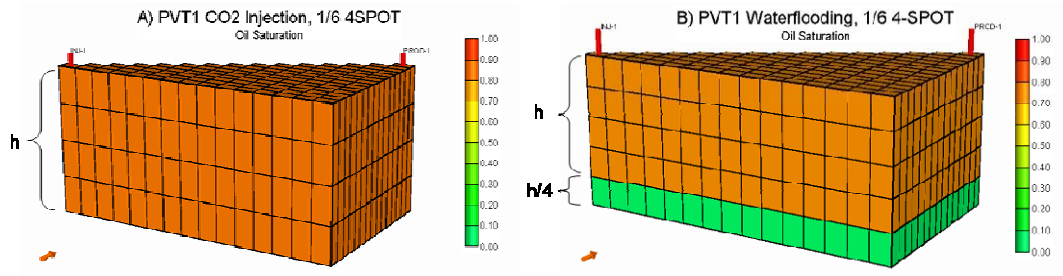
Figure **4-7**: Layering in Reservoir Models (4-SPOT)

A sensitivity analysis was performed to determine the appropriate completion for the producers. A 4-spot model was built using an area of 60 acres with 15x15x5 blocks. The reservoir properties used are the same as those used in the grid size sensitivity analysis, which are found in Table **4-2**. For all waterflooding cases, the given thickness corresponds only to the entire oil zone. The water zone thickness is set as ¼ of the oil zone thickness.

Four different completion schemes were evaluated as shown in Table **4-3**. From the results, the maximum recovery is achieved when the producer is completed in the three upper layers. Therefore, all waterflooding models are built using this completion scheme.

Table **4-3**: Sensitivity Analysis on Well Completion for Waterflooding Models

Completion of Producer	Completion of Injector	Cumulative Oil Production (STB)	Abandonment Time (days)
Layer 1	Layer 5	494,493	692
Layer 1 & 2	Layer 5	495,691	520
Layer 1, 2 & 3	Layer 5	496,858	463
Layer 1, 2, 3 & 4	Layer 5	493,154	409

4.5 Relative Permeability and Capillary Pressure

Typically, separate screening criteria are created for sandstone or carbonates formation types [Taber and Martin, 1983, and Taber et al., 1997]. The relative permeability curves used in the present work are characteristic of sandstone rocks. The three-phase relative permeability curves are generated using Corey's correlations [Corey, 1954].

In miscible displacement processes, viscous forces and gravitational effects are more important than capillary effects. Therefore, capillary pressure is set to zero for these two processes. Also, one set of relative permeability curves is used for all cases undergoing CO_2 and N_2 miscible displacement processes. These curves are shown in Figure **4-8**. The initial water saturation of the models is set to the connate water saturation, and the reservoir is considered to be saturated (no free gas).
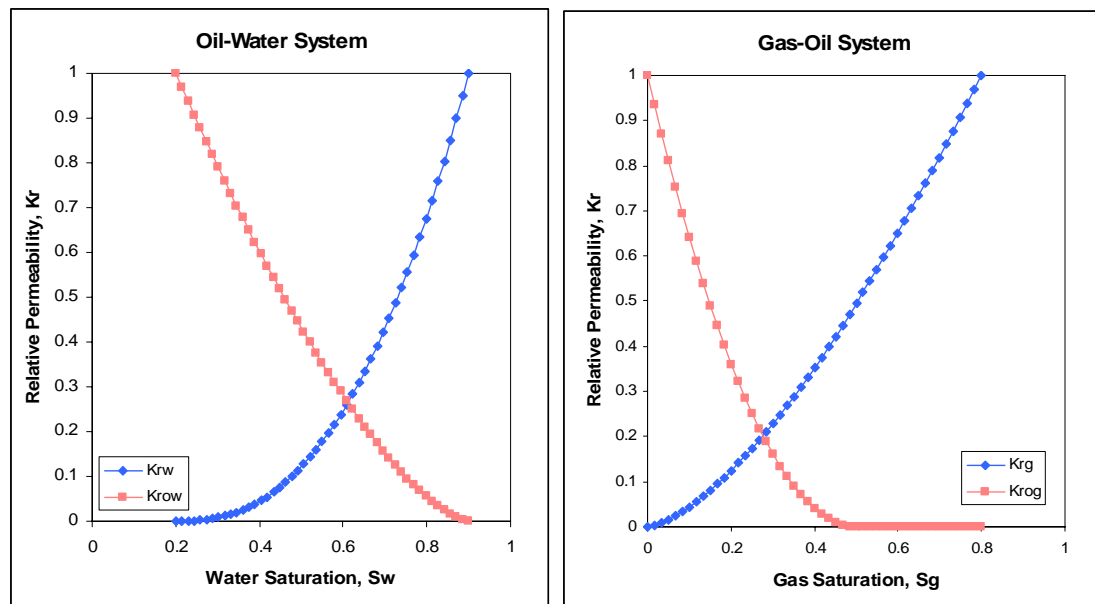
Figure **4-8**: Three-Phase Relative Permeability Curves

On the contrary, the effects of capillary pressure are among the most significant forces in immiscible displacement processes. Therefore, a good representation of the fluid flow in waterflooding models should take into account the influence of the capillary pressure. Capillary pressure, p_c, is incorporated into the waterflooding models using Corey's correlation (1954):

$$p_c = \frac{C}{\sqrt{\dfrac{Sw - Sw_{irr}}{1 - So_r - Sw_{irr}}}} \qquad\qquad \textbf{4.1}$$

where Sw_{irr} is the irreducible water saturation (fraction), So_r is the residual water saturation in the presence of water (fraction) and C is a constant. The constant C is usually determined experimentally for a given system. It defines the capillary pressure at the residual oil saturation. Different values of C are specified accordingly for the water-oil and gas-oil systems.

Water saturation changes drastically during waterflooding processes. Then, different values of irreducible water saturation and residual oil saturation are specified in the waterflooding models. The reservoirs are oil saturated at initial conditions. The relative permeability curves are functions of these saturations. As a result, each waterflooding model also incorporates a different set of relative permeability curves calculated with Corey's correlations [Corey, 1954]. In steam injection processes, water condensates in the reservoir due to heat losses encountered. Accordingly, capillary pressure is also incorporated into these models. Also different values of oil and water saturations are implemented in this process as they affect the relative permeability curves.

4.6 Operational and Abandonment Conditions

The operational conditions consist of the method applied to control the production or injection in the wells. In general, a well can be operated by controlling either its pressure or its flow rate. It is convenient to operate the wells using pressure control if the reservoir is subject to a miscible displacement process. In this way, it is possible to assure observation of miscibility. By the same token, proper control of the steam quality is fundamental in steam injection applications. This can be only achieved by controlling the injector by pressure. In the present study the wells are operated by bottom hole pressure (BHP) control. Pressure could be also controlled at the head of the well but that requires a completion design that is not included in the reservoir model.

4.6.1 Miscible Displacement Processes

For the miscible displacement processes, it would be desirable to set up the same pressure ranges of solvent injection in order to generate comparable cases. Nonetheless, Figure **4-3** showed that different combinations of fluid compositions and solvents lead to different MMP. For fluid #1, the highest calculated N_2-MMP value is about 7000 psia, while the highest calculated CO_2-MMP value is 5200 psia. Then, different ranges of injection pressure should be considered for each solvent when using fluid #1. On the other hand, N_2-and CO_2-MMP values for fluid #2 and #3 present similar calculated values (around 2700 psia). Therefore, the ranges of injection pressures can be set the same when using fluid #2 and fluid #3.

The production pressures must be set below the initial pressure to generate sufficient drawdown. It is obvious that these pressures will be below the MMP, but reservoir pressure is maintained above the MMP throughout most of the reservoir. Miscibility is expected to develop through a multi-contact process. A transition single-phase between the solvent and the oil is formed initially around the injector. The transition will move towards the producers as injection/production takes place, sweeping the oil on its path. By the time the solvent breaks through, most of the oil has been already produced. So the immiscibility around the producer will have a slight effect on the ultimate recovery.

The ranges of production pressure are set the same for both miscible displacement processes, but the range varies depending upon the fluid type under study. Since the CO_2- and N_2-MMP values for fluid #1 are higher than that of fluids #2 and #3, the production pressure limits when using fluid #1 are higher.

The highest injection pressures for PVT#1 undergoing nitrogen and carbon dioxide injection were set at 8000 psia. This value seems to be impractical as high pressure implies high operational cost associated to gas compression. However, a comprehensive evaluation of possible field development scenarios requires the study of different injection pressures. If the minimum injection pressure in miscible displacement projects is the MMP, the effects of pressure can be only analyzed by increasing injection BHP above the MMP. Hence, an analysis of whether the calculated MMP is practical or not should be performed. Yuan et al. (2005) reported experimental CO_2-MMP values varying from 1100 to 5000 psia for various types of oils. Similarly, Sebastian and Lawrence (1992) published experimental N_2-MMP values for different oils. They

reported values varied from 3600 to 9400 psia. Therefore, the calculated MMP for our hydrocarbon compositions can be considered reasonable. The selected injection pressure ranges allow the artificial neural networks to be fed with wide variety of scenarios, but some input combinations may not lead to a profitable process. It is up to the reservoir engineer to evaluate if these scenarios are economically feasible.

In practice, oil reservoirs are abandoned when the field is not considered to be economically feasible. The abandonment condition fixed for the miscible displacement model was set at 90% of molecular solvent fraction in the production stream. This condition is set considering that high concentration of solvent usually involves expensive separation procedures in the down stream direction of the process.

4.6.2 Waterflooding Processes

The operational pressure conditions for the models undergoing waterflooding were set the same as those used in the miscible displacement. The abandonment condition for the models undergoing water injection was set at 90% of water cut. This abandonment condition may seem too conservative since current technology may allow an efficient water/oil separation for higher water cut values. However, the waterflooding processes were built mainly for comparison purposes and most of the oil recovery is expected at early production time, before water breakthrough.

4.6.3 Steam Injection Processes

The operational production conditions in the models undergoing steam injection were set using a similar criterion as in the miscible displacement processes; production pressure below the initial reservoir pressure. However, the injection pressure ranges were selected using different criteria. The injection pressures were set above the initial reservoir pressure but at the same time they allowed the injected fluid to reach the bottom of the well with a steam quality of 1 (100% vapor). In addition, the injection pressure ranges were limited by the water critical conditions. In practice, steam is not injected above its critical pressure (3208.2 psia) due to operational cost.

The abandonment condition for the steam injection processes was set to a water-oil ratio (WOR) of 1000:1. This is the abandonment condition used by Willman et. al. (1961) in their steam models when they compared the recovery obtained by different scaled-laboratory studies undergoing water, hot water and steam injection. Even though a value of WOR of 1000 may seem high, it allows the recovery of a considerable amount of oil.

Figure **4-9** shows the WOR and recovery of a heavy oil reservoir model under steam injection. After steam breakthrough, WOR increases sharply but the oil recovery continues increasing rapidly until the steam quality observed at the producer stabilizes. Notice that little significant recovery is obtained at WOR higher than 1000.
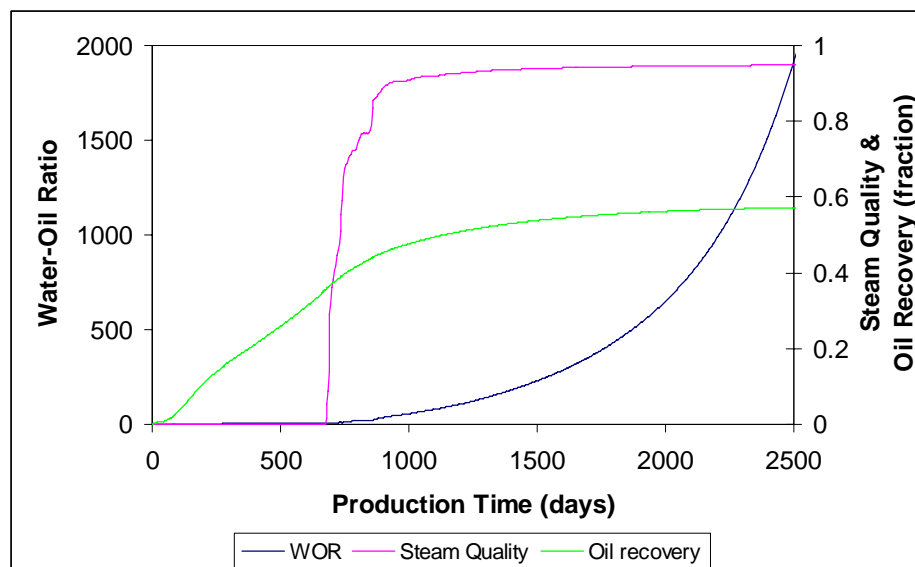
Figure **4-9**: WOR versus Time in Steam Injection IOR Process

Chapter 5

DEVELOPMENT OF THE ANN PREDICTION TOOL

Typically, screening criteria for IOR methods include no more than fluid and rock properties. More complete criteria are used to build the ANN model, where the reservoir performance and details of the field development plan are also taken into consideration. In this study, artificial neural networks are used to create two separate tools. While the first network provides comprehensive screening guidelines for oil reservoirs undergoing diverse IOR processes, a second network suggests recommended design parameters for those processes under consideration.

5.1 Networks for the Screening Tool-box

It is known that the higher the number of inputs/outputs in a network, the more the computational requirements. For convenience, the screening tool-box is structured using a series of different ANNs to reduce the complexity of the problem. Separate networks are created for each combination of problem parameters such as fluid composition, IOR process and well pattern. Note that the fluid composition implicitly brings in the effects of the hydrocarbon viscosity and specific gravity into the analysis. The screening tool-box can be considered with an architecture that contains several networks as shown Figure **5-1**. The selection of an appropriate individual expert system inside the tool-box will be done automatically by the program via a user-interface.
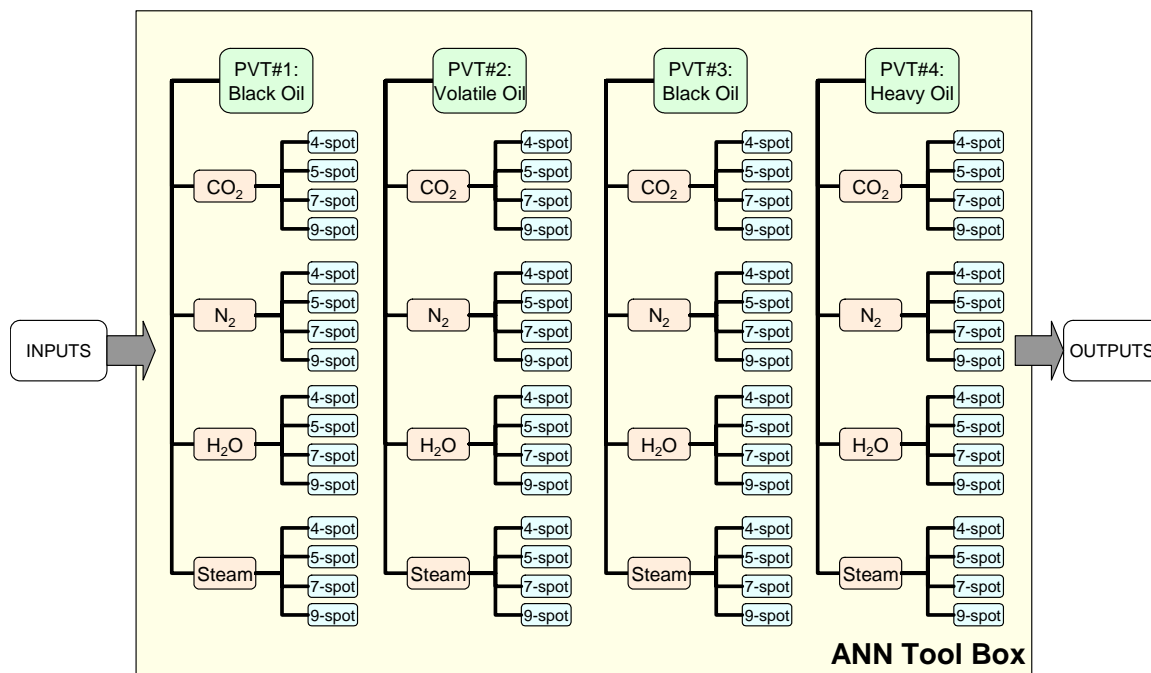
Figure **5-1**: Artificial Neural Network Tool-box Structure

As indicated earlier in Chapter 4, a diverse range of fluid properties is built into the network by using different hydrocarbon compositions. In the existing structure, each fluid undergoes four IOR methods: miscible carbon dioxide injection, nitrogen injection, waterflooding and steam injection. Furthermore, each IOR process is modeled using four well patterns. In consequence, a total of 64 individual artificial neural networks are needed to build the screening tool-box. The networks are built using Matlab®[5].

---

[5] MATLAB® is a high-performance language for technical computing developed by The MathWorks, Inc., 1994-2005.

5.1.1 Inputs and Outputs

Reservoir performance is the key factor to screen IOR methods. As a result, the output of the developed networks should provide the performance of a given reservoir under certain conditions. Since ANN is capable of finding non-linear relationships that characterize the physical phenomena between inputs and outputs, the network inputs should be the reservoir description. In this way, an effective connection between the reservoir characteristics and expected production is determined by the network.

The reservoir performance is a function of the natural reservoir characteristics such as fluid properties and rock properties. Furthermore, the reservoir performance is controlled by the design parameters, including the recovery technique, well pattern, well spacing and well operational conditions. Each network is developed for a given fluid composition/IOR method/well pattern. Then, rock properties, well spacing and operational conditions are the characteristics missing to complete the process description, which are given as inputs to the networks. The rock property inputs are permeability, porosity and thickness. Well spacing is given in the horizontal reservoir domain. The operational conditions are the production and injection pressures. These inputs are used to build the reservoir models described in Chapter 4. The corresponding network outputs are obtained from the simulation of each reservoir model.

The reservoir performance can be described by the oil production curves. Each simulation model provides cumulative oil production and oil production rate as functions of production time. One important observation is that the reservoir models produce oil for different periods of time, which provides production data within different timeframes.

Since the networks require data sets with the same length, it is not feasible to reproduce the entire curves exactly as calculated by the reservoir simulator. Instead, the reservoir performance is reproduced within fixed timeframe. The duration of a process time cannot be selected arbitrarily as it is controlled by the undergoing IOR process.

5.1.1.1 CO_2 and N_2 Miscible Displacement

Perhaps the most important event during the CO_2 and N_2 injection processes is the solvent breakthrough time (*BT*). This time is characteristic of each reservoir case and is a strong function of the recovery mechanism and the reservoir properties. On the other hand, the time to abandon the project is also characteristic of each model. As seen in Chapter 4, the abandonment time (*AT*) was set as a function of solvent molar fraction at the production stream. Therefore, the breakthrough time and abandonment time are used as outputs, as well as the corresponding oil production rate and cumulative oil production.

The *BT* is estimated from the solvent mole fraction curve. Figure **5-2** shows a typical S-shape of the CO_2 mole fraction data for a CO_2 injection process. Two straight trend lines are drawn at early time and at the sharp bend. The breakthrough time is read at the time where these two trends intersect.
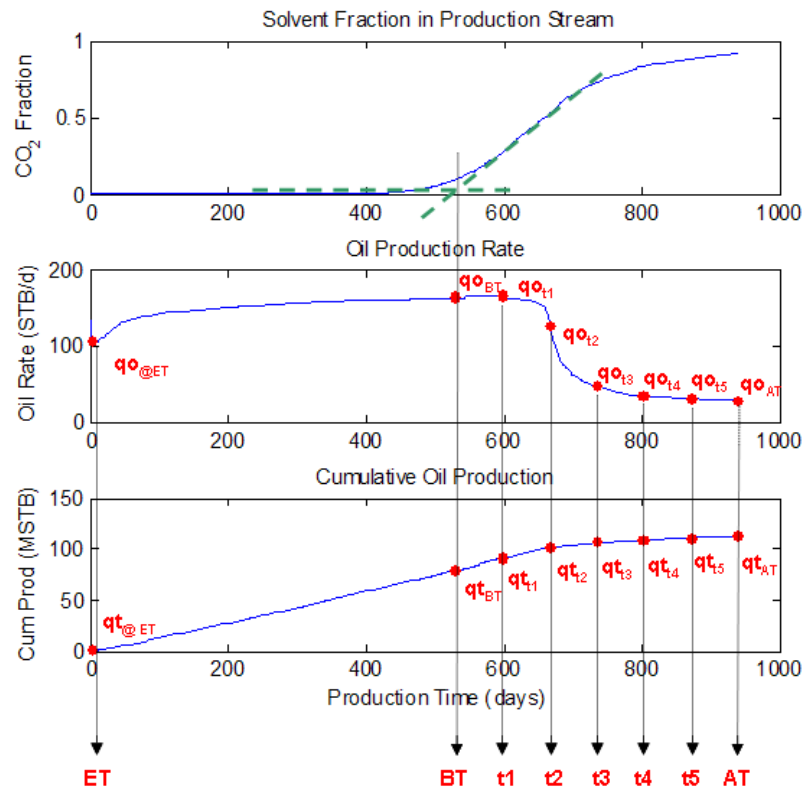
Figure **5-2**: Reservoir Performance for a Typical CO$_2$ Injection Process

Figure **5-2** also shows the oil production profiles for the same CO$_2$ injection process. The oil production rate curve exhibits the three typical stages of a hydrocarbon recovery process: ramp-up, plateau and decline. The ramp-up period is observed at the early production time when the production rate increases rapidly. The plateau slope is observed during the stable production period. The decline period is observed when the production rate decreases as production continues until the project is abandoned. It is obvious that the distinctive features of the production rate curve cannot be predicted using only *BT* and *AT*. Therefore, more pairs of time/production data should be included as outputs. Five evenly distributed times between *BT* and *AT* are also taken as network

outputs with their respective oil productions. It is noted that the recovery curves very stable before breakthrough. Then, the reservoir performance before *BT* is just represented by one point selected at early time (*ET*). Only production at that *ET* is fed to the networks since the early time is the same for all cases. Early time is fixed as 1, 2 or 5 days, depending on the network application that is modeled. In summary, the outputs of the miscible injection networks comprise 23 different variables.

5.1.1.2 Water Injection

Water breakthrough time is an important parameter in waterflooding processes since most of the oil recovery is expected to be achieved by the *BT*. The models undergoing water injection have initial water in place. Unfortunately, we cannot distinguish the in-place water from the injected water in the production stream in some models. Figure **5-3** shows the production profile and water cut for one case undergoing water injection. It can be seen that water is produced since the beginning of production. In addition, the water breakthrough time corresponding to the injected water cannot be obtained from this curve because of the lack of a defined inflection point. Therefore, *BT* was not used as an ANN output to build the oil profiles.
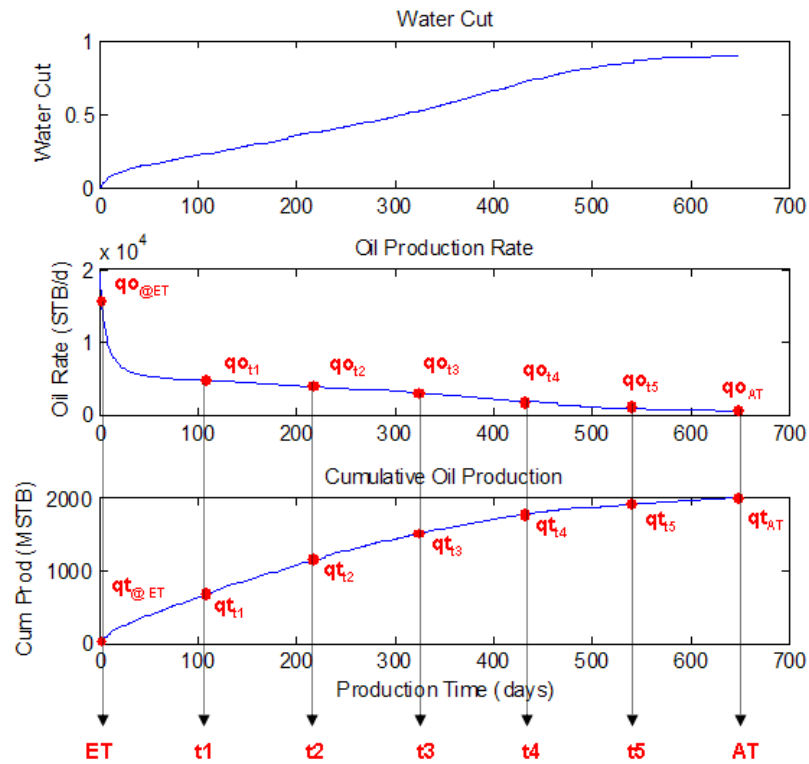
Figure **5-3**: Reservoir Performance for a Typical Waterflooding Process

Furthermore, it is noted that the oil production curve does not show the ramp-up period typically observed in miscible displacement. Instead, a sharp depletion behavior is observed due to the large drawdown experienced when the well is put on production. Production stabilizes but decreases continuously until the abandonment condition. Therefore, the oil production profile can be reproduced using five evenly separated times between 0 and *AT*. In addition, an early time production is used to reproduce the early depletion period. In summary, the outputs of the waterflooding networks comprise 20 different variables.

5.1.1.3 Steam Injection

The oil production profiles in steam injection processes present the most complex features. Willman et. al. (1961) were the first to identify these complex features. When steam is injected in a heavy oil reservoir, water and steam breakthrough (*SBT*) are observed. Therefore, the proper representation of the oil production curve requires these two times and their corresponding oil productions. Figure **5-4** shows a typical profile of steam injection into a heavy oil reservoir. A ramp-up period is easily identified where the oil production rate increases until water breakthrough is reached. After this, a plateau period is observed. The end of the plateau is identified by the steam breakthrough, which is defined by a kick. This kick also identifies the start of the decline period. We observed three additional picks during the decline period. These kicks are the result of gridding effects since they were only in existence in the models with thicknesses larger than 100 ft. The steam front moves in the actual reservoir as a continuous smooth s-shape phase. However, the numerical models with large thickness lead to four large vertical blocks. Therefore, the steam front advances through the grid model as a stair-shape phase. The three observed picks correspond to the steam front reaching the three lower blocks hosting the producer. These additional picks were ignored. For the suitable representation of the oil profile, two evenly distributed times/production values were selected between *BT* and *SBT*. In addition, an early time production and a mid value between *SBT* and *AT* were used to build the profiles. The early time was defined at the minimum oil rate before water breakthrough. In total, the networks' outputs of the steam injection into heavy oil reservoir include 21 different variables.
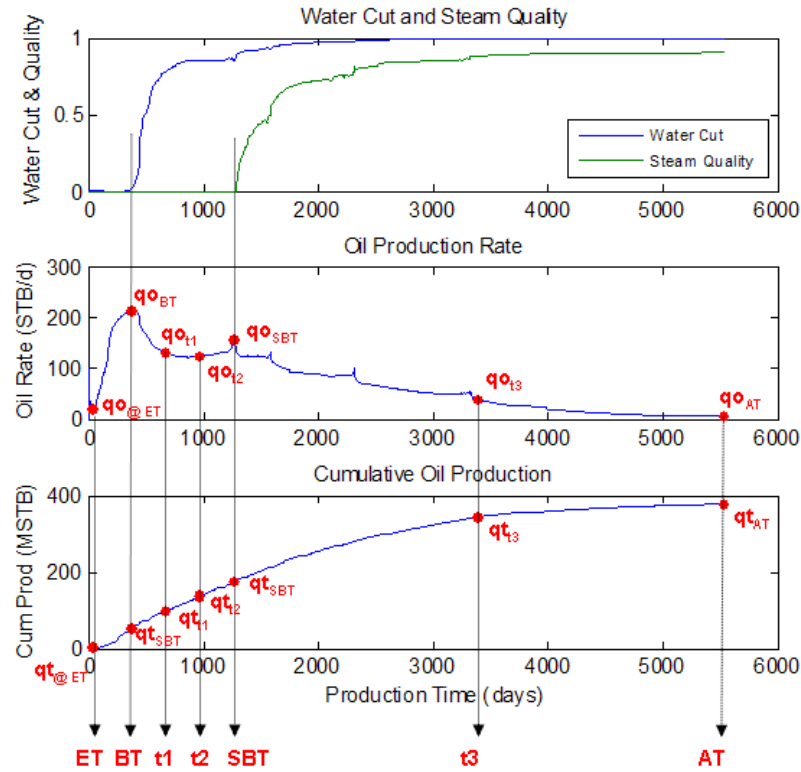
Figure **5-4**: Heavy Oil Reservoir Performance for a Typical Steam Injection Process

The oil profiles when steam was injected into a black oil reservoir were built using a different approach since they did not resemble the ones for heavy oil. The largest well pattern area used for heavy oil was 15 acres. However, it was not possible to use such a small well spacing with the black oil and volatile oil fluid systems since the abandonment condition would be reached immediately. When a large well spacing is used with steam injection, heat losses are found to be large. Therefore, the steam breakthrough cannot be observable. Even though steam is injected at the bottom of the well, the actual thermal mechanism is reduced to hot water drive. Furthermore, many of

the oil profiles obtained from the commercial simulator presented some numerical artifacts. Figure **5-5** shows the water cut and WOR for steam injection into a black oil reservoir. Steam never reaches the producer and water cut presents unexpected fluctuations after water breakthrough. Unfortunately, tuning the numerical simulator did not eliminate these fluctuations. In order to remove the noise, the abandonment condition for steam injection projects into black oil and volatile oil reservoirs was changed to a water cut value of 60%.
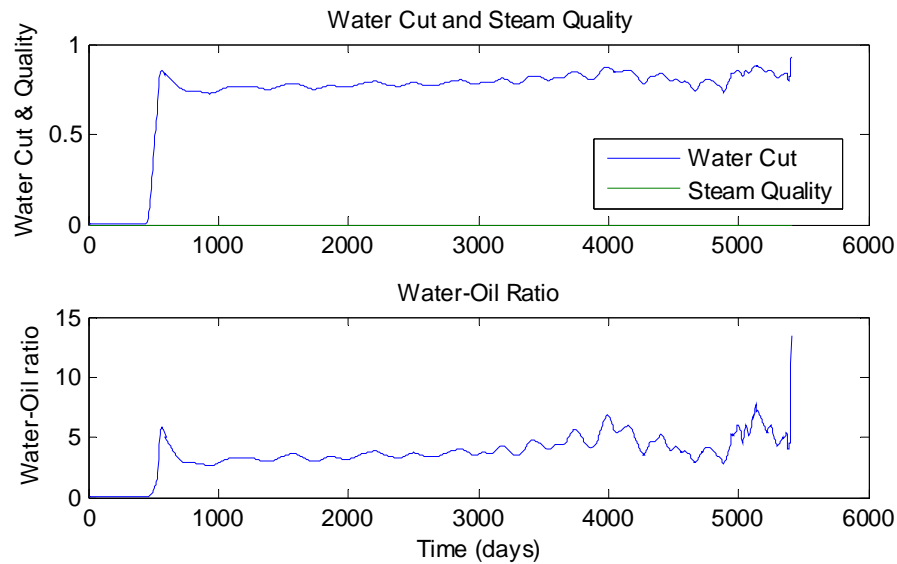
Figure **5-5**: Black Oil Reservoir Performance under Steam Injection

Figure **5-6** shows the oil profile using 60% water cut as abandonment condition. In order to build proper oil profiles three evenly distributed times between 0 and *BT* were used. A mid value between *BT* and *AT* was also used, as well as oil production at 0.1 days of production. The early depletion period was reproduced by selecting a production value

at 1/3 of time t_1. In summary, the networks' outputs of steam injection into non-heavy oil reservoirs comprise 23 different variables.
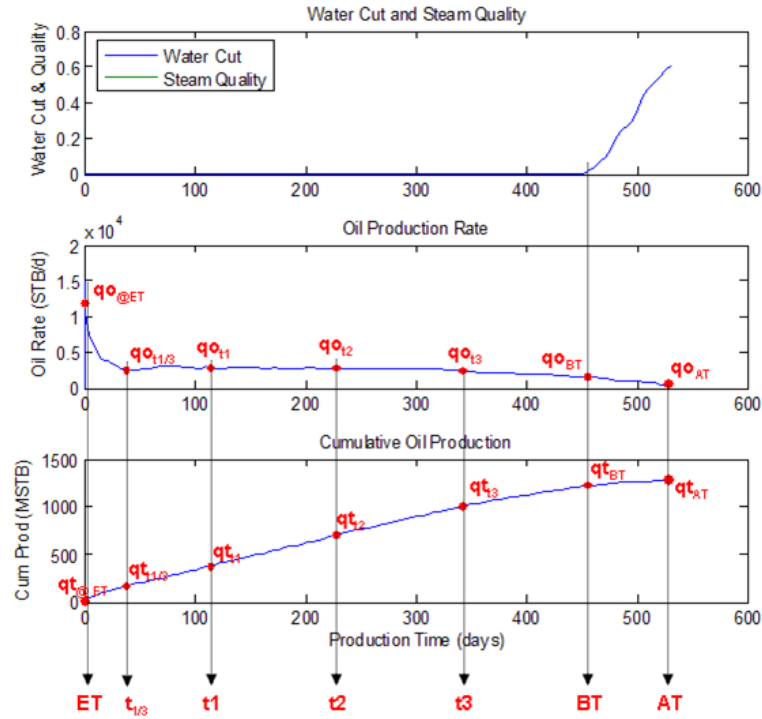
Figure **5-6**: Oil Profile for a Black Oil Reservoir under Steam Injection

5.1.2 Network for Miscible CO₂ Flooding Processes

The CO$_2$ miscible flooding network is the first network developed for the screening tool-box. The construction of this first proxy model was made in two stages in order to simplify the designing process. In the first stage, a reduced number of inputs and small data sets are used. This network architecture provides the basis to construct a more complex network in the second stage. In both stages, the networks predict the expected

oil production curves. The networks constructed in the second stage are the ones finally integrated into the tool-box.

5.1.2.1 Stage-One: Design Parameters as Inputs

A simple problem is studied in the first stage of the network design. A reservoir containing PVT#1 hydrocarbon composition is subjected to a CO_2 miscible injection process. The rock properties are maintained unchanged while the well spacing and operational conditions are modified in the reservoir models. Table **5-1** shows the reservoir properties specified in the reservoir model.

Table **5-1**: Reservoir Properties for Stage One Network

Parameter	Value
Initial Pressure	5000 psia
Initial Temperature	220°F
Initial Water Saturation	10 %
Horizontal Permeability	100 md
Vertical Permeability	10 md
Porosity	25 %
Thickness	50 ft

The ranges of input parameters used in this first stage network are given in Table **5-2**. The selection of the bottom hole pressure (*BHP*) limits are defined according to the CO_2-MMP value calculated for PVT#1 composition.

Table **5-2**: Data Ranges for ANN State One, CO_2 Injection, PVT #1

Design Parameter	Minimum	Middle	Maximum	Increment
Area (acres)	20	60	100	10
BHP Producer (psia)	3000	3500	4000	100
BHP Injector (psia)	6000	7000	8000	200

In order to train an ANN successfully, it is essential to feed the network with quality data that cover most of the possible scenarios under study. However, generation of data with these characteristics is impractical due to the computational time required. In real reservoir applications, a small number of production scenarios are evaluated. Similar approach was applied in this study but the scenarios are not selected randomly. Design of experiments is used to determine the minimum number of sensitive study cases that can cover the most characteristic possible combinations. This number of cases was calculated using a full factorial with a three-level design. With a 3-level design it is possible to capture the non-linearity effects of the inputs on the outputs as minimum, middle and maximum input values are combined. A 2-level design implies combination of minimum and maximums only. For three inputs in Stage-1 network, the 3-level full factorial design is 3^3, which means 27 sensitive cases are needed. In addition, 313 random combinations of inputs are generated, so 340 cases are simulated for each well pattern. That is, a total of 1360 simulation models for 4 patterns with fluid#1 undergoing CO_2 injection. The random cases are created using the increments specified in Table **5-2**. Input data-sets are checked to avoid repetition of cases. Since the total number of simulations is reasonably small, the models were generated using grid configurations of 40x40.

In this stage, one network is built per each well pattern. The networks forecast the expected oil production profile. Then, the specified outputs are the 23 time/production values necessary to reproduce the production curves. It is obvious that a poor network would be obtained if only three inputs are used to predict 23 targets. Therefore, five functional links are added as inputs. The functional links are the pressure gradient between the injector and the producer, the distance between injectors and producers, the distance between injectors, the geometric average of the bottom hole pressures of the producer and the injector, and the product of the area and production pressure. Bearing in mind that this problem requires 23 outputs, eight inputs may seem too few to effectively train this network. However, the outputs maintain close relationships between them, and the net should be able to capture the physical connection between production and time.

Different network architectures were tested in this stage in order to find the most appropriate architecture for the CO_2 miscible displacement process. The feedforward algorithm (*newff*) is widely used in neuro-simulation applications. Although this one provided good initial estimates, a modification of the *newff* was implemented with better results, which is the multilayer cascade feedforward back propagation (*newcf*). In the *newcf* algorithm the first hidden layer has weights coming from the input layer, and each following layer has connecting weights coming from all previous layers. The network design also included the Levenberg-Marquardt training function (*trainlm*) and the gradient descent with momentum weight and bias learning function (*learngdm*).

The complexity of this problem required two hidden layers for all four well patterns. Figure **5-7** shows the general network architecture used in the four networks. The transfer function used in the hidden layers is *tansig*, while the *purelin* transfer

function was used in the output layer. Each well pattern required different number of neurons in each layer. The number of neurons used for each well pattern is shown in Table **5-3**.

Table **5-3**: Stage One Hidden Layers for Each Well Pattern

	4-Spot	**5-Spot**	**7-Spot**	**9-Spot**
Neurons in Hidden Layer 1	40	60	50	50
Neurons in Hidden Layer 2	30	30	30	30
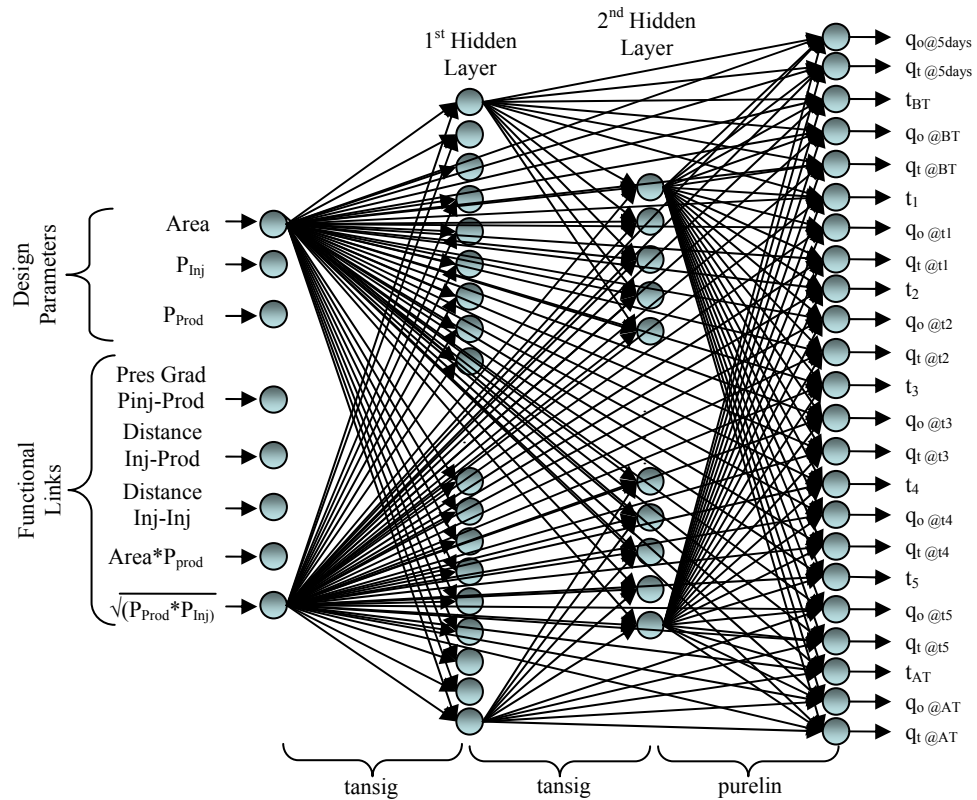
Figure **5-7**: Network Architecture for Stage-One Networks

The generated data were divided into three groups for training, validation and testing purposes. A total of 340 cases is divided in the following form: 290 cases are used for training, 50 for testing and 10 for validation. The 27 cases generated using design of experiments are included in the training set. The training and validation sets are given to the network during the training protocol. The network is trained exclusively with the training set but the LMS error is also calculated for the validation set. If the validation error is constant or increases after a certain amount of epochs, the training process is stopped to avoid overtraining. The values of weights and biases are taken when the error for the validation set was minimum. Figure **5-8** exhibits the performance of the network built of the CO_2 injection process with PVT#1 using a 4-spot well pattern. This network did not achieve the desired goal, 10^{-5} and the training process was stopped because the validation error increased in 5 consecutive epochs. The overall performance, or LMS error, was 0.00026.
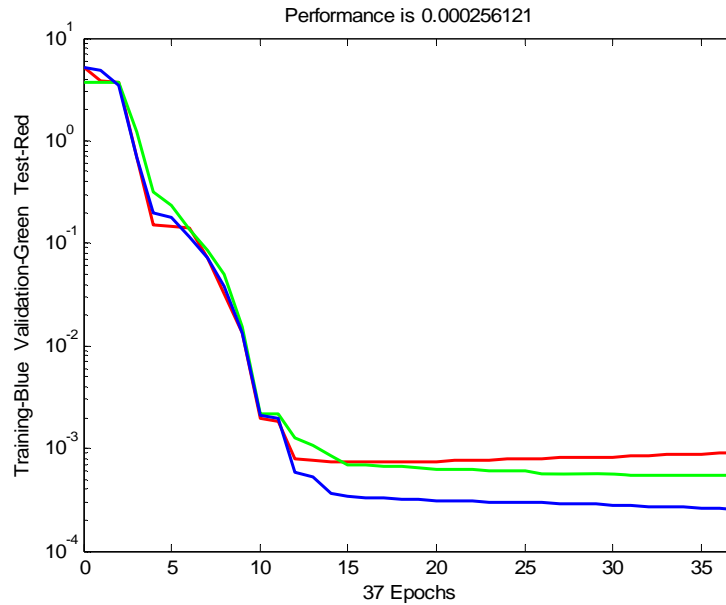
Figure **5-8**: Stage One Network Performance: CO_2 Injection – PVT#1 – 4-Spot

The performance of the network is then analyzed by comparing the desired outputs to the predicted ones. The results of the training and testing data sets are shown in Figure **5-9**, Figure **5-10** and Figure **5-11**. These figures show the times, cumulative oil production and oil production rates, respectively. The absolute error was calculated for each set of tested parameter, which is shown on the figures as well. The predicted oil production rate at breakthrough presented the minimum error (0.22%), while the oil production rate at t_1 presented the highest (4 %).
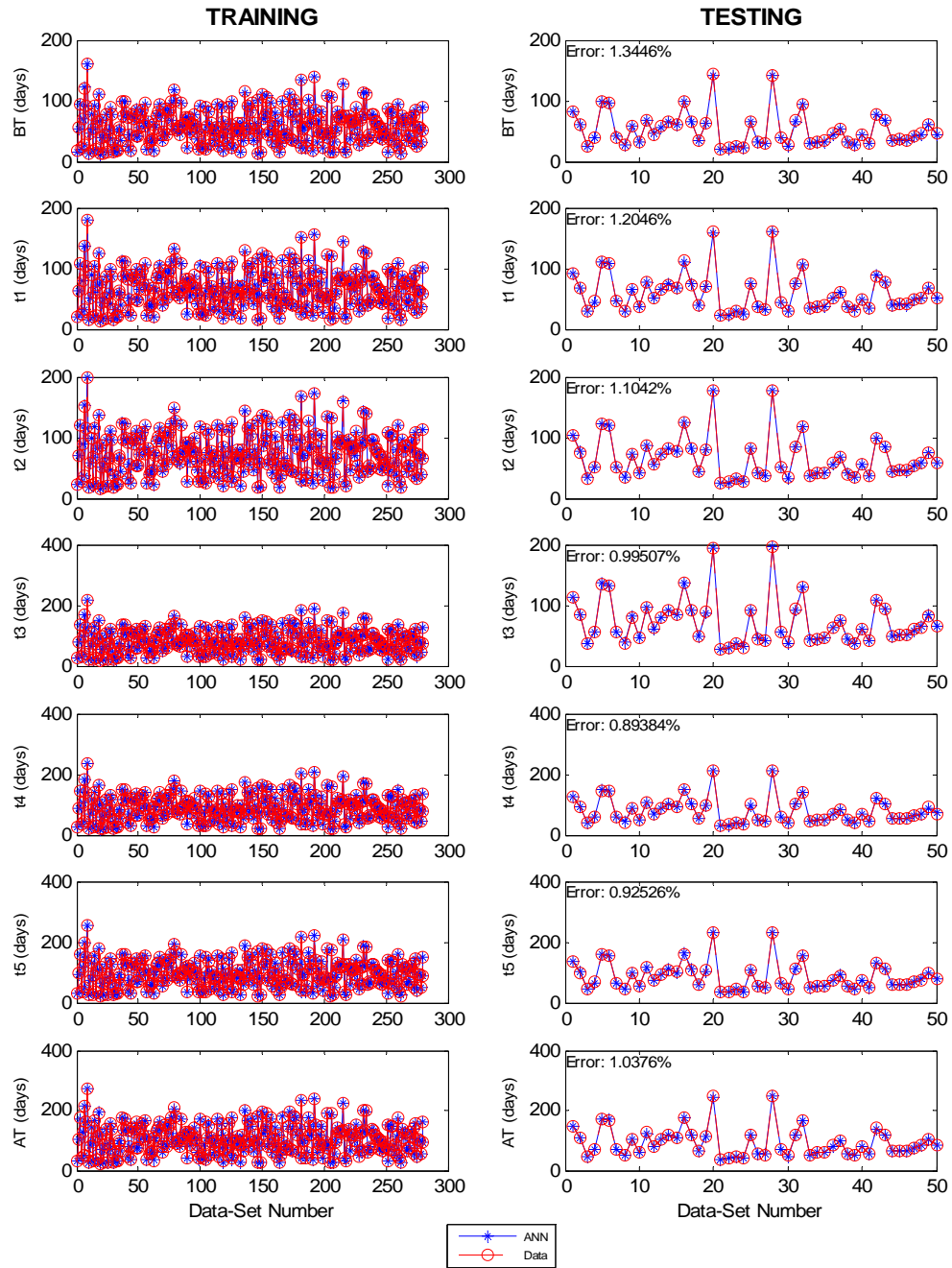
Figure **5-9**: Stage-1 Network Performance: Times (CO_2 Injection, PVT#1, 4-Spot)
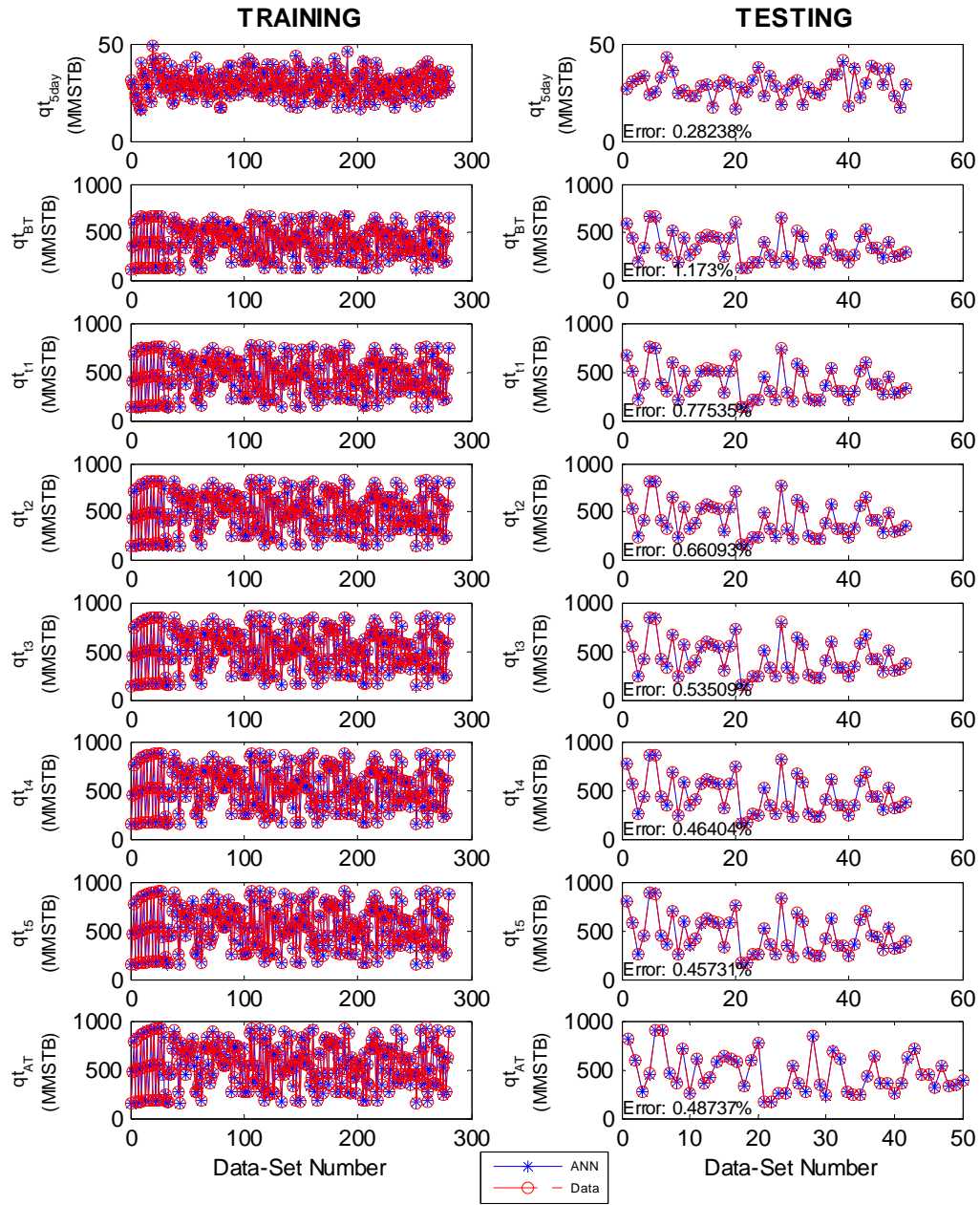
Figure **5-10**: Stage-1 Network Performance: Cumulative Oil Production (CO_2 Injection, PVT#1, 4-Spot)
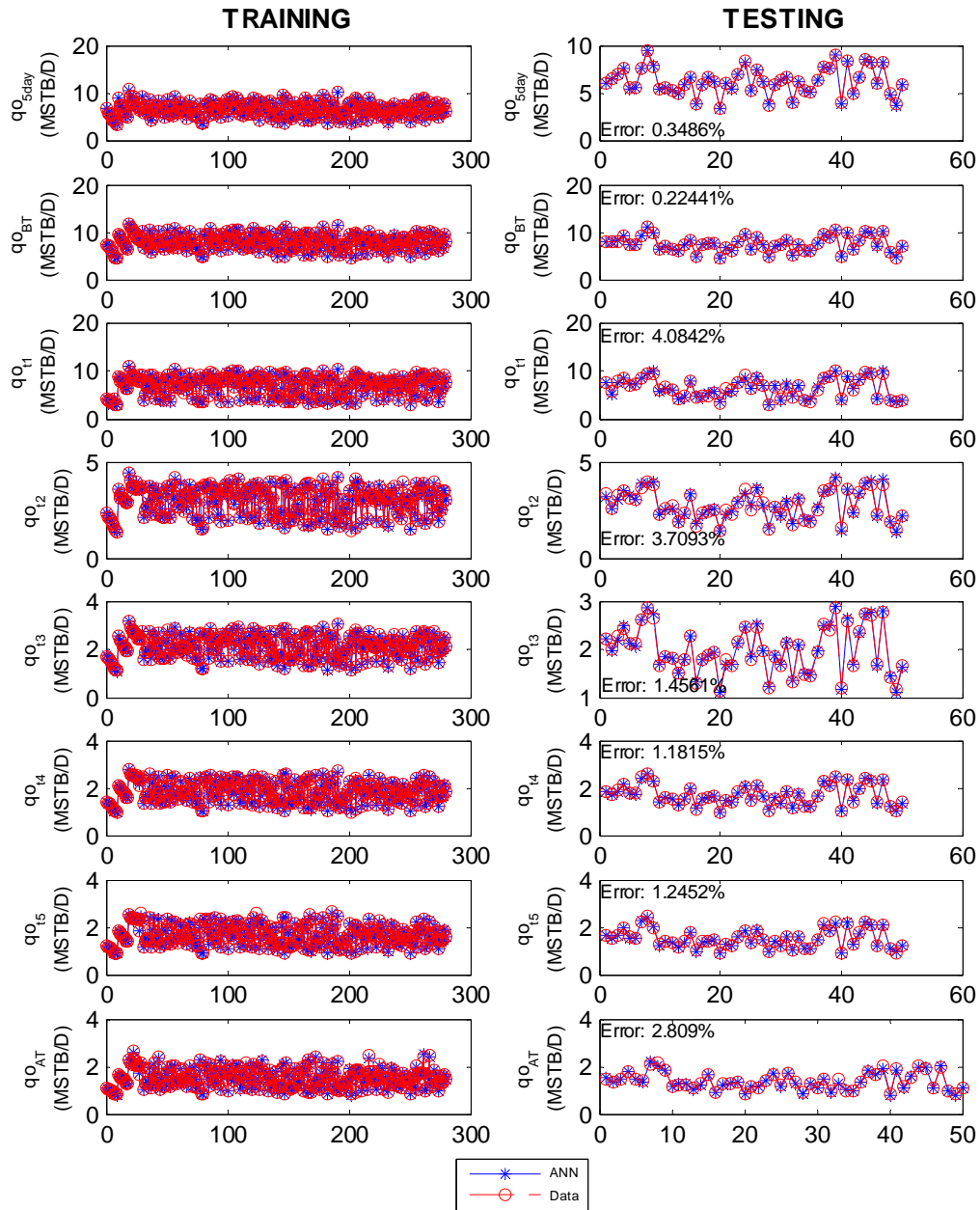
Figure **5-11**: Stage-1 Network Performance: Oil Production Rate (CO_2 Injection, PVT#1, 4-Spot)

The overall performance and the reported absolute error indicate that this network was successfully trained. However, absolute errors should not be the only set of criteria to evaluate the ANN since they sometimes lead to wrong conclusions. For example, values of permeability could vary between 2-1000 md. If the network predicts a value of 4 for the lower range limit, that represents 100% absolute error, which is interpreted as a poor network performance. On the other hand, if the network predicts a value of 950 for the highest limit, the absolute error would be 5%, which is interpreted as a good performance. However, the difference between 2 and 4 md is only 2 while the difference between 950 and 1000 md is 50, implying that the prediction of the lower limit of permeability is actually better than that of the upper limit.

Correlations between the predicted and desired outputs are also included in this analysis. For convenience, correlations are only shown for the best and the worst predicted outputs, as seen in Figure **5-12**. It is observed that the worst parameter's correlation is scattered but, in general, it shows that the network is able to predict the oil production rate at t_1 within an acceptable margin of error.

The results obtained by the network have been presented in a convenient form to assess the performance of the network so far. However, it is necessary to translate the results into a more suitable reservoir engineering approach. Each of the 23 outputs obtained from the network are used to construct the oil production profiles. The curves were constructed for all of the testing cases, but here only the best and worst curves are presented. The analysis of these two cases can implicitly reflect the overall performance of the other profiles.
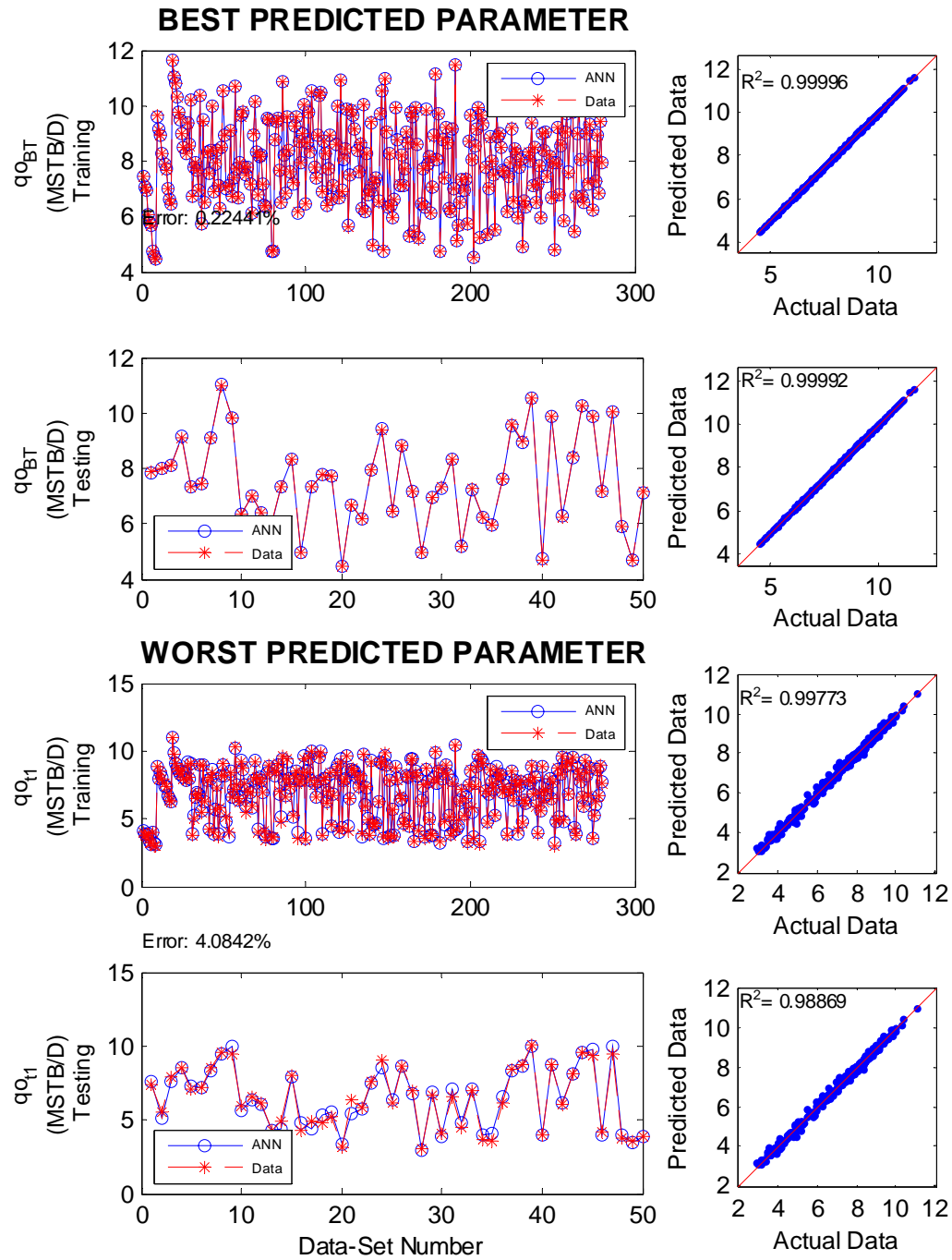
Figure **5-12**: Best and Worst Predicted Parameters, Stage-1 Network: CO₂ Injection, PVT#1, 4-Spot.

Figure **5-13** shows the best and worst fitted oil production profiles for the Stage-1 network built for CO_2 injection, PVT#1 and 4-spot well pattern. The fitting classification is based on the LMS error calculated for the 23 parameters used to construct the production curves for a given reservoir in the data set used in testing. The worst predicted curves have an LMS error of 3%, indicating that all other tested cases have errors that are even lower. Values of oil production rate at t_1 and t_2 are the ones with the highest deviation in the worst case. These two parameters describe the drastic oil rate drop as CO_2 breakthrough is achieved. This particular feature of the oil rate curve is difficult to reproduce since the data have a drastic change.
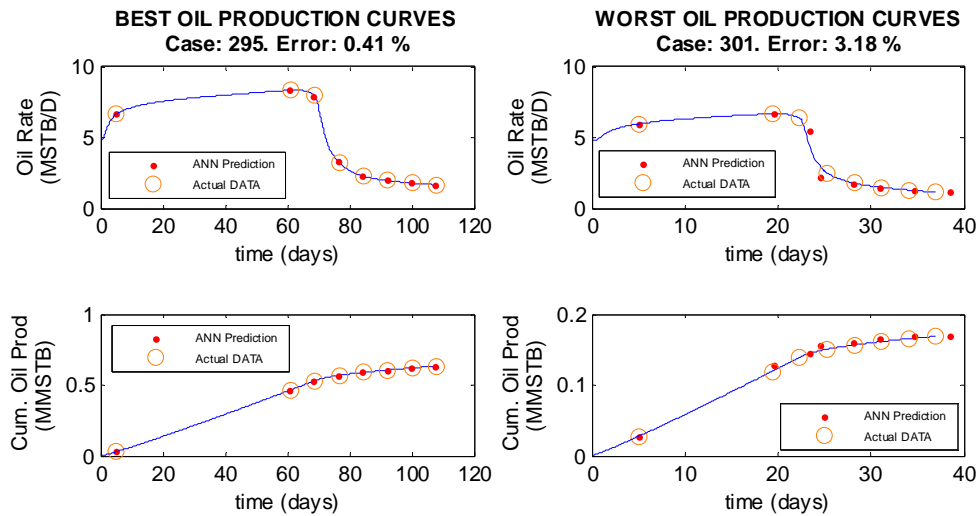
Figure **5-13**: Best and Worst Production Profiles Built using Stage-1 Network: CO_2 Injection, PVT#1, 4-Spot.

In general, similar results were obtained for the Stage-1 networks that predict the reservoir oil production using 5-spot, 7-spot and 9-spot well patterns. Table **5-4** shows

the absolute errors of each predicted parameter for all four well patterns simulated with Stage-1 networks. In general, the cumulative oil productions have the lower errors. This is because the cumulative curve is smooth. On the other hand, the oil production rates present the highest errors. This is because of the sharp changes of these curves. The general performance or LSM error of the 5-spot network is 0.0002, the 7-spot network is 0.0004 and the 9-spot is 0.012.

Table **5-4**: Absolute Errors Calculated Per Predicted Parameter from Stage-1 Networks

Parameter	Absolute Error (%)			
	4-SPOT	**5-SPOT**	**7-SPOT**	**9-SPOT**
BT	1.34	1.98	1.46	1.58
t1	1.20	1.25	1.00	1.45
t2	1.10	1.89	1.14	1.27
t3	1.00	1.70	1.02	1.58
t4	0.89	1.27	1.07	1.66
t5	0.93	1.70	0.92	1.65
AT	1.04	1.78	1.27	1.70
$qt_{@5days}$	0.28	0.37	0.23	0.24[*]
qt_{BT}	1.17	1.40	0.99	1.54
qt_{t1}	0.78	0.64	0.80	1.05
qt_{t2}	0.66	1.09	0.69	0.80
qt_{t3}	0.54	0.81	0.61	0.53
qt_{t4}	0.46	0.74	0.55	0.56
qt_{t5}	0.46	0.99	0.53	0.66
qt_{AT}	0.49	1.21	0.55	0.47
$qo_{@5days}$	0.35	0.72	0.26	0.26
qo_{BT}	0.22[*]	0.22[*]	0.20[*]	0.25
qo_{t1}	4.08[**]	1.70	3.18[**]	3.61[**]
qo_{t2}	3.71	2.88	2.89	2.32
qo_{t3}	1.46	3.05	1.51	1.97
qo_{t4}	1.18	4.76[**]	1.17	1.29
qo_{t5}	1.25	3.09	1.35	1.93
qo_{AT}	2.81	2.71	1.85	2.05

*:   Best Parameter
**: Worst Parameter

Figure **5-14**, Figure **5-15** and Figure **5-16** show the best and worst fitted oil production curves obtained with the Stage-1 networks for 5-spot, 7-spot and 9-spot well patterns. For all networks, the maximum LMS error of the curves did not exceed 4%, meaning that the networks were successfully trained. From the results obtained in this stage, it is evident that the network is able to find the relationship between the flow rates, the cumulative production and production times since all 23 outputs are accurately predicted using just 8 inputs.

Also, it is a particularly significant observation that all four well patterns produced networks with similar architectures. They only differ on the number of neurons in their hidden layers. This suggests that ANN architecture was able to effectively capture the thermodynamical and physical mechanisms of the CO_2 injection process taking place in a particular reservoir.
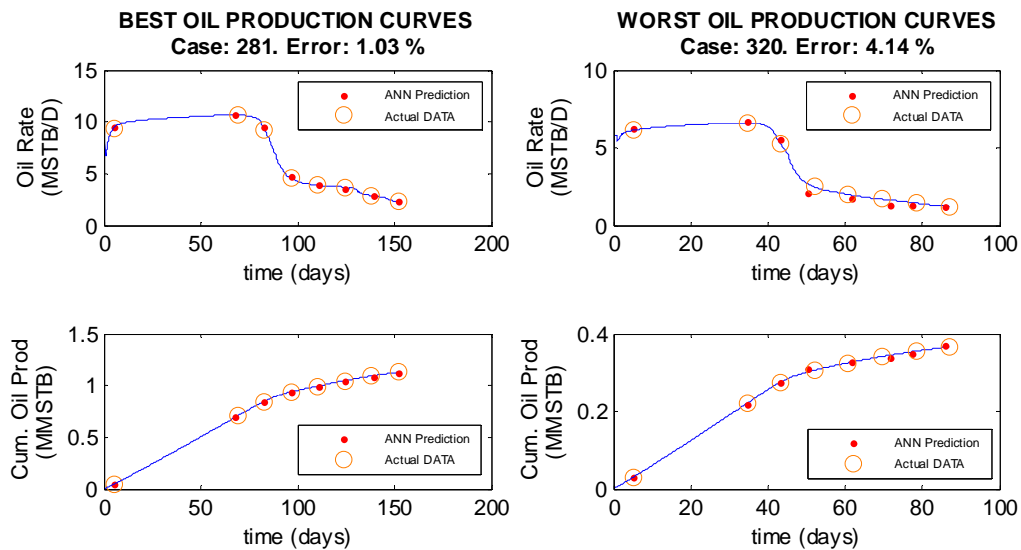
Figure **5-14**: Best and Worst Production Profiles Built using Stage-1 Network: CO_2 Injection, PVT#1, 5-Spot.
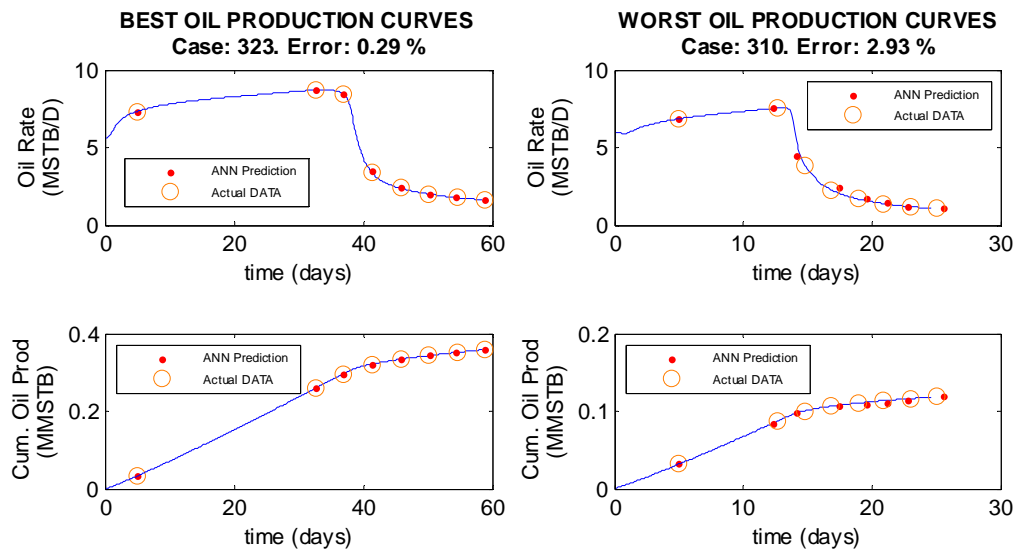
Figure **5-15**: Best and Worst Production Profiles Built using Stage-1 Network: CO$_2$ Injection, PVT#1, 7-Spot.
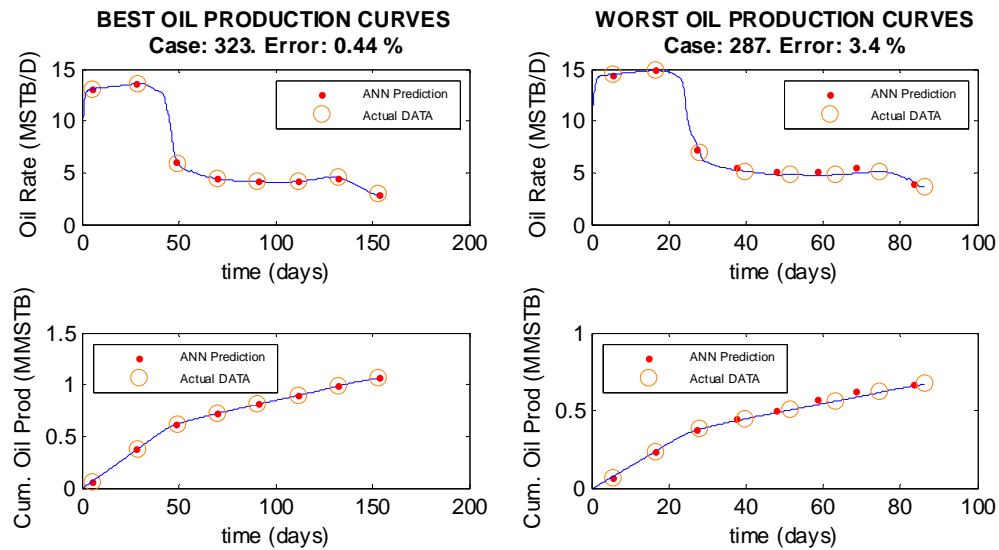
Figure **5-16**: Best and Worst Production Profiles Built using Stage-1 Network: CO$_2$ Injection, PVT#1, 9-Spot.

5.1.2.2 Stage-Two: Design Parameters and Rock Properties as Inputs

In the second stage, the complexity of the network is increased by feeding the proxy model with the reservoir rock properties such as permeability, porosity and thickness. As before, the well spacing, production pressure and injection pressure are the design parameters fed to the network. The outputs are the 23 targets used to reproduce the oil production curves. Once more, input functional links are used in order to help the learning process. This time, four functional links were introduced: pressure gradient between the injector and the producer, the distance between injectors and producers, the distance between injectors and the *kh* product. However, 9-spot networks were trained with five functional links since there are two different pressure gradients between the producer and the two injectors.

The simulation models for this stage were generated taking into account how the rock properties are found in real reservoirs. Typically, formations with low permeability also have low porosity. The proper field development for this kind of reservoirs implies a smaller well spacing. Therefore, the simulation data were generated in two groups or batches. In the first one, small reservoir areas are combined with low permeabilities and low porosities. In the second one, large areas are associated with high porosity and permeability. Table **5-5** shows the ranges of data considered in the batches.

Design of experiment with full factorial design was also used to generate a minimum number of sensitive models. Since the batches are separated by areas, 2-level design is applied to this parameter, while 3-level design is applied to the other five independent inputs. The non-linearity introduced by the areas are considered implicitly.

Between the two batches of data, four areas are provided. The 3-level full factorial design for five inputs gives 3^5=243 cases. Incorporating the 2-level design for the area, the number of minimum cases in one group is 243*2=486. Additionally, 514 random cases were also generated for each batch. That is, a 1000 different reservoir models per batch or 2000 cases per network.

The networks generated in this Stage-2 are the ones incorporated into the screening tool-box. As seen in Figure **5-1**, the tool-box consists of 64 networks. If each network requires 2000 models, it is necessary to generate 128,000 simulation cases for the entire tool-box. Considering the computational work involved in the generation of such a number of models, grid configurations of 15x15 blocks were used in this stage in order to have a controllable limit to simulation computing time.

Table **5-5**: Data Limits for ANN State 2 – CO_2 Injection Process

Input		Batch 1, Area<=100 acres			Batch 2, Area> 100 acres		
		min	mid	max	min	mid	max
Area (acres)		60	-	100	150	-	300
Kx=Ky (md)		10	50	100	200	350	500
h (ft)		10	50	200	10	100	200
Porosity (%)		15	25	40	20	30	40
PVT#1 (Pi=5000 psia)	P_{Prod} (psia)	3000	3500	4000	3000	3500	4000
	P_{Inj} (psia)	6000	7000	8000	6000	7000	8000
PVT#2 & 3 (Pi=3000 psia)	P_{Prod} (psia)	1000	1500	2000	1000	1500	2000
	P_{Inj} (psia)	4000	5000	6000	4000	5000	6000

The 2000 data sets were divided into three groups, 1600 cases were used for training, 200 for validation and 200 for testing. The 972 models created using design of experiments were included in the training data set. The network architecture used in this stage is similar to that in Stage-1. The algorithm uses a multilayer cascade feedforward back propagation network (*newcf*) with *trainlm* and *learngdm* functions. The net structure connects 10 inputs (3 design parameters, 3 rock properties and 4 functional links) with 23 outputs. The hidden layers use *tansig* transfer function while *purelin* is used in the output layer. Figure **5-17** shows the architecture of the Stage-2 networks.
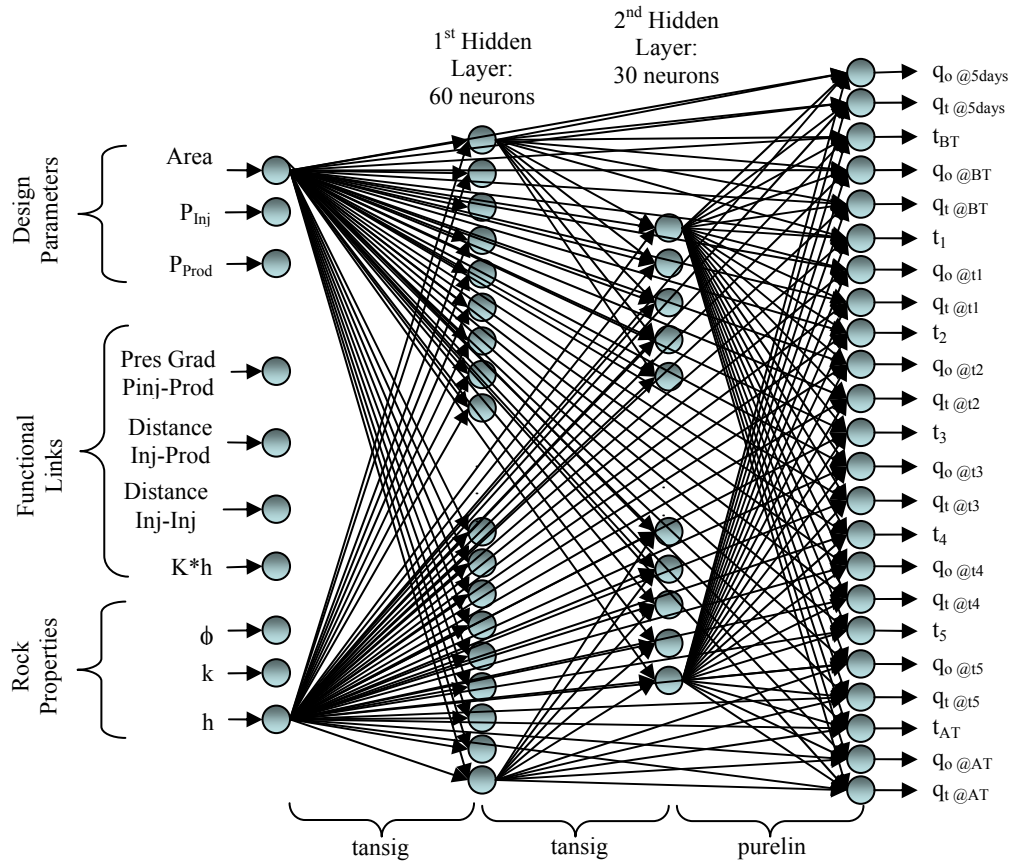
Figure **5-17**: Network Architecture for Stage-Two Networks

The first well pattern modeled in the Stage-2 network was the 4-spot. The network was efficiently trained with 60 neurons in the first hidden layer and 30 neurons in the second hidden layer. Figure **5-18** shows the best and worst parameters obtained after training. The worst parameter was the oil production rate at t_3, with an absolute error of 36%. The correlation between the predicted oil production and the actual value is a somewhat scattered. In order to assess whether the ANN was successfully trained, the oil production curves were constructed. Figure **5-19** shows the best and worst oil production profiles for the Stage-2 Network with 4-Spot, PVT#1, CO_2 injection. The worst curves presented an LMS error of 82%. Although most of the oil curves presented errors of approximately 10%, indicating that this network can be improved.

The cascade feedforward network algorithm proved to be the more adequate for the displacement process under study so far. Different combinations of number of neurons, number of layers, transfer functions and functional links were tested unsuccessfully suggesting that the problem could be attributed to the generation of the reservoir data and not the network itself.

The first 486 training values plotted shown in Figure **5-18** correspond to the first batch of data, while the following 486 are the second batch. The last 628 data sets are the models randomly created. It is noted that oil rates obtained from batch 2 have a wider range than oil rates from batch 1. It seems that the network had difficulties in correlating oil rates within different ranges. A way to work around this issue was to train two separate networks with each batch of input data. This procedure was first tested on the 4-spot well pattern.
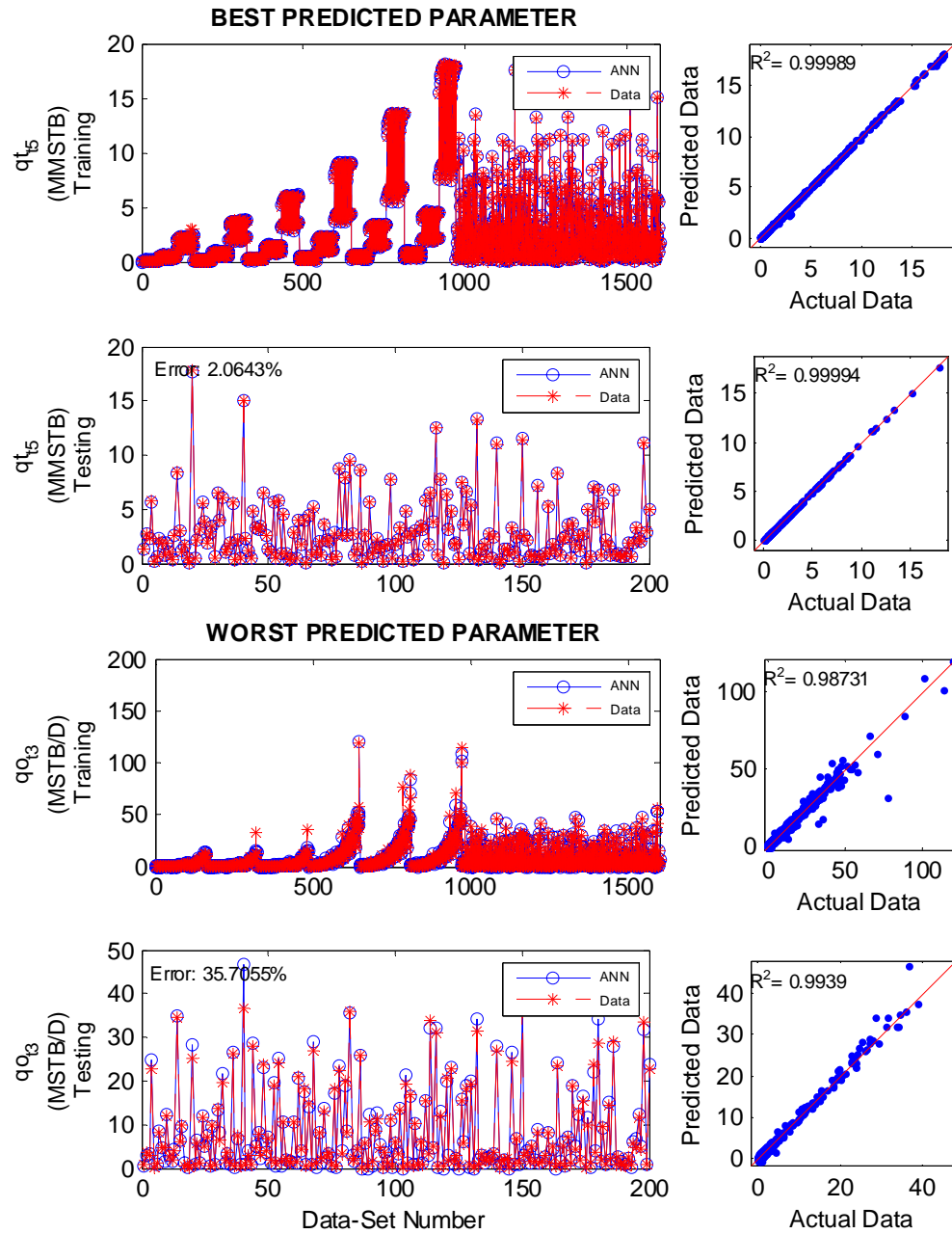
Figure **5-18**: Best and Worst Predicted Parameters, Stage-2 Network: CO_2 Injection, PVT#1, 4-Spot, Batch 1 and 2 combined.
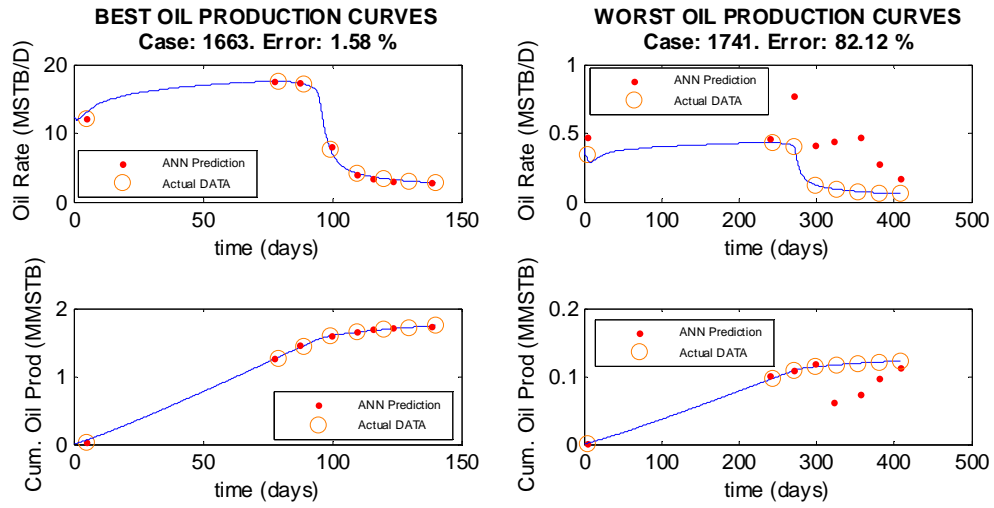
Figure **5-19**: Best and Worst Production Profiles Built using Stage-2 Network: CO_2 Injection, PVT#1, 4-Spot.

The two networks are designed with the same architecture shown in Figure **5-17**. Each data batch is divided into three groups: 800 cases for training, 100 for validation and 100 for testing. The 486 cases created using design of experiments are intentionally included in the training set. Figure **5-20** shows the best and worst parameters obtained after training a Stage-2 networks for 4-spot using CO_2 injection, PVT#1, Batch 1. The worst parameter in this case was oil production rate at t_2 with an error of 33%, which is lower than the ones in the case with both batches together. The correlation between predicted and actual values is more scattered than before. Nonetheless, it is necessary to analyze the oil production curves.
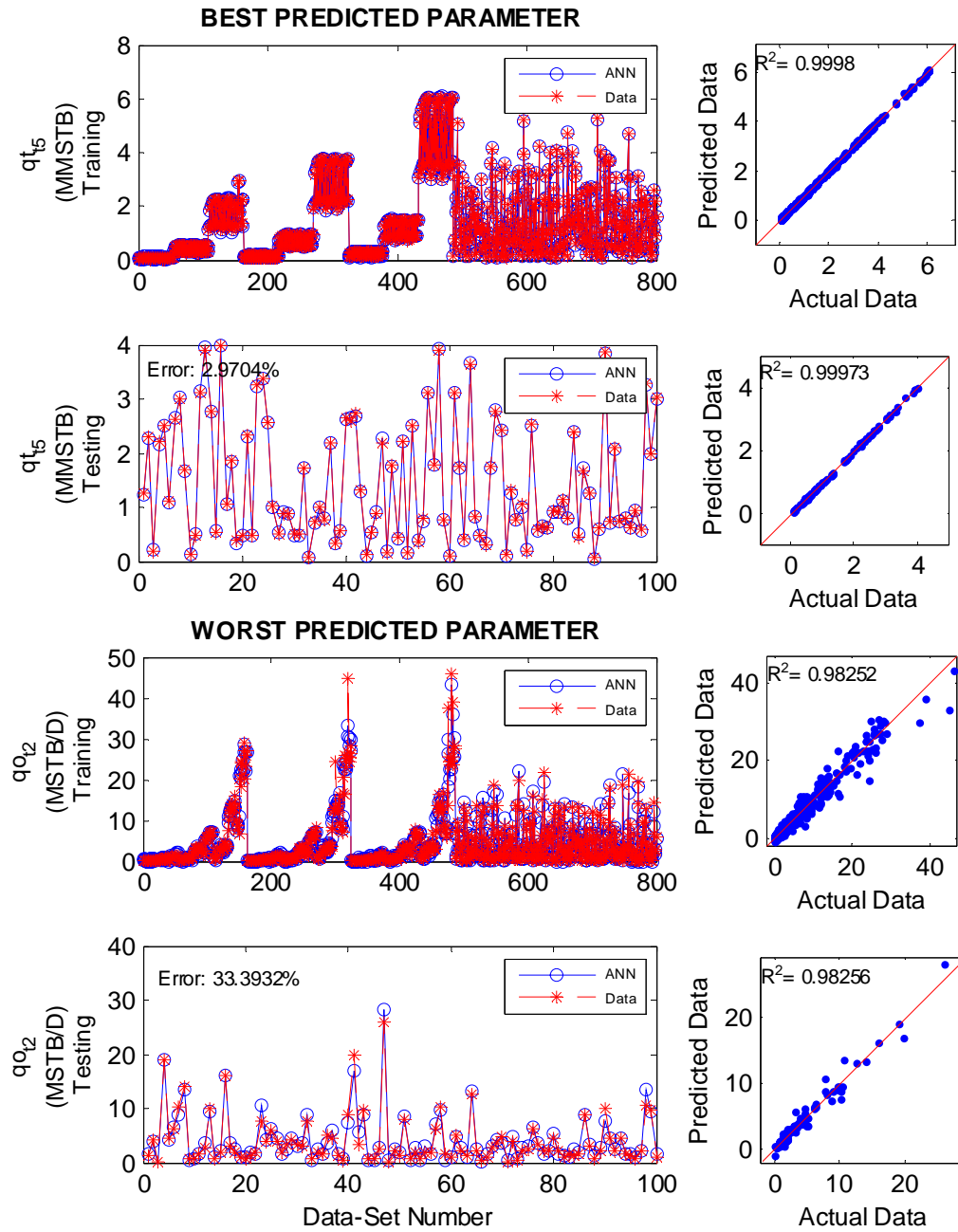
Figure **5-20**: Best and Worst Predicted Parameters, Stage-2 Network: CO$_2$ Injection, PVT#1, 4-Spot. Batch 1 (Small Areas)

Figure **5-21** shows the best and worst production curves. The highest LMS error was reduced to 36% and, in overall, the curves presented an average error of 7%. Since the efficiency of the network has been evidently improved, separate networks are constructed for each data batch. It is important to consider that each blue box shown in Figure **5-1** representing a well pattern will now contain two networks, one for the small area data sets (batch 1) and one for the large areas (batch 2). Thus, the total number of individual ANNs constituting the tool-box is doubled to 128.
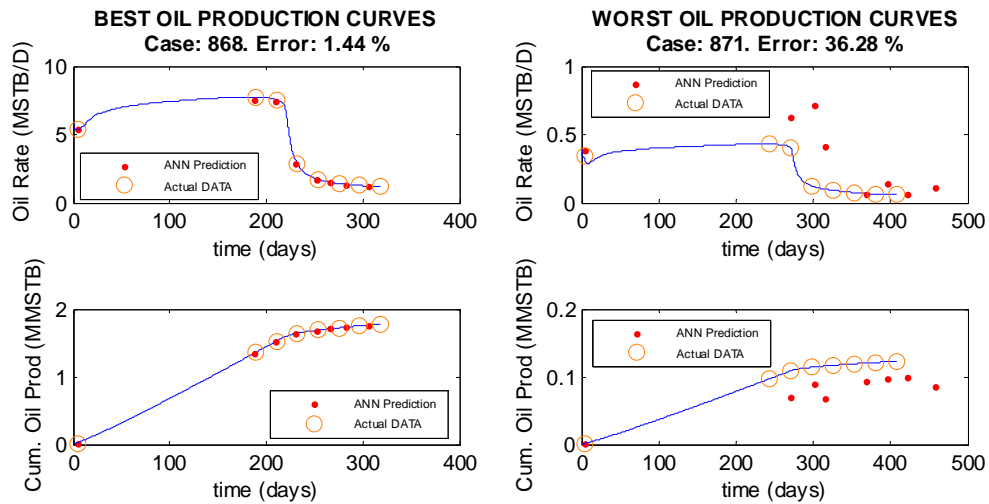
Figure **5-21**: Best and Worst Production Profiles Built using Stage-2 Network: CO_2 Injection, PVT#1, 4-Spot. Batch 1 (Small Areas)

A further modification is done to the net by applying the logarithm function to the actual outputs. As the logarithm function scales the data into a smaller range, the effects of wide output ranges should be minimized. Figure **5-22** shows the worst parameter obtained after training the same network with log-output. It is observed that the

correlation between actual and predicted log-output is less scattered, indicating a better network performance. Also, the same figure shows the correlation between outputs after the logarithm function was removed. Obviously, the data are still scattered. Figure **5-23** exhibits the best and worst parameters obtained from this network. The results are displayed after the log function is removed. The worst parameter was the oil production rate at t_2 with an error of 21%.
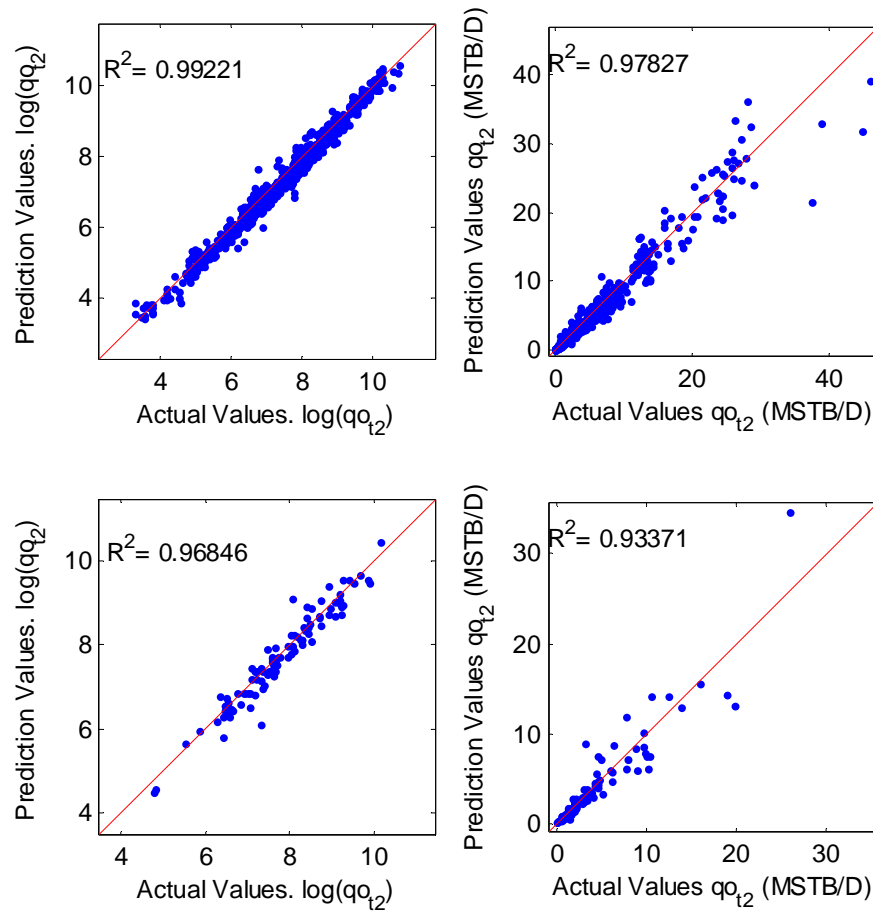
Figure **5-22**: Comparison between Log(qo_{t2}) and Actual Output (qo_{t2})
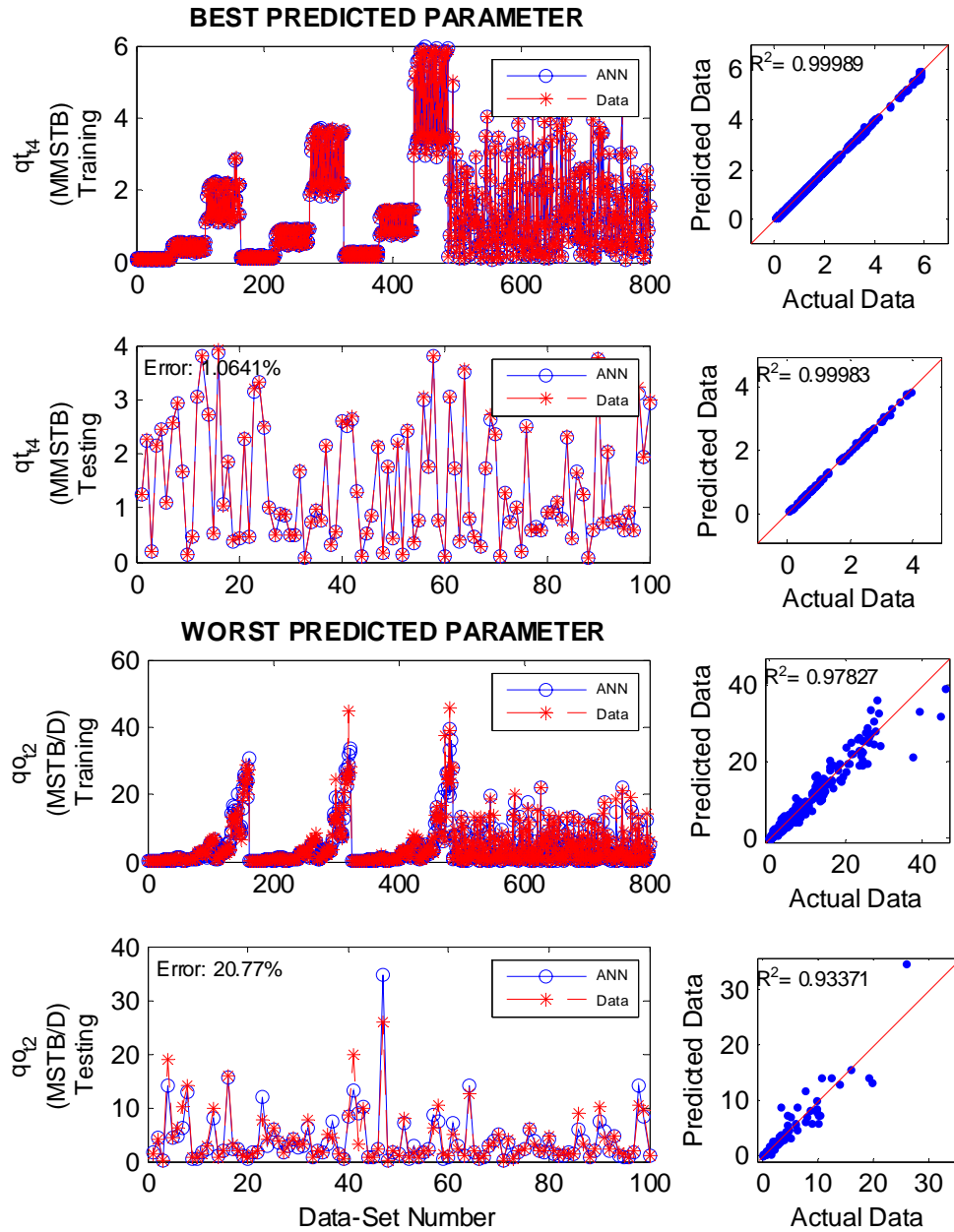
Figure **5-23**: Best and Worst Production Profiles Built using Stage-2 Network: CO_2 Injection, PVT#1, 4-Spot. Batch 1 (Small Areas). Results after Removing Functional Link log(output).
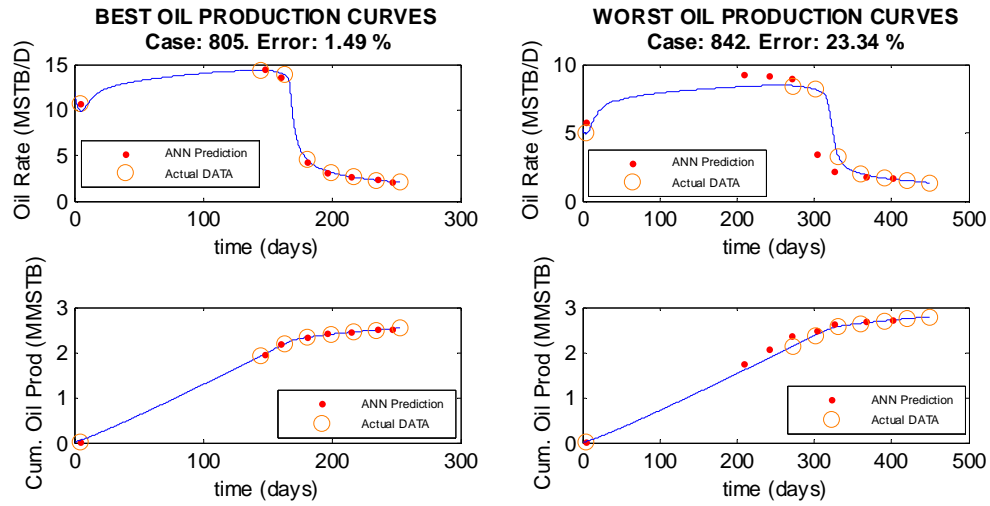
Figure **5-24**: Best and Worst Production Profiles Built using Stage-2 Network: CO_2 Injection, PVT#1, 4-Spot. Batch 1 (Small Areas), Using Logarithm in Outputs.

The best and worst predictions for oil curves by this network are presented in Figure **5-24**. The maximum error was reduced to 23%, and the average error for all curves is around 4.5%.

Since the logarithm functional link applied to the outputs successfully improved the overall network performance, we tested the network applying this functional link to both inputs and outputs. In addition, the ultimate oil recovery was also introduced as an additional output. Therefore, a new network was built with 24 outputs. Figure **5-25** shows the best and worst parameters obtained by this network.
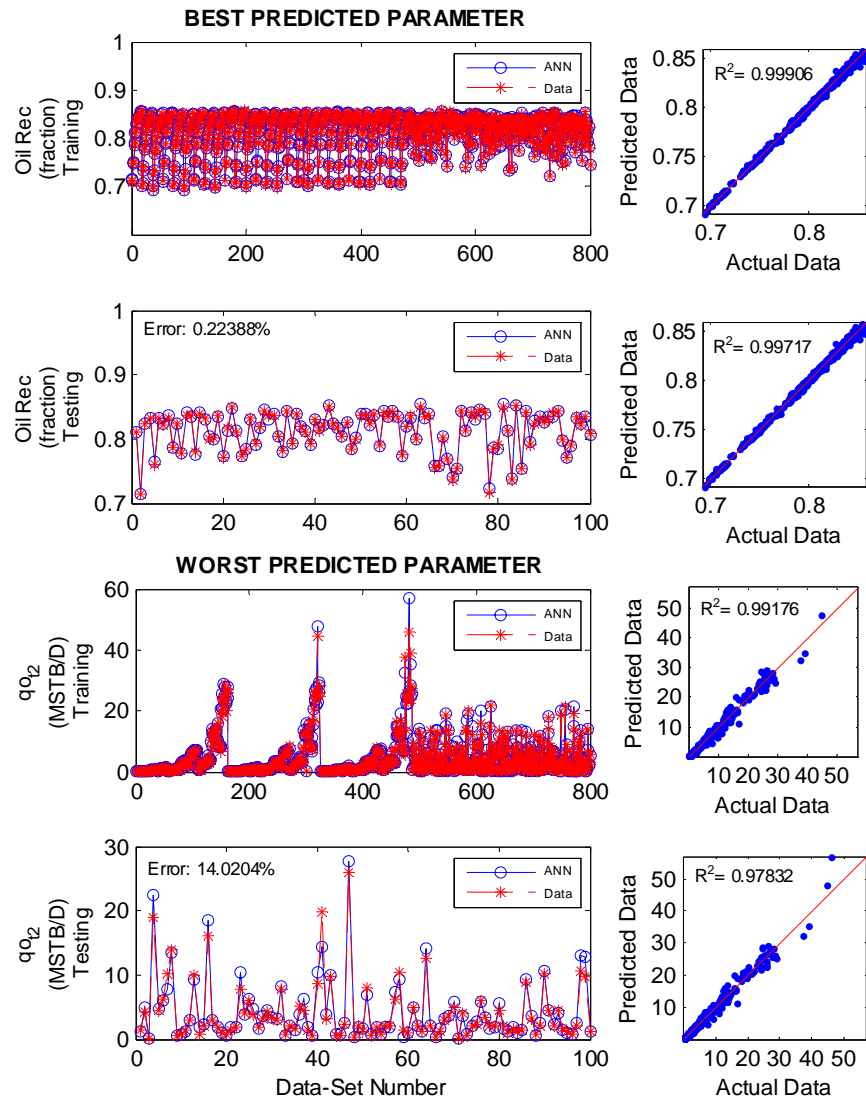
Figure **5-25**: Best and Worst Production Profiles Built using Stage-2 Network: CO_2 Injection, PVT#1, 4-Spot. Batch 1 (Small Areas). Functional Link log(input) & log(output).

The worst parameter, oil rate at t_2, presented an error of 14%, which is even lower than before. The parameter that showed the lowest error was the total oil recovery, which

was less than 1%. This was expected since oil recovery fraction is bounded between 0 and 1.

Figure **5-26** shows the best and worst oil production profiles. It is evident that the log function helped to improve the performance of the network. In all further networks developed in this study, the log function is applied to all inputs and outputs. The functional link is removed from the outputs before the oil production curves are constructed, and errors are calculated on the actual outputs, after removing the log function.
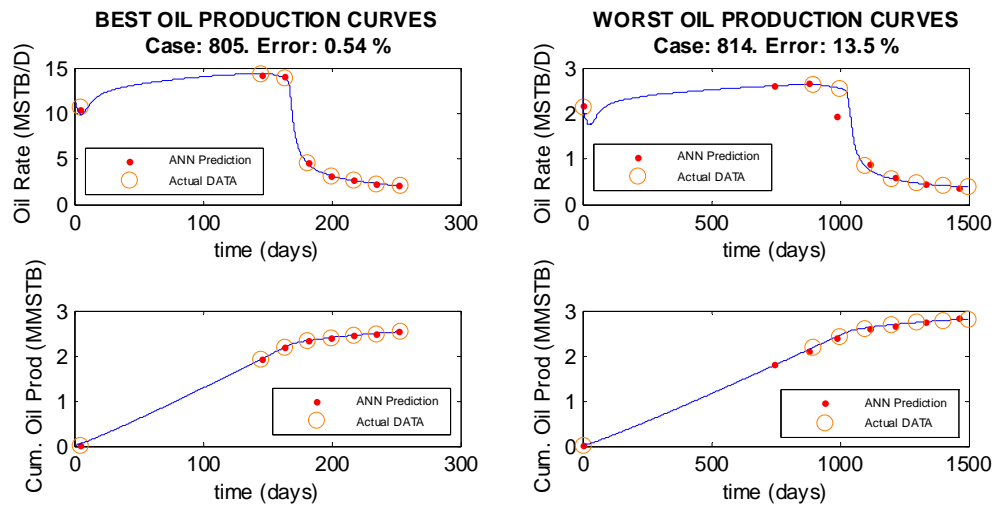
Figure **5-26**: Best and Worst Production Profiles Built using Stage-2 Network: CO_2 Injection, PVT#1, 4-Spot. Batch 1 (Small Areas), Using Logarithm in Inputs & Outputs.

Similar networks were developed for 5-spot, 7-spot and 9-spot well patterns for large and small area data sets with PVT#1 undergoing CO_2 injection, and all well patterns with PVT#2 and PVT#3. Diverse reservoir models were generated with PVT#4

undergoing CO_2 injection. However, no measurable oil production was observed in these models as the abandonment condition, 90% of CO_2 in the production stream, was achieved almost immediately after the wells are brought to operation. Therefore, it was not possible to build the networks that combine this IOR process with a heavy oil hydrocarbon composition.

Table **5-6**, Table **5-7** and Table **5-8** show the absolute errors per parameter predicted for PVT#1, PVT#2 and PVT#3 respectively. In general, the cumulative oil productions are the best predicted outputs while the oil production values are the hardest variables to forecast. Cumulative oil production and time are monotonically increasing variables, while the oil production rate is not. The sharp change in oil production rate after breakthrough generates non-linearity effects in the network.

Each of these networks was initially setup with the same architecture implemented in Stage-2, 4-Spot, PVT#1 case. In all cases, the initial response of the network was adequate. However, this was the starting point in tuning each net. Some of the modifications included the evaluation of transfer functions, number of layers, number of neurons, functional links, training protocols, etc. The modifications were first applied one by one to determine the most sensitive ones. Combinations of them were evaluated afterwards.

A preliminary evaluation of the diverse architectures was performed on a network that has only two outputs: the oil production rate at t_1 and breakthrough time. This approach reduces the training time while one of the hardest parameter to train is under observation. If a change makes a positive impact in the performance, the full network with 24 outputs would be trained with that change. However, none of the evaluated

architectures provided any major improvement. All Stage-2 networks generated so far in

the present study have the same architecture.

Table **5-6**: Absolute Error Per Predicted Parameter. Stage-2 Network, PVT#1, CO_2 Injection

Parameter	Absolute Error (%)							
	4-Spot		5-Spot		7-Spot		9-Spot	
	A≤ 100	A> 100	A≤ 100	A> 100	A≤ 100	A> 100	A≤ 100	A> 100
BT	2.98	1.78	0.88	0.78	1.93	1.84	3.62	12.51
t1	2.11	1.38	1.08	0.96	1.95	1.62	4.62	8.10
t2	1.67	0.97	1.15	1.33	2.46	1.90	6.22	7.10
t3	1.16	1.04	1.65	1.59	2.76	2.12	7.40	5.89
t4	0.92	0.94	1.80	1.79	3.18	2.51	7.62	5.07
t5	0.74	1.09	2.08	2.08	3.43	2.76	7.20	8.29
AT	0.78	1.13	2.37	2.16	3.71	2.83	7.68	7.84
$qt_{@ET}$	0.86	1.12	1.36	1.22	1.37	1.79	5.21	6.34
qt_{BT}	3.25	1.83	0.71	0.82	2.33	2.04	4.46	4.18
qt_{t1}	2.44	1.35	0.82	1.02	2.33	1.84	5.02	4.50
qt_{t2}	1.40	1.00	1.13	0.98	1.69	1.48	3.35	6.75
qt_{t3}	0.52	0.75	0.79	0.87	1.04	0.99	3.04	5.90
qt_{t4}	0.43	0.67	0.84	0.67	0.96	0.99	2.08	2.87[*]
qt_{t5}	0.39	1.00	0.80	0.71	1.04	0.93	2.43	5.63
qt_{AT}	0.38	0.52	0.86	0.74	1.13	1.01	1.56[*]	3.88
$qo_{@ET}$	1.06	1.60	1.55	1.36	1.72	2.28	5.10	9.13
qo_{BT}	0.49	0.63	0.80	0.80	0.61[*]	0.71[*]	3.00	7.21
qo_{t1}	1.67	1.44	1.40	1.47	1.92	1.16	7.83	6.80
qo_{t2}	14.02[**]	8.34[**]	6.03	5.98	12.12[**]	13.02[**]	17.98[**]	14.61
qo_{t3}	6.34	6.19	6.78	7.44[**]	8.19	7.52	15.78	19.92[**]
qo_{t4}	3.73	3.88	7.01[**]	6.20	5.46	5.55	14.77	13.41
qo_{t5}	2.19	3.07	5.20	6.17	4.51	4.95	11.63	12.52
qo_{AT}	2.27	3.51	5.04	5.49	4.72	5.48	9.63	13.28
Oil Rec.	0.22[*]	0.26[*]	0.48[*]	0.59[*]	0.91	0.75	12.43	15.43

*: Best Parameter
**: Worst Parameter

Table **5-7**: Absolute Error Per Predicted Parameter. Stage-2 Network, PVT#2, CO_2 Injection

Parameter	Absolute Error (%)							
	4-Spot		5-Spot		7-Spot		9-Spot	
	A≤ 100	A> 100	A≤ 100	A> 100	A≤ 100	A> 100	A≤ 100	A> 100
BT	1.42	2.52	2.04	1.61	2.57	4.44	1.38	1.53
t1	1.14	1.87	1.78	2.06	1.92	2.70	0.86	0.76
t2	0.95	1.68	2.76	1.74	1.79	2.46	0.84	0.79
t3	1.01	1.90	1.62	1.88	2.17	2.85	0.88	1.03
t4	1.14	2.13	1.49	2.11	2.47	3.15	0.93	0.92
t5	1.10	2.10	2.30	2.31	2.26	3.46	1.00	0.90
AT	1.17	2.32	1.44	2.10	2.30	3.83	0.95	1.16
$qt_{@ET}$	1.75	2.39	3.43	2.05	2.17	1.86	0.68	1.27
qt_{BT}	1.40	2.50	1.60	2.38	3.15	4.83	1.45	1.51
qt_{t1}	0.83	1.69	1.29	1.40	1.41	2.79	0.95	0.82
qt_{t2}	0.64	1.84	1.65	1.74	1.62	1.91	0.64	0.64
qt_{t3}	0.66	1.31	1.49	1.34	1.28	1.91	0.57	0.69
qt_{t4}	0.48	1.33	1.14	1.39	1.05	1.34	0.46	0.62
qt_{t5}	0.47	1.21	1.77	2.79	0.93	1.12	0.44	0.53
qt_{AT}	0.39	0.78	0.83	1.22	1.03	1.13	0.37	0.39
$qo_{@ET}$	2.69	2.17	3.72	1.77	2.50	1.65	1.27	1.30
qo_{BT}	1.23	1.62	2.07	1.55	1.95	1.54	0.72	0.25
qo_{t1}	1.75	1.95	2.61	1.86	2.02	2.02	1.62	1.10
qo_{t2}	4.74	4.31	3.16	2.79	4.32	3.62	2.57[**]	3.71[**]
qo_{t3}	2.72	4.99	3.52	4.62	4.53	6.52	2.18	2.90
qo_{t4}	3.56	6.68	3.77	5.24	6.12	10.41	1.98	2.13
qo_{t5}	5.14[**]	9.22	4.31	6.67	9.37	14.32	1.61	1.65
qo_{AT}	4.87	10.58[**]	4.37[**]	7.95[**]	10.45[**]	17.80[**]	0.65	1.21
Oil Rec.	0.15[*]	0.32[*]	0.24[*]	0.41[*]	0.30[*]	0.37[*]	0.06[*]	0.06[*]

*: Best Parameter
**: Worst Parameter

Table **5-8**: Absolute Error Per Predicted Parameter. Stage-2 Network, PVT#3, CO_2 Injection

Parameter	Absolute Error (%)							
	4-Spot		5-Spot		7-Spot		9-Spot	
	A≤ 100	A> 100	A≤ 100	A> 100	A≤ 100	A> 100	A≤ 100	A> 100
BT	0.81	0.53	0.34	0.72	0.90	0.76	0.73	0.73
t1	0.46	0.55	0.33	0.42	0.65	0.76	0.71	0.73
t2	0.50	0.72	0.29	0.39	0.71	0.71	0.82	0.60
t3	0.66	0.88	0.27	0.61	0.84	0.74	0.97	0.64
t4	0.39	0.43	0.23	0.57	0.72	0.60	1.00	0.66
t5	0.43	0.55	0.35	0.42	0.75	0.51	0.94	0.73
AT	0.43	0.50	0.32	0.59	0.64	0.56	1.04	0.65
$qt_{@ET}$	0.91	0.95	0.65	0.86	1.96	1.25	2.12	0.74
qt_{BT}	0.57	0.65	0.39	0.65	1.07	1.04	0.71	0.77
qt_{t1}	0.50	0.75	0.35	0.58	0.82	1.08	0.86	0.86
qt_{t2}	0.32	0.84	0.28	0.59	0.91	0.84	0.77	0.67
qt_{t3}	0.39	0.48	0.24	0.60	0.77	0.77	0.63	0.61
qt_{t4}	0.49	0.77	0.28	0.53	0.63	1.00	0.63	0.61
qt_{t5}	0.35	0.42	0.27	0.49	0.72	0.93	0.51	0.46
qt_{AT}	0.61	0.32	0.19	0.43	0.74	0.63	0.35	0.30
$qo_{@ET}$	1.28	0.95	0.74	1.80	2.49	1.01	2.37	0.90
qo_{BT}	0.47	0.63	0.34	0.26	0.98	0.66	0.41	0.40
qo_{t1}	0.48	1.05	0.32	0.24	0.72	0.71	0.31	0.28
qo_{t2}	0.65	0.79	0.30	0.75	0.81	0.93	0.88	0.58
qo_{t3}	0.85	0.86	0.58	0.86	1.16	1.00	1.38	0.76
qo_{t4}	1.35	2.23	1.20	1.31	1.74	2.30	1.78	1.00
qo_{t5}	2.05[**]	2.66[**]	1.49[**]	2.04[**]	2.79[**]	3.12	3.41	2.11
qo_{AT}	1.81	2.33	1.06	1.48	1.94	3.27[**]	5.62[**]	3.47[**]
Oil Rec.	0.05[*]	0.07[*]	0.05[*]	0.08[*]	0.07[*]	0.16[*]	0.10[*]	0.15[*]

*:   Best Parameter
**: Worst Parameter

An important observation is that the same architecture was able to reproduce the behavior of the reservoirs holding different hydrocarbon compositions. This implies that the network is able to effectively describe the displacement mechanism under different miscibility conditions. Oil production curves were generated using the Stage-2 networks. Some characteristic examples are included in Appendix C.

5.1.3 Network for Miscible N_2 Flooding Processes

Miscible nitrogen displacement is also simulated in this study. The models were generated following the same procedure as in miscible carbon dioxide displacement. A set of networks were designed for a given combination of specific fluid/well pattern/area range. However, the networks were built in one stage. Provided that the physics involved in a CO_2 displacement mechanism are similar to that in a N_2 process, no major changes in the network architecture were expected.

The inputs and outputs for N_2 injection are similar to the ones used in for CO_2 injection. The reservoir description and field development associated parameters are fed to the network. These inputs are extended by implementing functional links. The networks predict the reservoir behavior, and oil production curves are constructed from the predicted targets. In general, the reservoir models simulating nitrogen displacement are built using the same properties used in CO_2 injection, but the pressure injection range is different for PVT#1 hydrocarbon composition due to higher N_2-MMP value. Table **5-9** shows the data limits used in the reservoir models undergoing nitrogen injection.

Table **5-9**: Data Limits for ANN – N$_2$ Injection Process

Input		Batch 1, Area<=100 acres			Batch 2, Area> 100 acres		
		min	mid	max	min	mid	Max
Area (acres)		60	-	100	150	-	300
Kx=Ky (md)		10	50	100	200	350	500
h (ft)		10	50	200	10	100	200
Porosity (%)		15	25	40	20	30	40
PVT#1 (Pi=5000 psia)	P$_{Prod}$ (psia)	3000	3500	4000	3000	3500	4000
	P$_{Inj}$ (psia)	7000	7500	8000	7000	7500	8000
PVT#2 & 3 (Pi=3000 psia)	P$_{Prod}$ (psia)	1000	1500	2000	1000	1500	2000
	P$_{Inj}$ (psia)	4000	5000	6000	4000	5000	6000

A total of 1000 reservoir simulation cases were generated for each area data batch. As before, the design of experiment protocol was applied to generate 486 characteristic cases and the rest were generated randomly. The design of each network started with the same architecture as used for CO_2 displacement. Although some combinations of functions, neurons and layers were evaluated, the CO_2 network architecture prevailed as the best approach to our problem.

The cumulative oil production parameters are the best fitted outputs of the proxy model. They have the lowest error while the oil production rates have the highest. The behavior of the oil reservoir undergoing N_2 injection is very similar as in CO_2 injection. Figure **5-27** shows the oil production profiles for 4-Spot, PVT#1, small areas (batch1). It is clear that a reservoir undergoing CO_2 or N_2 injection behaves in a similar fashion. The cumulative oil production is smooth while the oil rate severely changes as nitrogen reaches the injector. This explains why the same network architecture developed for CO_2

applications was easily applied to N_2 injection. Oil production curves developed for other well patterns and fluid types are included in Appendix C.
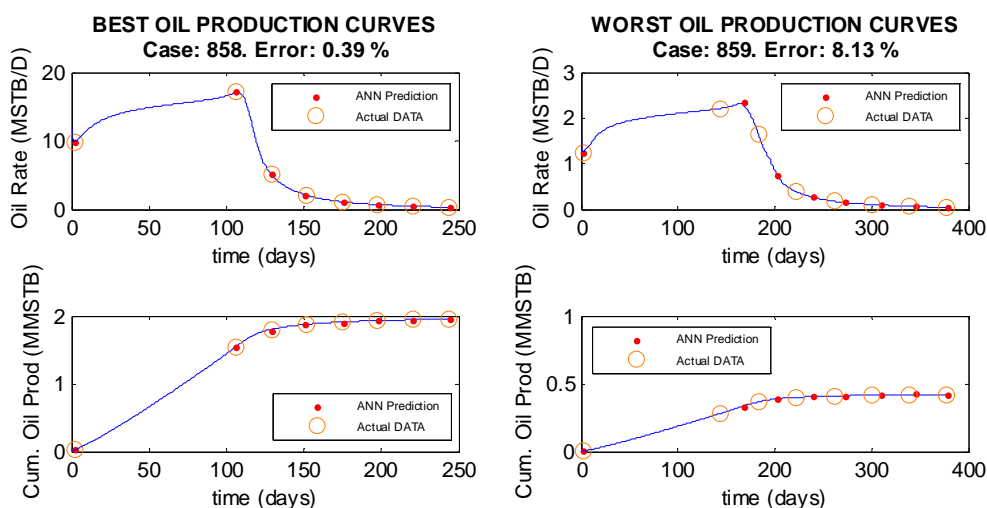
Figure **5-27**: Best and Worst Production Profiles Built using Stage-2 Network: N_2 Injection, PVT#1, 4-Spot. Batch 1 (Small Areas)

Table **5-10**, Table **5-11** and Table **5-12** summarize the performance of the trained networks for the PVT#1, PVT#2 and PVT#3 under nitrogen injection. No significant oil production was observed in the reservoir models holding a heavy oil hydrocarbon composition undergoing nitrogen injection as the abandonment condition was achieved almost immediately after the wells became operational. Then, networks that combine nitrogen injection with PVT#4 were not built.

Table **5-10**: Absolute Error Per Predicted Parameter. Stage-2 Network, PVT#1, N_2 Injection

Parameter	Absolute Error (%)							
	4-Spot		5-Spot		7-Spot		9-Spot	
	A≤ 100	A> 100	A≤ 100	A> 100	A≤ 100	A> 100	A≤ 100	A> 100
BT	2.03	2.02	0.55	0.82	1.17	1.35	0.49	0.66
t1	1.37	1.36	0.45	0.85	0.98	1.37	0.47	0.92
t2	1.01	1.14	0.61	1.08	1.08	1.78	0.59	0.97
t3	0.91	1.15	0.68	1.21	1.20	2.37	0.63	1.11
t4	0.89	1.24	0.77	1.26	1.26	2.68	0.68	1.17
t5	0.85	1.37	0.83	1.43	1.51	2.81	0.80	1.28
AT	0.81	1.47	0.86	1.45	1.54	3.04	0.78	1.27
$qt_{@ET}$	0.79	0.63	0.62	0.49	0.74	1.51	0.50	0.51
qt_{BT}	2.38	2.58	0.59	1.01	1.35	1.74	0.53	0.72
qt_{t1}	1.05	1.40	0.47	0.81	0.75	1.31	0.24	0.49
qt_{t2}	0.56	1.01	0.39	0.66	0.60	0.95	0.29	0.72
qt_{t3}	0.52	0.84	0.34	0.66	0.50	0.81	0.41	0.66
qt_{t4}	0.44	0.69	0.30	0.57	0.56	1.10	0.29	0.46
qt_{t5}	0.49	0.75	0.31	0.57	0.43	1.48	0.22	0.56
qt_{AT}	0.41	0.69	0.27	0.53	0.43	0.97	0.20	0.29
$qo_{@ET}$	0.79	0.56	0.69	0.47	0.84	1.80	0.72	0.56
qo_{BT}	1.12	1.21	0.53	0.78	0.67	1.00	0.35	0.46
qo_{t1}	9.09[**]	5.44[**]	1.80	2.32	5.74[**]	7.88	0.53	0.84
qo_{t2}	5.54	5.29	1.31	2.61	5.54	8.60	0.31	0.55
qo_{t3}	3.44	4.91	1.50	2.87	4.94	9.22	0.48	0.92
qo_{t4}	2.78	4.70	1.90	3.19	4.70	9.47	3.79	5.30
qo_{t5}	2.48	4.65	2.16	3.56	4.79	10.58[**]	4.17[**]	6.84[**]
qo_{AT}	2.51	4.51	2.45[**]	3.95[**]	5.20	10.22	2.90	4.84
Oil Rec.	0.25[*]	0.45[**]	0.19[*]	0.34[*]	0.28[*]	0.36[*]	0.08[*]	0.12[*]

*: Best Parameter
**: Worst Parameter

Table **5-11**: Absolute Error Per Predicted Parameter. Stage-2 Network, PVT#2, N_2 Injection

Parameter	Absolute Error (%)							
	4-Spot		5-Spot		7-Spot		9-Spot	
	A≤ 100	A> 100	A≤ 100	A> 100	A≤ 100	A> 100	A≤ 100	A> 100
BT	1.49	1.44	2.02	2.35	1.36	1.25	18.28	12.91
t1	1.13	1.29	1.10	1.51	1.17	2.05	3.78	3.28
t2	0.97	1.39	0.93	1.28	1.43	2.86	2.33	1.83
t3	0.95	1.50	0.92	1.31	1.71	3.52	1.58	1.19
t4	0.98	1.65	0.93	1.41	1.91	3.97	1.32	1.01
t5	1.00	1.74	0.94	1.49	2.02	4.27	1.31	0.93
AT	1.05	1.86	1.04	1.54	2.11	4.52	1.12	1.07
$qt_{@ET}$	1.62	2.24	1.32	0.92	1.68	1.24	2.50	1.68
qt_{BT}	1.72	1.36	2.09	2.50	1.68	1.28	20.43**	15.9**
qt_{t1}	0.82	0.90	0.72	0.72	0.87	0.78	2.26	1.74
qt_{t2}	0.70	0.72	0.69	0.61	0.72	0.71	1.79	1.18
qt_{t3}	0.63	0.67	0.54	0.57	0.75	0.61	1.55	1.09
qt_{t4}	0.68	0.70	0.54	0.59	0.73	0.54	1.99	0.91
qt_{t5}	0.61*	0.65	0.55	0.58	0.57	0.54	1.74	1.40
qt_{AT}	0.62	0.72	0.55	0.49*	0.56*	0.55	1.50	1.53
$qo_{@ET}$	2.91	1.95	2.39	1.16	1.99	1.58	2.53	1.74
qo_{BT}	4.33	4.49	2.88	2.69	3.69	3.52	2.98	2.70
qo_{t1}	5.99	6.08	4.10**	5.42**	6.24	9.96	7.17	5.64
qo_{t2}	7.30**	7.91**	3.64	4.43	7.21**	12.35**	3.51	2.45
qo_{t3}	4.32	4.70	3.73	4.07	4.43	7.32	2.10	2.36
qo_{t4}	1.48	2.23	2.32	2.58	2.73	4.63	4.79	4.18
qo_{t5}	0.84	1.36	0.95	1.28	1.71	3.21	2.19	1.93
qo_{AT}	0.65	1.05	0.79	0.98	1.07	2.09	1.80	1.12
Oil Rec.	0.66	0.58*	0.53*	0.52	0.60*	0.54*	0.47*	0.54*

*: Best Parameter
**: Worst Parameter

Table **5-12**: Absolute Error Per Predicted Parameter. Stage-2 Network, PVT#3, N_2 Injection

Parameter	Absolute Error (%)							
	4-Spot		5-Spot		7-Spot		9-Spot	
	A≤ 100	A> 100	A≤ 100	A> 100	A≤ 100	A> 100	A≤ 100	A> 100
BT	0.72	1.37	0.70	1.03	0.82	1.16	1.29	1.48
t1	0.51	0.98	0.53	0.75	0.72	1.03	0.73	0.96
t2	0.40	0.72	0.44	0.63	0.55	0.74	0.49	0.62
t3	0.31	0.57	0.42	0.59	0.49	0.62	0.51	0.58
t4	0.30	0.44	0.40	0.55	0.39	0.56	0.56	0.55
t5	0.28	0.49	0.39	0.61	0.39	0.51	0.58	0.52
AT	0.31	0.48	0.40	0.61	0.36	0.41	0.58	0.53
$qt_{@ET}$	0.76	1.08	0.37	0.40	0.98	0.92	0.78	0.34
qt_{BT}	0.79	1.55	0.80	1.10	0.88	1.25	1.40	1.62
qt_{t1}	0.57	1.10	0.64	0.85	0.78	1.26	0.79	1.06
qt_{t2}	0.48	0.85	0.45	0.65	0.62	0.85	0.36	0.49
qt_{t3}	0.36	0.68	0.31	0.42	0.52	0.60	0.33	0.37
qt_{t4}	0.33	0.54	0.23	0.30	0.50	0.53	0.33	0.36
qt_{t5}	0.30	0.47	0.24	0.29	0.52	0.32	0.34	0.29
qt_{AT}	0.33	0.44	0.21	0.26	0.50	0.39	0.36	0.24
$qo_{@ET}$	0.73	1.09	0.55	0.41	1.22	0.90	0.91	0.66
qo_{BT}	0.65	0.68	0.34	0.39	0.48	0.49	0.26[*]	0.28
qo_{t1}	0.97	0.94	0.78	0.75	0.95	1.13	1.58	1.83[**]
qo_{t2}	1.94	3.39	1.32	1.43	2.84	2.70	1.19	1.19
qo_{t3}	3.37[**]	5.08[**]	1.85[**]	2.40[**]	3.68[**]	3.61	0.81	0.90
qo_{t4}	2.25	4.24	1.24	1.70	3.14	3.89[**]	1.01	0.96
qo_{t5}	1.61	3.16	0.89	1.43	2.15	3.11	2.10[**]	1.39
qo_{AT}	1.40	1.70	0.85	0.97	1.53	2.43	1.35	1.23
Oil Rec.	0.27[*]	0.43[*]	0.19[*]	0.21[*]	0.43[*]	0.26[*]	0.30	0.22[*]

*: Best Parameter

**: Worst Parameter

5.1.4 Network for Waterflooding Processes

A specific network was developed per well pattern/fluid type combination. Nevertheless, data generation of the networks for water injection followed a different procedure. Each waterflooding model was built using different sets of relative permeability curves and capillary pressure. Then, the variables used to generate these curves were included as part of the inputs, together, with the design parameters and rock properties. The data were generated in two batches as it was done for the miscible displacement networks. Table **5-13** shows the data ranges considered for the waterflooding cases.

Table **5-13**: Data Limits for ANN – Waterflooding Process

Input		Batch 1, Area<=100 acres			Batch 2, Area> 100 acres		
		min	mid	max	min	mid	max
Area (acres)		60	-	100	150	-	300
Kx=Ky (md)		10	-	100	200	-	500
h (ft)		50	-	200	50	-	200
Porosity (%)		15	-	40	20	-	40
Swirr (fraction)		0.15	-	0.3	0.15	-	0.3
Sor (fraction)		0.15	-	0.4	0.15	-	0.4
C_{oil} (dimensionless)		0.5	-	4	0.5	-	4
C_{gas} (dimensionless)		0.1	-	0.3	0.1	-	0.3
PVT#1 (Pi=5000 psia)	P_{Prod} (psia)	2000	3000	4000	3000	3000	4000
	P_{Inj} (psia)	6000	6500	7000	6000	7000	8000
PVT#2 & 3 (Pi=3000 psia)	P_{Prod} (psia)	1000	1500	2000	1000	1500	2000
	P_{Inj} (psia)	4000	5000	6000	4000	5000	6000

Design of experiment with full factorial was also applied to generate a minimum amount of characteristic cases. It should be noted that this network has 10 independent parameters. A 3-level design applied to these variables would require the generation of 3^{10}=59049 cases, which is unfeasible. In order to reduce the amount of minimum cases to a practical number, different design levels were used. The 3-level design was only applied to the most significant parameters, which are the injection and production pressures. A 2-level design was applied to the rest of the variables. However, this design would require the generation of 2^8*3^2=2304 cases. Considering that some random cases are also necessary to train the network properly, the memory requirements to develop a network with this amount of data sets are again considered to be too large. Then, it was necessary to reduce the number of independent inputs. The capillary pressure constant for gas, C_{gas}, was tied to its oil counterpart C_{oil}. That is, when the minimum limit of C_{oil} is used, the minimum value of C_{gas} is also used. Likewise, if the maximum value of C_{oil} is used, the maximum limit of C_{gas} is also used. This approach was implemented since the initial gas saturation was set to zero in all models, and free gas is not expected to develop as the reservoir pressure remains above the saturation value. With 9 independent parameters, the minimum number of cases is reduced to 2^7*3^2=1152 cases. Additionally, 848 random cases were generated for each batch. That is, 2000 different reservoir models per batch or 4000 per well pattern.

Since the physics of waterflooding projects are, to some extent, simpler than those in miscible displacement, the networks were generated in only one stage. These networks are incorporated into the screening tool-box. The architecture of the network is very similar to the ones developed for miscible displacement processes, as it can be seen in

Figure **5-28**. The network has 13 inputs, including the same functional links used in the previous networks. The outputs consist of the 20 values of time/oil production parameters to build the production profiles as shown before in Figure **5-3**. The ultimate recovery fraction is also predicted by this network. The logarithm functional link is applied to all inputs and outputs to help the performance of the network.
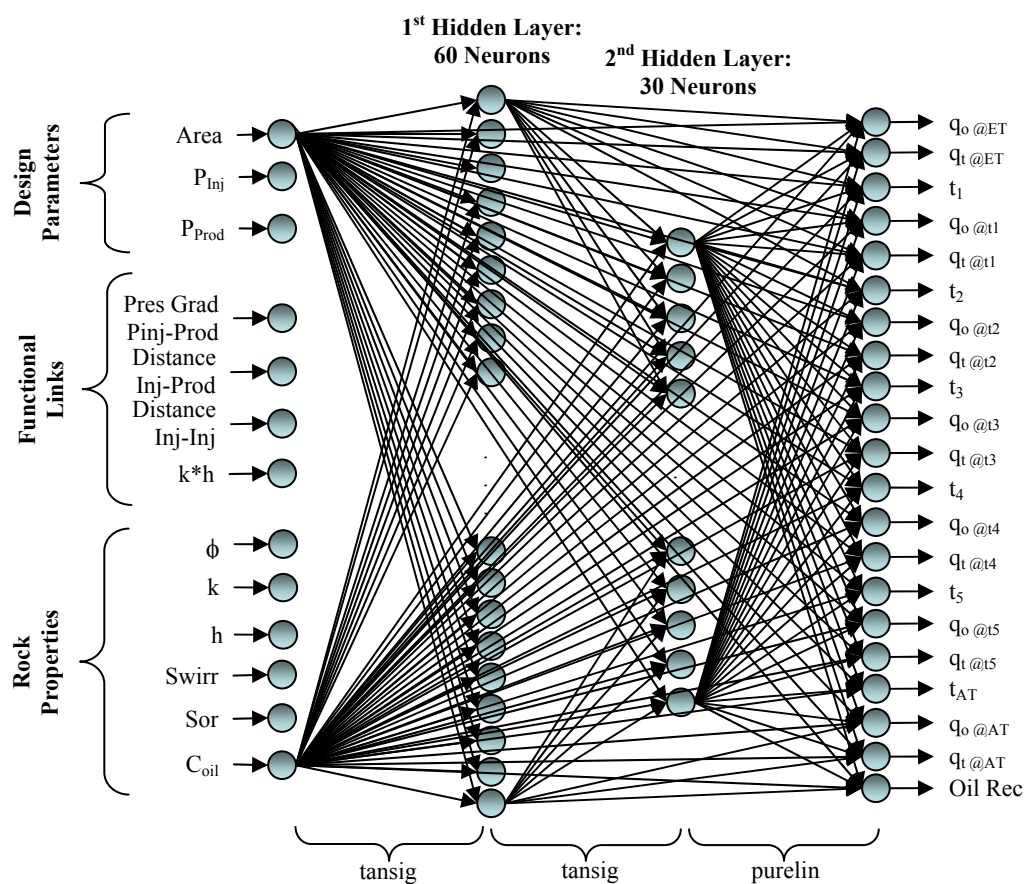
Figure **5-28**: Network Architecture for Waterflooding Projects

While a different number of neurons, layers, transfer functions, training functions and functional link combinations were tested, the architecture shown in Figure **5-28** was

the one that provided the best results. This was used in both batches, in 4-spot, 5-spot, 7-spot and 9-spot with PVT#1, PVT#2 and PVT#3. All networks were built using 60 neurons in the first hidden layer and 30 in the second one, with "*trainlm*" and "*learngdm*" functions. It was not possible to build networks for PVT#4 undergoing water injection since no significant oil was produced from these reservoir models. The injected water did not sweep the oil thus the abandonment condition (90% of water cut) was achieved almost immediately after the wells became operational.

Figure **5-29** shows the oil production profile for the best and worst testing cases using the network for 4-Spot, PVT#1, Batch 1. The worst profile has an error of 5%, while the average error for the oil production profiles generated using this network is 1%. The other characteristic oil profiles generated using the waterflooding networks can be found in Appendix C. In general, they are very similar to the one presented in Figure **5-29**.
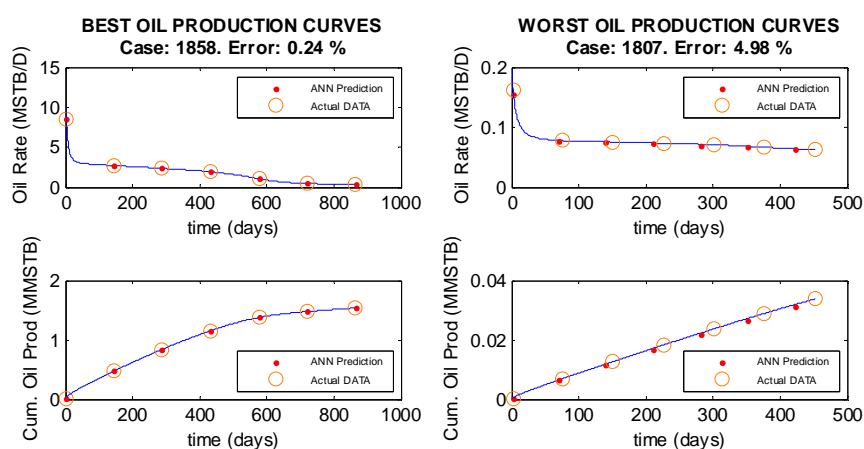
Figure **5-29**: Best and Worst Production Profiles Built using Water Injection Network, PVT#1, 4-Spot. Batch 1 (Small Areas)

Table **5-14,** Table **5-15** and Table **5-16** show the absolute errors per parameter predicted for PVT#1, PVT#2 and PVT#3, respectively. In general, the errors are very low. The oil production rate is the parameter that usually presented the highest deviation, as it was observed in the miscible displacement networks. It is noted that oil rate at t_4 seems to be the parameter with the highest error in most cases. This is not unexpected as the oil production rate has a change in its slope, which occurs when the injected water breaksthrough.

Table **5-14**: Absolute Error Per Predicted Parameter. Stage-2 Network, PVT#1, Water Injection

Parameter	Absolute Error (%)							
	4-Spot		5-Spot		7-Spot		9-Spot	
	A≤ 100	A> 100	A≤ 100	A> 100	A≤ 100	A> 100	A≤ 100	A> 100
t1	1.05	1.47	1.73	1.40	1.45	1.27	1.92	1.83
t2	1.04	1.46	1.79	1.38	1.48	1.34	1.94	1.95
t3	1.04	1.42	1.92	1.37	1.45	1.29	1.79	1.95
t4	1.07	1.47	1.83	1.37	1.41	1.32	1.87	1.86
t5	1.04	1.42	1.66	1.38	1.43	1.32	1.80	2.00
AT	1.05	1.43	1.68	1.36	1.54	1.32	1.88	1.94
$qt_{@ET}$	1.10	1.42	2.38	0.99	2.21	1.65	2.16	1.18
qt_{t1}	1.16	1.49	1.95	1.40	1.45	1.45	2.28**	2.14**
qt_{t2}	1.04	1.45	1.56	1.38	1.27	1.39	2.21	2.12
qt_{t3}	0.92	1.37	1.71	1.26	1.27	1.21	2.07	2.01
qt_{t4}	0.77	1.12	1.72	1.14	1.33	1.13	2.00	1.92
qt_{t5}	0.69	1.07	1.66	1.20	1.19	1.05	2.02	1.90
qt_{AT}	0.65	0.94	1.74	1.10	1.04	1.00	1.95	1.73
$qo_{@ET}$	1.24	1.51	2.99**	1.21	3.06	1.65	2.08	1.27
qo_{t1}	0.62	0.79	1.44	0.93	1.18	0.91	1.79	0.75*
qo_{t2}	0.59	0.71	1.75	0.68	2.10	1.14	1.52	0.88
qo_{t3}	1.14	1.45	2.32	1.14	2.45	1.24	1.71	0.95
qo_{t4}	2.57**	2.55**	2.67	1.63**	3.21**	2.25**	1.42	0.94
qo_{t5}	1.85	2.29	1.76	1.60	2.65	1.72	1.54	1.28
qo_{AT}	0.31*	0.42*	0.74*	0.65*	0.46	0.48*	0.74*	0.50
Oil Rec.	0.67	0.89	1.15	0.94	1.03*	0.85	1.48	1.68

*: Best Parameter
**: Worst Parameter

Table **5-15**: Absolute Error Per Predicted Parameter. Stage-2 Network, PVT#2, Water Injection

Parameter	Absolute Error (%)							
	4-Spot		**5-Spot**		**7-Spot**		**9-Spot**	
	A≤ 100	**A> 100**	**A≤ 100**	**A> 100**	**A≤ 100**	**A> 100**	**A≤ 100**	**A> 100**
t1	2.51	4.70	2.46	2.17	3.04	4.38	1.41	1.45
t2	2.51	4.73	2.46	2.20	2.93	4.24	1.35	1.09
t3	2.52	4.84	2.48	2.21	2.98	4.24	1.35	0.99
t4	2.49	4.85	2.53	2.27	3.01	4.10	1.39	0.95
t5	2.58	4.73	2.44	2.25	2.95	4.25	1.37	0.97
AT	2.50	4.79	2.42	2.19	2.97	4.21	1.38	0.94
$qt_{@ET}$	2.33	3.86	2.85	2.34	2.23	3.21	2.31	1.92
qt_{t1}	1.99	3.90	2.91	1.89	2.67	4.05	1.99	1.84
qt_{t2}	2.15	3.71	2.99	1.69	2.41	3.75	1.55	1.18
qt_{t3}	2.25	3.49	2.72	1.62	2.28	3.42	1.44	0.96
qt_{t4}	2.26	3.05	2.48	1.43	2.08	3.06	1.37	0.85
qt_{t5}	2.03	2.81	2.29	1.34	1.95	3.01	1.29	0.85
qt_{AT}	1.99	2.94	2.23	1.50	2.08	2.91	1.24	0.77
$qo_{@ET}$	3.13	4.47	3.64	3.85	3.12	4.15	2.88[**]	2.46
qo_{t1}	2.73	4.96	3.35	3.04	2.95	3.45	2.55	2.55[**]
qo_{t2}	3.25	4.55	2.99	2.45	3.86	3.77	1.53	1.26
qo_{t3}	4.16	6.36	3.92	3.47	5.34	5.44	1.69	1.42
qo_{t4}	7.89[**]	11.79[**]	6.94[**]	5.99[**]	9.49[**]	12.26[**]	1.96	1.63
qo_{t5}	5.06	6.67	6.84	5.29	6.56	5.77	3.25	2.47
qo_{AT}	5.54	9.19	4.40	3.89	8.78	7.97	1.47	1.41
Oil Rec.	1.66[*]	2.56[*]	1.72[*]	1.14[*]	1.80[*]	2.44[*]	0.91[*]	0.64[*]

*: Best Parameter
**: Worst Parameter

Table **5-16**: Absolute Error Per Predicted Parameter. Stage-2 Network, PVT#3, Water Injection

Parameter	Absolute Error (%)							
	4-Spot		5-Spot		7-Spot		9-Spot	
	A≤ 100	A> 100	A≤ 100	A> 100	A≤ 100	A> 100	A≤ 100	A> 100
t1	0.77	1.47	1.22	1.11	1.07	1.51	2.22	1.74
t2	0.76	1.39	1.17	1.10	1.08	1.57	2.20	1.48
t3	0.79	1.36	1.18	1.08	1.07	1.47	2.19	1.48
t4	0.77	1.36	1.21	1.05	1.10	1.51	2.21	1.51
t5	0.80	1.36	1.18	1.11	1.10	1.49	2.19	1.48
AT	0.79	1.37	1.19	1.08	1.11	1.49	2.18	1.55
$qt_{@ET}$	0.94	1.55	1.47	1.50	1.06	1.50	1.92	1.74
qt_{t1}	1.01	1.56	1.51	1.41	1.15	1.48	2.26**	2.37**
qt_{t2}	0.77	1.47	1.19	1.18	0.92	1.26	2.19	1.71
qt_{t3}	0.67	1.29	1.07	1.08	0.74	1.16	2.08	1.55
qt_{t4}	0.61	1.28	0.86	0.86	0.59	0.92	2.08	1.44
qt_{t5}	0.60	1.26	0.88	0.86	0.51	0.82	2.06	1.32
qt_{AT}	0.57*	1.22	0.84	0.80*	0.49	0.86	2.03	1.32
$qo_{@ET}$	0.97	1.89**	1.77	1.72	1.50	1.67	2.00	2.15
qo_{t1}	0.86	1.07	1.41	1.45	0.87	1.22	1.67	1.27
qo_{t2}	0.94	1.16	1.14	1.46	0.94	1.20	1.62	1.15
qo_{t3}	1.25	1.76	1.57	1.37	1.57	1.69	1.75	0.91
qo_{t4}	1.86**	1.73	1.88**	1.43	3.57**	2.34	1.40	1.05
qo_{t5}	1.49	1.46	1.57	1.80**	2.10	2.53**	1.68	1.40
qo_{AT}	0.61	0.72*	0.75*	0.91	1.00	0.74	0.84*	0.71*
Oil Rec.	0.46	1.12	0.78	0.86	0.47*	0.66*	1.50	1.16

*: Best Parameter
**: Worst Parameter

5.1.5 Network for Steam Injection Processes

Steam injection projects are the most complex IOR methods covered in the present study. Hence, the artificial neural networks developed for this recovery process are also the most challenging proxy models. In addition to the input parameters used in waterflooding, this network also incorporates the injection temperature as one of the design parameters. Pressure and temperature injection are the most crucial independent variables for the proper reservoir modeling Together, they control the steam quality. Therefore, this independent variable is included as one of the network's inputs.

In a real field application, steam is not injected above its critical pressure due to economical constraints, as compression of steam above its critical pressure becomes too expensive. A given hydrocarbon fluid similar to PVT#1 won't be a possible candidate for steam injection since its initial pressure, 5000 psia, is way above the critical water pressure, 3208.2 psia. Then, a reservoir model for PVT#1 undergoing steam injection is not built. The initial pressure of reservoirs holding PVT#2 and PVT#3, 3000 psia, is very close to the water critical pressure. Although that leads to a narrow range of injection pressures, steam injection was still applied to these fluids for comparison purposes against miscible displacement and waterflooding methods.

Table **5-17** shows the data limits used in the development of the networks for PVT#2 and PVT#3. It is noted that this IOR recovery method involves 11 independent variables. It is not feasible to apply a 3-level design to all parameters as it would require $3^{11}=177147$ minimum number of characteristic cases. In order to use the design of experiment protocol with full factorial, different design levels were implemented. The 3-

level design was applied only to the injection temperature and pressure as they are the most critical parameters. A 2-level design was applied to the other independent variables. As in waterflooding, the constant C_{oil} was tied to C_{gas} to reduce the number of independent variables. Moreover, *Swirr* was tied to *So* to reduce even further the number independent variables to 9. With this approach, the minimum number of required cases is $2^7*3^2=1152$ cases. In addition, 848 random cases were modeled for each batch. In total, 2000 cases were modeled for each steam injection network. The proxy models were trained with 1800 data sets, 100 cases were used for validation and 100 cases were used for testing.

Table **5-17**: Data Limits for ANN – PVT#2 & PVT#3 under Steam Injection Process

Input		Batch 1, Area<=100 acres			Batch 2, Area> 100 acres		
		min	mid	max	min	mid	max
Area (acres)		60	-	100	150	-	300
Kx=Ky (md)		10	-	100	200	-	500
h (ft)		50	-	200	50	-	200
Porosity (%)		15	-	40	20	-	40
Swirr (fraction)		0.15	-	0.3	0.15	-	0.3
Sor (fraction)		0.15	-	0.4	0.15	-	0.4
C_{oil} (dimensionless)		0.5	-	4	0.5	-	4
C_{gas} (dimensionless)		0.1	-	0.3	0.1	-	0.3
ΔTemp (F)		30	45	60	30	45	60
PVT#2 & 3 (Pi=3000 psia)	P_{Prod} (psia)	2000	-	2500	2000	-	2500
	P_{Inj} (psia)	3100	3150	3200	3100	3150	3200

The same network architecture used in the previous recovery methods was used for steam. Initially, the same inputs as in waterflooding were used together with injection temperature. However, the network performance was poor. The previous input networks

provided an excellent description of the flow in porous media transport, but they did not account for the heat transport phenomena. More inputs were required due to the complexity of the IOR method under study. Figure **5-30** shows a schematic of the developed structure.
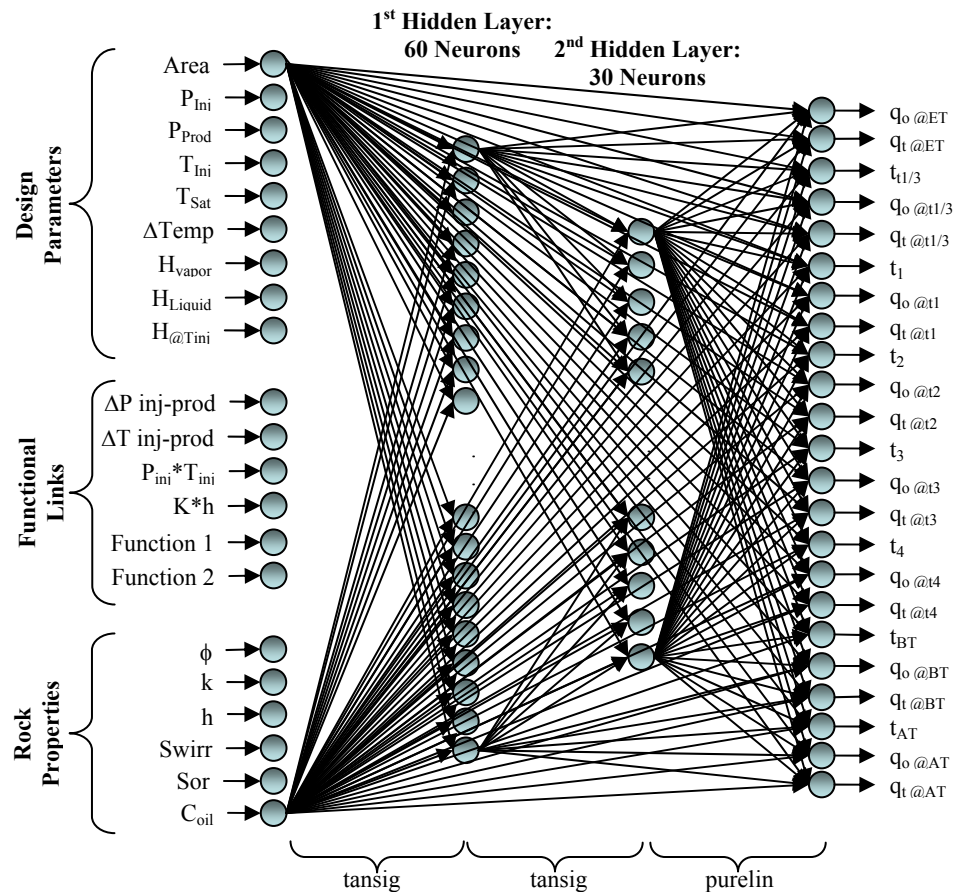
Figure **5-30**: Network Architecture for Steam Injection Projects

The design parameters now include injection temperature, saturation temperature, and the temperature difference between these two values (*ΔTemp*). Additionally, enthalpy values of vapor, liquid and injection conditions are provided (H_{vapor}, H_{liquid}, $H_{@Tinj}$). New functional links were incorporated. Those are temperature gradient between the injector

and producer, the product of injection temperature and injection pressure, and two functions derived from the independent inputs. Function 1, shown in Eq. **5.1**, resembles Darcy's Law but uses temperature difference instead of pressure.

$$Function1 = A \times h \times \phi \times (1 - Swirr - Sor) \times \frac{(T_{initial} - 220)}{\log(dist_{inj-prod})}$$

5.1

The second function, shown in Eq. **5.2**, resembles an equation of state where the reservoir volume is used instead of fluid volume.

$$V_{Res} = A \times h \times \phi \times (1 - Swirr - Sor)$$
$$Function2 = \frac{1}{V_{res}} - \frac{1}{V_{res}^3 + 2 \times V_{res}}$$

5.2
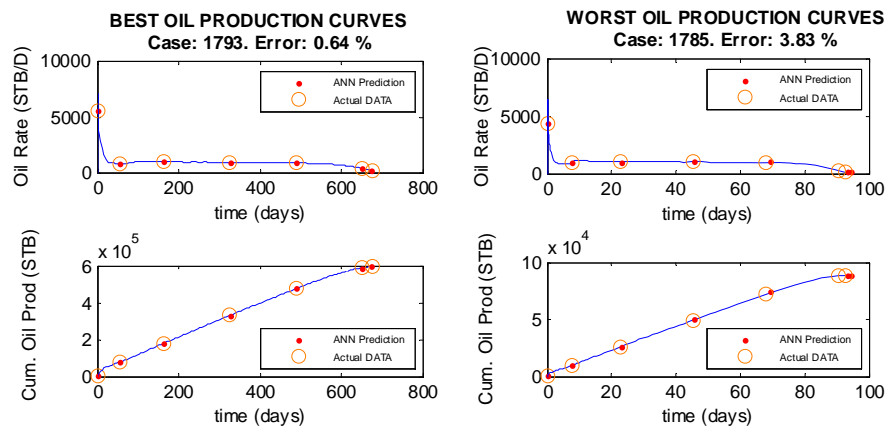
Figure **5-31**: Best and Worst Production Profiles Built using Stage-2 Network: Steam Injection, PVT#2, 4-Spot. Batch 1 (Small Areas)

Figure **5-31** shows the best and worst predicted oil production curves while testing the network 4-spot, PVT#2 under steam injection. The worst profile showed an error of 4 % while the average oil profile curve's error was 2 %. The characteristic

profiles generated while testing the rest of the steam injection networks for PVT#2 and

PVT#3 are shown in Appendix C.

Table **5-18** and Table **5-19** shows the absolute error of the predicted parameters

using for PVT#2 and PVT#3. In general, among the predicted parameters the highest

deviation was displayed by oil production rate.

Table **5-18**: Absolute Error Per Predicted Parameter. Stage-2 Network, PVT#2, Steam Injection

Parameter	Absolute Error (%)							
	4-Spot		5-Spot		7-Spot		9-Spot	
	A≤ 100	A> 100	A≤ 100	A> 100	A≤ 100	A> 100	A≤ 100	A> 100
$t_{1/3}$	1.13	0.77	1.19	0.98	1.70	1.11	1.74	1.78
t1	1.05	0.74	1.21	0.80	1.44	1.03	1.72	1.71
t2	1.01	0.76	1.33	0.87	1.59	1.04	1.68	1.67
t3	1.06	0.70	1.24	1.11	1.72	1.06	1.70	1.77
BT	1.08	0.78	1.35	1.01	1.62	1.08	1.90	1.72
AT	1.05	0.81	1.33	1.00	1.45	0.84	1.54	2.61
$qt_{@ET}$	0.52*	0.31*	0.73*	0.50*	0.73*	0.47*	0.75*	0.58*
$qt_{t1/3}$	1.36	1.02	1.81	1.28	1.93	1.45	1.95	1.80
qt_{t1}	1.11	0.97	1.59	1.09	2.10	1.19	2.68	2.65
qt_{t2}	0.96	0.67	1.23	0.85	1.50	1.07	1.94	1.82
qt_{t3}	0.81	0.64	1.33	0.77	1.31	0.94	1.42	1.46
qt_{BT}	0.63	0.58	0.91	0.68	1.11	0.70	0.83	0.73
qt_{AT}	0.77	0.48	1.06	0.68	1.27	0.83	1.03	0.85
$qo_{@ET}$	0.49	0.28	0.70	0.41	0.91	0.54	0.62	0.60
$qo_{t1/3}$	3.63	2.76	4.41	3.61	4.78	3.47	5.89	4.67
qo_{t1}	2.55	1.55	1.95	1.41	3.17	2.06	3.54	2.73
qo_{t2}	1.72	1.20	1.79	1.37	2.31	1.52	2.16	1.79
qo_{t3}	2.44	1.62	2.27	2.01	2.88	1.66	4.97	3.53
qo_{BT}	9.84**	5.38**	17.24**	7.67**	14.31**	10.34**	18.15**	15.09**
qo_{AT}	4.75	3.61	7.85	5.06	6.61	3.83	4.21	3.13

*: Best Parameter
**: Worst Parameter

Table **5-19**: Absolute Error Per Predicted Parameter. Stage-2 Network, PVT#3, Steam Injection

Parameter	Absolute Error (%)							
	4-Spot		5-Spot		7-Spot		9-Spot	
	A≤ 100	A> 100	A≤ 100	A> 100	A≤ 100	A> 100	A≤ 100	A> 100
$t_{1/3}$	1.13	0.77	1.19	0.98	1.70	1.11	1.74	1.78
t1	1.05	0.74	1.21	0.80	1.44	1.03	1.72	1.71
t2	1.01	0.76	1.33	0.87	1.59	1.04	1.68	1.67
t3	1.06	0.70	1.24	1.11	1.72	1.06	1.70	1.77
BT	1.08	0.78	1.35	1.01	1.62	1.08	1.90	1.72
AT	1.05	0.81	1.33	1.00	1.45	0.84	1.54	2.61
$qt_{@ET}$	0.52	0.31	0.73	0.50	0.73*	0.47*	0.75	0.58
$qt_{t1/3}$	1.36	1.02	1.81	1.28	1.93	1.45	1.95	1.80
qt_{t1}	1.11	0.97	1.59	1.09	2.10	1.19	2.68	2.65
qt_{t2}	0.96	0.67	1.23	0.85	1.50	1.07	1.94	1.82
qt_{t3}	0.81	0.64	1.33	0.77	1.31	0.94	1.42	1.46
qt_{BT}	0.63	0.58	0.91	0.68	1.11	0.70	0.83	0.73
qt_{AT}	0.77	0.48	1.06	0.68	1.27	0.83	1.03	0.85
$qo_{@ET}$	0.49*	0.28*	0.70*	0.41*	0.91	0.54	0.62*	0.60*
$qo_{t1/3}$	3.63	2.76	4.41	3.61	4.78	3.47	5.89	4.67
qo_{t1}	2.55	1.55	1.95	1.41	3.17	2.06	3.54	2.73
qo_{t2}	1.72	1.20	1.79	1.37	2.31	1.52	2.16	1.79
qo_{t3}	2.44	1.62	2.27	2.01	2.88	1.66	4.97	3.53
qo_{BT}	9.84**	5.38**	17.24**	7.67**	14.31**	10.34**	18.15**	15.09**
qo_{AT}	4.75	3.61	7.85	5.06	6.61	3.83	4.21	3.13

*:   Best Parameter
**: Worst Parameter

The network architecture for PVT#4 is very similar to the architecture developed for PVT#2 and PVT#3. The only difference is that an additional functional link was incorporated into the input layer. The third functional link is given by Eq. **5.3**:

$$Function3 = k \times h \times \frac{(P_{inj} - P_{prod})}{\log(H_{liq})}$$

5.3

Table **5-20** shows the data limits used in the generation of the data sets. The
maximum injection pressure was set as 1400 psia. A higher limit could have been used
but that would lead to too high injection temperatures, which are not feasible.

Table **5-20**: Data Limits for ANN – PVT#4 under Steam Injection Process

Input		Batch 1, Area<=100 acres			Batch 2, Area> 100 acres		
		min	mid	max	min	mid	max
Area (acres)		1	-	5	1	-	15
Kx=Ky (md)		500	-	2500	5000	-	15000
h (ft)		20	-	200	20	-	200
Porosity (%)		20	-	40	20	-	40
Swirr (fraction)		0.15	-	0.35	0.15	-	0.35
Sor (fraction)		0.2	-	0.4	0.2	-	0.4
C_{oil} (dimensionless)		0.5	-	4	0.5	-	4
C_{gas} (dimensionless)		0.1	-	0.3	0.1	-	0.3
dTemp (F)		30	45	60	30	45	60
PVT#4 (Pi=1000 psia)	P_{Prod} (psia)	600	-	900	600	-	900
	P_{Inj} (psia)	1100	1250	1400	1100	1250	1400

Figure **5-32** shows the best and worst oil profile obtained while testing the
network. The worst profile presented an error of 8%, while the average error for all oil
production prediction was 3.6%.
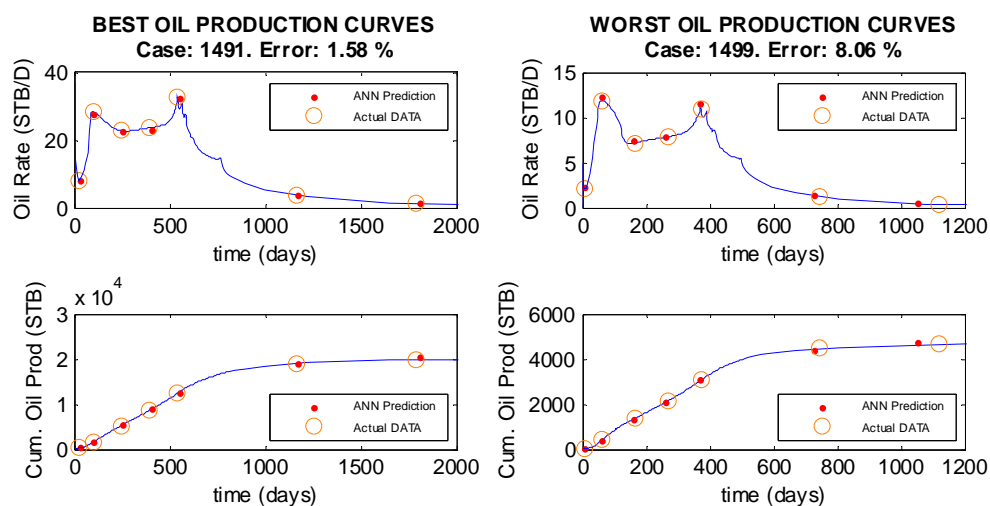
Figure **5-32**: Best and Worst Production Profiles Built using Steam Injection Network, PVT#4, 4-Spot. Batch 1 (Small Areas)

Table **5-21** summarizes the absolute errors per parameter obtained while testing the network with PVT#4 undergoing steam injection. In general, the early time (*ET*) is the parameter that presented the highest deviation. This is because *ET* was extracted from the numerical simulator at the minimum oil production rate after the well is put on production. There was no other simulator output that helped to validate this value.

Table **5-21**: Absolute Error Per Predicted Parameter. Stage-2 Network, PVT#4, Steam Injection

Parameter	Absolute Error (%)							
	4-Spot		5-Spot		7-Spot		9-Spot	
	A≤ 100	A> 100	A≤ 100	A> 100	A≤ 100	A> 100	A≤ 100	A> 100
ET	13.96**	10.12**	9.27**	8.75**	11.69**	12.90**	19.50	16.47**
BT	2.89	3.47	4.10	4.27	3.22	7.56	5.27	4.06
t1	1.99	2.31	2.24	4.25	2.54	5.74	3.56	3.22
t2	2.01	2.29	2.24	3.56	3.49	6.25	3.77	3.06
SBT	1.76	2.33	1.97	4.91	2.95	7.19	4.13	3.32
t3	2.37	1.99	1.50	3.69	2.68	4.70	3.31	2.25
AT	2.89	2.20	1.38	3.79	2.80	4.94	3.28	2.04
$qt_{@ET}$	10.59	8.37	7.75	8.51	10.44	12.20	19.99**	15.52
qt_{BT}	4.58	4.32	5.26	6.13	5.22	7.17	5.82	3.35
qt_{t1}	2.01	2.25	1.70	3.40	2.07	6.28	3.16	2.35
qt_{t2}	2.21	1.85	1.42	3.67	3.30	7.35	3.68	3.15
qt_{SBT}	2.11	2.27	1.74	3.61	1.98	6.48	3.99	2.92
qt_{t3}	1.64	1.22	1.00	2.60	1.91	3.43	2.04	1.69
qt_{AT}	1.25*	1.22*	0.97*	2.29	1.56	3.19	1.45*	2.53
$qo_{@ET}$	3.10	3.35	2.47	4.32	3.81	5.38	3.02	2.94
qo_{BT}	1.36	1.28	1.28	1.57*	1.53*	3.19*	3.37	1.27*
qo_{t1}	2.35	2.21	1.77	2.72	2.04	4.78	2.40	2.07
qo_{t2}	2.32	2.55	2.21	2.34	2.56	4.22	2.30	2.15
qo_{BT}	3.87	4.14	4.15	4.04	3.13	5.57	4.18	4.41
qo_{t3}	4.22	5.12	2.35	5.83	3.31	6.43	6.63	4.63
qo_{AT}	7.07	2.78	2.26	3.94	3.75	6.14	2.29	3.39

*:   Best Parameter
**: Worst Parameter

5.1.6 Relevancy of Inputs to the Developed Networks for the Screening Tool-Box

Different inputs have been used in the development of the networks for the screening tool-box. It is always desirable to determine which inputs parameters have the highest impact on the network performance, especially when few data is available or the available reservoir model presents some uncertainties.

The relevancy of the input parameters to the different networks is obtained directly from the weight values of the input layer. The larger the input layer weight, the higher the connection between the inputs and the network. This connection can be observed graphically by using the Hinton plot, as shown in Figure **5-33**.
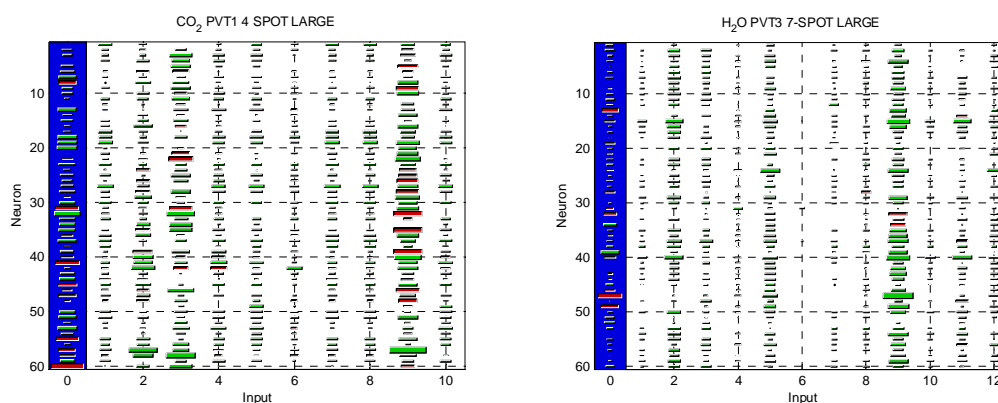
Figure **5-33**: Hinton Graphs for Screening Tool-Box's Networks

On the white background, each square's area represents a weight's magnitude. Each column represents the weights connecting each input with the neurons in the first layer. Usually, the neurons in each column have similar connecting weights as it can be

seen in Figure **5-33**. The biases are shown in the first column with blue background. Each red square represents a negative value while the green color denotes a positive value.

The relevancy of the inputs can be determined by adding the absolute values of the weights corresponding to that input. That is, the values of the weights per column. The input with the highest summed weight value is the one that has the highest impact on the network, while the input with the lowest summed value has the lowest impact.

The weights of all networks were ranked in a descending order so that the value of 1 corresponds to the input with the highest impact. Table **5-22** shows the sorting of the weights per input parameter for each CO_2 injection network as well as the average sorting of all CO_2 injection networks. In general, the product *kh* has the lowest relevancy while the pressure gradient between the injector and the producer has the highest relevancy. Although the functional links helped to improve the performance of the networks, it is more useful for the reservoir engineer to sort only the rock and fluid properties since these are the parameters that are input into the tool-box. The reservoir properties sorted in descending order of relevancy for CO_2 injection process are injection pressure, production pressure, permeability, area, porosity and thickness.

Table **5-22**: Sorting of Weights for CO_2 Injection Networks

PVT	Spot	Size	Input Parameter										
			Area	P_{prod}	P_{inj}	K	h	poro	d_{i-i}	d_{i-p}	P_{grad}	P_{grad2}	K*h
#1	4	Large	8	3	2	4	6	10	7	9	1	-	5
		Small	7	3	2	4	6	5	9	8	1	-	10
	5	Large	7	3	2	6	4	10	8	9	1	-	5
		Small	5	3	2	4	10	8	6	7	1	-	9
	7	Large	9	2	3	6	4	7	8	-	1	-	5
		Small	5	2	3	8	6	9	4	-	1	-	7
	9	Large	7	4	3	11	9	5	8	6	1	2	10
		Small	10	4	1	5	6	11	8	9	2	3	7
#2	4	Large	6	3	2	5	9	4	8	7	1	-	10
		Small	7	4	2	3	9	10	8	6	1	-	5
	5	Large	7	3	2	5	9	4	8	6	1	-	10
		Small	9	3	2	4	10	5	7	8	1	-	6
	7	Large	5	3	2	7	8	6	4	-	1	-	9
		Small	6	4	3	5	8	2	7	-	1	-	9
	9	Large	8	4	3	5	10	6	9	7	2	1	11
		Small	9	4	1	10	5	11	8	7	2	3	6
#3	4	Large	6	2	3	4	8	9	5	7	1	-	10
		Small	6	2	3	4	10	5	8	7	1	-	9
	5	Large	4	3	2	7	10	8	5	6	1	-	9
		Small	7	5	3	2	10	4	6	8	1	-	9
	7	Large	4	3	2	6	8	7	5	-	1	-	9
		Small	6	3	2	4	9	7	5	-	1	-	8
	9	Large	7	4	1	11	6	5	8	9	2	3	10
		Small	7	4	1	6	10	5	8	9	2	3	11
Average Sorting			6	4	2	5	10	7	8	9	1	3	11

Table **5-23** shows the sorting of the weights per input parameter for each N_2 injection network as well as the average sorting of all N_2 injection networks. The most and least relevant inputs are the same as in the CO_2 injection networks: injection pressure and the *kh* product. The reservoir properties organized in descending order of relevancy for N_2 injection process are injection pressure, production pressure, permeability, thickness, area and porosity.

Table **5-23**: Sorting of Weights for N$_2$ Injection Networks

PVT	Spot	Size	Input Parameter										
			Area	P$_{prod}$	P$_{inj}$	K	h	poro	d$_{i-i}$	d$_{i-p}$	P$_{grad}$	P$_{grad2}$	K*h
#1	4	Large	6	2	3	8	4	10	7	5	1	-	9
		Small	6	2	3	4	8	9	7	5	1	-	10
	5	Large	9	2	3	5	4	6	8	10	1	-	7
		Small	8	6	2	5	3	4	9	10	1	-	7
	7	Large	4	6	2	9	3	7	5	-	1	-	8
		Small	5	4	3	2	7	9	6	-	1	-	8
	9	Large	8	4	3	6	5	10	9	7	2	1	11
		Small	11	6	5	4	3	7	9	10	2	1	8
#2	4	Large	6	3	2	7	9	8	5	4	1	-	10
		Small	6	3	2	4	10	5	7	8	1	-	9
	5	Large	8	3	1	5	6	4	9	7	2	-	10
		Small	8	3	1	4	6	5	10	9	2	-	7
	7	Large	5	3	2	4	7	9	6	-	1	-	8
		Small	6	4	2	3	9	7	5	-	1	-	8
	9	Large	6	4	3	8	9	10	7	5	1	2	11
		Small	6	2	9	3	10	1	7	8	4	5	11
#3	4	Large	6	3	1	9	8	4	7	5	2	-	10
		Small	8	3	1	4	6	7	10	9	2	-	5
	5	Large	8	3	1	5	4	10	9	7	2	-	6
		Small	8	3	1	4	6	10	7	9	2	-	5
	7	Large	4	3	1	6	7	8	5	-	2	-	9
		Small	7	3	1	4	9	5	6	-	2	-	8
	9	Large	5	4	1	8	9	10	6	7	3	2	11
		Small	6	4	1	10	5	11	7	8	3	2	9
Average Sorting			**7**	**4**	**3**	**5**	**6**	**9**	**8**	**10**	**1**	**2**	**11**

Table **5-24** shows the sorting of the weights per input parameter for each waterflooding network as well as the average sorting of all waterflooding injection networks. The most relevant inputs are the C_{oil} coefficient for the capillary pressure curves and the pressure gradient between the injector and the producer. The parameters with the lowest impact on the network are the porosity and the distances between the wells. The reservoir properties arranged in descending order of relevancy for water injection process are C_{oil} coefficient, production pressure, thickness, residual oil,

saturation, injection pressure, permeability, area, irreducible water saturation and porosity.

Table **5-24**: Sorting of Weights for H_2O Injection Networks

PVT	Spot	Size	Area	P_{prod}	P_{inj}	K	h	poro	S_{wirr}	S_{or}	C_{oil}	$d_{inj\text{-}inj}$	$d_{inj\text{-}prod}$	P_{grad}	P_{grad2}	K*h
								Input Parameter								
1	4	Large	8	4	13	11	1	12	7	6	2	10	9	5	-	3
		Small	12	2	10	6	5	9	7	4	1	13	11	3	-	8
	5	Large	7	5	13	9	2	11	12	10	1	8	6	4	-	3
		Small	10	2	9	4	13	5	6	3	1	12	11	8	-	7
	7	Large	9	5	11	10	2	7	12	6	1	8	-	4	-	3
		Small	10	4	11	7	2	12	8	6	1	9	-	3	-	5
	9	Large	12	4	13	8	1	14	9	7	2	10	11	6	5	3
		Small	10	2	13	7	8	5	9	6	1	12	11	3	4	14
2	4	Large	8	4	2	12	5	13	11	10	3	7	9	1	-	6
		Small	9	3	2	11	5	13	12	6	4	10	8	1	-	7
	5	Large	9	4	2	8	5	13	12	7	3	11	10	1	-	6
		Small	11	2	4	6	13	7	8	5	3	10	12	1	-	9
	7	Large	8	5	3	11	4	12	10	9	1	7	-	2	-	6
		Small	7	3	2	10	5	12	11	6	4	8	-	1	-	9
	9	Large	9	5	7	12	2	14	13	8	1	10	11	3	4	6
		Small	14	4	2	9	11	7	8	3	1	12	13	6	5	10
3	4	Large	7	3	13	9	4	10	12	11	1	6	8	2	-	5
		Small	12	4	6	7	3	10	9	5	1	13	11	2	-	8
	5	Large	7	9	11	12	2	13	10	8	1	6	5	3	-	4
		Small	12	4	9	2	8	7	10	6	1	11	13	3	-	5
	7	Large	9	2	5	11	3	12	8	7	1	10	-	4	-	6
		Small	10	5	4	9	2	12	8	6	1	11	-	3	-	7
	9	Large	10	5	14	8	2	13	12	3	1	9	11	6	7	4
		Small	11	9	4	3	14	5	8	2	1	13	12	6	7	10
Average Sorting			**10**	**3**	**8**	**9**	**4**	**14**	**11**	**6**	**1**	**12**	**13**	**2**	**5**	**7**

Table **5-25** shows the sorting of the weights per input parameter for each steam injection network. Since the sorting of the weights for the heavy oil networks was significantly different from PVT2 and PVT3 networks, two values of average sorting were calculated, one comprising all heavy oil networks (PVT4) and one for all black oil and light oil networks (PVT2 and PVT3). It was expected that the inputs in the heavy oil

networks have different relevancies than the black oil and light oil networks undergoing steam injection since steam breakthrough was not observed in the black oil or volatile oil systems.

Table **5-25**: Sorting of Weights for Steam Injection Networks

PVT	Spot	Size[*]	Area	P_{prod}	P_{inj}	K	h	poro	S_{wirr}	S_{or}	C_{oil}	T_{inj}	T_{sat}	ΔT	H_{liq}	H_{vap}	H_{Tinj}	P_{grad}	T_{grad}	function1	kh	$P_{inj}*T_{inj}$	function2	function3
2	4	S	14	8	10	19	4	13	17	16	21	18	12	9	5	6	7	3	15	2	11	20	1	-
		L	8	13	11	17	5	15	20	16	21	18	12	10	4	6	7	2	9	3	14	19	1	-
	5	S	10	4	14	20	5	13	18	16	21	17	11	9	6	7	8	3	12	2	15	19	1	-
		L	10	9	13	20	6	16	19	18	21	14	12	5	7	8	4	3	11	2	17	15	1	-
	7	S	15	5	9	20	4	14	16	17	21	18	11	10	7	6	8	2	13	3	12	19	1	-
		L	13	4	11	19	9	17	18	15	21	12	7	10	6	8	5	3	16	2	20	14	1	-
	9	S	14	12	7	20	5	11	18	15	21	17	8	6	10	9	3	4	16	2	13	19	1	-
		L	9	12	13	19	11	14	20	17	21	15	7	6	5	8	4	3	10	2	18	16	1	-
3	4	S	10	13	5	20	3	11	17	19	21	16	6	14	7	9	8	4	15	2	12	18	1	-
		L	9	13	11	19	7	14	18	20	21	16	10	8	5	4	6	3	12	2	15	17	1	-
	5	S	16	11	8	20	5	14	19	18	21	12	10	4	7	6	9	3	17	2	13	15	1	-
		L	12	17	8	20	4	19	18	15	21	11	10	7	6	9	5	3	13	2	16	14	1	-
	7	S	19	8	10	20	5	17	14	18	21	11	12	6	7	9	4	3	13	1	16	15	2	-
		L	14	16	10	20	4	19	18	17	21	11	9	6	5	7	8	3	12	2	15	13	1	-
	9	S	15	13	8	19	4	11	16	18	21	12	10	5	7	9	6	3	20	2	14	17	1	-
		L	9	16	10	18	7	15	14	13	21	19	8	12	5	3	6	4	11	2	17	20	1	-
Average			12	11	10	20	4	14	19	17	21	15	9	8	6	7	5	3	13	2	16	18	1	12
4	4	S	12	8	18	11	13	10	2	1	14	6	15	17	4	3	7	5	16	22	20	19	21	9
		L	17	8	15	16	19	10	2	1	9	7	14	11	3	5	6	4	18	20	21	12	22	13
	5	S	10	8	16	12	13	11	2	1	9	6	18	14	5	4	7	3	15	20	21	17	22	19
		L	15	9	10	13	20	18	2	1	11	4	16	12	7	6	5	3	8	19	21	14	22	17
	7	S	14	8	17	10	12	9	3	2	11	7	18	15	4	1	5	6	19	21	20	16	22	13
		L	18	8	9	15	14	12	2	1	17	3	13	10	5	7	4	6	22	19	21	11	20	16
	9	S	12	8	14	11	17	15	1	2	9	7	13	16	6	3	4	5	19	21	20	18	22	10
		L	16	5	14	13	15	9	1	2	10	8	18	12	7	6	3	4	19	21	20	17	22	11
Average			15	8	14	11	16	10	2	1	9	7	18	12	5	3	6	4	19	20	21	17	22	13

[*]Size: S=small, L=large

The reservoir properties listed in descending order of relevancy for the light and black oil networks are thickness, injection pressure, production pressure, area, porosity,

injection temperature, residual oil saturation, irreducible water saturation, permeability and C_{oil} coefficient. The reservoir properties sorted in descending order of relevancy for the heavy oil models undergoing steam injection are residual oil saturation, irreducible water saturation, injection temperature, production pressure, C_{oil} coefficient, porosity, thickness, injection pressure, area and thickness.

5.1.7 User Interface Screening Tool-box

A total of 96 artificial neural networks were developed in order to forecast the performance of various hydrocarbon reservoirs under diverse operating conditions. These networks were trained and tested with data not exposed to the ANNs beforehand. In order to access easily all developed networks, it is necessary to provide a user-network interface. When all networks are integrated into a single application, we create a powerful screening tool-box for diverse IOR recovery methods.
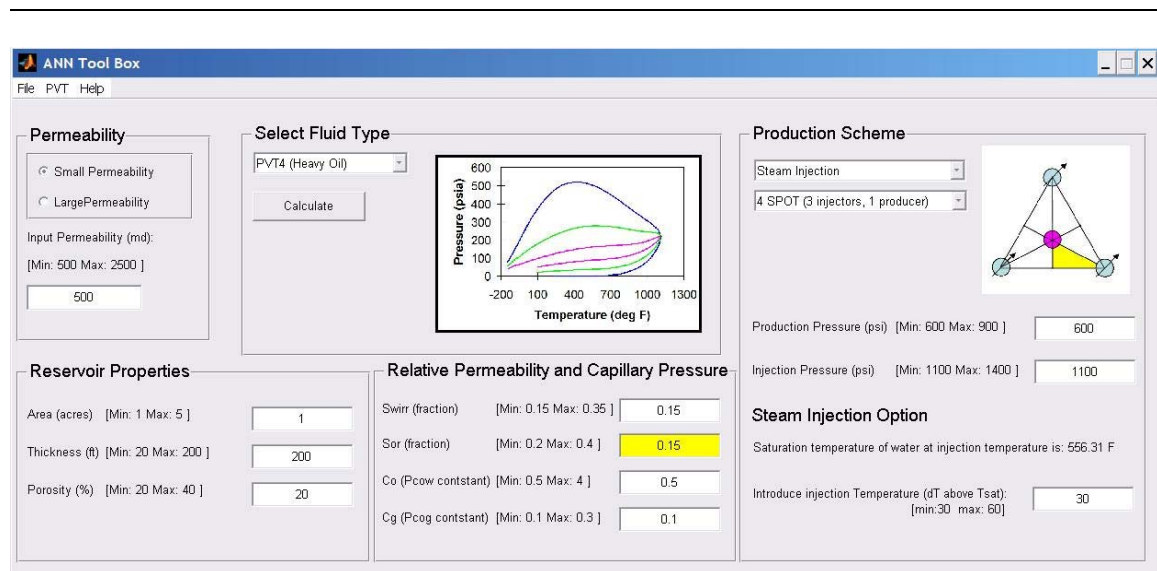
Figure **5-34**: User Interface for Screening Tool-box

Figure **5-34** shows the principal panel of the developed screening tool-box. The interface organizes conveniently the networks and provides a flexible way to forecast oil production for new reservoirs, as long as the input parameters are within the data ranges used to train the networks. The panel shows graphically the selected well pattern and fluid phase envelope. However, more details of the fluid composition are provided in the PVT tab. Figure **5-35** shows the details for fluid #3.
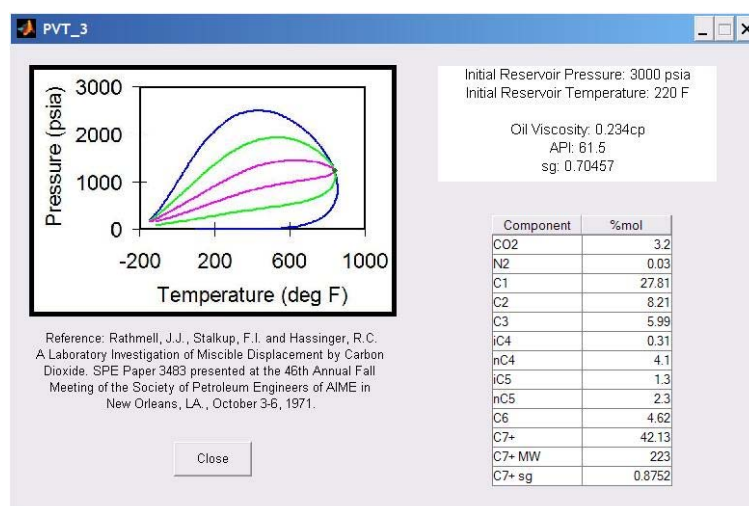
Figure **5-35**: Fluid Details in the Screening Tool-box

Relative permeability and capillary pressure panel becomes available only if either waterflooding or steam injection methods is selected. If the steam injection option is selected, the interface determines the saturation temperature for the given injection pressure. The injection temperature is then entered by the user as a gradient above the saturation value. When the user enters an out-of-range value, the corresponding box is colored in yellow, as shown in Figure **5-34**. If the user clicks on the calculate bottom

while one or more variables are out of range, the interface pops up an error message as shown in Figure **5-36**.
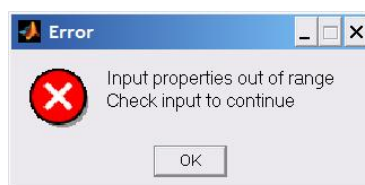
Figure **5-36**: Error Message for Out-of-Range Inputs

Similarly, a message pops up if the selected combination of PVT/IOR method corresponds to a network that was not built-in the tool-box. Figure **5-37** shows the message for a 4-spot, PVT#4 and CO_2 injection.
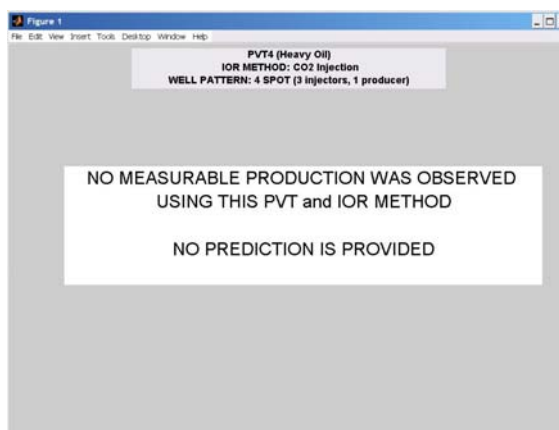
Figure **5-37**: Error Message for Non-Existing Networks

If all inputs are in-range, the tool-box predicts the expected oil production. The predicted profiles are plotted using the forecast parameters. In addition, these parameters are shown in a table that can easily copy into the clipboard. Figure **5-38** shows an example of the graphical output.
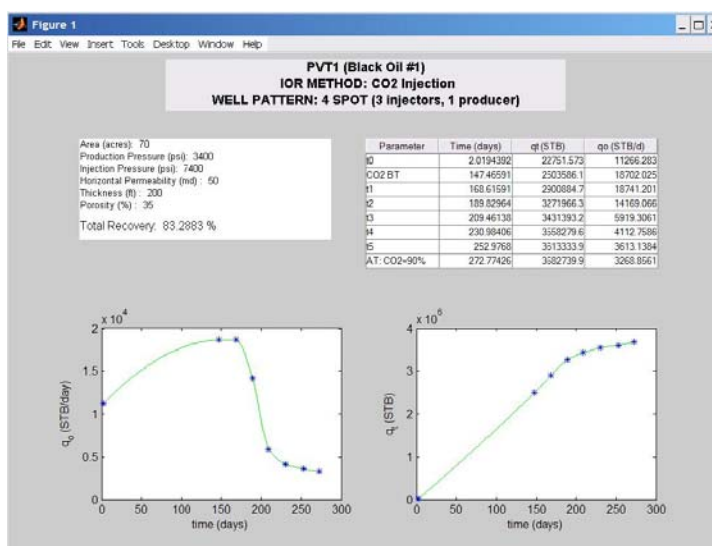
Figure **5-38**: Screening Tool-box Graphical Output

5.2 Networks for the IOR Project Design Tool-box

In this section, an artificial neural network tool-box is constructed to provide the reservoir engineer with guidelines for possible project design parameters. This tool-box is based on the inverse of the problem studied in the screening tool-box, where the appropriate field development plan is predicted on the basis of the desired oil recovery and natural reservoir characteristics of a given field.

The tool-box is a user interface that calls the appropriate ANN to predict the development plan from the characteristics of the reservoir. The diverse networks inside the tool were designed for a given fluid type, IOR process and well pattern (similar to the screening tool-box's networks). This second application of neuro-simulation uses the same data sets generated for the screening tool-box. At the end, 96 individual networks are trained, one for each batch of input data generated for the forward application.

Figure **5-39** shows a schematic of how the inverse tool works. The inputs are the expected total recovery, abandonment time and reservoir natural characteristics, which are the permeability, porosity, thickness and fluid type. The parameters for the relative permeability curves and capillary pressure are also requested for predictions using water and steam injection methods. The outputs are the field development plan, which consists of the design parameters that are under control of the reservoir engineer. These parameters comprise the operation pressures at the wells, well spacing and well pattern. Given that the networks are trained per fluid type/IOR process/well pattern combination, the recovery method must be provided as an input to the tool-box. Different areas are evaluated internally in the ANN tool. The bottom hole pressures are calculated for all

possible combinations of user inputs, areas and well patterns. The optimum case per well pattern is selected by the tool-box, which is the case that requires the lower injection pressure. When the selected IOR method is steam injection, different temperatures and areas are evaluated internally and the outputs include the injection temperature associated to the optimum predicted case.
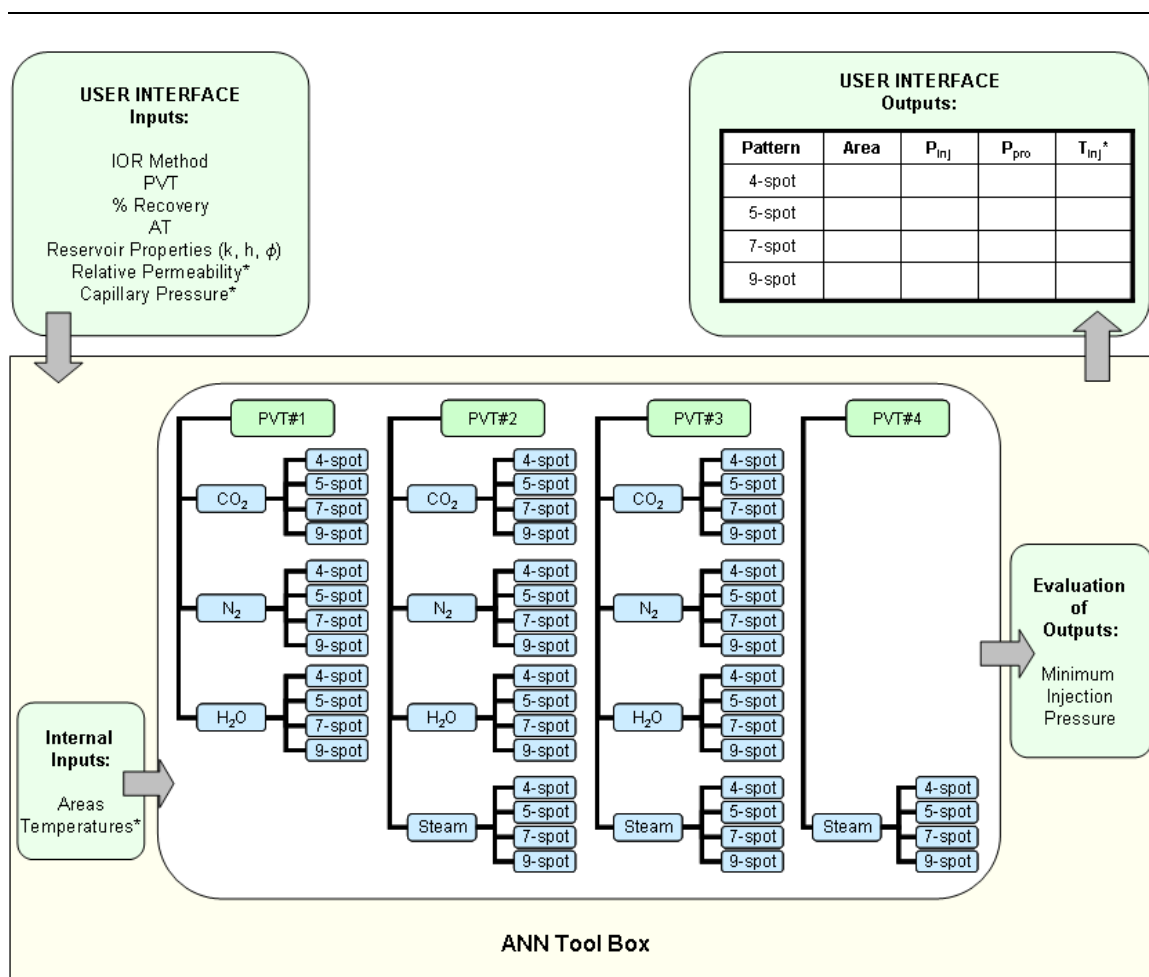
Figure **5-39**: ANN Tool-box for IOR Project Design

The inputs and outputs of the networks are not the same as those of the tool-box. Since an evaluation of different areas is performed by the interface, area must be an input to the network as part of the reservoir properties and ultimate recovery. On the other hand, the network outputs are only required to provide the injection and production pressure. The interface provides not only pressures but area for each well pattern.

5.2.1 Miscible Displacement Networks

A simple network was initially developed for CO_2 injection processes. The architecture, shown in Figure **5-40**, is simpler than the one used in the forward application. The network consists of 7 inputs: the desired oil recovery, the life time of the project or abandonment time, permeability, porosity, thickness and area. Also, the *kh* product was fed to the network as a functional link. The logarithmic functional link was applied to all inputs and outputs since it helped to improve the network's performance in the forward application.

The network was designed using a multilayer cascade feedforward back propagation (*newcf*) with Levenberg-Marquardt training function (*trainlm*) and gradient descent with momentum weight and bias learning function (*learngdm*). The first hidden layer required 20 neurons and the second 10 neurons.

Similar as in the IOR screening tool-box, each network is trained with 1000 input data-set. They are divided into three groups: 800 for training, 100 for testing and 100 for validation.
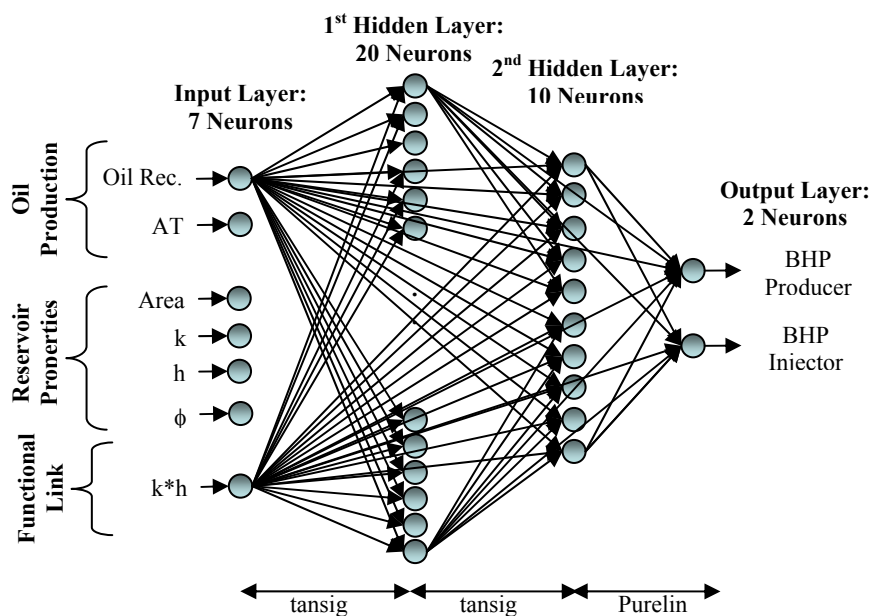
Figure **5-40**: First Network Architecture for Field Development Plan

Figure **5-41** shows the results of training and testing of the networks for a 4-spot pattern using small areas (batch 1) for PVT#1 undergoing CO_2 injection. The areas evaluated for this batch goes from 60 to 100 acres, with increments of 10. The correlations between the actual and predicted pressures were colored according to the area values. This particular network predicted pressure with low errors and the correlation between predicted and actual pressures is slightly scattered.

Similar networks were constructed for 5-spot, 7-spot and 9-spot, PVT#1, undergoing CO_2 and N_2 injection. Figure **5-42** shows the correlation between actual and predicted pressures in the testing phase, and it is clear that some predictions present high dispersion. For example, the correlation for production pressure in the network of 9-spot

with CO_2 injection is highly scattered. The analysis of the correlations suggests that some networks have a poor performance.
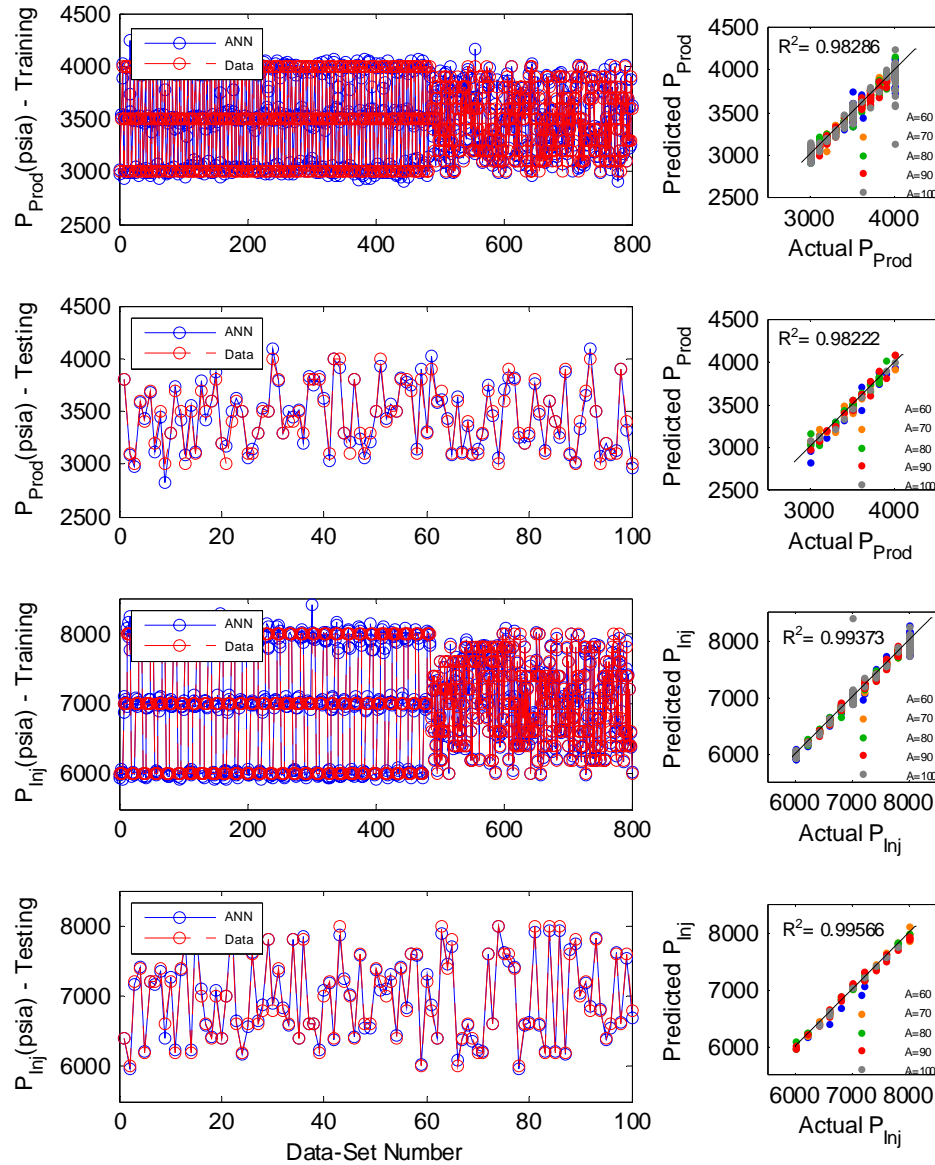
Figure **5-41**: Inverse Network. 4-Spot, CO_2 Injection, PVT#1. Batch 1 (Small Areas)
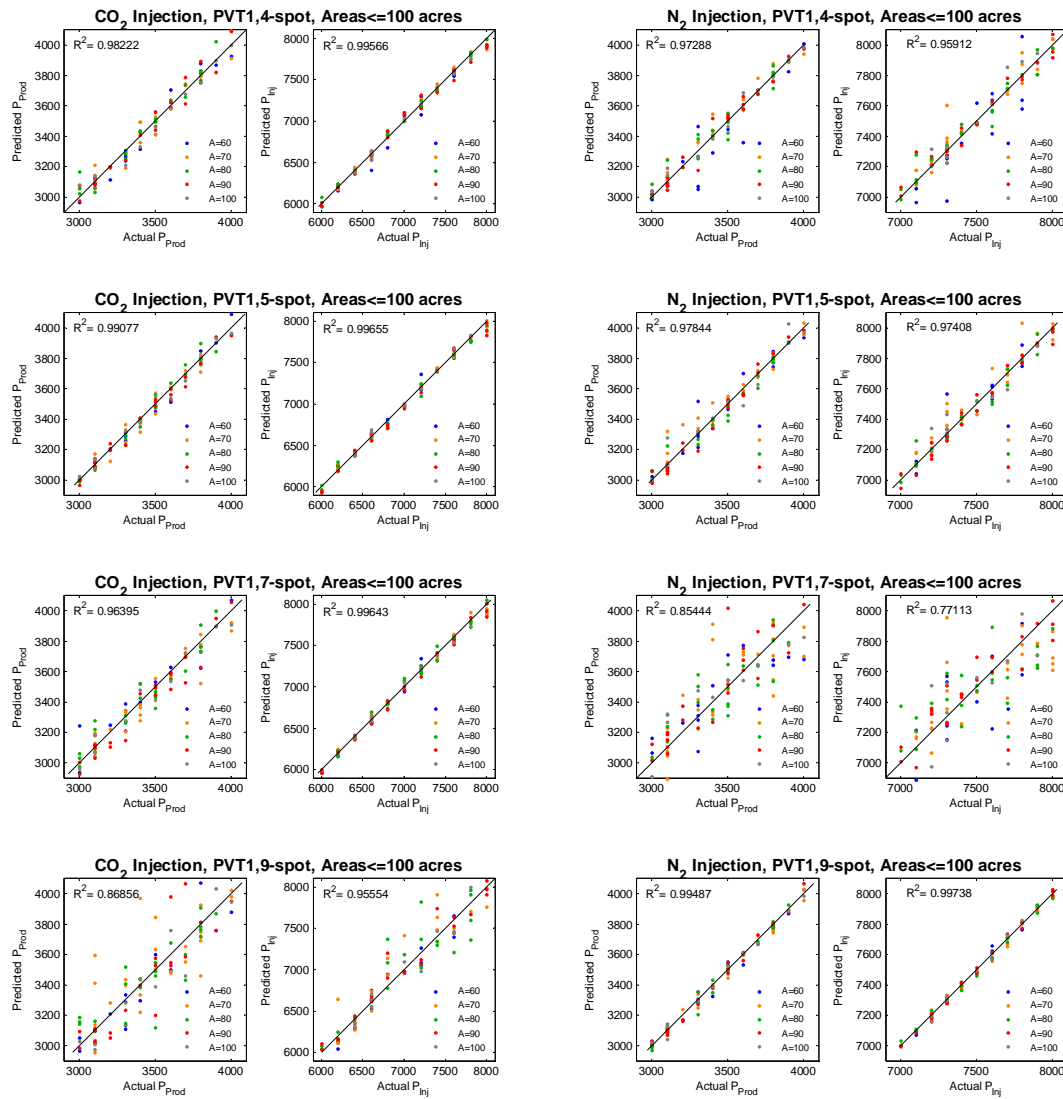
Figure **5-42**: Correlation Between Actual and Predicted Pressures. CO_2 and N_2 Injection, PVT#1, Batch 1 (Small Areas)

Although the networks for the inverse application seemed simpler than the developed in the screening tool-box since they predict only two outputs, in reality, they are more complex. The forward networks proved that it is possible to capture the relationship between the entire oil production profile data and the rock properties, fluid

properties and design parameters. In the inverse network, it was not possible to predict the operation pressures when only part of the reservoir performance obtained from the numerical simulator is given as inputs.
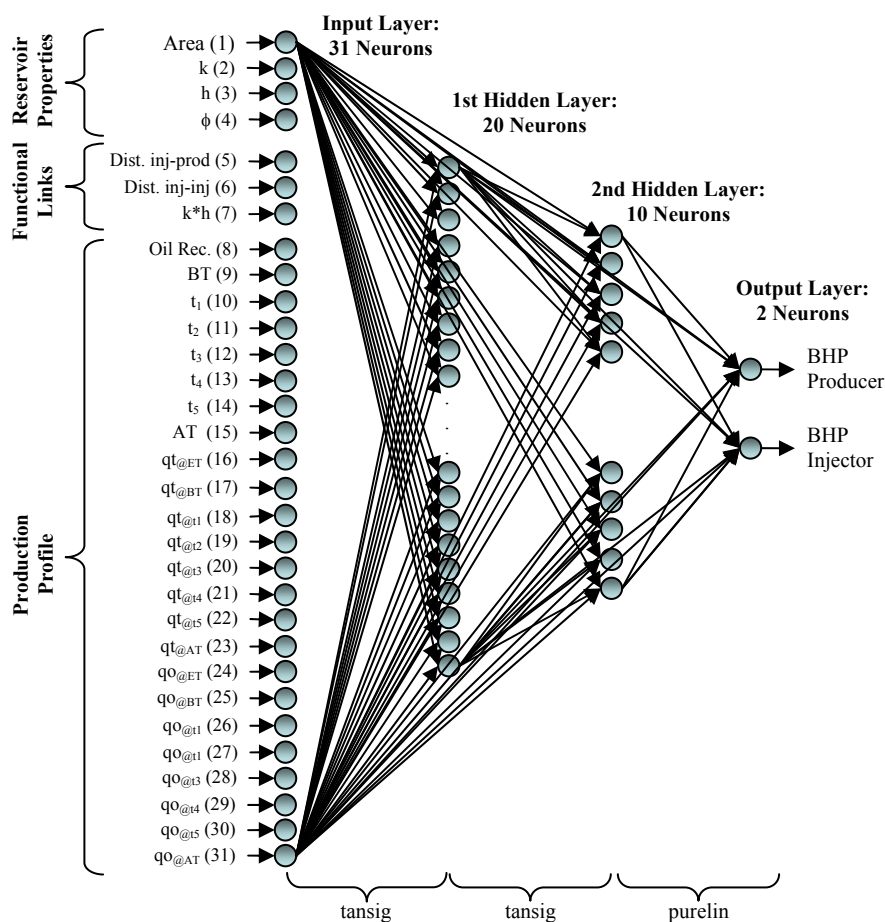
Figure **5-43**: Second Network Architecture for Field Development Plan

In order to evaluate the influence of the entire oil production curves on the prediction of pressures, a new network was built providing the values of time, cumulative production and production rate as additional inputs. Figure **5-43** shows the architecture of

this second network. Distances between wells were given as functional links. Also, the

logarithm function is applied to all inputs and outputs.
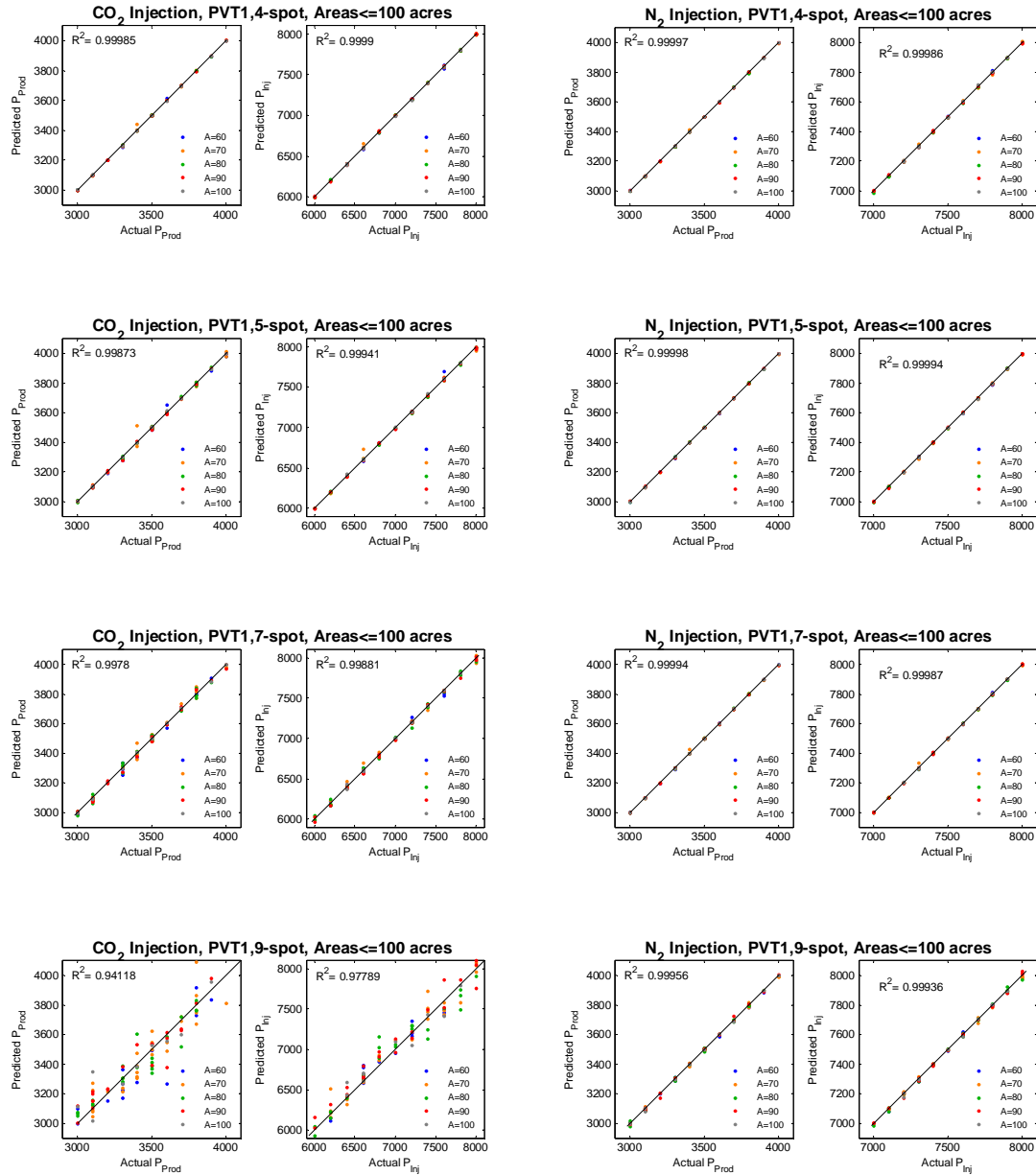
Figure **5-44**: Correlation Between Actual and Predicted Pressures (Testing). Miscible Displacement, PVT#1, Batch 1 (Small Areas), Second Network.

Figure **5-44** shows the pressure correlations obtained with the testing data sets for PVT#1 undergoing N_2 and CO_2 injection. It is obvious that the networks can predict accurately the production and injection pressures when the entire oil profile is given as an input. In order to establish which inputs have the highest impact on the performance of the network, a Hinton graph of weight matrix and bias vector was created. The Hinton graphs for PVT#1, batch 1, undergoing CO_2 and N_2 injection are shown in Figure **5-45**.
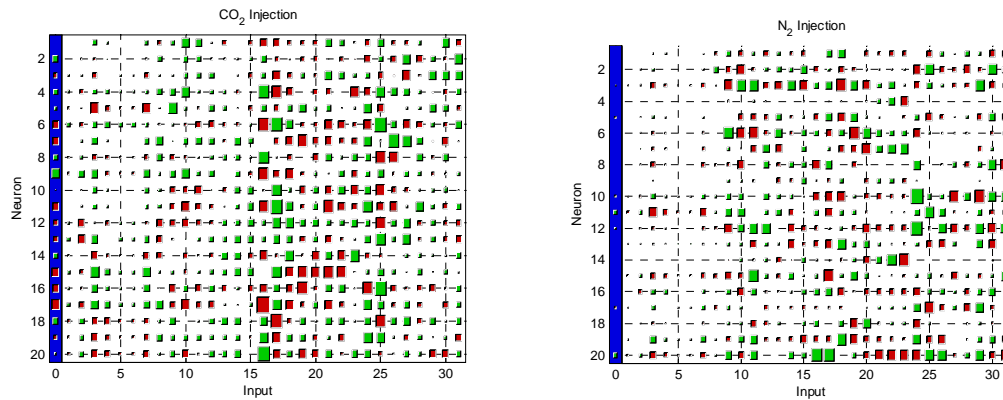
Figure **5-45**: Hinton Graphs for Second Inverse Network, batch 1, PVT#1, CO_2 and N_2 Injection.

In the Hinton graphs, the inputs with the highest impact correspond to the oil production curves. For CO_2 injection, inputs 16 to 26 have higher weights, which correspond to the cumulative oil production and oil rate values. For N_2 injection, the inputs with the highest weights are 9 to 31, which correspond to the entire oil production parameters as seen in Figure **5-43**.

The observations from the Hinton graphs indicate that oil recovery and abandonment time are not sufficient to provide accurate predictions. The complete oil

profile is necessary to incorporate the drive mechanisms involved in the miscible displacement processes into the network.

The objective of designing the inverse tool-box is to recommend diverse field development scenarios to the petroleum engineer before the reservoir is produced. Thus, the engineer can predict the reservoir performance using the suggested design parameters. Nevertheless, it is impossible to have the oil performance as part of the inputs in the inverse tool-box.

A workaround for this problem was to create a series of two networks, where the first network predicts the complete oil production profile from the reservoir characteristics and the oil recovery, and the second one incorporates the oil profile to finally forecast the operation pressures as shown in Figure **5-46**.
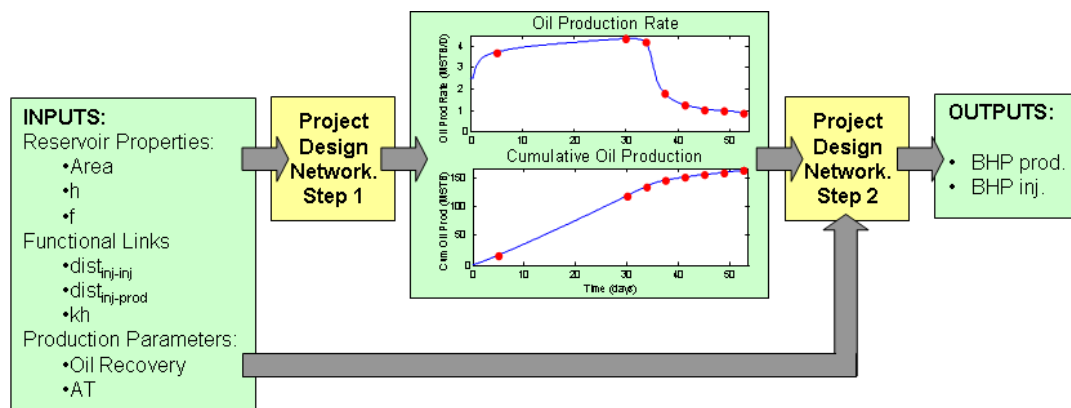
Figure **5-46**: Schematic of Inverse Network Steps

Generating two networks in series duplicates the number of required networks from 96 to 192, which may seem as laborious. In reality, building two networks in series

is convenient as it generates the complete oil profiles in a mid stage without the use of the forward networks.

The network architecture of Step 1 is shown in Figure **5-47** while the network architecture for Step 2 is the one shown previously in Figure **5-43**.
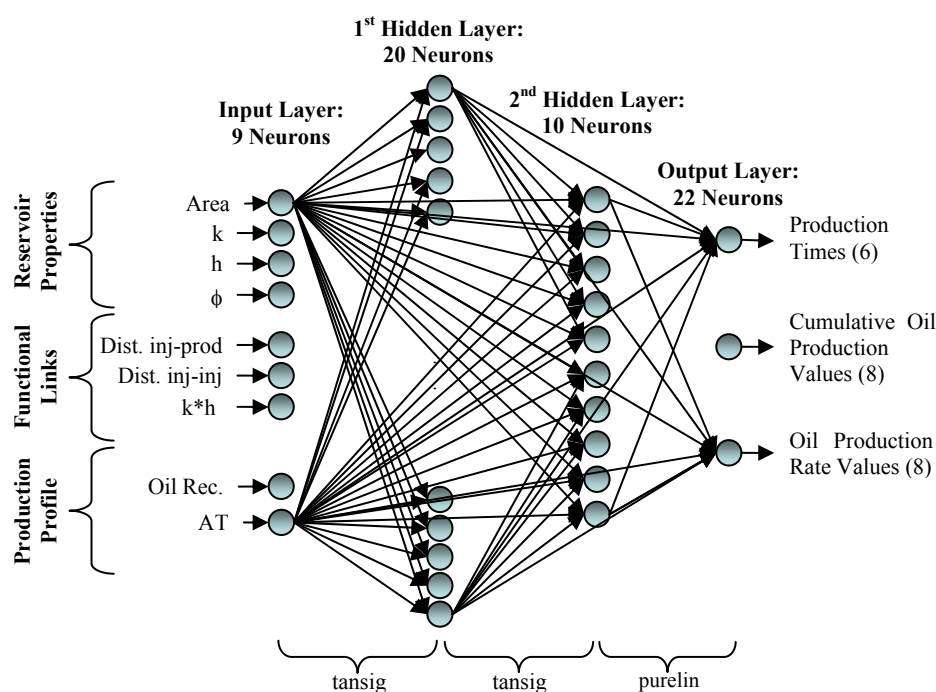
Figure **5-47**: Network Architecture for Field Development Plan – Step 1

Figure **5-48** shows the best and worst predicted parameters obtained from the Step-1 network for 4-Spot, PVT#1 with CO_2 injection. The error of the worst parameters was about 9%, while the average error was about 2%. These results indicate that the developed step-1 network effectively provides the complete oil production profile.
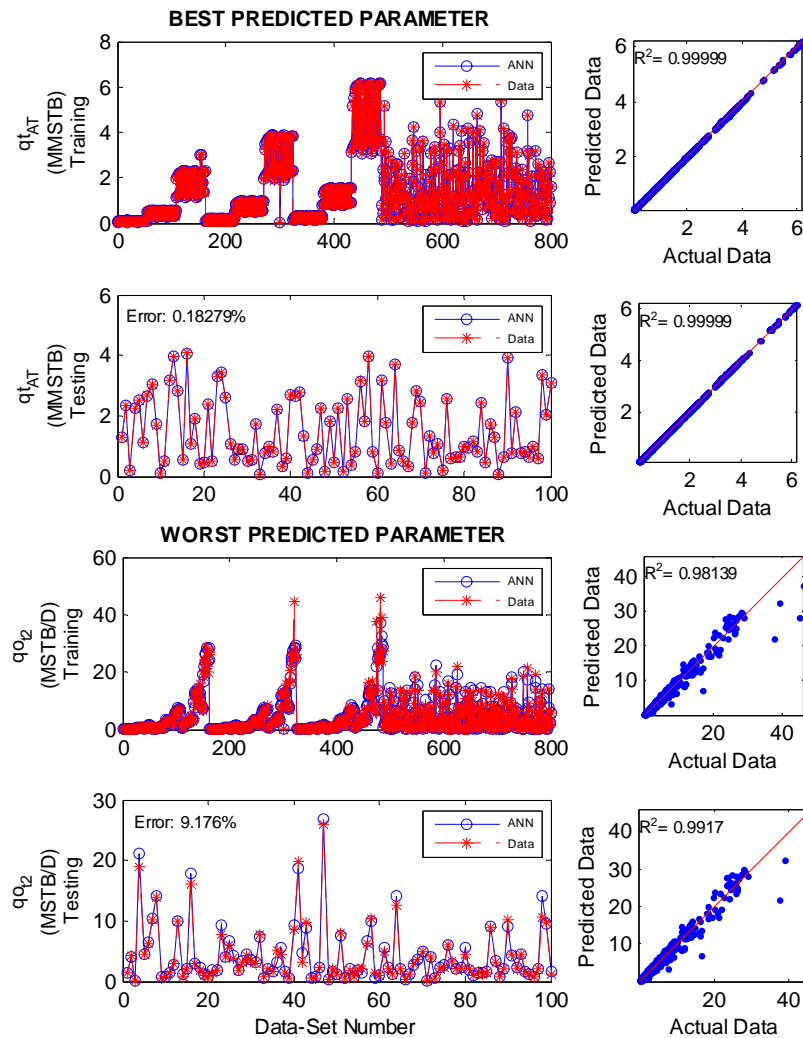
Figure **5-48**: Best and Worst Predicted Parameters using Inverse Network, Step-1, Batch 1, 4-Spot, PVT#1, CO_2 Injection.

An important observation is that the most significant inputs in forward networks were the pressures. Figure **5-49** shows the Hinton graphs for the forward and inverse networks using 4-Spot, PVT#1, Batch 1, CO_2 injection. In the forward case, the weights with the highest impact on this network are inputs 2, 3 and 9, which correspond to

production pressure, injection pressure and pressure gradient between wells. In the inverse case, the most influential inputs are 8 and 9, which are the oil recovery and abandonment time. This comparison implies that the influence of the pressures is overcome by the oil recovery and *AT*. Furthermore, it is clear that the relationship between the oil profile and the oil recovery and *AT* is stronger than the relationship between the operation pressures and the profiles since the inverse network provides comparable results with a less number of neurons per layer. Thus, the artificial neural networks are able to capture the connection between the diverse oil profile variables extracted from the numerical simulator.
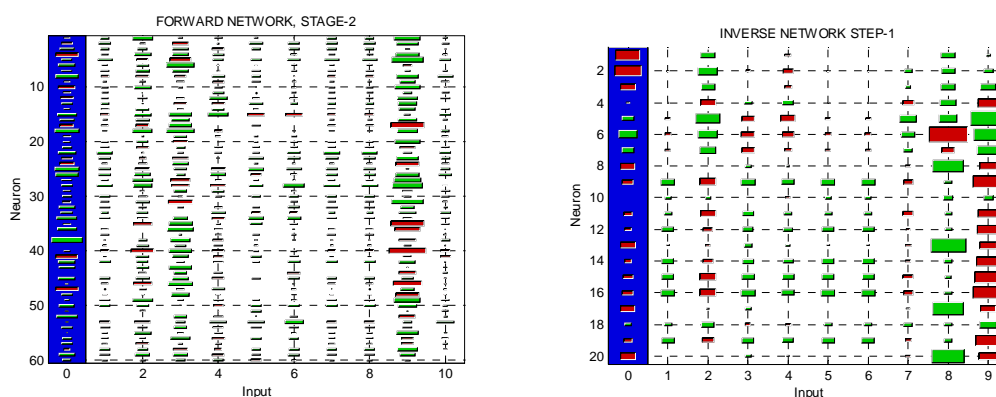
Figure **5-49**: Comparison of Hinton Graphs in Forward and Inverse Networks: Batch 1, 4-Spot, PVT#1, CO_2 Injection, (small areas).

Table **5-26** summarizes the absolute errors for the 22 predicted parameters for PVT#1 under CO_2 injection. The response of the network is very similar to the response observed in the forward application networks, where the oil production rate values were the most difficult variables to predict.

Table **5-26**: Absolute Error per Predicted Parameter. Inverse Network – Step-1. PVT#1, CO_2 Injection.

Parameter	Absolute Error (%)							
	4-Spot		5-Spot		7-Spot		9-Spot	
	A≤ 100	A> 100	A≤ 100	A> 100	A≤ 100	A> 100	A≤ 100	A> 100
BT	1.61	1.33	4.09	4.07	4.01	3.95	5.05	6.03
t_1	1.22	0.84	2.75	2.75	2.67	2.73	2.44	2.88
t2	0.92	0.72	1.92	1.85	1.80	1.80	1.41	1.65
t3	0.61	0.48	1.21	1.25	1.16	1.16	0.81	1.00
t4	0.38	0.34	0.82	0.73	0.68	0.74	0.57	0.64
t5	0.22	0.29	0.36	0.35	0.35*	0.35*	0.28*	0.41*
$qt_{@ET}$	2.29	2.76	10.72	8.63	6.00	4.34	6.48	10.51
qt_{BT}	1.81	1.12	0.71	0.80	1.82	1.94	3.20	3.64
qt_{t1}	1.31	0.91	1.33	1.44	1.35	1.34	1.89	3.33
qt_{t2}	0.76	0.58	1.62	1.56	0.75	0.72	2.34	2.63
qt_{t3}	0.35	0.29*	0.84	0.88	0.44	0.45	1.99	1.84
qt_{t4}	0.21	0.30	0.59	0.47	0.41	0.48	1.64	1.37
qt_{t5}	0.27	0.39	0.25	0.40	0.37	0.41	1.29	1.18
qt_{AT}	0.18*	0.29	0.24*	0.31*	0.38	0.49	1.23	1.24
$qo_{@ET}$	2.13	2.61	8.95	6.18	5.42	3.79	4.85	8.68
qo_{BT}	0.64	0.93	3.86	4.14	2.97	2.76	3.57	5.17
qo_{t1}	1.35	1.61	3.97	4.38	2.19	2.65	10.21**	12.49**
qo_{t2}	9.18**	10.46**	8.21	9.77	9.96**	11.10**	8.64	9.91
qo_{t3}	4.85	4.82	11.54**	10.47**	4.68	5.23	4.83	4.92
qo_{t4}	3.20	2.61	8.99	8.42	3.32	3.61	4.12	4.64
qo_{t5}	2.12	2.34	6.85	5.84	2.68	3.94	5.52	5.20
qo_{AT}	2.43	3.36	5.07	4.88	3.28	4.00	9.64	7.92

*: Best Parameter
**: Worst Parameter

Table **5-27** and Table **5-28** shows the error summary of the predicted pressure from the inverse networks developed for CO_2 and N_2, respectively.

Table **5-27**: Summary of Predicted Pressures in Inverse Network Step-2, CO_2 injection Processes

Fluid Type	Well Pattern	Area (acres)	Production Pressure				Injection Pressure			
			Min. Error (%)	Ave. Error (%)	S. D. Error (%)	Max. Error (%)	Min. Error (%)	Ave. Error (%)	S. D. Error (%)	Max. Error (%)
PVT #1	4-Spot	≤ 100	0.002	0.07	0.13	1.24	0.0001	0.08	0.10	0.89
		> 100	0.002	0.26	0.39	2.50	0.002	0.21	0.24	1.52
	5-Spot	≤ 100	0.002	0.07	0.13	1.24	0.0001	0.08	0.10	0.89
		> 100	0.0002	0.45	0.49	2.83	0.001	0.31	0.34	1.70
	7-Spot	≤ 100	0.0001	0.43	0.39	2.15	0.007	0.33	0.27	1.54
		> 100	0.020	0.69	0.62	3.51	0.009	0.48	0.38	1.87
	9-Spot	≤ 100	0.030	2.23	1.88	9.19	0.001	1.39	1.15	5.29
		> 100	0.009	1.11	1.06	4.79	0.010	0.85	0.73	4.08
PVT #2	4-Spot	≤ 100	0.038	1.60	1.28	7.62	0.006	0.53	0.45	2.35
		> 100	0.002	1.09	0.97	4.97	0.000	0.61	0.46	2.45
	5-Spot	≤ 100	0.040	1.06	0.90	5.03	0.002	0.51	0.44	2.44
		> 100	0.013	0.98	1.41	12.03	0.002	0.59	0.87	7.60
	7-Spot	≤ 100	0.014	1.74	1.55	8.55	0.011	0.63	0.58	2.89
		> 100	0.014	2.12	1.52	7.00	0.004	0.66	0.55	2.21
	9-Spot	≤ 100	0.003	2.24	1.72	8.05	0.006	0.67	0.77	4.99
		> 100	0.011	0.45	0.33	1.36	0.002	0.19	0.13	0.58
PVT #3	4-Spot	≤ 100	0.006	0.41	0.38	2.21	0.001	0.14	0.14	0.95
		> 100	0.001	0.20	0.20	1.32	0.002	0.08	0.07	0.44
	5-Spot	≤ 100	0.001	0.21	0.20	1.22	0.000	0.07	0.07	0.40
		> 100	0.005	0.21	0.24	1.99	0.0004	0.09	0.11	0.91
	7-Spot	≤ 100	0.002	0.48	0.44	2.17	0.002	0.19	0.17	0.88
		> 100	0.001	0.31	0.30	2.17	0.001	0.09	0.10	0.70
	9-Spot	≤ 100	0.003	0.53	1.01	7.50	0.0003	0.20	0.36	2.42
		> 100	0.016	0.73	1.38	10.21	0.002	0.26	0.42	3.33

Table **5-28**: Summary of Predicted Pressures in Inverse Network Step-2, N_2 injection Processes

Fluid Type	Well Pattern	Area (acres)	Production Pressure				Injection Pressure			
			Min. Error (%)	Ave. Error (%)	S. D. Error (%)	Max. Error (%)	Min. Error (%)	Ave. Error (%)	S. D. Error (%)	Max. Error (%)
PVT #1	4-Spot	≤ 100	0.0003	0.05	0.05	0.34	0.0002	0.05	0.05	0.21
		> 100	0.004	0.23	0.31	2.52	0.006	0.17	0.18	1.25
	5-Spot	≤ 100	0.0002	0.04	0.03	0.18	0.0003	0.03	0.03	0.15
		> 100	0.003	0.08	0.08	0.34	0.001	0.08	0.06	0.28
	7-Spot	≤ 100	0.001	0.05	0.08	0.78	0.001	0.04	0.06	0.52
		> 100	0.009	0.29	0.26	1.35	0.002	0.18	0.17	0.91
	9-Spot	≤ 100	0.002	0.20	0.17	0.85	0.004	0.11	0.09	0.41
		> 100	0.003	0.27	0.26	1.79	0.0003	0.14	0.14	0.95
PVT #2	4-Spot	≤ 100	0.002	0.97	0.78	3.79	0.000	0.12	0.10	0.58
		> 100	0.0004	1.19	1.27	8.34	0.000	0.15	0.11	0.49
	5-Spot	≤ 100	0.0001	0.55	0.53	2.28	0.002	0.15	0.12	0.61
		> 100	0.004	0.64	0.58	3.08	0.001	0.11	0.11	0.61
	7-Spot	≤ 100	0.031	1.20	0.99	5.69	0.004	0.18	0.12	0.57
		> 100	0.100	1.67	1.27	5.46	0.009	0.19	0.16	1.04
	9-Spot	≤ 100	0.012	1.01	1.86	11.51	0.003	0.12	0.15	0.91
		> 100	0.015	0.63	0.50	2.03	0.000	0.10	0.07	0.29
PVT #3	4-Spot	≤ 100	0.013	0.43	0.57	3.16	0.0002	0.14	0.18	1.09
		> 100	0.003	0.81	0.77	2.93	0.001	0.33	0.28	1.29
	5-Spot	≤ 100	0.004	0.36	0.33	1.60	0.002	0.13	0.10	0.48
		> 100	0.007	1.60	1.49	6.54	0.017	0.52	0.38	2.19
	7-Spot	≤ 100	0.003	0.82	0.84	4.56	0.003	0.31	0.29	1.48
		> 100	0.010	0.87	0.67	3.15	0.001	0.29	0.22	0.86
	9-Spot	≤ 100	0.001	1.26	1.08	5.72	0.018	0.44	0.37	2.07
		> 100	0.034	1.45	1.00	4.78	0.002	0.47	0.35	1.62

One important observation is that the injection pressure prediction is always better than the production pressure prediction. This was also consistently observed in the results from the first inverse network. The displacement mechanisms under consideration in this study depend on the minimum miscible pressure. The injection pressure is the only variable that can control whether the miscibility conditions will be achieved or not. Therefore, a limited range of pressure is suitable for miscible displacement applications. On the other hand, production pressure has an effect on the final recovery of the field.

The lower the bottom hole pressure, the higher the oil production. However, there is more flexibility in the range of production pressures, as long as there is enough pressure drawdown around the producer. Then, it is clear that the network is able to find a better connection between the reservoir performance and the injection pressure.

Correlations between actual and predicted pressures were calculated for all miscible displacement cases under study. These correlations are included in Appendix C.

5.2.2 Waterflooding Networks

The inverse networks for waterflooding recovery mechanism were also developed in two steps. The oil production profile parameters are calculated in the Step 1, while the operation pressures are calculated in Step 2. The architecture for Step 1 waterflooding network is shown in Figure **5-50**, whereas Figure **5-51** shows the architecture for Step 2 waterflooding network. The logarithm function is applied to all inputs and outputs.

Figure **5-52** shows the pressure correlations obtained from the inverse network Step 2 for PVT#2. A higher dispersion is observed compared to the results obtained in the miscible displacement case. In water injection, both pressures play an important role. The injection pressure maintains pressure while the production pressure controls the amount of produced fluid, including water. To some extend, the producer governs the abandonment condition imposed as a water cut constraint. Accordingly, it is concluded that the network is finding more challenging to relate both pressures to the drive mechanism involved in waterflooding.
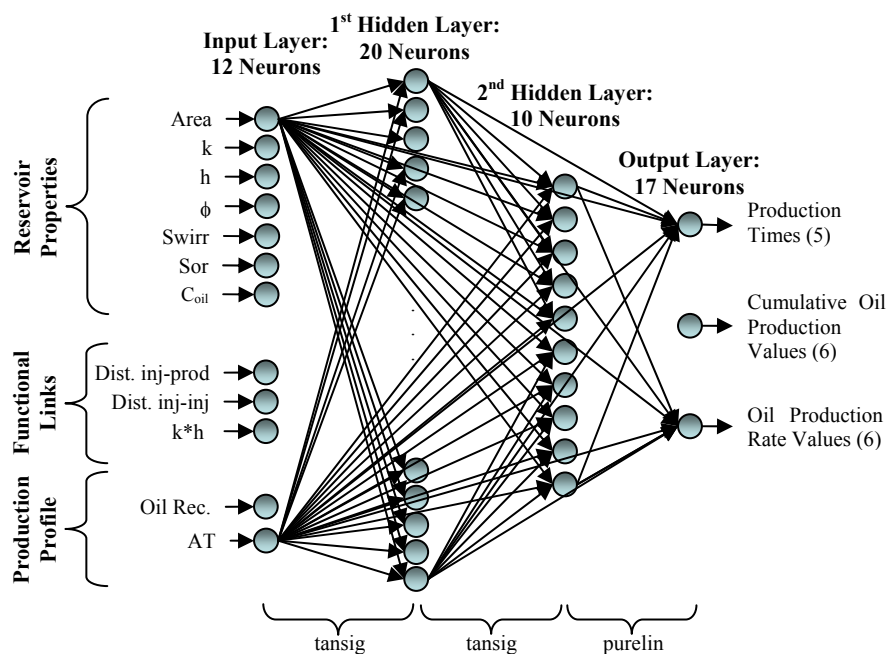
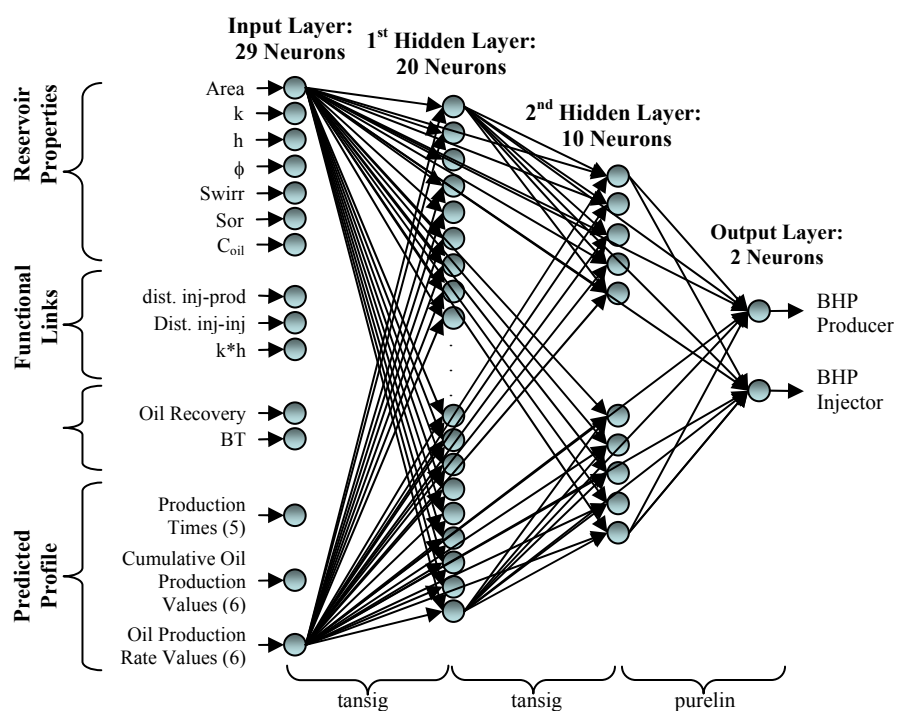Figure **5-50**: Inverse Network Architecture for Water Injection – Step 1

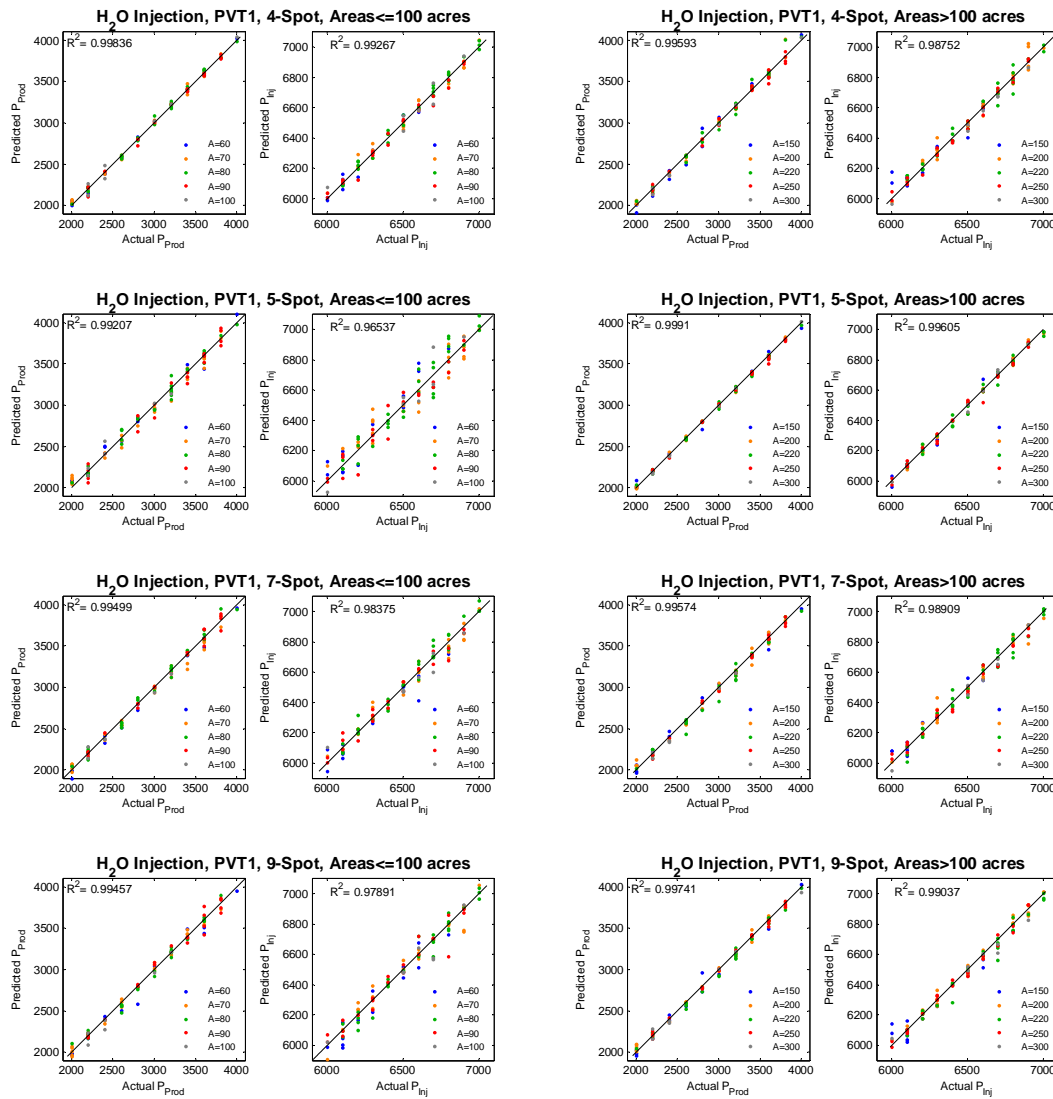Figure **5-51**: Inverse Network Architecture for Water Injection – Step 2

Figure **5-52**: Correlation Between Actual and Predicted Pressures (Testing). Waterflooding, PVT#1, Step-2 Inverse Network.

Table **5-29** summarizes the calculated errors for all water injection cases under study. Although the maximum error for production pressure seems very large, these values do not represent the network performance as they may be the result of a particular

case with high deviation. The average error and standard deviation show that the networks provide prediction within acceptable margin of deviation. Also, they show that predicted injection pressures are slightly better than the predicted production pressures.

Table **5-29**: Summary of Predicted Pressures in Inverse Network Step-2, H_2O Injection Processes

Fluid Type	Well Pattern	Area (acres)	Production Pressure				Injection Pressure			
			Min. Error (%)	Ave. Error (%)	S. D. Error (%)	Max. Error (%)	Min. Error (%)	Ave. Error (%)	S. D. Error (%)	Max. Error (%)
PVT #1	4-Spot	≤ 100	0.016	1.02	0.94	4.22	0.001	0.43	0.34	1.49
		> 100	0.000	1.42	1.26	5.76	0.006	0.53	0.49	2.95
	5-Spot	≤ 100	0.045	2.25	1.65	7.51	0.015	0.98	0.70	2.76
		> 100	0.000	0.66	0.66	4.30	0.008	0.30	0.26	1.24
	7-Spot	≤ 100	0.002	1.64	1.24	5.33	0.004	0.62	0.51	2.81
		> 100	0.016	1.54	1.26	6.24	0.002	0.53	0.41	2.08
	9-Spot	≤ 100	0.013	1.63	1.42	7.55	0.004	0.67	0.67	3.14
		> 100	0.058	1.22	1.07	5.87	0.021	0.48	0.42	2.39
PVT #2	4-Spot	≤ 100	0.016	1.54	1.26	6.24	0.002	0.53	0.41	2.08
		> 100	0.040	4.12	4.81	29.88	0.054	0.93	0.70	3.16
	5-Spot	≤ 100	0.008	2.70	2.76	14.53	0.031	0.81	0.81	4.85
		> 100	0.015	4.38	4.76	33.74	0.039	0.89	0.76	4.25
	7-Spot	≤ 100	0.016	3.19	2.66	13.49	0.000	0.69	0.64	4.52
		> 100	0.016	3.74	3.74	23.69	0.016	1.02	0.86	3.73
	9-Spot	≤ 100	0.078	4.96	4.09	21.08	0.007	1.15	1.08	4.70
		> 100	0.095	3.93	3.85	19.28	0.001	0.88	0.73	3.15
PVT #3	4-Spot	≤ 100	0.275	4.86	4.41	23.20	0.014	1.39	1.11	5.94
		> 100	0.075	4.60	4.34	18.39	0.001	1.37	1.14	5.43
	5-Spot	≤ 100	0.048	3.91	3.08	13.95	0.002	1.08	0.91	5.16
		> 100	0.018	3.25	2.49	9.51	0.008	1.14	0.89	4.62
	7-Spot	≤ 100	0.028	6.40	6.10	30.73	0.000	1.74	1.39	6.96
		> 100	0.021	5.58	5.02	24.35	0.026	1.55	1.34	6.53
	9-Spot	≤ 100	0.008	3.15	3.62	31.65	0.001	1.15	0.87	4.10
		> 100	0.064	2.21	2.07	8.16	0.012	0.87	0.60	2.48

5.2.3 Steam Injection Networks

The steam injection networks were also developed in two steps. The structure of the first step is similar to the waterflooding, which was shown in Figure **5-50**. They only differ in the number of neurons in the output layer. In steam injection network, the oil profile consists of 5 values of production time, 7 values of cumulative oil production and 7 values of oil production rate, for a total of 19 neurons in the output layer.

The design parameters for a steam injection project besides the operation pressures should include the injection temperature. The appropriate combination of temperature and pressure at the injector defines the difference between hot water injection from steam injection. Thus, temperature was initially set as one of the outputs from the Step 2 inverse network. The architecture of the Step 2 network is similar to the one shown in Figure **5-51**, with the difference that the output layer includes the injection temperature.

Figure **5-53** shows the results obtained from one network that predicted the operation conditions at the wells from the reservoir properties and the complete oil production profile. It is evident that the network cannot predict the temperature accurately. The predicted pressures, though present a high deviation, are not as deviated as temperature.

Different training protocols were tried in order to design a network that predicts accurately the operation temperature. However, none of the designs provided acceptable results.
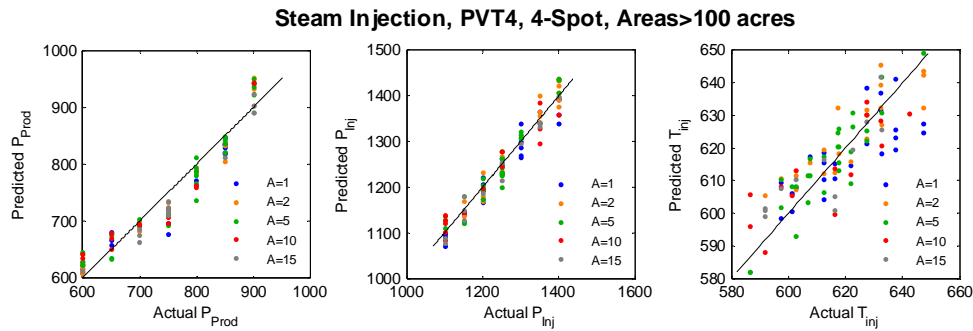
Figure **5-53**: Prediction of Operation Pressure and Temperature.

The idea of predicting temperature was to include it as part of the design parameters that the tool-box provides to the user. Then, a workaround for this problem was to use the tool-box itself to evaluate values of temperature as it is done for the areas. The temperature is specified as an input of the inverse networks. For each predicted set of operation pressures, there is a corresponding value of temperature. The tool-box evaluates diverse scenarios, and provides the optimum case based on minimum injection pressure criterion. Selecting the minimum injection pressure also leads to an optimum injection temperature. The lower the pressure, the lower is the required temperature to form steam with quality of one.

Figure **5-54** and Figure **5-55** shows the architectures of the Step 1 and Step 2 inverse networks for steam injection, respectively. Notice that the temperature is given to the networks as the gradient above the saturation temperature. The saturation temperature is calculated from the injection pressure in the tool-box, and the injection temperature is calculated by adding these two values. In addition, function 2 given earlier in Eq. **5.2** is used as a functional link.
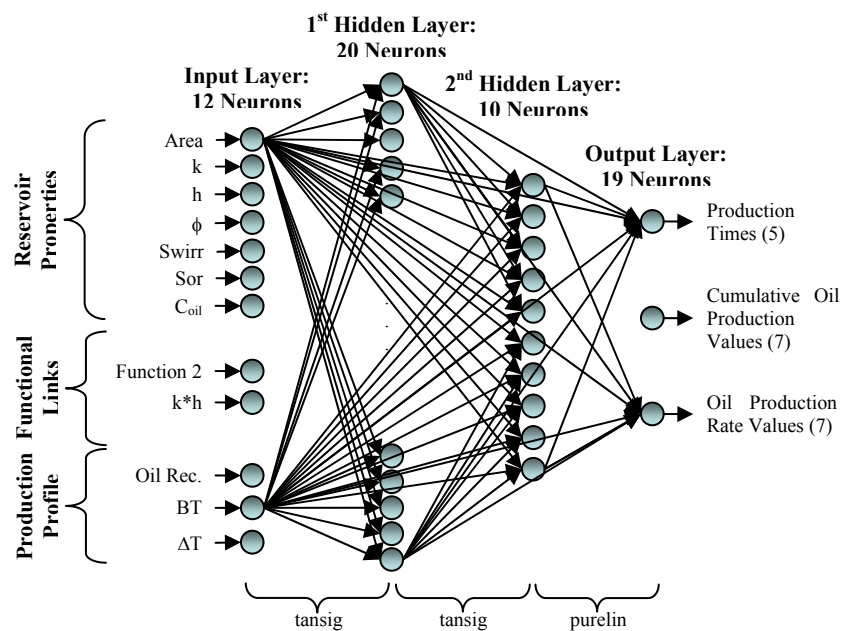
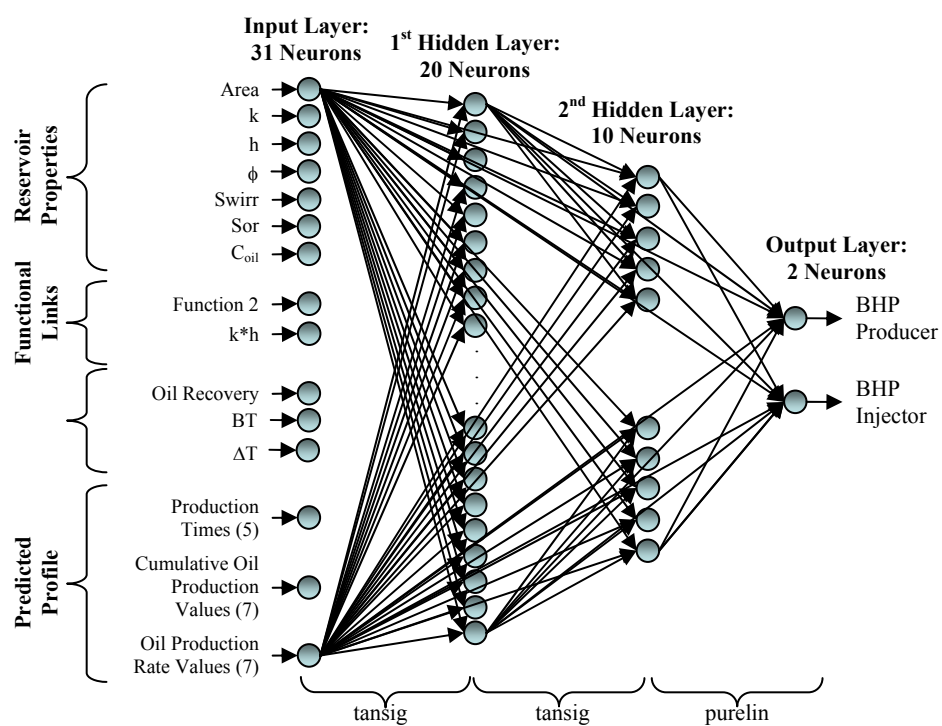Figure **5-54**: Inverse Network Architecture for Steam Injection – Step 1

Figure **5-55**: Inverse Network Architecture for Steam Injection – Step 2

Figure **5-56** shows the predicted pressures when steam is injected into a reservoir holding fluid PVT#2. It seems that the injection pressure presents a higher deviation. However, that is a visual artifact of the scales used. Table **5-30** shows a summary of the calculated errors. The results show that the deviation among these operation conditions is analogous. In general, these predictions imply an efficient network performance.
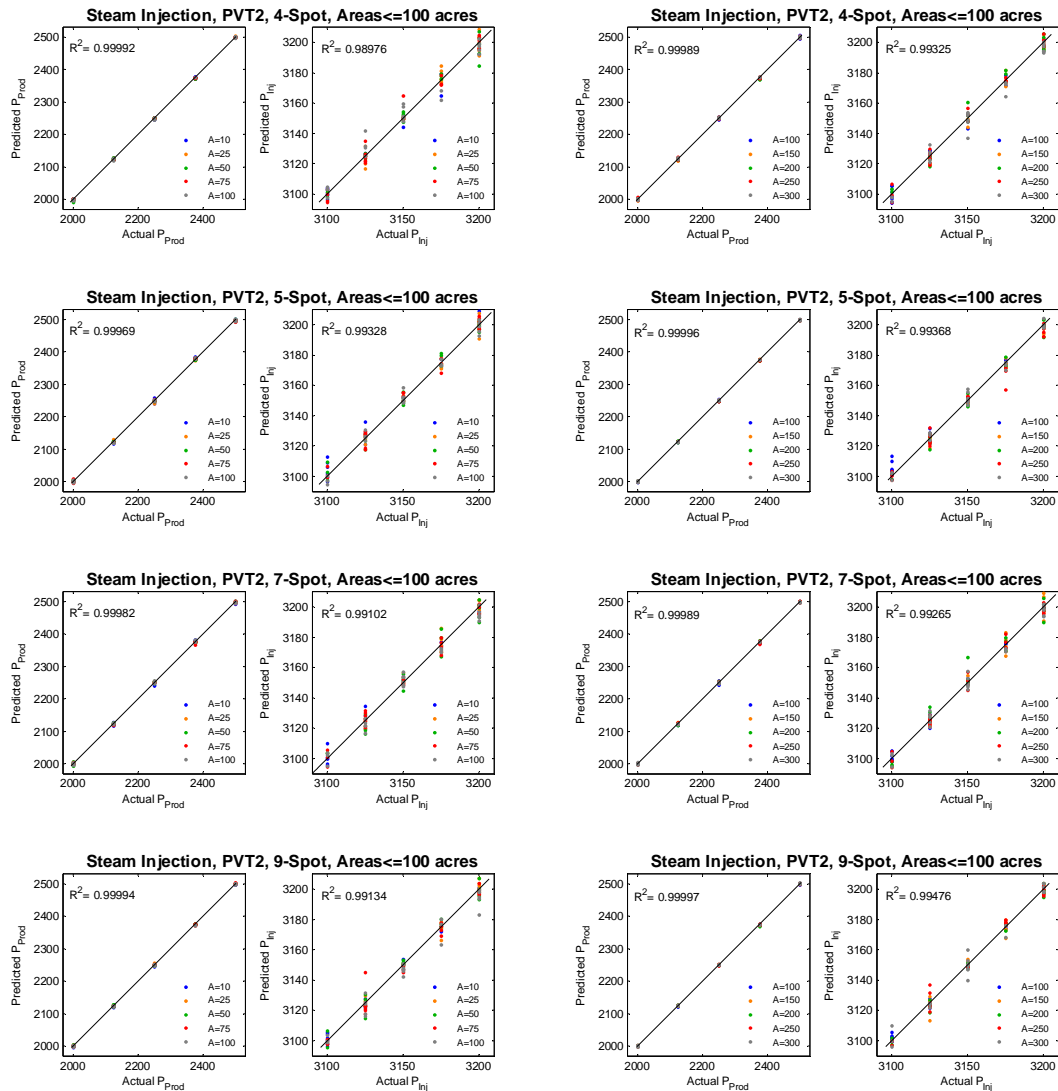
Figure **5-56**: Correlation Between Actual and Predicted Pressures (Testing). Steam Injection, PVT#1, Batch 1&2, Step-2 Inverse Network.
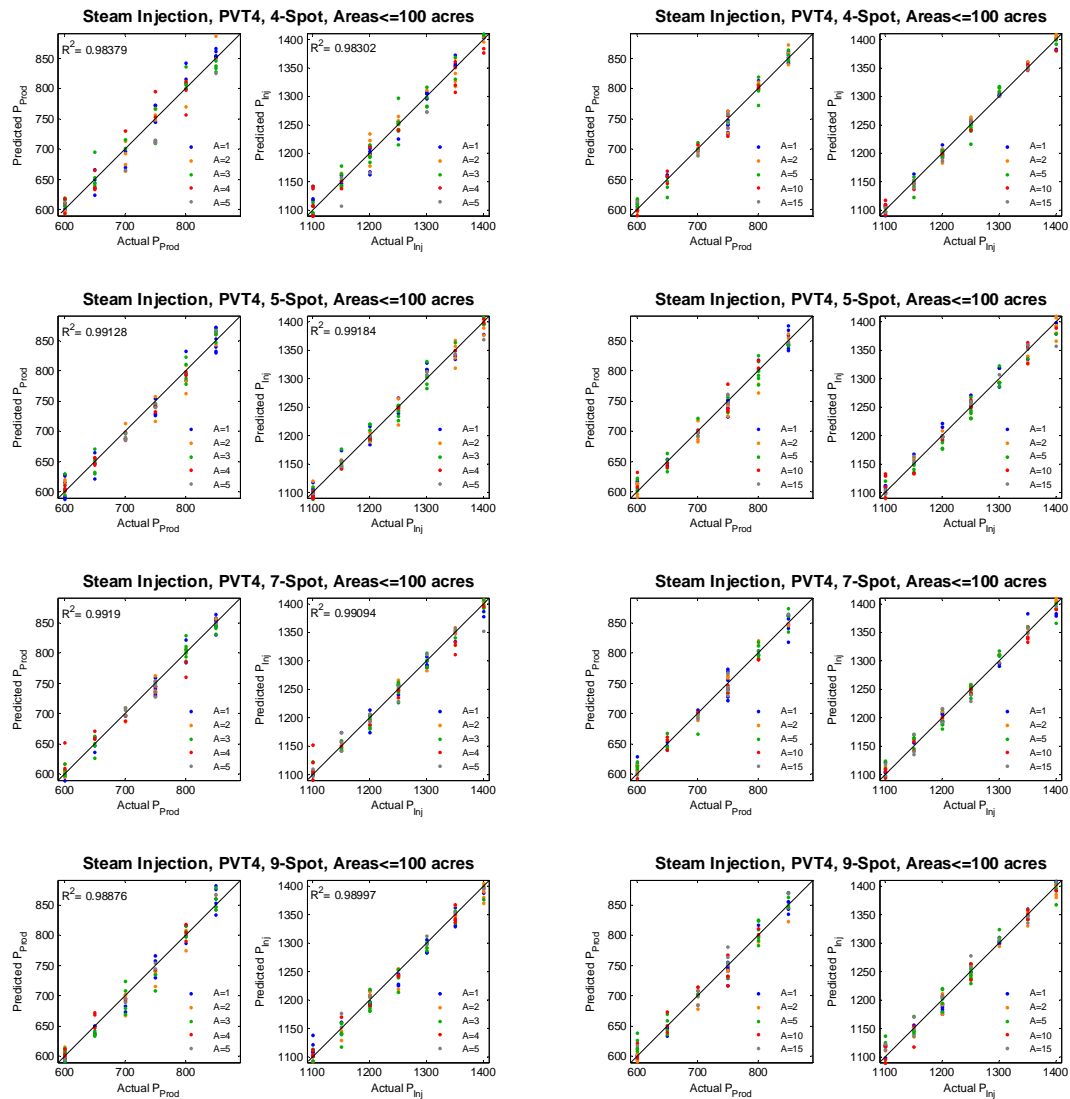
Figure **5-57**: Correlation Between Actual and Predicted Pressures (Testing). Steam Injection, PVT#4, Step-2 Inverse Network.

Figure **5-57** shows the predicted pressures using PVT#4. These results show that the chosen architecture for steam injection was adequate as the pressures are predicted within acceptable deviation. Moreover, production pressures show a slightly higher deviation, as it can be seen in Table **5-30**. This was not observed in either PVT#2 or

PVT#3. This outcome could be a consequence of the heat front never reaching the producer in the modeled cases with PVT#2 and PVT#3. Evidently, it is more complex for the network to capture the thermal effects around the producer.

Table **5-30**: Summary of Predicted Pressures in Inverse Network Step-2, Steam Injection Processes

Fluid Type	Well Pattern	Area (acres)	Production Pressure				Injection Pressure			
			Min. Error (%)	Ave. Error (%)	S. D. Error (%)	Max. Error (%)	Min. Error (%)	Ave. Error (%)	S. D. Error (%)	Max. Error (%)
PVT #2	4-Spot	≤ 100	0.000	0.08	0.07	0.45	0.000	0.12	0.11	0.54
		> 100	0.001	0.10	0.07	0.32	0.006	0.11	0.08	0.41
	5-Spot	≤ 100	0.001	0.16	0.11	0.50	0.003	0.10	0.09	0.41
		> 100	0.001	0.06	0.04	0.19	0.001	0.09	0.09	0.56
	7-Spot	≤ 100	0.002	0.11	0.09	0.45	0.001	0.12	0.09	0.42
		> 100	0.004	0.09	0.07	0.29	0.004	0.10	0.09	0.54
	9-Spot	≤ 100	0.000	0.07	0.06	0.28	0.003	0.10	0.11	0.65
		> 100	0.001	0.05	0.04	0.27	0.001	0.08	0.08	0.38
PVT #3	4-Spot	≤ 100	0.001	0.04	0.03	0.14	0.001	0.05	0.05	0.19
		> 100	0.000	0.03	0.03	0.13	0.002	0.05	0.05	0.28
	5-Spot	≤ 100	0.003	0.11	0.10	0.63	0.002	0.08	0.07	0.41
		> 100	0.0001	0.06	0.05	0.22	0.0001	0.09	0.11	0.91
	7-Spot	≤ 100	0.001	0.07	0.05	0.20	0.0001	0.06	0.06	0.36
		> 100	0.0004	0.06	0.05	0.20	0.0001	0.07	0.05	0.21
	9-Spot	≤ 100	0.001	0.07	0.06	0.27	0.0001	0.08	0.07	0.33
		> 100	0.0003	0.04	0.03	0.16	0.002	0.08	0.10	0.88
PVT #4	4-Spot	≤ 100	0.006	1.98	1.66	6.92	0.028	1.18	0.96	3.82
		> 100	0.008	1.13	0.93	4.53	0.001	0.62	0.50	2.66
	5-Spot	≤ 100	0.002	1.58	1.20	5.14	0.002	0.81	0.63	2.52
		> 100	0.003	1.52	1.18	5.79	0.001	0.91	0.67	3.06
	7-Spot	≤ 100	0.014	1.35	1.29	8.70	0.008	0.81	0.75	4.70
		> 100	0.047	1.43	1.06	4.94	0.018	0.82	0.57	2.48
	9-Spot	≤ 100	0.032	1.72	1.40	7.83	0.007	0.91	0.69	3.46
		> 100	0.004	1.61	1.25	6.48	0.024	0.91	0.69	3.34

5.2.4 Relevancy of Inputs to Developed Networks for the Project Design Tool-Box

The relevancy of the inputs to the networks developed for the project design toolbox was also determined. The sorting of the properties indicates what reservoir properties should be entered into the tool-box carefully. Table **5-31** shows the sorting of the weights per input parameter for each CO_2 injection network as well as the average sorting of all CO_2 injection networks. The reservoir properties sorted in descending order of relevancy for these networks are abandonment time, oil recovery, permeability, porosity, area and thickness.

Table **5-31**: Sorting of Weights for CO_2 Injection Project Design Networks

PVT	Spot	Size	Input Parameters								
			Area	K	h	poro	$d_{inj\text{-}inj}$	$d_{inj\text{-}prod}$	kh	Oil Rec	AT
1	4	Small	8	3	4	9	6	7	5	1	2
		Large	9	3	4	5	8	7	6	2	1
	5	Small	8	2	5	6	7	9	4	3	1
		Large	8	3	4	6	7	9	5	2	1
	7	Small	5	8	3	2	-	4	7	1	6
		Large	3	2	6	8	-	4	7	5	1
	9	Small	5	6	9	7	4	3	8	2	1
		Large	4	3	9	8	5	6	7	2	1
2	4	Small	7	3	8	4	5	6	9	2	1
		Large	7	3	6	4	9	8	5	2	1
	5	Small	7	4	8	3	6	5	9	2	1
		Large	7	3	9	4	6	8	5	2	1
	7	Small	5	3	8	4	-	6	7	2	1
		Large	7	2	6	4	-	8	5	3	1
	9	Small	8	2	9	3	7	6	5	4	1
		Large	5	3	9	8	6	7	4	2	1
3	4	Small	7	3	6	4	8	9	5	2	1
		Large	6	3	4	8	5	7	9	2	1
	5	Small	5	3	9	4	6	7	8	1	2
		Large	8	3	6	4	9	7	5	1	2
	7	Small	6	4	7	3	-	5	8	1	2
		Large	5	3	8	6	-	4	7	2	1
	9	Small	7	5	3	6	8	9	4	2	1
		Large	7	3	4	6	8	9	5	1	2
Average Sorting			**6**	**3**	**7**	**4**	**8**	**9**	**5**	**2**	**1**

Table **5-32** shows the sorting of the weights per input parameter for each N$_2$ injection network as well as the average sorting of all N$_2$ injection networks. The reservoir properties listed in descending order of relevancy for these networks are abandonment time, oil recovery, permeability, porosity and thickness.

Table **5-32**: Sorting of Weights for N$_2$ Injection Project Design Networks

| PVT | Spot | Size | Input Parameters | | | | | | | | |
			Area	K	h	poro	d$_{inj-inj}$	d$_{inj-prod}$	kh	Oil Rec	AT
1	4	Small	7	5	3	6	8	9	4	2	1
		Large	9	3	4	6	8	7	5	2	1
	5	Small	8	3	5	4	9	7	6	2	1
		Large	7	3	6	4	9	8	5	2	1
	7	Small	7	5	3	8	-	6	4	2	1
		Large	8	2	4	5	-	7	6	3	1
	9	Small	9	4	3	6	7	8	5	2	1
		Large	7	3	5	4	9	8	6	2	1
2	4	Small	4	7	8	3	5	6	9	1	2
		Large	8	3	6	4	7	9	5	2	1
	5	Small	8	3	9	4	7	6	5	2	1
		Large	9	3	6	4	8	7	5	1	2
	7	Small	5	4	7	3	-	6	8	2	1
		Large	3	5	8	7	-	4	6	2	1
	9	Small	5	8	6	9	3	4	7	2	1
		Large	7	2	3	9	6	5	4	8	1
3	4	Small	8	3	5	4	9	7	6	1	2
		Large	7	3	5	4	9	8	6	1	2
	5	Small	9	4	3	6	8	7	5	1	2
		Large	9	3	6	5	8	7	4	1	2
	7	Small	8	3	5	4	-	7	6	1	2
		Large	8	3	6	4	-	7	5	2	1
	9	Small	7	5	3	6	8	9	4	2	1
		Large	9	2	6	4	7	8	5	3	1
Average Sorting			**8**	**3**	**5**	**4**	**9**	**7**	**6**	**2**	**1**

Table **5-33** shows the sorting of the weights per input parameter for each waterflooding network as well as the average sorting of all water injection networks. The reservoir properties listed in descending order of relevancy for these networks are oil

recovery, abandonment time, thickness, C_{oil} coefficient, residual oil saturation, permeability, irreducible water saturation and porosity.

Table **5-33**: Sorting of Weights for H_2O Injection Project Design Networks

| PVT | Spot | Size | Input Parameter | | | | | | | | | | | |
			Area	K	h	poro	S_{wirr}	S_{or}	C_{oil}	$d_{inj-inj}$	$d_{inj-prod}$	kh	Oil Rec	AT
1	4	Small	10	8	4	9	6	3	5	12	11	7	1	2
		Large	10	6	4	9	8	5	1	12	11	7	3	2
	5	Small	10	8	4	9	7	5	3	12	11	6	1	2
		Large	12	6	4	8	9	5	3	10	11	7	1	2
	7	Small	10	7	2	9	8	5	3	-	11	6	1	4
		Large	11	6	4	9	8	5	3	-	10	7	1	2
	9	Small	12	7	3	8	9	6	2	11	10	5	1	4
		Large	10	5	3	9	7	4	6	12	11	8	1	2
2	4	Small	6	11	8	12	10	3	7	4	5	9	1	2
		Large	11	5	3	7	12	4	6	9	10	8	1	2
	5	Small	6	9	8	10	11	3	4	5	7	12	1	2
		Large	10	7	4	12	6	2	5	9	11	8	1	3
	7	Small	10	7	5	8	9	3	4	-	11	6	1	2
		Large	10	7	3	8	9	5	4	-	11	6	2	1
	9	Small	8	10	2	12	11	4	5	9	7	6	1	3
		Large	9	8	2	12	7	3	4	10	11	6	1	5
3	4	Small	12	7	3	8	9	5	4	11	10	6	2	1
		Large	9	5	1	8	12	7	3	10	11	6	4	2
	5	Small	11	7	4	9	8	5	2	10	12	6	1	3
		Large	11	6	3	8	9	7	4	10	12	5	1	2
	7	Small	10	8	5	9	7	3	2	-	11	6	1	4
		Large	11	5	3	8	9	4	7	-	10	6	2	1
	9	Small	11	8	4	9	7	5	2	12	10	6	1	3
		Large	12	6	2	9	8	5	4	11	10	7	1	3
Average Soting			**11**	**7**	**3**	**9**	**8**	**5**	**4**	**10**	**12**	**6**	**1**	**2**

Table **5-34** shows the sorting of the weights per input parameter for each waterflooding network. Similar to the screening networks, the responses of the steam networks with heavy oil were different from those with light and black oil networks. Therefore, the average sorting of all networks with heavy oil is reported separately from the light and black oils. The reservoir properties organized in descending order of impact

for the light and black oil networks are abandonment time, area, thickness, permeability, residual oil saturation, porosity, irreducible water saturation, C_{oil} coefficient and ΔT. For the heavy oil networks, the properties listed in descending order are residual oil saturation, irreducible water saturation, abandonment time, oil recovery, area, thickness, permeability, porosity, C_{oil} coefficient and ΔT.

Table **5-34**: Sorting of Weights for Steam Injection Project Design Networks

PVT	Spot	Size[*]	Area	K	h	poro	S_{wirr}	S_{or}	C_{oil}	ΔT	FL1[**]	kh	Oil Rec	AT
2	4	S	5	6	4	8	10	9	11	12	1	7	2	3
		L	4	6	5	10	9	7	12	11	2	8	1	3
	5	S	7	4	5	8	9	6	11	12	2	10	1	3
		L	3	5	7	9	10	6	12	11	2	8	1	4
	7	S	5	4	7	9	8	6	11	12	2	10	1	3
		L	3	5	8	9	7	6	11	12	4	10	1	2
	9	S	5	7	4	9	10	6	11	12	1	8	2	3
		L	4	7	6	9	8	5	12	11	2	10	1	3
3	4	S	5	6	4	8	10	9	11	12	1	7	2	3
		L	4	5	9	8	7	6	12	11	2	10	1	3
	5	S	5	6	4	7	9	8	11	12	2	10	1	3
		L	4	6	5	9	10	7	12	11	1	8	2	3
	7	S	5	8	3	7	10	9	11	12	1	6	2	4
		L	4	6	7	9	8	5	12	11	2	10	1	3
	9	S	5	10	4	7	8	6	11	12	1	9	2	3
		L	4	9	5	8	7	6	11	12	1	10	2	3
Average Sorting			**4**	**6**	**5**	**8**	**9**	**7**	**11**	**12**	**2**	**10**	**1**	**3**
4	4	S	6	9	7	10	2	1	12	11	5	8	4	3
		L	7	10	6	8	2	1	11	12	4	9	5	3
	5	S	6	8	7	10	2	1	11	12	5	9	3	4
		L	6	8	7	9	2	1	11	12	3	10	5	4
	7	S	6	10	7	9	2	1	11	12	3	8	4	5
		L	6	10	7	8	2	1	12	11	4	9	5	3
	9	S	6	10	7	8	2	1	11	12	3	9	4	5
		L	6	7	9	11	2	1	10	12	5	8	4	3
Average Sorting			**6**	**9**	**7**	**10**	**2**	**1**	**11**	**12**	**4**	**8**	**5**	**3**

Size[*]: S=small, L=large
FL1[**]: Functional Link 1

5.2.5 User Interface for IOR Project Design Tool-box

A total of 196 inverse networks were developed in order to determine the development plan parameters for particular reservoirs. These networks were incorporated into a tool-box that evaluates diverse production schemes with the aim to suggest optimum scenarios. The tool-box consists of a graphical user interface (*GUI*) where the reservoir characteristics and field development parameters are evaluated by accessing the built inverse networks, selection of optimum scenarios is performed and results are provided graphically.

The networks incorporated in the project design tool-box were built with the data sets generated for the screening tool-box. Design of experiments was applied to the network inputs to ensure an efficient network performance in a wide range of inputs limits. The inputs to the forward networks were the same input variables to the numerical reservoir simulation, so that the forward networks were designed under a strict control. In the inverse application, some network inputs are values calculated by the simulator. Therefore, it is not possible to control theirs limits. That is the case of abandonment time and total oil recovery, whose limits are controlled by many factors such as the recovery mechanism, thermodynamics, Darcy's Law, continuity equation, energy balance, etc. Then, it is not possible to generate extensive input data sets for the inverse application using design of experiments.

The limits for *AT* and oil recovery used in the project design tool-box were defined by the highest and lowest values calculated by the numerical reservoir, while the reservoir characteristics were limited as in the forward tool. Some combinations of

network inputs may be within the allowable input data ranges. However, they may lead to wrong results as the inverse networks may predict operation conditions that are not within the specified ranges used in the design of experiments. The tool-box was designed considering this problem.

Inside the tool-box, five values of areas are evaluated to provide an optimum production scheme per well pattern. The selection of these areas was not arbitrary as they match the area values specified when generating the data sets using the design of experiments. Then, five sets of field development plan are forecasted. The tool identifies the production scheme with the minimum injection pressure, and verifies if the predicted injection and production pressures are within the pressure limits given to the numerical simulator. For example, the water was injected between 4000 and 6000 psia for the cases with PVT#2 and PVT#3, while oil was produced within 1000 and 2000 psia. If the optimum case leads to pressures that are out of these ranges, the tool-box eliminates the case and selects the second minimum pressure. If all five scenarios lead to operation pressures out of range, the tool will indicate that some illogical results were obtained with the entered inputs. The minimum injection pressure selection also removes the issue of uniqueness encountered when two different reservoir cases may produce the same oil recovery. Since the networks involve some numerical errors, the pressure limits were expanded by 15%. That is, if the maximum injection pressure is 4000 psia, the tool-box will account 4600 psia as a permissible result.

Table **5-35** and Table **5-36** summarize the *AT* and oil recovery limits obtained from the reservoir simulator for all cases under study. It is clear that *AT* and oil recovery are within different limits depending upon the recovery method, fluid and well pattern.

This incorporates a major constrain in the design of the tool-box as it was not possible to evaluate and compare different IOR methods at the same time. Comparison between IOR methods must be done manually by the user who should provide adequate inputs that works for all IOR methods. Comparisons of different well patterns were performed by taking common limits of *AT* and recovery for all well patterns. The limits were defined by the highest and lowest values among the patterns. Unfortunately, this increases the probability of ending with illogical results.

Table **5-35**: Abandonment Time and Oil Recovery Limits for PVT#1 Inverse Networks

Fluid	IOR	Area	4 Spot		5 Spot		7 Spot		9 Spot	
			AT	%Rec	AT	%Rec	AT	%Rec	AT	%Rec
PVT1	CO$_2$	Large	30	69	30	70	14	69	25	42
			669	86	815	80	365	86	873	82
		Small	43	69	43	67	21	69	40	44
			4169	86	4971	80	2467	86	5443	81
	N$_2$	Large	23	38	24	37	13	39	24	39
			349	44	382	42	171	42	395	43
		Small	31	38	37	34	18	39	35	39
			2138	44	2410	41	1038	43	2430	42
	H$_2$O	Large	25	4	29	4	12	4	9	4
			3115	65	3729	65	1475	65	2443	65
		Small	87	4	36	3	83	4	11	2
			66254	63	21291	63	61167	63	14573	60

Table **5-36**: Abandonment Time and Oil Recovery Limits for PVT#2, PVT#3 & 4 Inverse Networks

Fluid	IOR	Area	4 Spot		5 Spot		7 Spot		9 Spot	
			AT	%Rec	AT	%Rec	AT	%Rec	AT	%Rec
PVT2	CO_2	Large	16	89	18	86	7	89	20	87
			290	93	326	90	146	93	546	89
		Small	85	92	24	86	11	89	29	87
			133	93	1986	90	870	93	3487	89
	N_2	Large	13	59	7	53	7	53	16	54
			313	71	154	69	154	69	379	63
		Small	20	58	23	50	9	52	22	54
			1942	72	2380	64	923	70	2355	64
	H_2O	Large	20	16	23	15	10	15	9	9
			2265	72	2578	72	1127	72	893	69
		Small	28	15	30	14	14	15	12	9
			14777	72	15637	70	7577	72	5816	68
	Steam	Large	39	17	33	16	20	17	17	15
			5308	37	4690	35	2531	35	2939	34
		Small	14	16	19	15	12	16	10	14
			1946	35	10581	33	9106	35	8449	31
PVT3	CO_2	Large	22	91	22	80	11	91	22	85
			540	92	539	82	261	92	526	87
		Small	32	91	31	79	16	91	31	85
			3388	92	3346	81	1635	92	3285	87
	N_2	Large	21	66	22	66	10	66	21	71
			503	92	563	81	244	93	534	88
		Small	29	66	30	66	14	66	30	71
			3138	92	3527	80	1518	92	3365	88
	H_2O	Large	26	5	27	4	2	5	10	2
			3098	64	4059	64	259	63	2701	62
		Small	35	5	37	4	17	5	12	2
			18520	62	22552	62	9715	62	15663	60
	Steam	Large	81	19	73	17	37	19	77	15
			7036	43	10832	41	5670	43	10767	35
		Small	81	19	42	17	22	19	45	15
			10781	43	10842	40	10816	43	10897	35
PVT4	Steam	Large	20	29	20	32	12	34	19	32
			10815	58	10909	54	10065	58	10837	53
		Small	110	28	121	29	55	27	111	32
			10948	58	10880	54	10927	58	10905	54

Figure **5-58** shows the main panel of the project design tool-box. As in the screening tool-box, the user can select within four hydrocarbon compositions, four well patterns and four different IOR methods. If the user enters an input out of range, the corresponding box turns yellow for warning. If the user clicks on the calculate button with an out of range input, an error message is displayed, as shown in Figure **5-36**.
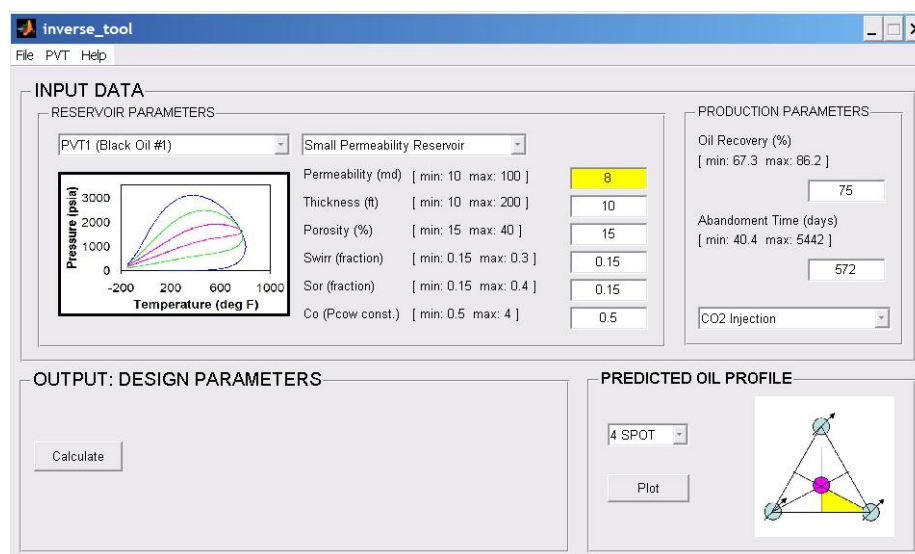
Figure **5-58**: User Interface for IOR Project Design Tool-box

If a combination of PVT#1 and steam injection method is selected, the tool-box shows a warning indication that the process is not feasible, as shown in Figure **5-59**.
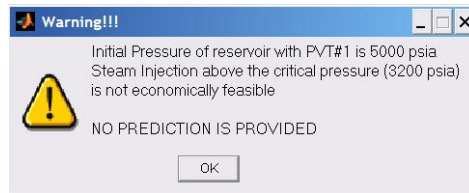
Figure **5-59**: Warning for PVT#1 and Steam Injection Input Selection

Likewise, if the user selects PVT#4 and any method aside from steam injection, the tool-box pops the warning message shown in Figure **5-60**.
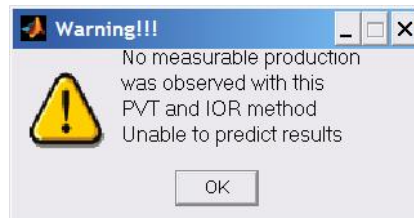
Figure **5-60**: Warning for PVT#4 and IOR Method Selection

If the user clicks on the plot button when any of the parameters combinations lead to a non-exiting network, an "unable to plot" message pops up. Similarly, if the combination of parameters leads to an exiting network but the design parameters were not calculated, an error message is also displayed. Examples of these messages are shown in Figure **5-61**.

Figure **5-61**: Plotting Error Messages

When a set of inputs provides results within the permissible pressure limits, the main panel provides the design parameters in a table as shown in Figure **5-62**. For steam injection evaluations, temperature is also returned in the table. This table is only generated if logical results are found for at least one well pattern. Otherwise, an error message appears as shown in Figure **5-63**.
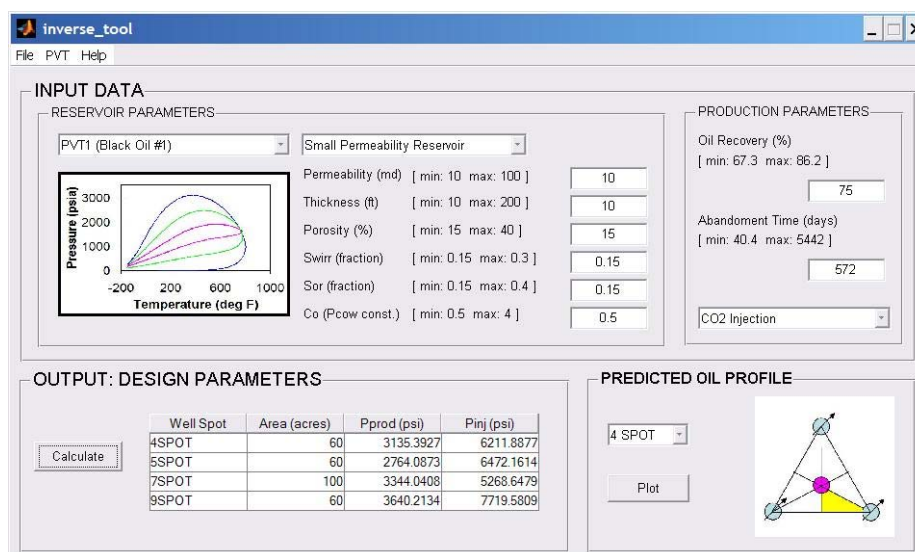
Figure **5-62**: Tabular Outputs from IOR Project Design Tool-box

Figure **5-63**: Error Message for Illogical Results

Once the design parameters are determined, the user can visualize the oil production profiles by plotting the desired well pattern, as shown in Figure **5-64**. Also, the oil profiles parameters are summarized in a table and they can be easily copied into the clipboard.
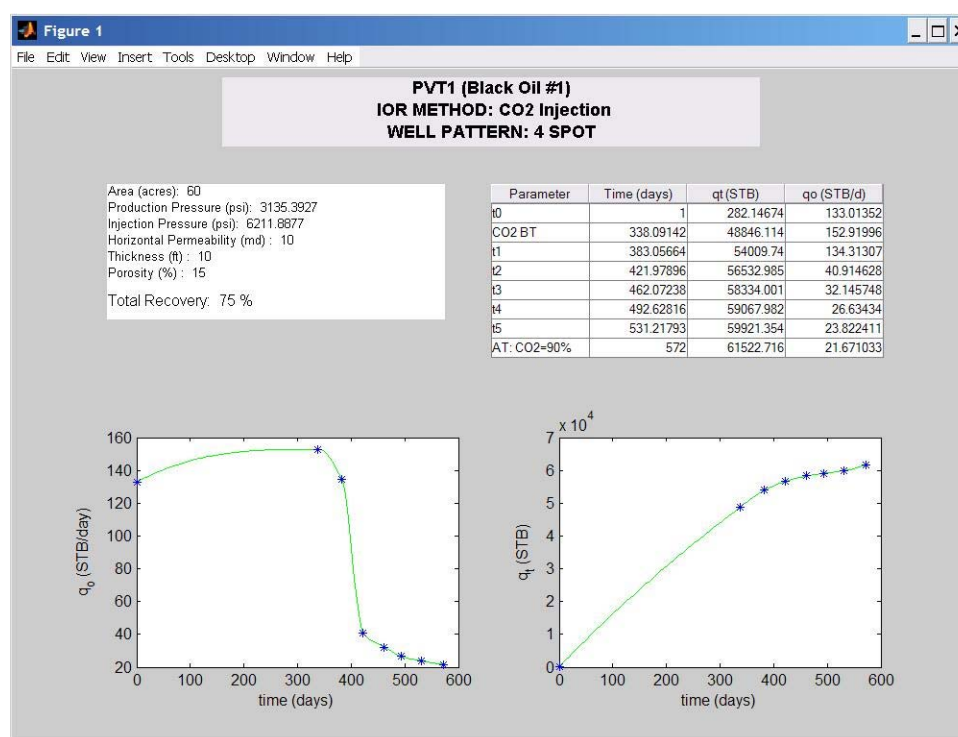
Figure **5-64**: Predicted Oil Production Profile using the Project Design Tool-box

5.3 Performance of the Tool-Boxes

Each of the built networks has been exhaustively tested to ensure and demonstrate the capabilities of the tool-boxes. The screening capabilities of the tool-box can be deduced directly from the results when the networks are tested. This tool operates as an interactive graphics interface for easy access of the ANNs. On the other hand, the project design tool-box operation is more complex as diverse comparisons are executed internally within the interface. The tests performed on each network allow the tool to have a series of well trained expert systems working in a concatenated mode, but they do not show how the inverse application works. Accordingly, it is necessary to evaluate some case studies in order to assess the performance of the project design tool-box. Table **5-37** shows the input parameters used to generate the study cases, which are new data sets not used in training or testing before.

The project design tool-box was used to evaluate and provide appropriate field development plans. The proposed operation schemes were verified against the commercial simulator. Since the predicted operation pressures had a wide range of values, the case studies were also evaluated using the screening tool-box. In this way, the performance of the forward application tool is also under examination and results between both tools boxes are compared against the simulator output. In some cases, the project design tool-box provided scenarios that resulted in pressures outside of the existing operable ranges. Still, the response was analyzed and compared with the help of the commercial simulator assuming that the pressures were reasonable.

Table **5-38** shows the field development plans proposed by the project design network for a reservoir containing a hydrocarbon of PVT#1 composition. Each production scheme, when feasible, was verified by running the corresponding model with the reservoir simulator. The deviation between the predicted cases and the simulator were calculated and are also reported in Table **5-38**. It is observed that some of the operational pressures were predicted within 15% of the out of range values. In some cases, the predicted pressures were not physically possible; such as the case when water is injected in a small 7-spot well configuration as the suggested production pressure is above the initial reservoir pressure.

Table **5-37**: Input Parameters in Study Cases

Fluid	IOR	Area	k (md)	h (ft)	φ (%)	Swirr	Sor	Co	Cg	Oil Rec (%)	AT (days)
PVT1	CO$_2$	Large	400	50	25	-	-	-	-	79.17	104
		Small	50	200	35	-	-	-	-	83.44	274
	N$_2$	Large	400	50	25	-	-	-	-	39.86	66.4
		Small	50	200	35	-	-	-	-	40.16	185.4
	H$_2$O	Large	200	50	30	0.25	0.15	0.5	0.1	60	282
		Small	50	200	35	0.25	0.15	4	0.3	51.09	1264.5
PVT2	CO$_2$	Large	200	100	30	-	-	-	-	87	116
		Small	50	200	35	-	-	-	-	91.80	125
	N$_2$	Large	200	100	30	-	-	-	-	58	116
		Small	50	200	35	-	-	-	-	59	116
	H$_2$O	Large	400	50	35	0.15	0.25	4	0.1	45	276
		Small	50	200	35	0.25	0.15	4	0.3	51	1264
	Steam	Large	400	50	35	0.15	0.25	4	0.1	24.75	435
		Small	10	50	40	0.25	0.2	4	0.3	29.40	4182
PVT4	Steam	Large	400	50	35	0.15	0.25	4	0.1	45	276
		Small	2500	20	35	0.3	0.35	4	0.1	41	1352

Part of the idea of extending the pressure limits by 15% was to evaluate the tool-boxes' performance with inputs beyond their designed original conditions. When either injection or production pressure is not close to the actual pressure limits, the toolboxes can still forecast oil production profiles and provide an adequate production plan. In some cases, if both predicted operation pressures were above or below the pressures limits, it was more difficult for the networks to reproduce the reservoir response.

Table **5-38**: Field Development Plans Determined by Project Design Network for PVT1

IOR	Small/ Large	Pattern	Area (acres)	P_{prod} (psia)	P_{inj} (psia)	Inverse Error (%)	Forward Error (%)
CO_2	S	4 Spot	60	3770	7145	4.9	4.1
		5 Spot	60	3037	7381	9.8	3.1
		7 Spot	100	4294*	5733*	59.9	11.8
		9 Spot	60	3752*	7829	16.7	12.1
	L	4 Spot	150	4047*	6028	5.3	3.1
		5 Spot	150	4130*	6580*	4.8	3.2
		7 Spot	220	4050	5328	22.3	18.5
		9 Spot	150	3975	6581	11.2	25.9
N_2	S	4 Spot	60	3772	7453	10.3	7.7
		5 Spot	100	3276	8459*	23.5	1.7
		7 Spot	60	4849**	5964	36.3	NA
		9 Spot	60	3653	7822	10.1	9.5
	L	4 Spot	150	4033*	6292*	18.6	16.9
		5 Spot	150	4948**	7668	4.3	NA
		7 Spot	250	4163*	6134*	12.3	8.6
		9 Spot	150	3985	6700*	28.6	27.6
H_2O	S	4 Spot	60	3941	6518	0.8	1.0
		5 Spot	60	2331	5303*	2.3	9.2
		7 Spot	60	5139**	5548	NA	NA
		9 Spot	70	2763	5337*	9.0	4.3
	L	4 Spot	150	1777*	7382*	6.7	1.7
		5 Spot	150	2400	5398*	52.5	8.9
		7 Spot	NA	NA	NA	NA	NA
		9 Spot	NA	NA	NA	NA	NA

*: Pressure within 15% out of range
**: Pressure is more than 15% out of range
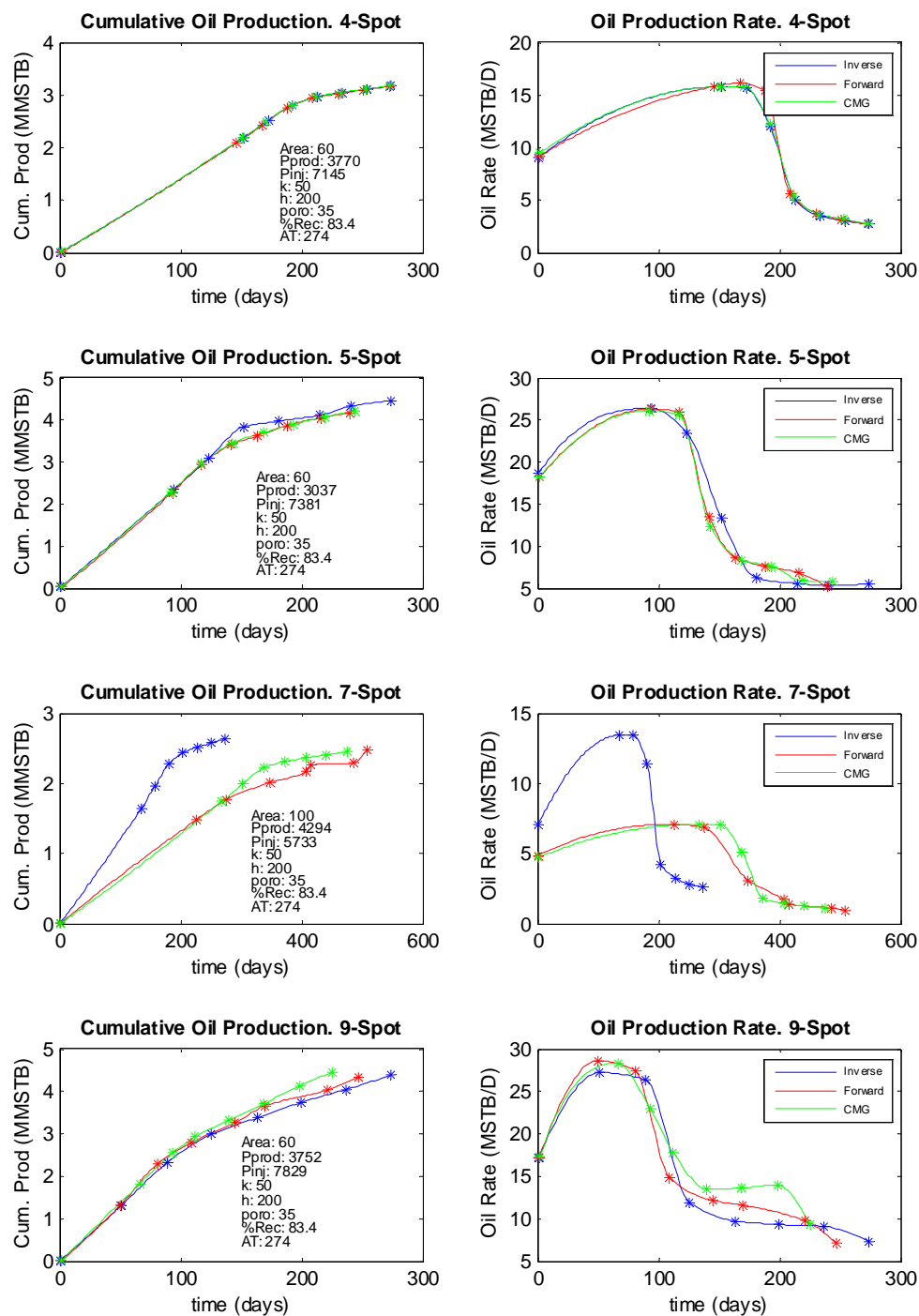
Figure **5-65**: Comparison of Results for PVT1 Undergoing CO_2 Injection (Small Areas)

Figure **5-65** shows the oil production profiles predicted by the toolboxes and the corresponding profile generated by the reservoir simulator. It is clear that the forward application provides accurate results, even when the input pressures were outside the limits. The oil profile obtained for 7-spot configuration reveals the limitations of the inverse application. While both suggested pressures are within the permitted 15% range, the forward tool is capable of reproducing the profile, but the inverse tool is not able to perform similarly. Furthermore, it is noted that the cumulative oil production values are better predicted than the oil production rates, as the monotonic behavior of the cumulative curves facilitates the performance of the networks.

Table **5-39** shows the development plans obtained for diverse reservoirs containing a hydrocarbon of PVT#2 fluid composition. The results, in general, are comparable to the results obtained using PVT#1.

Table **5-39**: Field Development Plans Determined by Project Design Network for PVT2

IOR	Small/ Large	Pattern	Area (acres)	Pprod (psia)	P$_{inj}$ (psia)	T$_{inj}$ (^{o}F)	ΔT	Inverse Error (%)	Forward Error (%)
CO_2	S	4 Spot	60	1773	5187	-	-	28.6	32.4
		5 Spot	NA	NA	NA	-	-	NA	NA
		7 Spot	60	2218*	3779*	-	-	10.7	8.0
		9 Spot	NA	NA	NA	-	-	NA	NA
	L	4 Spot	NA	NA	NA	-	-	NA	NA
		5 Spot	150	1023	3821	-	-	13.4	2.9
		7 Spot	NA	NA	NA	-	-	NA	NA
		9 Spot	150	2075	5392	-	-	154.5	154.1
N_2	S	4 Spot	60	566**	4662**	-	-	9.8	NA
		5 Spot	60	1121	5512*	-	-	2.7	1.5
		7 Spot	60	2206*	3852*	-	-	6.2	3.7
		9 Spot	60	1014	5332	-	-	4.4	3.6
	L	4 Spot	150	1253	3675*	-	-	9.5	3.4
		5 Spot	150	2070*	4537	-	-	3.7	14.0
		7 Spot	150	4044**	3660*	-	-	NA	NA
		9 Spot	150	1831	4422	-	-	7.7	3.2
Steam	S	4 Spot	25	2645*	3052*	758	60	9.9	6.9
		5 Spot	NA	NA	NA	NA	NA	NA	NA
		7 Spot	75	2247	3053*	728	30	6.5	4.7
		9 Spot	NA	NA	NA	NA	NA	NA	NA
	L	4 Spot	300	2745*	3576*	733.2	30	20.1	8186.9
		5 Spot	NA	NA	NA	NA	NA	NA	NA
		7 Spot	200	2843*	3313*	734.5	30	***	***
		9 Spot	NA	NA	NA	NA	NA	NA	NA

*: Pressure within 15% out of range
**: Pressure is more than 15% out of range
***: Simulator did not reach a solution due to small time steps

Figure **5-66** shows the oil production curves for PVT#2 undergoing N_2 injection with large areas. The results show that the project design toolbox was able to suggest production scenarios within a low margin of error. Furthermore, the forward tool-box was also able to reproduce the response of the reservoir. On the other hand, Table **5-40** also shows that it was difficult to obtain adequate scenarios for most of the steam injection cases. The reason is that the initial pressure in reservoir containing PVT#2 is very close

to the critical pressure of steam (3000 psia). The injection pressure for steam injection in PVT#2 was set between 3100 to 3200 psia. Then, there is a high probability that the predicted scenario resulted in pressure ranges away from the permissible values.
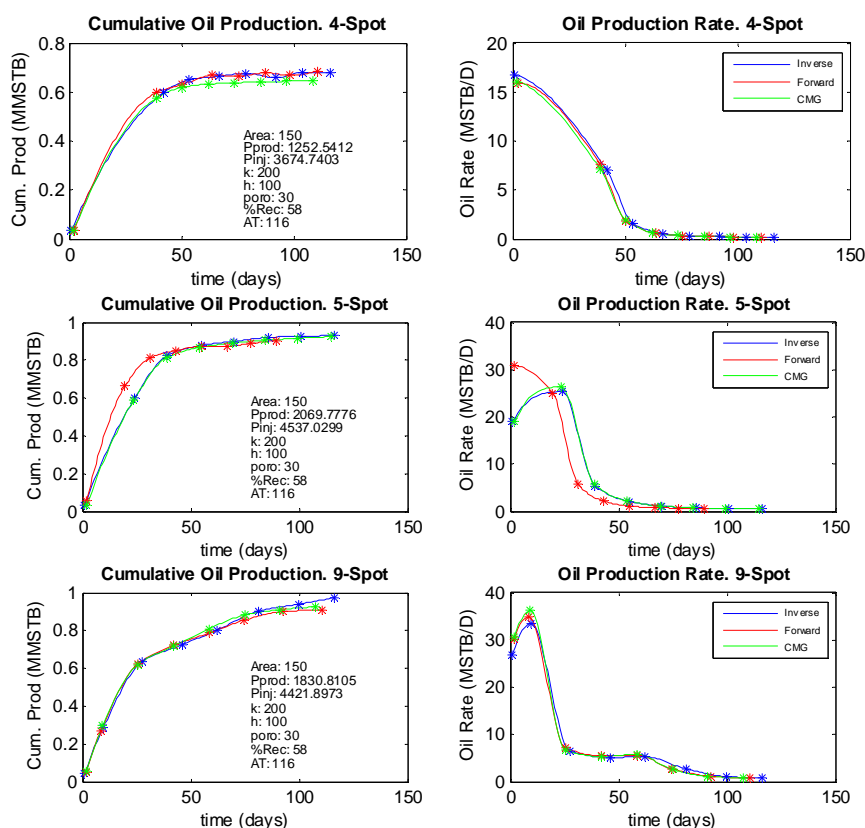
Figure **5-66**: Comparison of Results for PVT2 Undergoing N_2 Injection (Large Areas)

Figure **5-67** shows the cases of production profiles for PVT#2 undergoing steam injection. The profiles obtained for small areas indicate that the project design tool-box proposed adequate field development plans as their predicted injection pressures are very close to the lower permissible limit. However, the profiles obtained for the large area

cases display significantly high disparities. In fact, this response is anticipated as the forecasted injection pressures are above the critical pressure of steam.
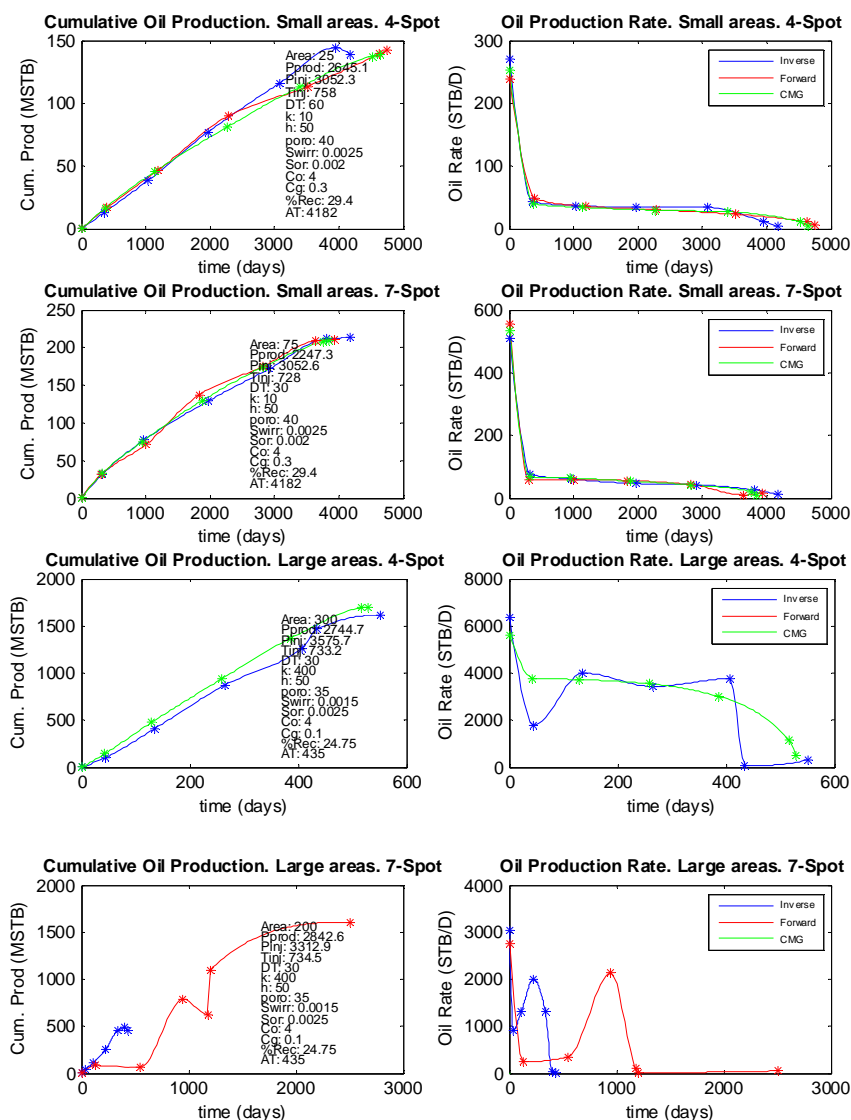
Figure **5-67**: Comparison of Results for PVT2 Under Steam Injection

A further evaluation of the large areas was carried out by combining the same reservoir properties used for the PVT#2, steam injection and large areas with different values of estimated production. When using an abandonment time of 500 days with a

total recovery of 30 %, the project design provided schemes with pressures within the limits. Table **5-41** shows the results for the second case studies. For this new combination of *AT* and oil recovery, none of the operational pressures are away from the permissible 15%. Also, it was possible to obtain a production scheme using a 9-spot well arrangement.

Table **5-41**: New Field Development Plans for PVT#2, Steam Injection, Large Areas

Pattern	Area (acres)	Pprod (psia)	P_{inj} (psia)	T_{inj} (°F)	ΔT	Inverse Error (%)	Forward Error (%)
4 Spot	100	2853*	3135	732	30	24.7	58.6
5 Spot	NA	NA	NA	NA	NA	NA	NA
7 Spot	300	2681*	3140	732	30	13.9	5.9
9 Spot	250	2495	3082*	729	30	8.1	2.4

*: Pressure within 15% out of range

Figure **5-68** shows the corresponding oil profiles for the second case studies. The predictions obtained from both tool-boxes for curves for 7-spot and 9-spot display accurate results. However, the forward tool provided a poor prediction of the 4-spot scheme. The predicted injection pressure for this specific case is within the existing limits while the predicted production pressure is at the upper 15% limit. This indicates that the permitted range of 15% is too wide for steam injection methods. The tool-box evaluation methodology demonstrates that different combination of the expected total recovery and project life time provide diverse field development strategies. This represents a significant advantage for reservoir appraisal as many scenarios can be under consideration at the same time.
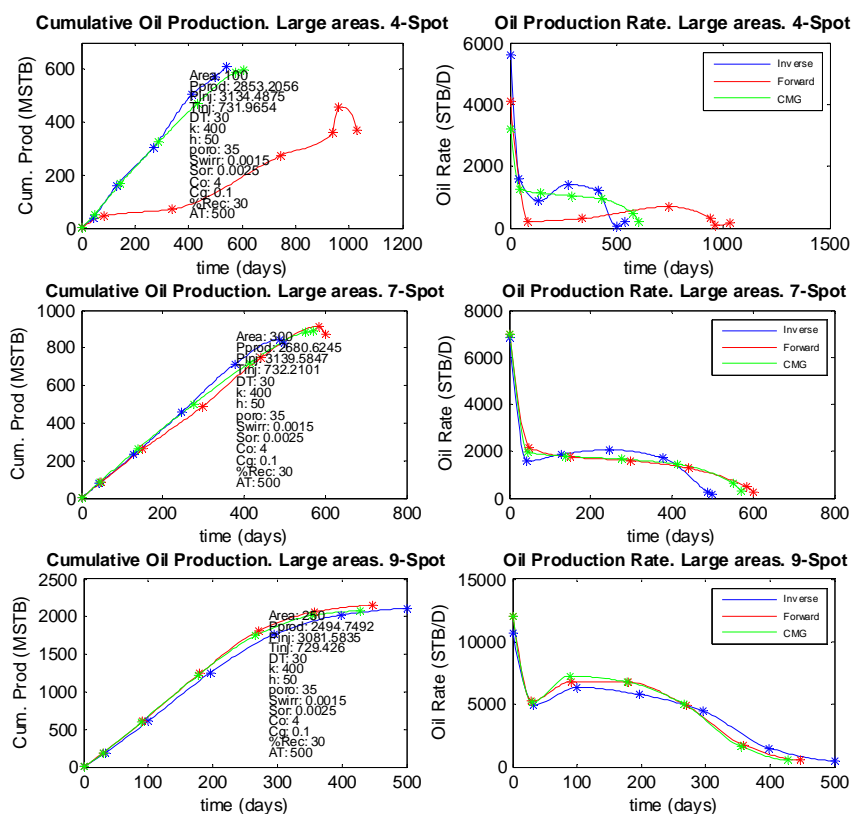
Figure **5-68**: Comparison of Results for PVT#2 Undergoing N₂ Injection (Large Areas). Second Case Studies.

In general, the results from the case studies indicate that the field development plans obtained with the project design tool-box can be verified using the screening tool-box within an acceptable margin of error. The combined use of the project design and screening tool-boxes provides a powerful application for hydrocarbon reservoir evaluations. This methodology should help the reservoir engineer to eliminate production scenarios that are not efficient from the beginning.

5.4 Recommended Implementation Protocol for Field Applications

Reservoir engineers rely on conventional simulation and screening criteria in order to evaluate the most appropriate production scenario for green and mature reservoirs. The tools developed in this study can be used as the screening criteria in order to minimize the number of possible production scenarios to be simulated.

In order to evaluate a given reservoir with the developed tool-boxes, the average properties of the reservoir under study should be entered into the project design tool-box. Each layer of the reservoir can be evaluated separately as long as the layer thickness is within the limits of the tool. If the layers are very thin, the reservoirs should be evaluated using the average properties of all layers.

The user should select the hydrocarbon composition that is closer to the real reservoir fluid. Then, the different values of estimated recovery and project abandonment time can be evaluated for each recovery method. This procedure should provide different well pattern options if the combination of *AT* and oil recovery are physically possible. If these parameters lead to unpractical schemes, different pairs of *AT* and recovery should be evaluated.

The oil production curves are generated for each of the recommended well patterns. Then, these curves can be exported and validated using the screening tool-box. The average reservoir properties, fluid type, recovery method and well pattern are entered into the screening tool. The oil production curves are generated for each case and they should be compared with the curves obtained before. A good match of the oil production curves indicates that the process under study is feasible.

A major advantage of following this protocol is that the rapid response of the tool-boxes provides the user with the necessary information for further economic analysis in a matter of seconds. Calculations of the present value can be easily estimated from the oil production rate curve, which helps to decide which process and development plan are more appropriate for a given reservoir.

5.5 Recommendations for Further Expansion of the Tool-Boxes

Using different PVT's instead of fluid properties as inputs in the tool-boxes provides an important advantage versus the published screening criteria by Taber and Martin (1983) and Taber et. al. (1997). Hydrocarbon compositions allow the artificial neural network applications to evaluate wider ranges of property combinations.

The screening criteria and project design applications developed in this study were built using four specific hydrocarbons compositions. However, the tool-boxes are intended to be expanded in the future by incorporating new sets of PVT data.

It is recommended to incorporate various PVT's that varies from light oils to heavy oils with varying initial reservoir pressures. Even though some of the heavy oil reservoir models developed in this study did not provide significant production, the models simulated with some other heavy oil compositions and undergoing CO_2, N_2 and water injection should be evaluated with the help of a commercial simulator. Some of this recovery processes may lead to significant oil production when they are applied to heavy oils with characteristics that are different from the PVT#4.

Chapter 6

CONCLUSIONS

The following achievements have been realized in the study presented in this thesis:

- A multilayer cascade feedforward back propagation network algorithm was effectively implemented to simulate miscible displacement, waterflooding and steam injection recovery methods using artificial intelligent protocols.

- The logarithmic function applied to the inputs and outputs proved to improve the network performance as it scales down the target ranges.

- The constructed networks were able to describe the displacement mechanism under different miscibility conditions given that the same network architecture was efficient for different hydrocarbon compositions. Moreover, the same network also captured the similarities between carbon dioxide and nitrogen displacement mechanisms as the same network architecture was successfully applied in both CO_2 and N_2 injection.

- The networks developed for waterflooding and steam injection applications were trained efficiently with an architecture similar to the miscible displacement applications. The expert systems also captured effectively the displacement mechanisms involved in these processes since two network structures were used in steam drive and water drive mechanisms, respectively.

- Artificial neural network was able to relate oil production rate, cumulative oil production and production time given that the proxy models predicted successfully the production curves using a considerably smaller number of input patterns.

- Targets that exhibit a monotonically increasing behavior facilitate the network training process. Cumulative oil production and production time were accurately predicted while the oil production rate was the hardest variable to forecast due to its sharp drop as solvent breakthrough is achieved.

- Two networks built in series helped to incorporate the complete oil profiles as a mid stage in the inverse expert systems as the oil recovery and abandonment time were not sufficient to provide accurate predictions. Nevertheless, the neuro-simulation application recognized stronger relationships between the oil profile and the oil recovery and abandonment time than the relationships between the operation pressures and the oil profiles since the inverse protocol provided comparable results with a simpler network architecture.

- ANN was able to recognize the pronounced effects that injection pressure has in miscible displacement processes. Networks developed for the project design tool-box established a strong connection between oil recovery and injection pressure. The connection with the production pressure was not as strong as its prediction presented high levels of dispersion.

- The inverse proxy models identified similar level of impact of the injection and production pressures on the water drive mechanism since both parameters presented similar deviations.

- Extension of the permissible operation condition limits in the project design application allowed more flexibility in the assessment of optimum development plans. However, better production scenarios are provided if the tool is used within the operating ranges as established with the design of experiment protocol.

- The project design tool-box demonstrated to help in the quantitative project assessment if proper combinations of expected project time and oil recovery are provided for the same reservoir. Its use, when combined with the screening network application, facilitates the evaluation and validation of the proposed production scenarios.

Bibliography

Abou-Kassem, J., Farouq, S. and Islam, R.: Petroleum Reservoir Simulation. Gulf Publishing Company. Houston, Texas, ISBN 0-9765113-6-3, 2006.

Ayala, L.F., Ertekin, T. and Adewumi, M.: Optimized Exploitation of Gas-Condensate reservoir Using Neuro-Simulation. SPE paper 88471 presented at the Asia Pacific Oil and Gas Conference and Exhibition, Perth, Australia,18-20 October, 2004.

Corey, A. T.: The Interrelation between Gas and Oil Relative Permeabilities. Producers Monthly, November 1954, p. 38-41.

Craig, Forrest: The Reservoir Engineering Aspects of Waterflooding. Monograph Volume 3 of the Henry L. Doherty Series, Fourth Edition, Dallas, ISBN 0-89520-202-6, 1993.

Demuth, H., Beale, M. and Hagan, M.: Neural Network Toolbox 5 User's Guide, The MathWorks, Inc., Natick, Massachusetts, 2007.

Ertekin, T., Abou-Kassem, J. and King, G.: Basic Applied Reservoir Simulation, SPE Textbook Series Vol. 7. Richardson, Texas, ISBN 1-55563-089-8, 2001.

Fausett, Laurene: Fundamentals of Neural Networks: Architectures, Algorithms and Applications, Prentice-Hall, Inc., New Jersey, ISBN 0-13-334186-0, 1994.

Fizoorabadi, A. and Aziz, K.: Analysia and Correlation of Nitrogen and Lena-Gas Miscibility Pressure. SPE Paper 13669. SPE Reservoir Engineering, November 1986, p. 575-582.

Frick, T. C. and Taylor, R. W.: Petroleum Production Handbook. McGraw-Hill Book Company. York, PA. 1962. Volume 2, Ch. 41.

Gorucu, F. B.: Optimization of Carbon Dioxide Sequestration Process Design Parameters, Master's Thesis in Petroleum and Natural Gas Engineering, The Pennsylvania State University, University Park, 2005.

Gorucu, F.B., Ertekin, T., Bromhal, G. S., Smith, D. H., Sams, W.N., Jikich, S.:"A Neurosimulation Tool for Predicting Performance in Enhance Coalbed Methane and CO_2 Sequestration Projects, SPE paper 97164 presented at the 2005 SPE Annual Technical Conference and Exhibition held in Dallas, Texas, 9-12 October, 2005.

Green, D. and Willhite, G.: Enhanced Oil Recovery, SPE Textbook Series Vol. 6. Richardson, Texas, ISBN 1-55563-077-4, 2003.

Hagan, M., Demuth, H. and Beale, M.: Neural Network Design, PWS Pub.,1st Edition, Boston, ISBN 7-111-10841-8, 1996.

Herning and Zipperer. Gas und Wasserfach, v. 79, 49.1936.

Holm, L. and Josendal, V.: Effect of Oil Composition on Miscible-type Displacement by Carbon Dioxide. SPE paper 8814. SPE Journal, February 1982, p. 87-98.

Hudgins, D., Llave, F. and Chung, F.: Nitrogen Miscible Displacement of Light Crude Oil: A Laboratory Study," SPE paper 17322 presented at SPE/DOE Enhanced Oil Recovery Symposium, Tulsa, April 1988.

Jarrel, P., Fox, C., Stein, S. and Johns, R.: Practical Aspects of CO_2 Flooding, SPE Monograph Volume 22, Henry L. Doherty Series, Richardson, TX, ISBN 1-55563-096-0, 2002.

Jessen, M., Michelsen, M. and Stenby, E.: Effective Algorithm for calculation of Minimum Miscibility Pressure. SPE Paper 50632 presented at the 1998 SPE European Petroleum Conference held in The Hague, The Netherlands, 20-22 October 1998.

Johns, R. and Orr, F.: Miscible Displacement of Multicomponent Oils. SPE Paper 30798. SPE Journal, March 1996, p. 39-50.

Jossi, J. , Stiel, L. and Thodos, G.: The Viscosity of Pure Substances in the Dense Gaseous and Liquid Phases, AIChE Journal., vol. 8, issue 1, p. 59-63, 1962.

Lake, Larry: Enhance Oil Recovery. Prentice-Hall, Inc., New Jersey, ISBN 0-13-281601-6, 1989.

Maren, A., Harston, C and Pap, R.: Handbook of Neural Computing Applications. Academic Press, Inc., San Diego, ISBN 0-12-546090-2, 1990.

McCain, William D.: The Properties of Petroleum Fluids. Second Edition, PennWell Publishing Company, Tulsa, Oklahoma, 1990. ISBN 0-87814-335-1.

Odusote, O. Ertekin, T., Smith, D. H., Sams, W.N., Jikich, S.: Carbon Dioxide Sequestration in Coal Seams: A parametric Study and Development of a Practical Prediction/Screening Tool Using Neuro-Simulation. SPE paper 90055 presented at the SPE Annual Technical Conference and Exhibition held in Houston, Texas, 26-29 September, 2004.

Papp, I. Lakes, B. Palasthy, G. and Tromboczky, S.: Enhanced Recovery for Selected Components of a Highly Volatile Oil. SPE paper 39689 presented at the 1998 SPE/DOE Improved Oil Recovery Symposium held in Tulsa, Oklahoma, 19-22 April 1998.

Patterson, D. W.: Artificial Neural Networks, Theory and Applications. Prentice-Hall, Inc., Singapore, ISBN 0-13-295353-6, 1996.

Peneloux, A., Rauzy, E., and Freze, R.: "A Consistent Correction for Redlich-Kwong-Soave Volumes," Fluid Phase Equilibria, Vol. 8, 1982, p. 7-23.

Rathmell, J.J., Stalkup, F.I. and Hassinger, R.C.: A Laboratory Investigation of Miscible Displacement by Carbon Dioxide. SPE Paper 3483 presented at the 46th Annual Fall Meeting of the Society of Petroleum Engineers of AIME in New Orleans, LA., October 3-6, 1971.

Sebastian, H. M. and Lawrence, D. D.: Nitrogen Minimum Miscibility Pressures. SPE paper 24134 presented at the SPE/DOE Eighth Symposium on Enhance Oil Recovery held in Tulsa, Oklahoma, April 22-24, 1992.

Stalkup, Fred: Miscible Displacement. SPE Monograph Volume 8, Henry L. Doherty Series, Dallas, ISBN 0-89520-319-7, 1983.

Taber, J. J. and Martin, F. D.: Technical Screening Guides for the Enhance Recovery of Oil. SPE paper 12069 presented at the 58th Annual Technical Conference and Exhibition held in San Francisco, CA, October 5-8, 1983.

Taber, J. J., Martin, F. D. and Seright, R. S.: EOR Screening Criteria Revisited- Part 1: Introduction to Screening Criteria and Enhance Recovery Filed Projects. SPE Paper 35385. SPE Reservoir Engineering, p. 189-198, 1997.

Taber, J. J., Martin, F. D. and Seright, R. S.: EOR Screening Criteria Revisited- Part 2: Application and Impact of Oil Prices. SPE Paper 35385. SPE Reservoir Engineering, p. 189-198, 1997.

Teletzke, G.F., Patel, P. D. Chen, A. L.: Methodology for Miscible Gas Injection EOR Screening. SPE paper 97650 presented at the SPE International Oil Recovery Conference in Asia Pacific held in Kuala Lumpur, Malaysia, 5-6 December 2005.

Vinsome, P.K.W., and Westerveld, J.: A Simple Method for Predicting Cap and Base Rock Heat Losses in Thermal Reservoir Simulators. JCPT, July-September 1980, p. 87-90.

Volek, C.W. and Pryor, J. A.: Steam Distillation Drive-Brea Field, California. SPE 3441, JPT August 1972, p. 899-906.

Yelling, W. and Metcalfe, R.: Determination and Prediction of CO_2 Minimum Miscibility Pressure. SPE paper 7477. JPT, January 1980, p. 160-168.

Yoon, P. and Thodos, G.: Viscosity of Nonpolar Gaseous Mixtures at Normal Pressures. AIChE Journal, v.16, issue 2, p. 300-304, 1970.

Yuan, H. and Johns, R. T.: Simplified Method for Calculation of Minimum Miscibility Pressure or Enrichment. SPE Paper 77381. SPE Journal December 2005, p. 416-425.

Yuan, H., Johns, R. T., Egwuenu, A. M. and Dindoruk, B.: Improved MMP Correlations for CO_2 Floods Using Analytical Gasflooding Theory. SPE paper 2005. SPE Reservoir Engineering, p. 418-425, October 2005.

Wang, Y. and Orr, F.: Calculation of Minimum Miscibility Pressure. SPE Paper 39683 presented at the 1998 SPE/DOE Improved Oil Recovery Symposium held in Tulsa, Okalahoma. 19-22 April 1998.

Willhite, Paul: Waterflooding. SPE Textbook Series Vol. 3. Richardson, Texas, ISBN 1-55563-005-7, 1986.

Willman, B. T., Valleroy, V. V., Runberg, G. W., Cornelius, A. J. and Powers, L. W.: Laboratory Studies of Oil Recovery by Steam Injection. SPE 1537-G, JPT July 1961, p 681-690.

Appendix A

Peng Robinson Equation of State

The general form of PR EOS is shown in Equation **A.1**:

$$P = \frac{R*T}{(\upsilon-b)} - \frac{\alpha*a}{\upsilon^2 + 2*b*\upsilon - b^2} \qquad \textbf{A.1}$$

Where T is the absolute temperature, P is the absolute pressure, R is the universal gas constant and υ is the molar volume. The α term is a parameter calculated using Equation **A.2** :

$$\alpha = \left[1 + \left(0.37464 + 1.54226*\omega - 0.26992*\omega^2\right)*\left(1-\sqrt{Tr}\right)\right]^2 \qquad \textbf{A.2}$$

and is a function of the acentric factor ω, which is calculated as:

$$\omega = \log\left(\frac{Pc}{Psat\big|_{Tr=0.7}}\right) \qquad \textbf{A.3}$$

In Equation **A.3**, Pc is the critical pressure and Psat is the saturation pressure at the reduce temperature (Tr) of 0.7. Parameters a and b are calculated using Equation **A.4** and Equation **A.5** respectively:

$$a = 0.45724*\frac{R^2 Tc^2}{Pc} \qquad \textbf{A.4}$$

$$b = 0.07780*\frac{R*Tc}{Pc} \qquad \textbf{A.5}$$

The PR cubic expression in Z, compressibility factor, is as presented in Equation **A.6** :

$$Z^3 - (1 - B)Z^2 + (A - 2B - 3B^2)Z - (AB - B^2 - B^3) = 0 \qquad \textbf{A.6}$$

where parameters A and B are calculated as:

$$A = \frac{\alpha a P}{R^2 T^2} \qquad \textbf{A.7}$$

$$B = \frac{bP}{RT} \qquad \textbf{A.8}$$

The values of a and b for the hydrocarbon mixture are determined by:

$$(\alpha a)_m = \sum \sum y_i y_j (\alpha a)_{i,j} ; (\alpha a)_{i,j} = \sqrt{(\alpha a)_i (\alpha a)_j (1 - k_{i,j})} \qquad \textbf{A.9}$$

$$b_m = \sum_i y_i b_i \qquad \textbf{A.10}$$

Cubic EOS provides a week prediction of the liquid phase. Peneloux et al. (1982) molar volume correction is also applied in order to improve the prediction of the liquid densities. This correction, usually referred to as volume shift, is shown in Equation **A.11**, which adds a third parameter to the EOS.

$$\upsilon_{Corrected} = \upsilon_{EOS} - \upsilon^* \qquad \textbf{A.11}$$

The compressibility factor can be also corrected as follows:

$$Z_{Corrected} = Z_{EOS} - \frac{P\upsilon^*}{RT} \qquad \textbf{A.12}$$

The molar volume υ^* is the third term added to the EOS, which is a function of the shift volume parameter Vs, the critical pressure and critical temperature and the component composition (z_i), as shown in Equation **A.13**:

$$\upsilon^* = \sum \frac{z_i Vs\Omega_b RTc_i}{Pc_i} \qquad \textbf{A.13}$$

For low pressure conditions, the viscosity of each hydrocarbon component is calculated using the correlation developed by Yoon and Thodos (1970):

$$\mu_{(low,i)} = (4.610 * Tr^{0.618} - 2.040 * e^{-0.449*Tr} + 1.94 * e^{-4.058*Tr} + 10^{-5} / \mu p \qquad \textbf{A.14}$$

where μp is the viscosity parameter, which is a function of the critical properties and the molecular weight (MW):

$$\mu p = \left(\frac{Tc}{MW^3 Pc^4} \right)^{1/6} \qquad \textbf{A.15}$$

Then, the viscosity of the mixture at low pressure is calculated using the mixing rule proposed by Herning and Zipperer (1936):

$$\mu_{(mix,low)} = \frac{\sum\limits_{i=1}^{nc} \mu_{(low,i)} x_i \sqrt{MW_i}}{\sum\limits_{i=1}^{nc} x_i \sqrt{MW_i}} \qquad \textbf{A.16}$$

The viscosity of the mixture at reservoir conditions is calculated from that one at low pressure using the correlation developed by Jossi, Stiel and Thodos (1962):

$$\left(\left(\mu_{(mix,res)} - \mu_{(mix,low)} \right) * \mu p_{mix} + 10^{-4} \right)^{0.25} =$$
$$0.10230 + 0.023364 * \rho_r * 0.058533 * \rho_r^2 - 0.040758 * \rho_r^3 + 0.0093324 * \rho_r^4 \qquad \textbf{A.17}$$

where ρ_r is reduced density of the mixture.

Appendix B

Sensitivity of the Numerical Model to the Grid Dimensions

The sensitivity analysis on the coarseness/fineness of the grid to be used in the reservoir simulation was performed using 5-spot (normal and direct line drive), 7-spot and 9-spot well patterns. Figures **B-1** to **B-4** show the variation of oil flow rates and CO_2 mol fractions in the producer using different block numbers for each well pattern. These figures illustrate that the simulation models are, at some extend, sensitive to the grid block number. However, the differences in the results are not that significant since the curves have similar trends for all studied cases. As it was noted in Chapter 4, the only exception to this observation is the grid made up of 10x10 blocks. At early production time, oil rate shows a notable deviation from the rest of the curves. Thus, 10x10 grid systems were not used in any of the simulation runs.
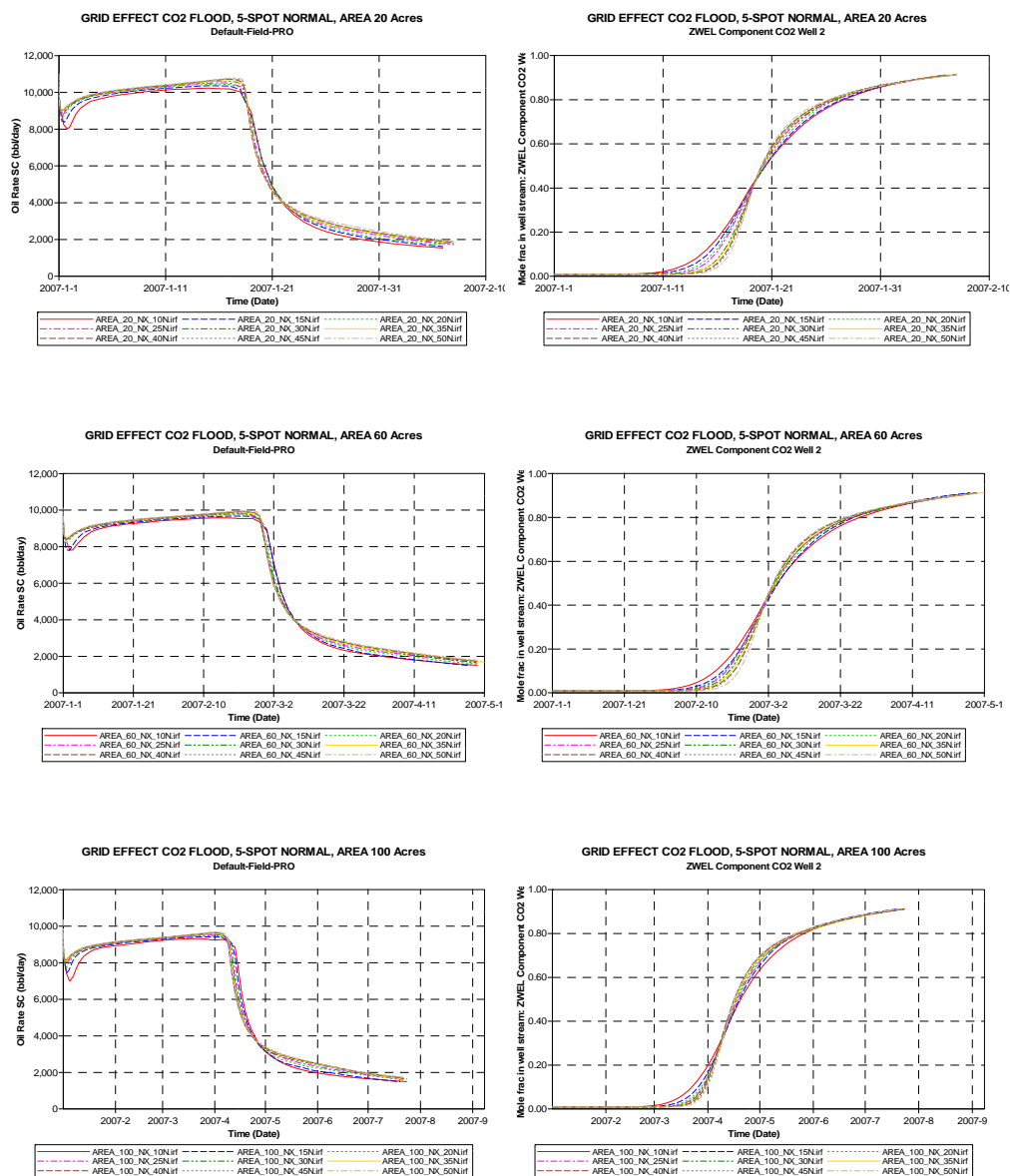
Figure **B-1**: Sensitivity Analysis on Grid Size – Normal 5-Spot Well Pattern
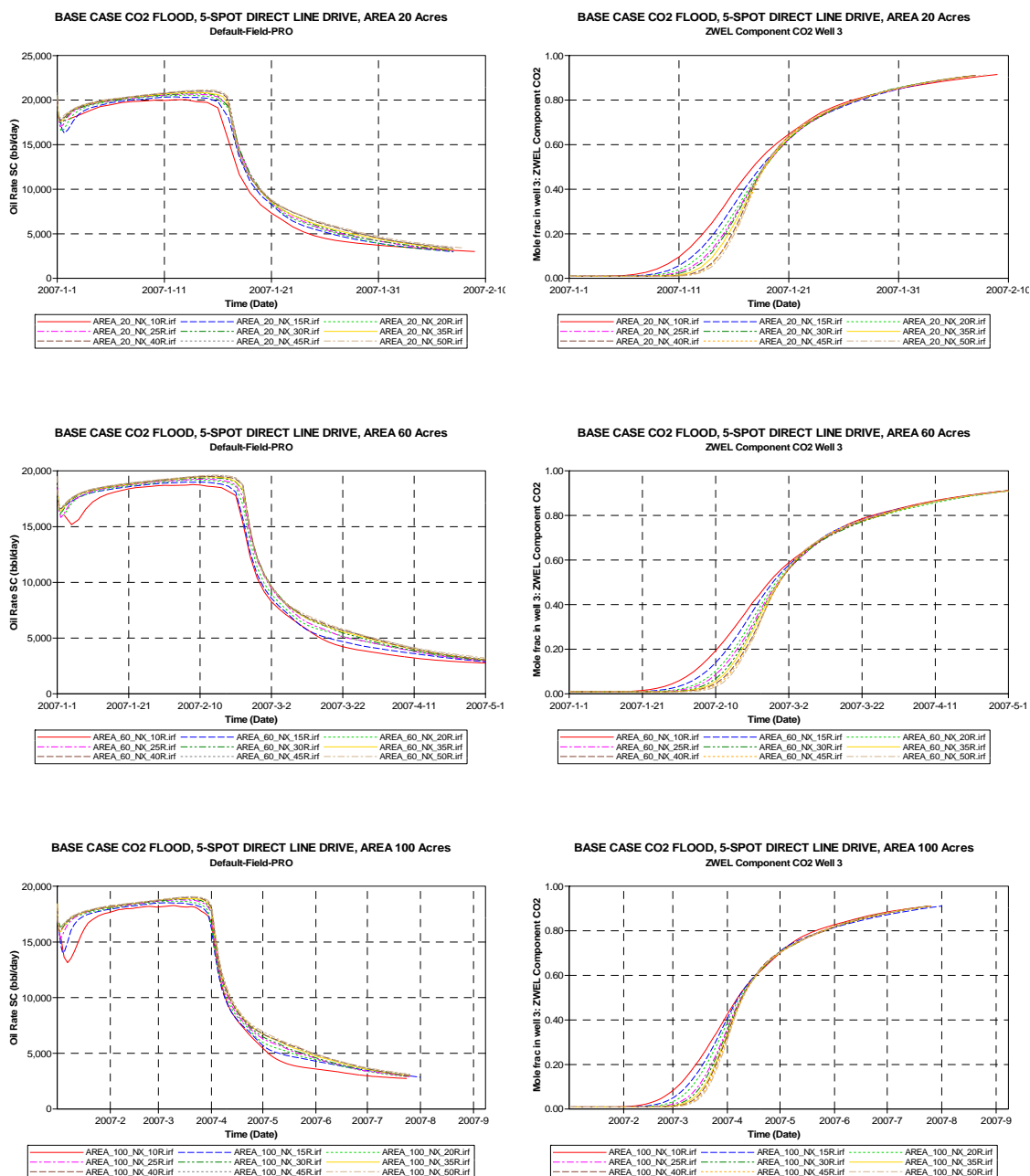
Figure **B-2**: Sensitivity Analysis on Grid Size – Direct Line Drive 5-Spot Well Pattern

\
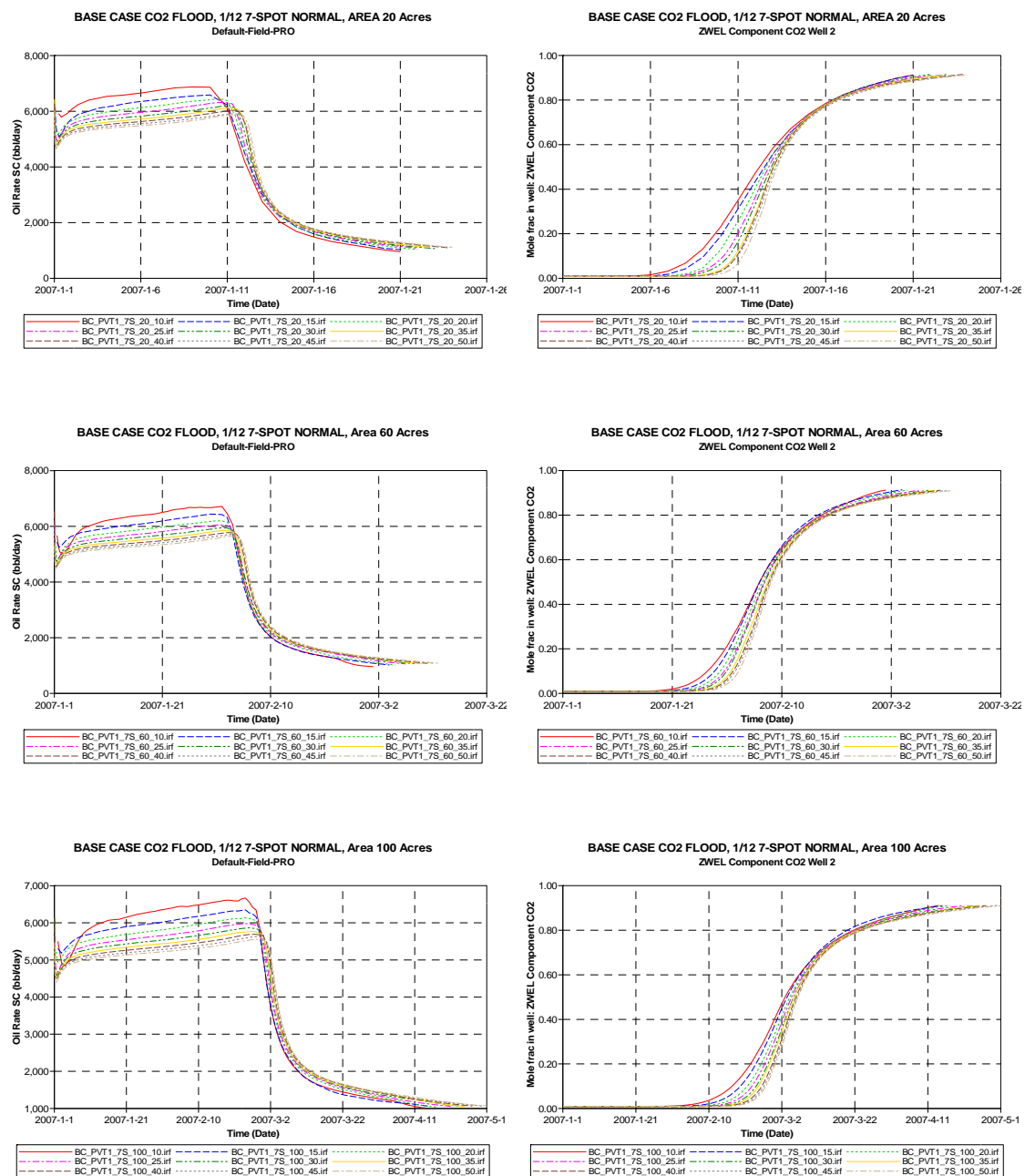
Figure **B-3**: Sensitivity Analysis on Grid Size – Normal 7-Spot Well Pattern
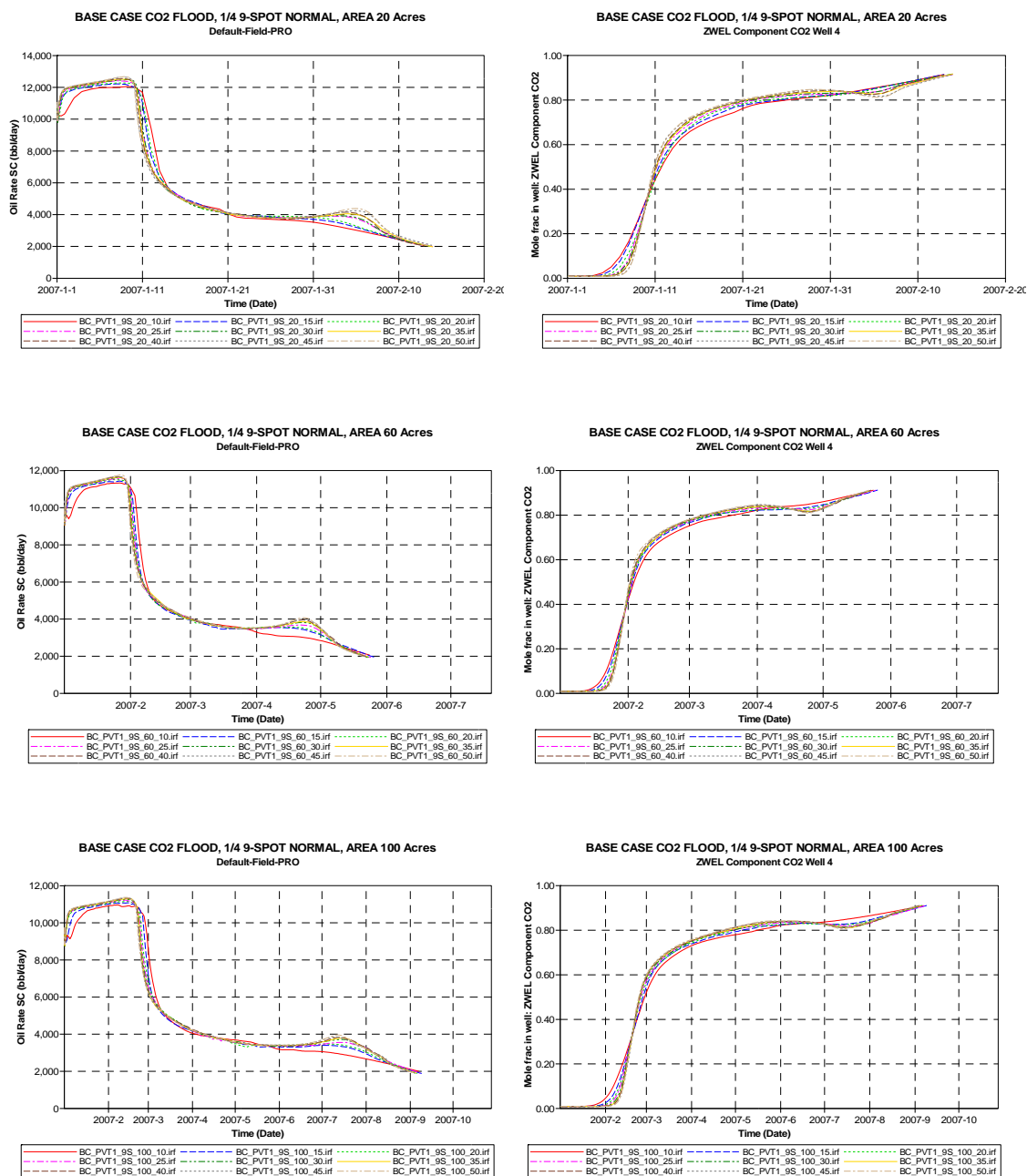
Figure **B-4**: Sensitivity Analysis on Grid Size – Normal 9-Spot Well Pattern

Appendix C

Oil Production Profiles and Operation Pressure Predictions

The present study involved extensive generation of networks to be included in the tool-boxes. Since results are in most cases very similar within one well pattern and IOR process, this appendix contains the most characteristic results obtained from the networks.

C.1 Networks in the Screening Tool-box

C.1.1 CO_2 Injection
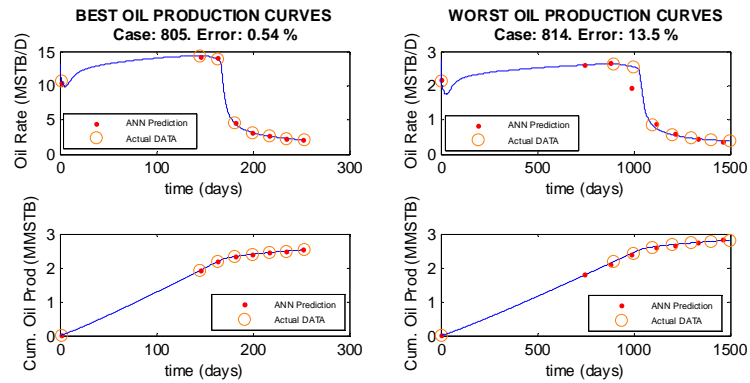
Figure **C-1**: Best and Worst Production Profile Built using Stage-2 Network: CO_2 Injection, PVT#1, 4-Spot. Batch 1 (Small Areas)
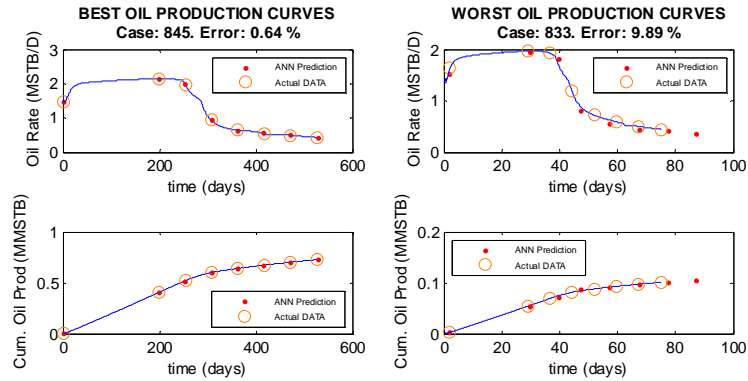
Figure **C-2**: Best and Worst Production Profile Built using Stage-2 Network: CO_2 Injection, PVT#1, 5-Spot. Batch 1 (Small Areas)
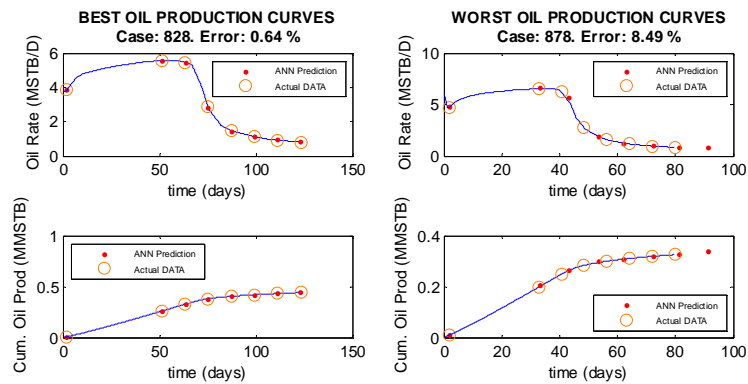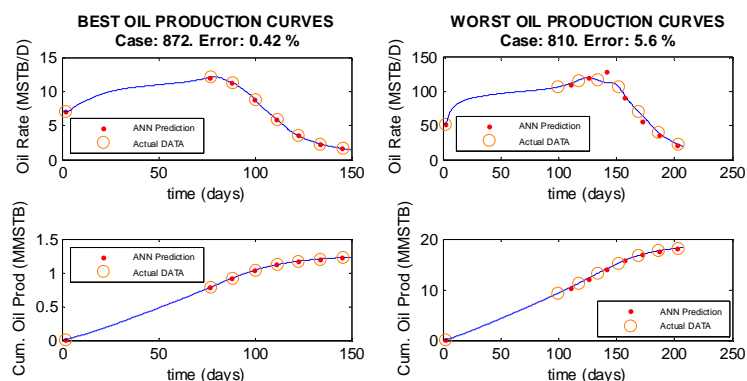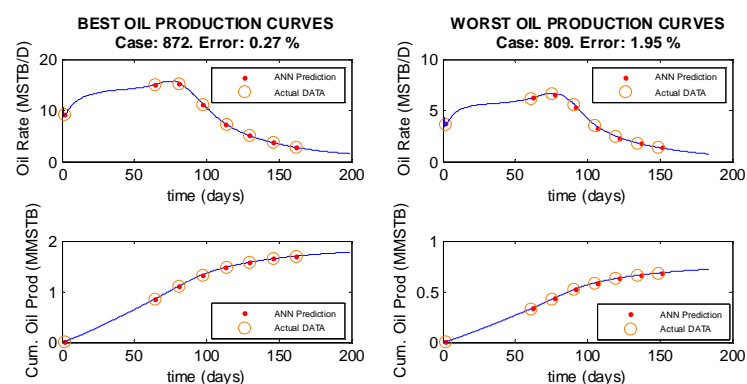

Figure **C-3**: Best and Worst Production Profile Built using Stage-2 Network: CO_2 Injection, PVT#1, 7-Spot. Batch 1 (Small Areas)
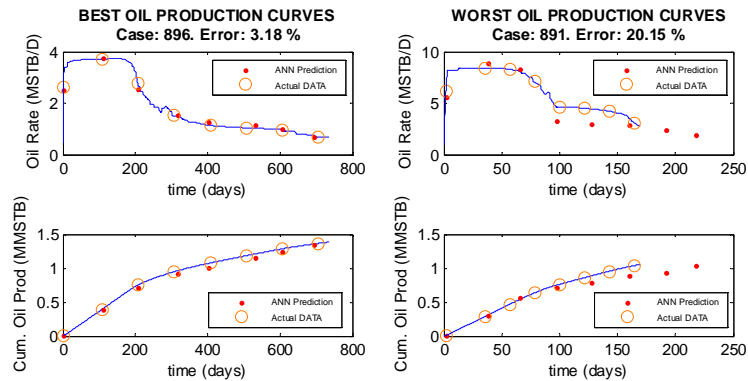
Figure **C-4**: Best and Worst Production Profile Built using Stage-2 Network: CO_2 Injection, PVT#1, 9-Spot. Batch 1 (Small Areas)
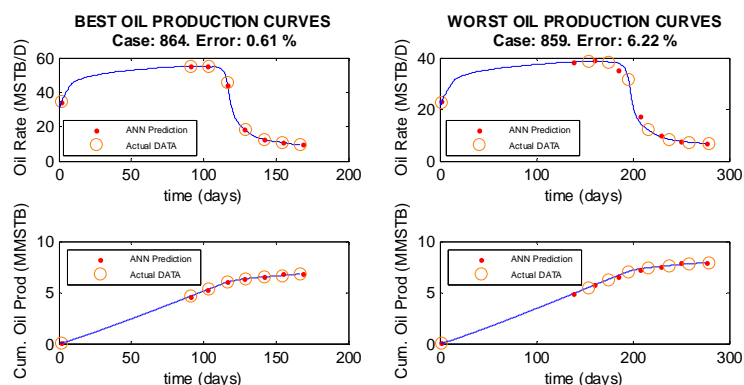
Figure **C-5**: Best and Worst Production Profile Built using Stage-2 Network: CO_2 Injection, PVT#1, 4-Spot. Batch 2 (Large Areas)
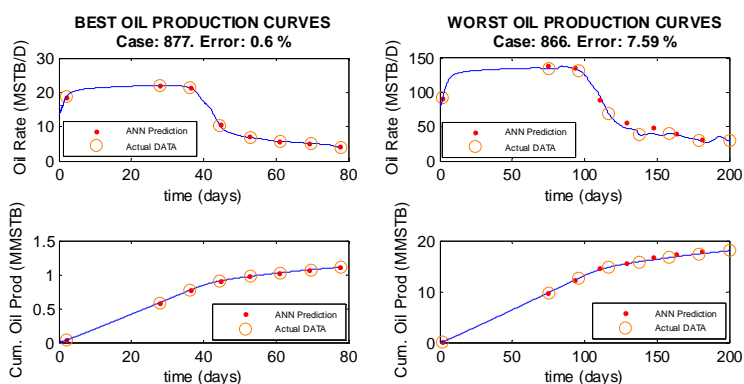
Figure **C-6**: Best and Worst Production Profile Built using Stage-2 Network: CO_2 Injection, PVT#1, 5-Spot. Batch 2 (Large Areas)
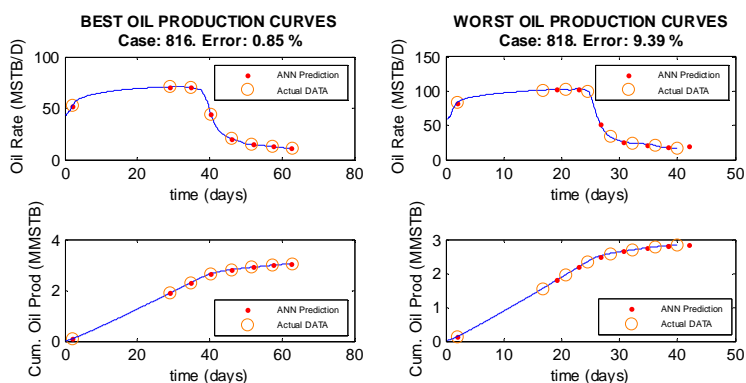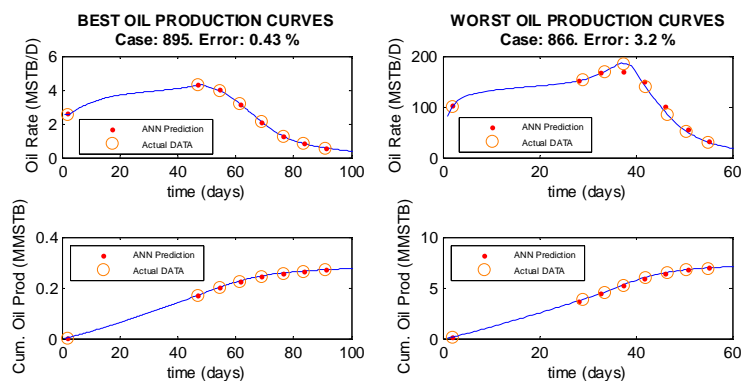

Figure **C-7**: Best and Worst Production Profile Built using Stage-2 Network: CO_2 Injection, PVT#1, 7-Spot. Batch 2 (Large Areas)
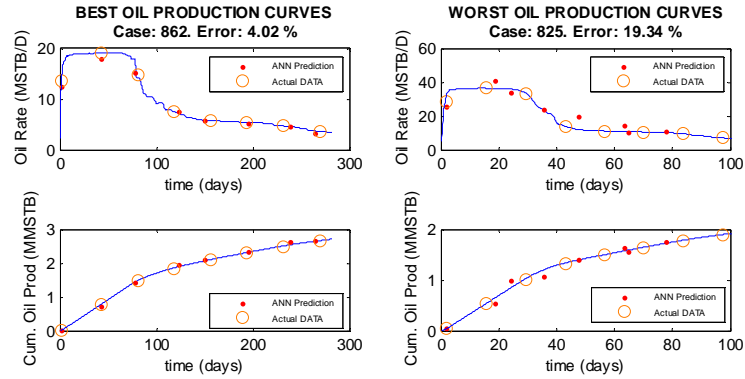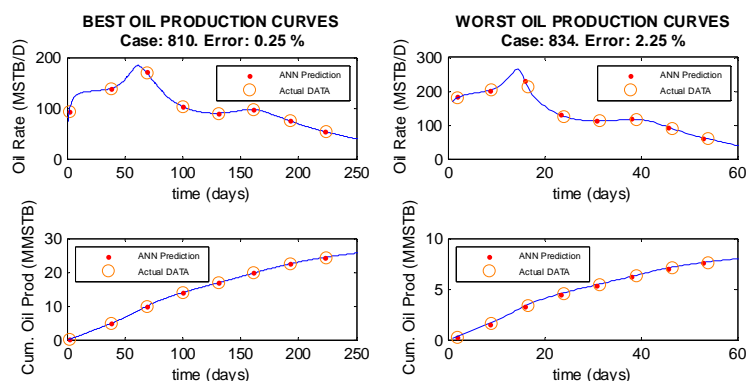
Figure **C-8**: Best and Worst Production Profile Built using Stage-2 Network: CO_2 Injection, PVT#1, 9-Spot. Batch 2 (Large Areas)
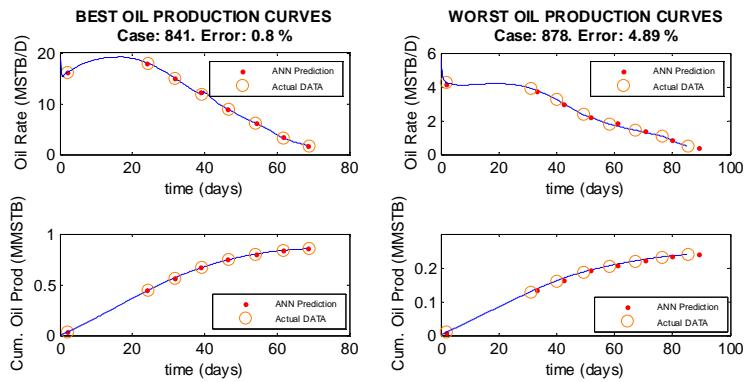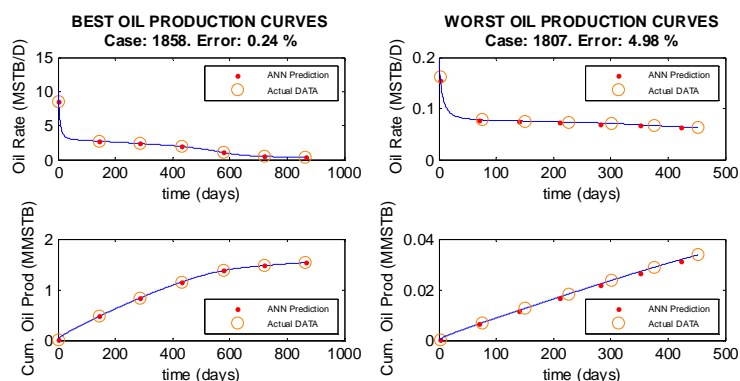

Figure **C-9**: Best and Worst Production Profiles Built using Stage-2 Network: CO_2 Injection, PVT#2, 4-Spot. Batch 1 (Small Areas)
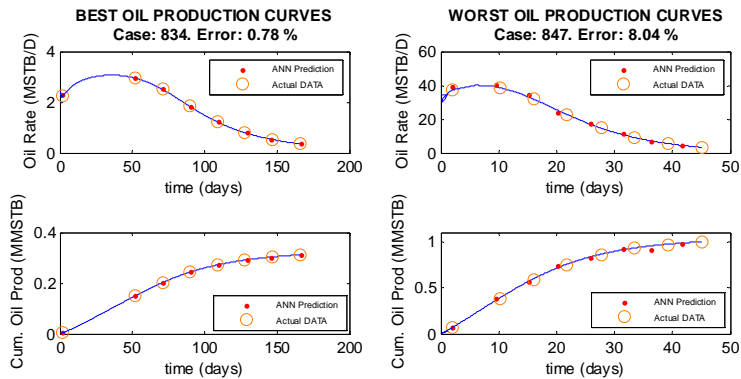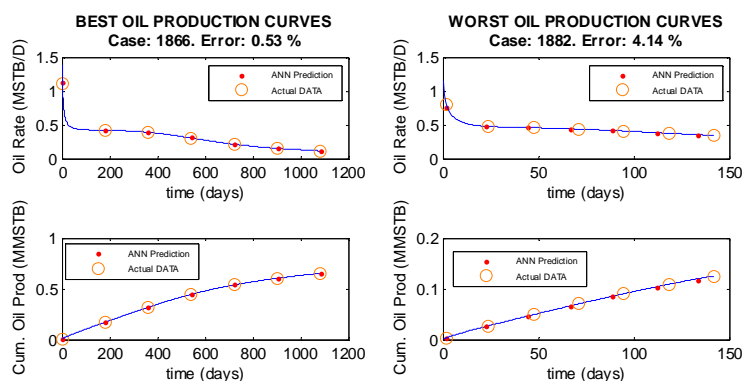

Figure **C-10**: Best and Worst Production Profiles Built using Stage-2 Network: CO_2 Injection, PVT#2, 5-Spot. Batch 1 (Small Areas)
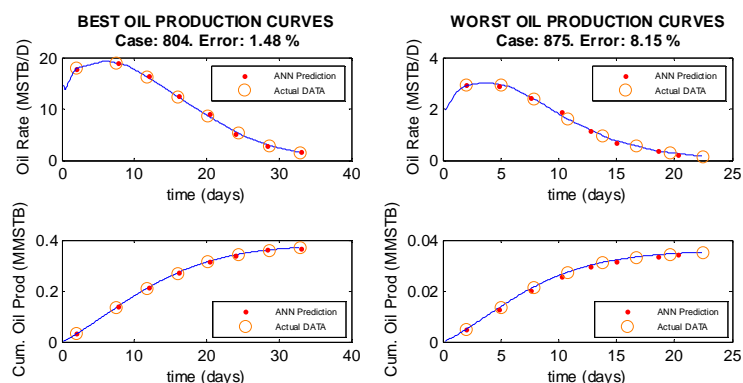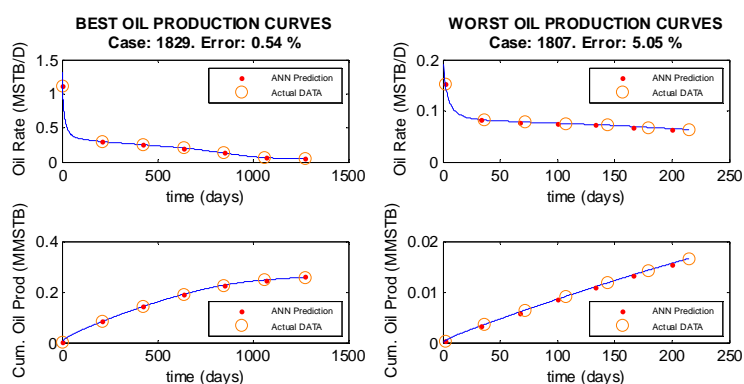
Figure **C-11**: Best and Worst Production Profiles Built using Stage-2 Network: CO_2 Injection, PVT#2, 7-Spot. Batch 1 (Small Areas)
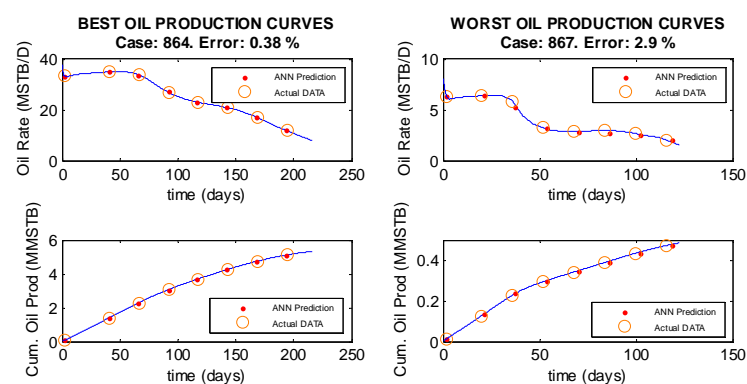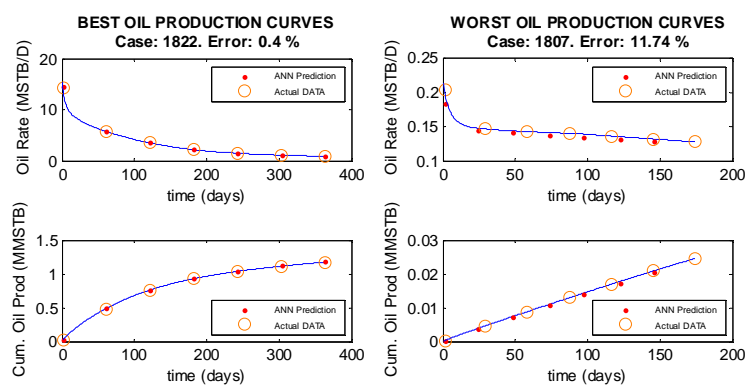

Figure **C-12**: Best and Worst Production Profiles Built using Stage-2 Network: CO_2 Injection, PVT#2, 9-Spot. Batch 1 (Small Areas)
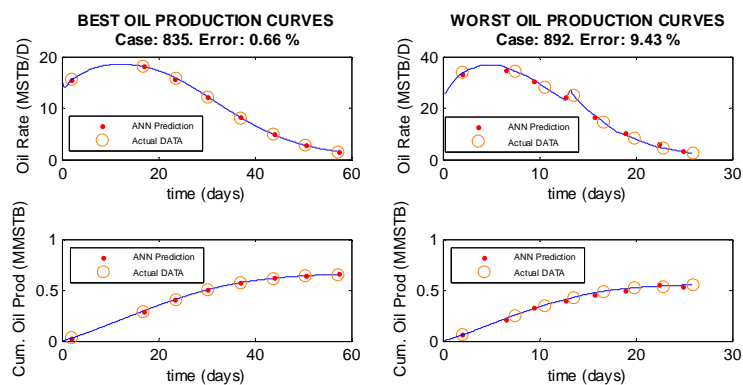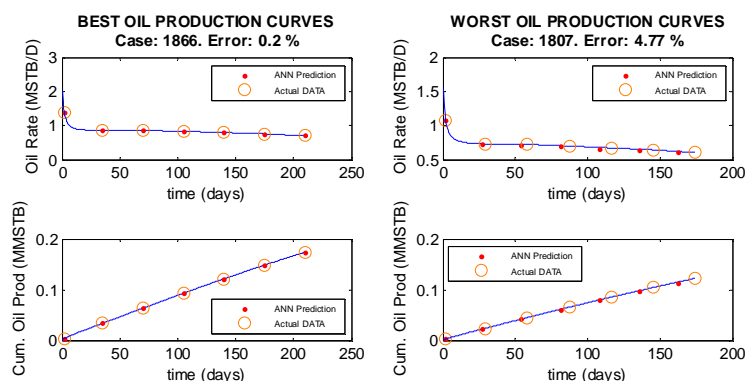

Figure **C-13**: Best and Worst Production Profiles Built using Stage-2 Network: CO_2 Injection, PVT#2, 4-Spot. Batch 2 (Large Areas)
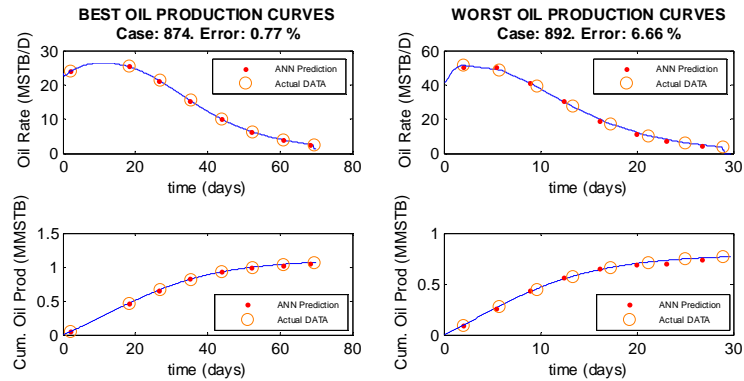
Figure **C-14**: Best and Worst Production Profiles Built using Stage-2 Network: CO_2 Injection, PVT#2, 5-Spot. Batch 2 (Large Areas)
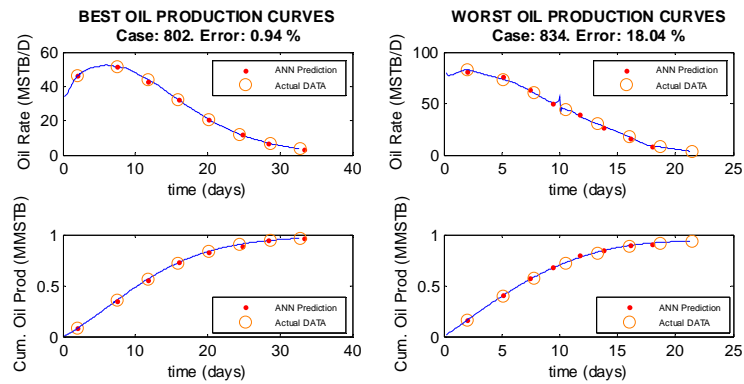
Figure **C-15**: Best and Worst Production Profiles Built using Stage-2 Network: CO_2 Injection, PVT#2, 7-Spot. Batch 2 (Large Areas)
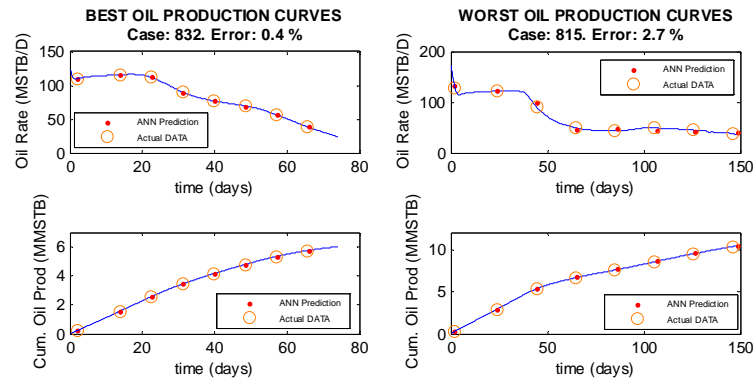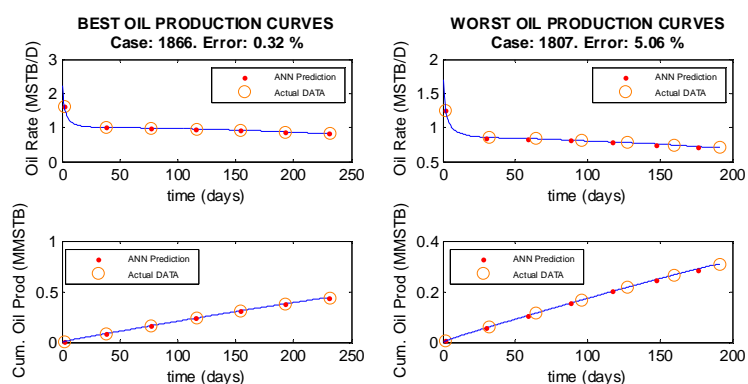

Figure **C-16**: Best and Worst Production Profiles Built using Stage-2 Network: CO_2 Injection, PVT#2, 9-Spot. Batch 2 (Large Areas)
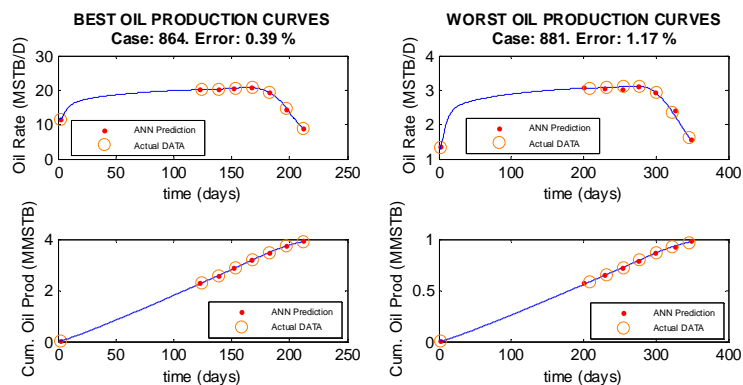
Figure **C-17**: Best and Worst Production Profiles Built using Stage-2 Network: CO_2 Injection, PVT#3, 4-Spot. Batch 1 (Small Areas)
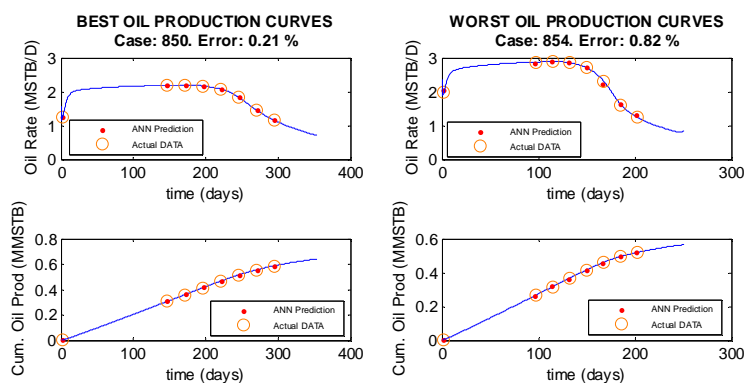
Figure **C-18**: Best and Worst Production Profiles Built using Stage-2 Network: CO_2 Injection, PVT#3, 5-Spot. Batch 1 (Small Areas)
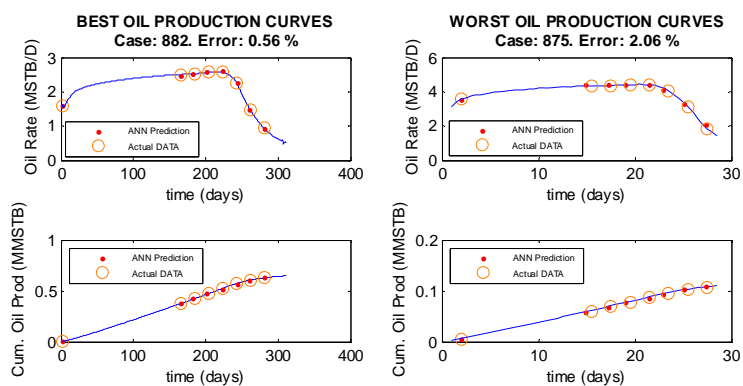
Figure **C-19**: Best and Worst Production Profiles Built using Stage-2 Network: CO_2 Injection, PVT#3, 7-Spot. Batch 1 (Small Areas)
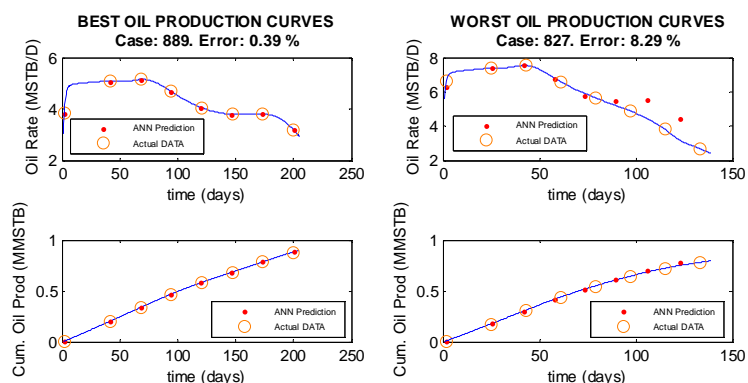
Figure **C-20**: Best and Worst Production Profiles Built using Stage-2 Network: CO_2 Injection, PVT#3, 9-Spot. Batch 1 (Small Areas)
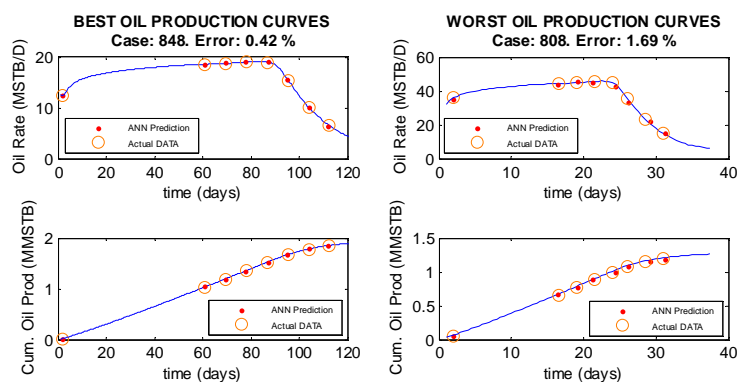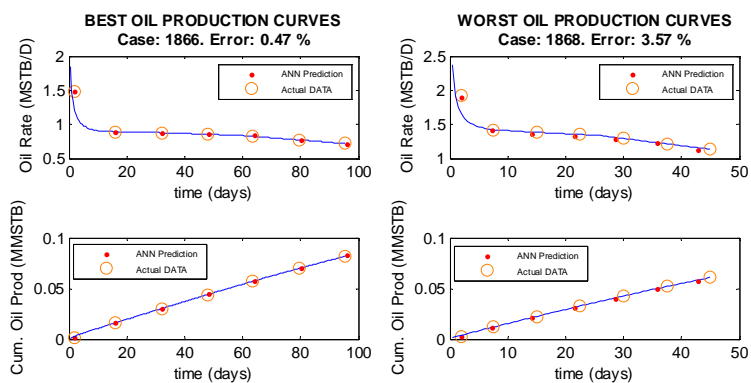

Figure **C-21**: Best and Worst Production Profiles Built using Stage-2 Network: CO_2 Injection, PVT#3, 4-Spot. Batch 2 (Large Areas)
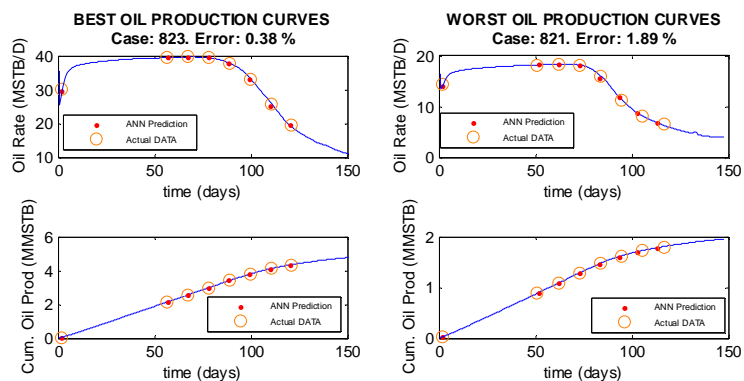
Figure **C-22**: Best and Worst Production Profiles Built using Stage-2 Network: CO_2 Injection, PVT#3, 5-Spot. Batch 2 (Large Areas)
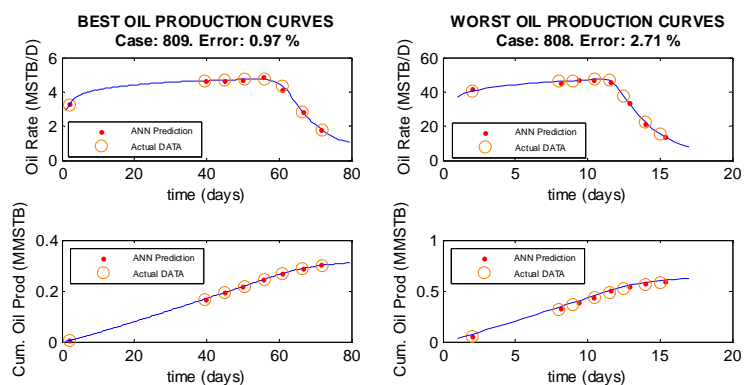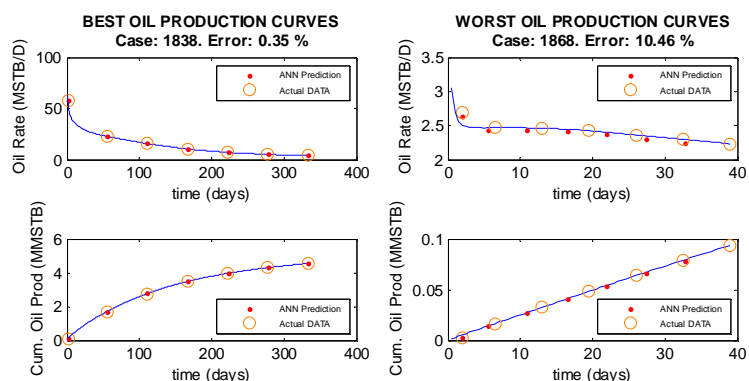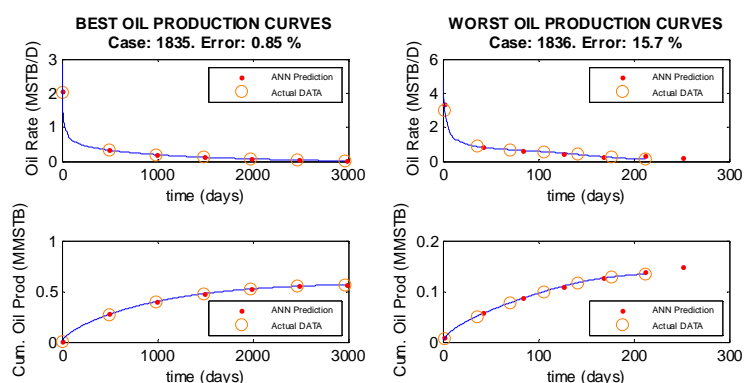
Figure **C-23**: Best and Worst Production Profiles Built using Stage-2 Network: CO_2 Injection, PVT#3, 7-Spot. Batch 2 (Large Areas)
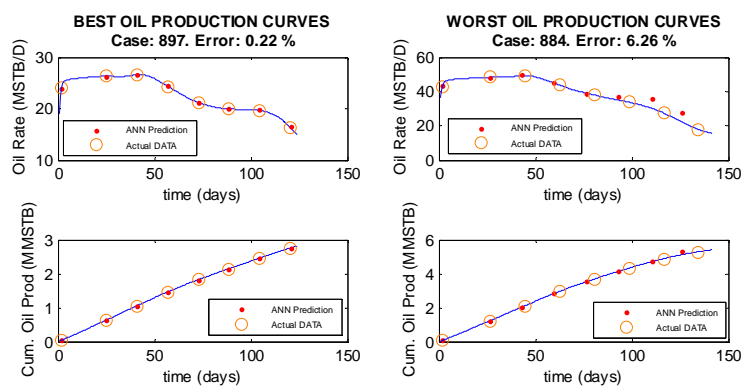
Figure **C-24**: Best and Worst Production Profiles Built using Stage-2 Network: CO_2 Injection, PVT#3, 9-Spot. Batch 2 (Large Areas)
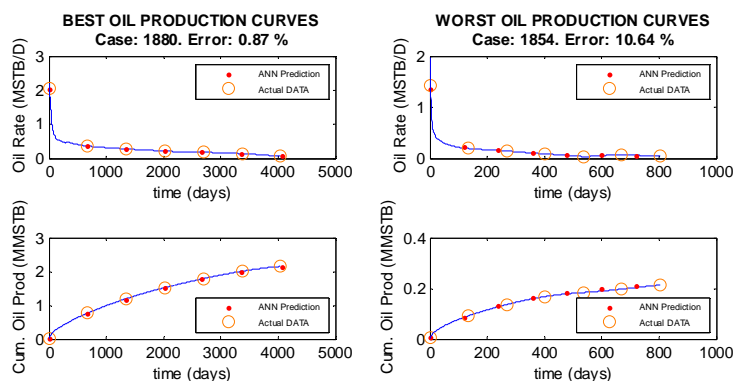
C.1.2 N₂ Miscible Injection
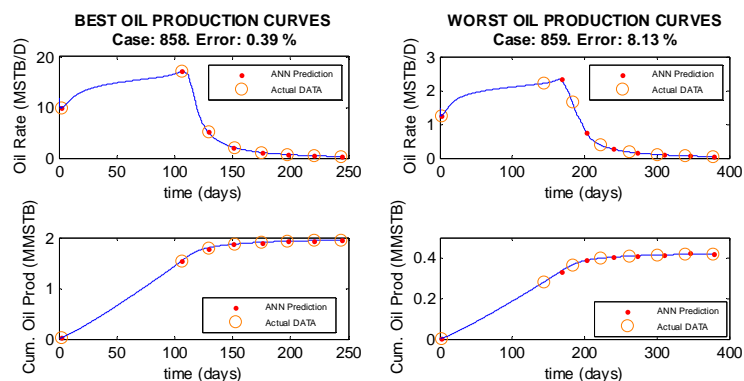
Figure **C-25**: Best and Worst Production Profiles Built using Stage-2 Network: N₂ Injection, PVT#1, 4-Spot. Batch 1 (Small Areas)
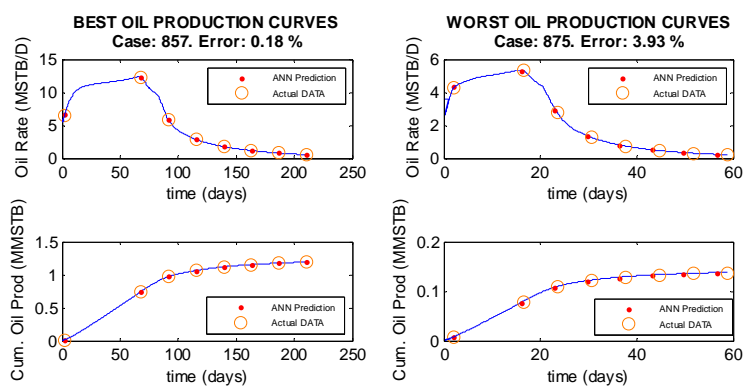
Figure **C-26**: Best and Worst Production Profiles Built using Stage-2 Network: N₂ Injection, PVT#1, 5-Spot. Batch 1 (Small Areas)
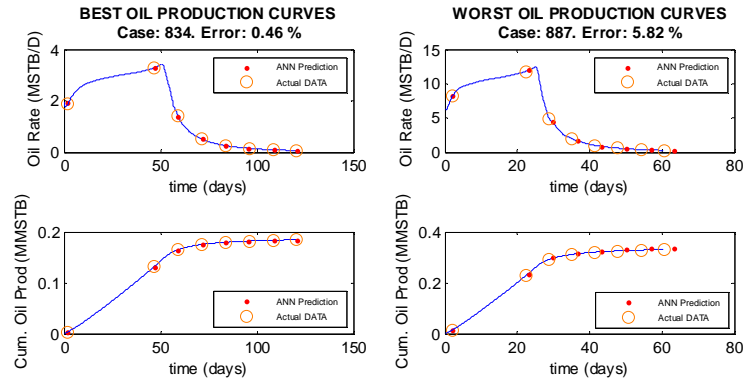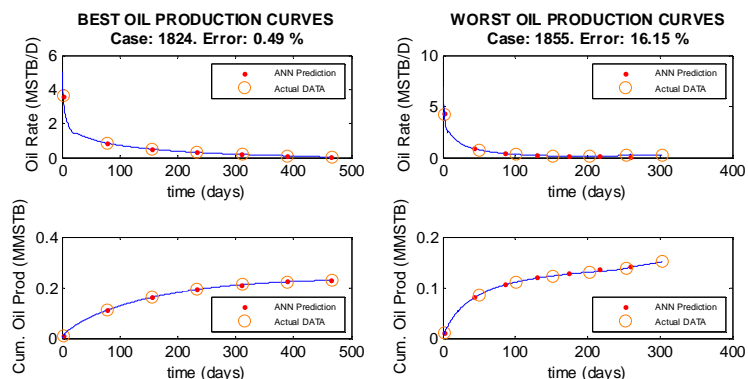
Figure **C-27**: Best and Worst Production Profiles Built using Stage-2 Network: N$_2$ Injection, PVT#1, 7-Spot. Batch 1 (Small Areas)
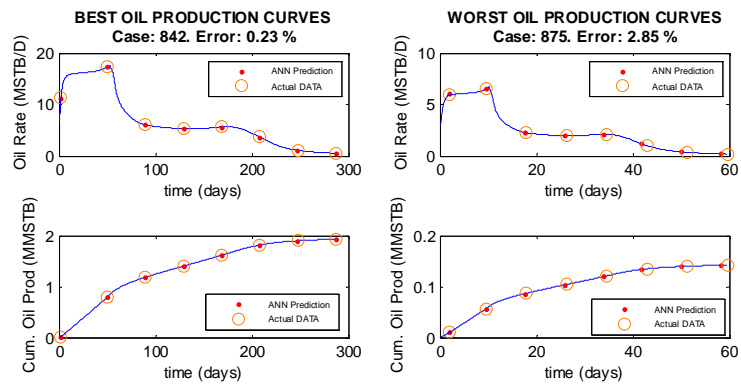
Figure **C-28**: Best and Worst Production Profiles Built using Stage-2 Network: N$_2$ Injection, PVT#1, 9-Spot. Batch 1 (Small Areas)
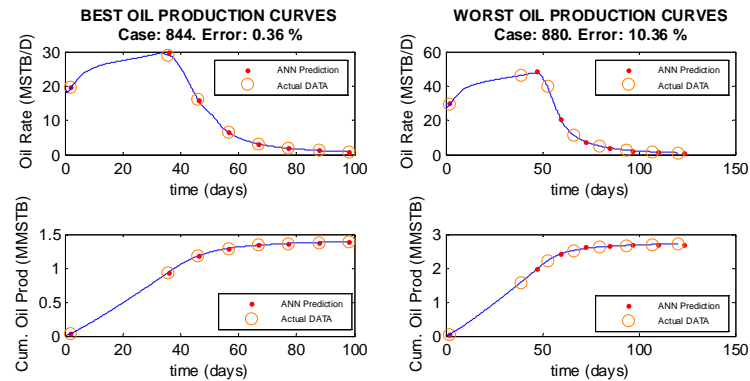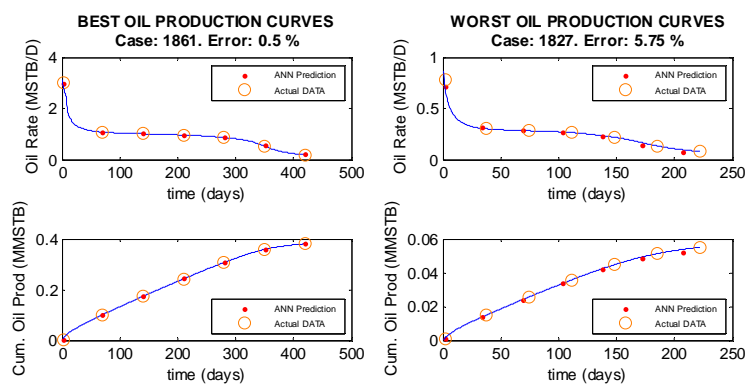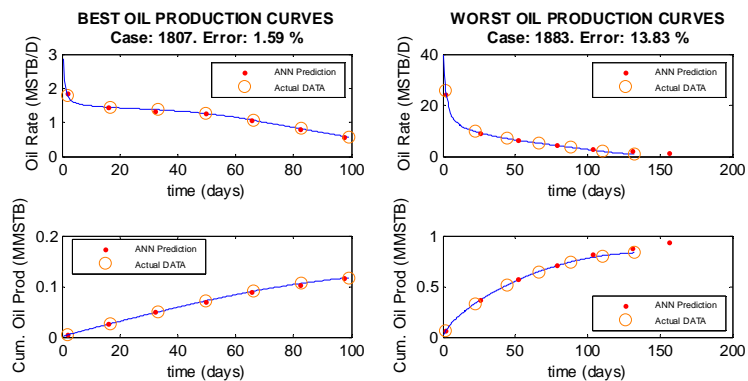

Figure **C-29**: Best and Worst Production Profiles Built using Stage-2 Network: N$_2$ Injection, PVT#1, 4-Spot. Batch 2 (Large Areas)
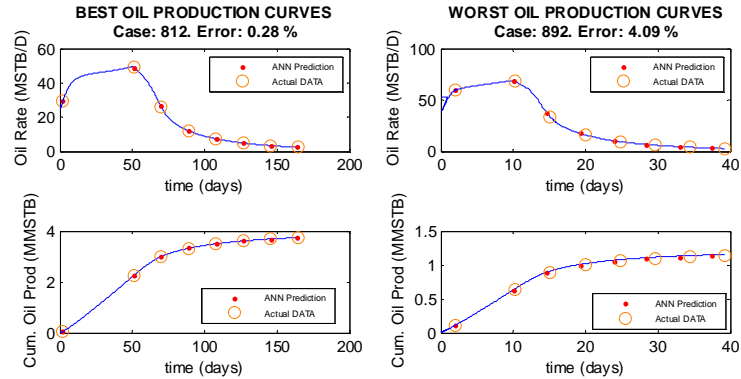
Figure **C-30**: Best and Worst Production Profiles Built using Stage-2 Network: N_2 Injection, PVT#1, 5-Spot. Batch 2 (Large Areas)
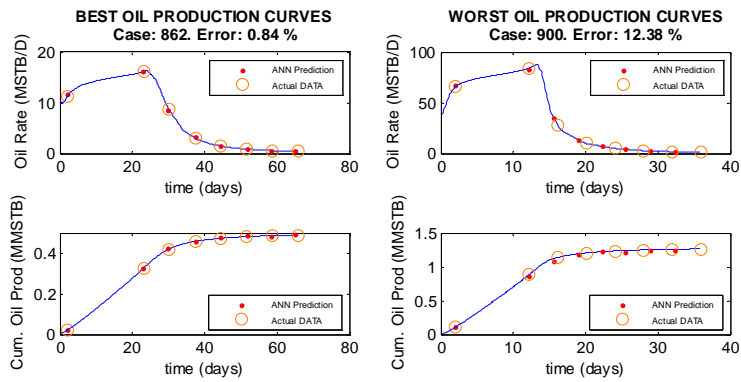
Figure **C-31**: Best and Worst Production Profiles Built using Stage-2 Network: N_2 Injection, PVT#1, 7-Spot. Batch 2 (Large Areas)
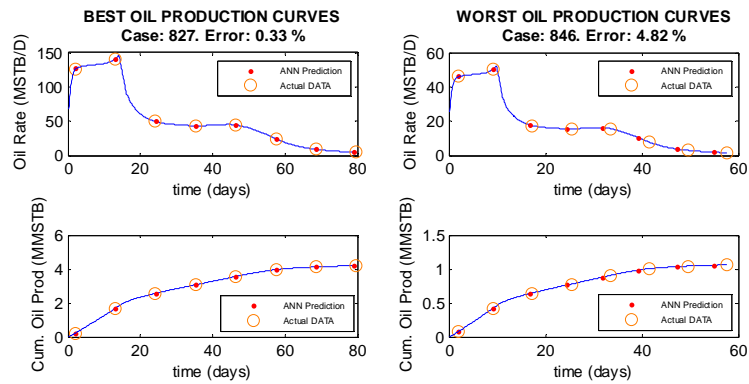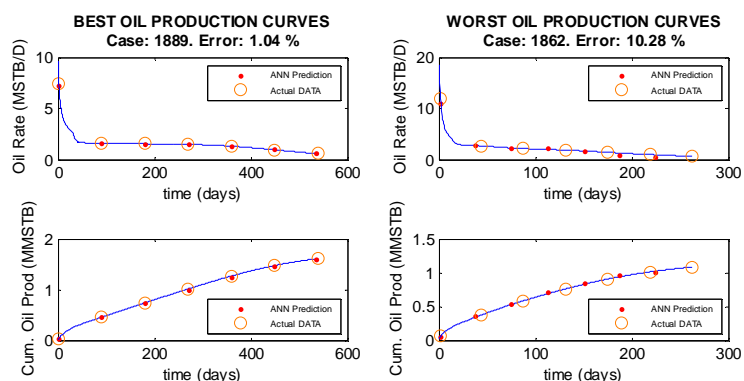

Figure **C-32**: Best and Worst Production Profiles Built using Stage-2 Network: N_2 Injection, PVT#1, 9-Spot. Batch 2 (Large Areas)
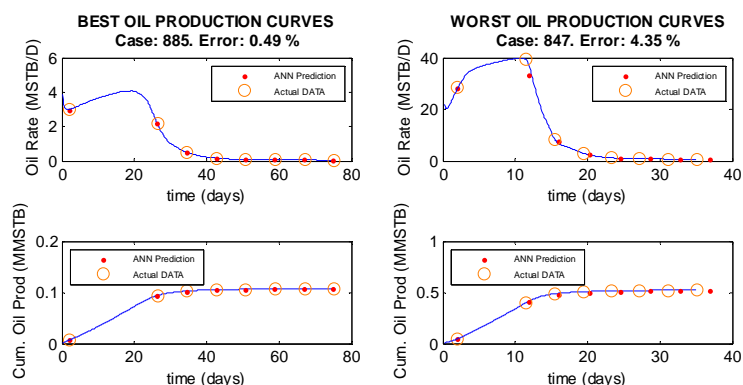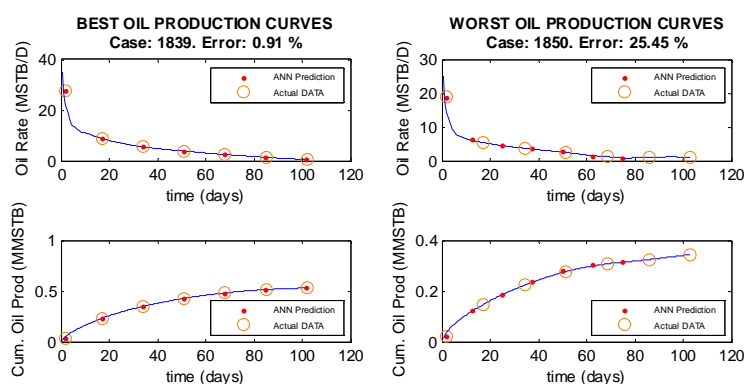
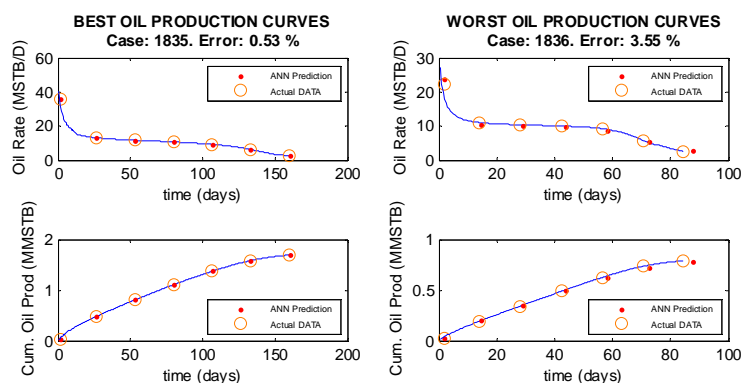Figure **C-33**: Best and Worst Production Profiles Built using Stage-2 Network: N$_2$ Injection, PVT#2, 4-Spot. Batch 1 (Small Areas)
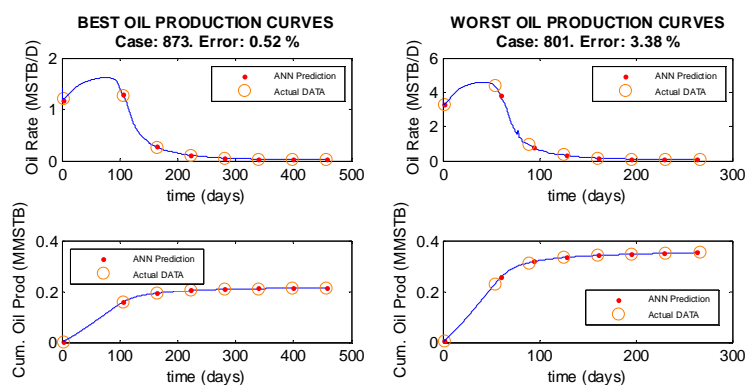
Figure **C-34**: Best and Worst Production Profiles Built using Stage-2 Network: N$_2$ Injection, PVT#2, 5-Spot. Batch 1 (Small Areas)
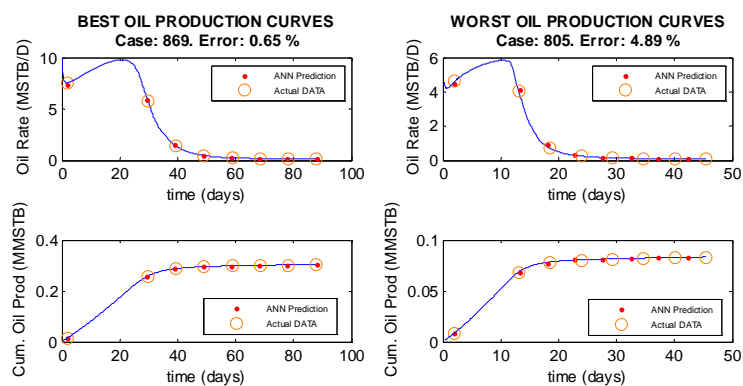
Figure **C-35**: Best and Worst Production Profiles Built using Stage-2 Network: N$_2$ Injection, PVT#2, 7-Spot. Batch 1 (Small Areas)
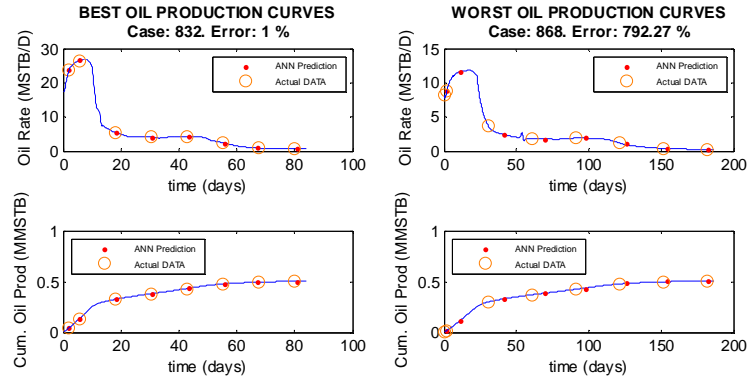
Figure **C-36**: Best and Worst Production Profiles Built using Stage-2 Network: N_2 Injection, PVT#1, 9-Spot. Batch 1 (Small Areas)
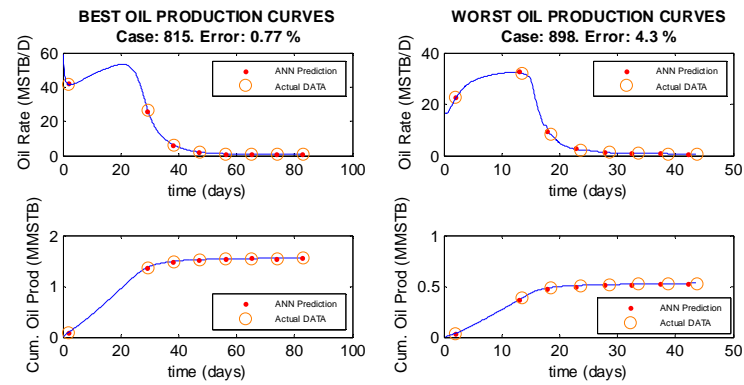
Figure **C-37**: Best and Worst Production Profiles Built using Stage-2 Network: N_2 Injection, PVT#2, 4-Spot. Batch 2 (Large Areas)
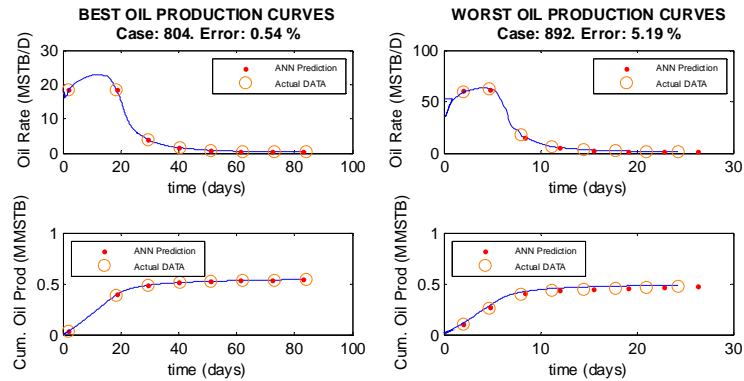
Figure **C-38**: Best and Worst Production Profiles Built using Stage-2 Network: N_2 Injection, PVT#2, 5-Spot. Batch 2 (Large Areas)
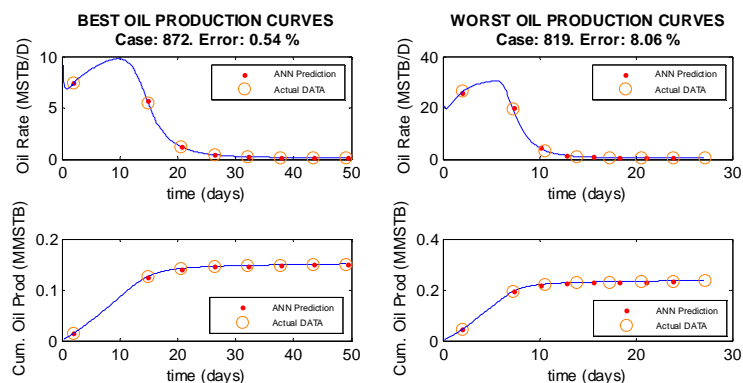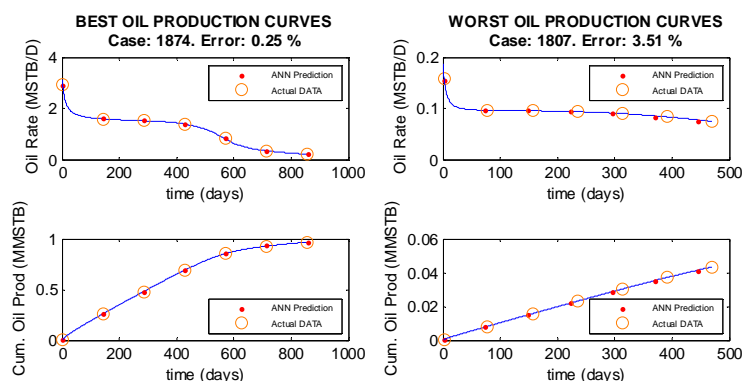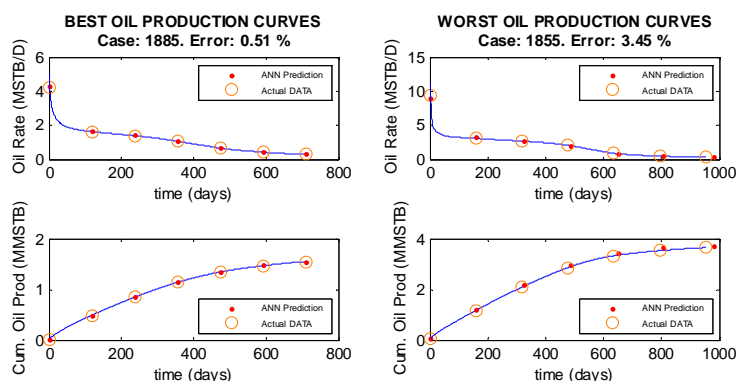
Figure **C-39**: Best and Worst Production Profiles Built using Stage-2 Network: N_2 Injection, PVT#2, 7-Spot. Batch 2 (Large Areas)
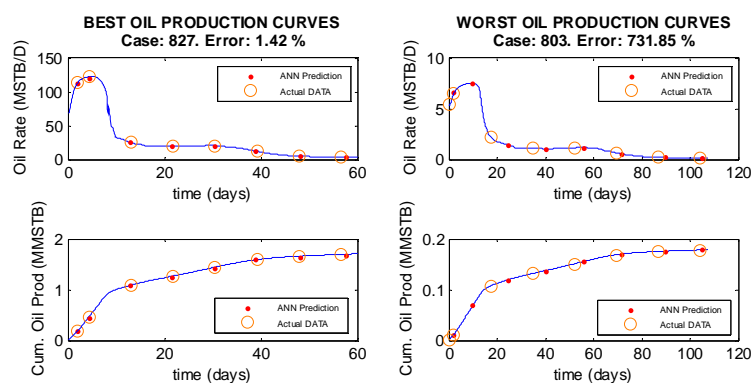
Figure **C-40**: Best and Worst Production Profiles Built using Stage-2 Network: N_2 Injection, PVT#2, 9-Spot. Batch 2 (Large Areas)
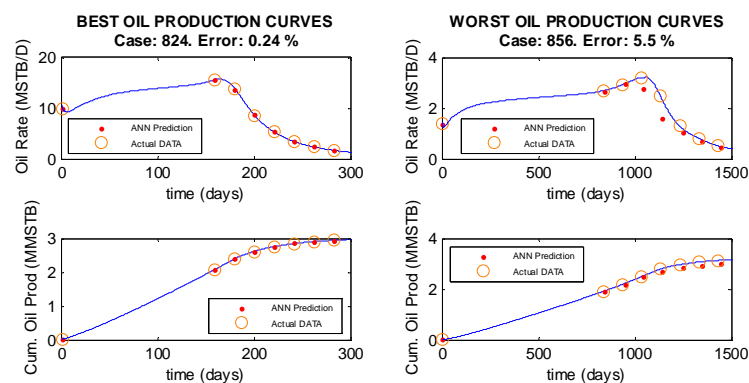
Figure **C-41**: Best and Worst Production Profiles Built using Stage-2 Network: N_2 Injection, PVT#3, 4-Spot. Batch 1 (Small Areas)
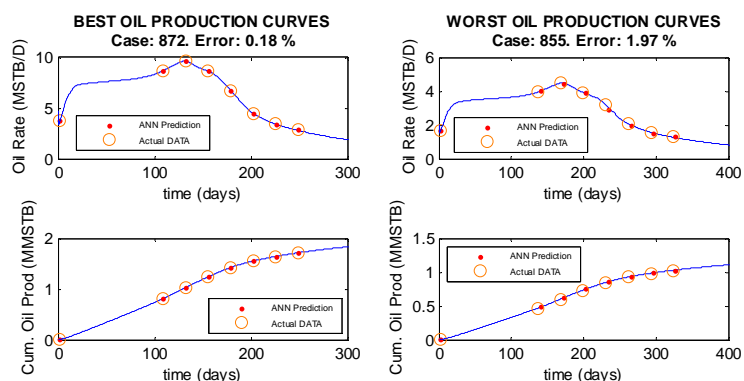
Figure **C-42**: Best and Worst Production Profiles Built using Stage-2 Network: N_2 Injection, PVT#3, 5-Spot. Batch 1 (Small Areas)
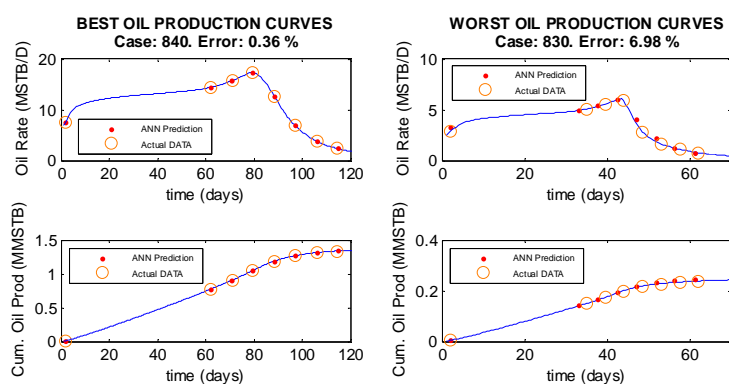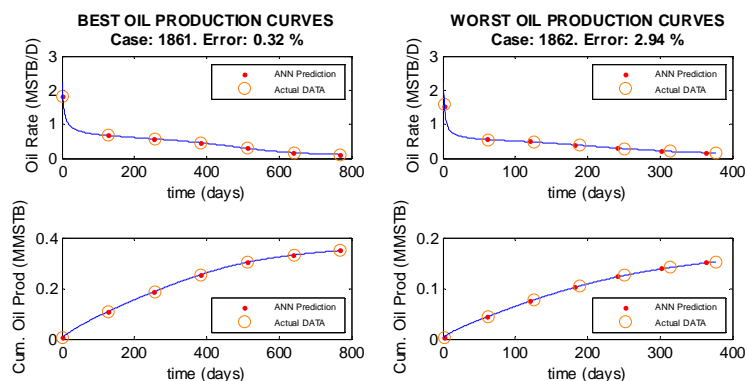

Figure **C-43**: Best and Worst Production Profiles Built using Stage-2 Network: N_2 Injection, PVT#3, 7-Spot. Batch 1 (Small Areas)
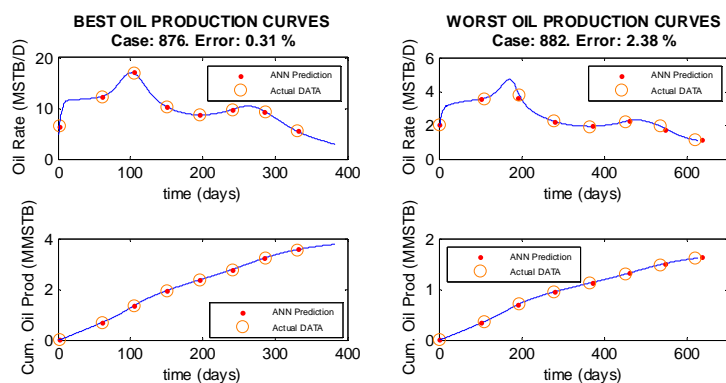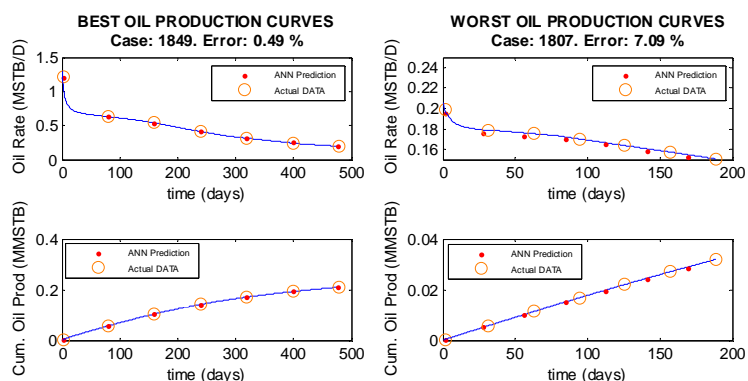

Figure **C-44**: Best and Worst Production Profiles Built using Stage-2 Network: N_2 Injection, PVT#3, 9-Spot. Batch 1 (Small Areas)
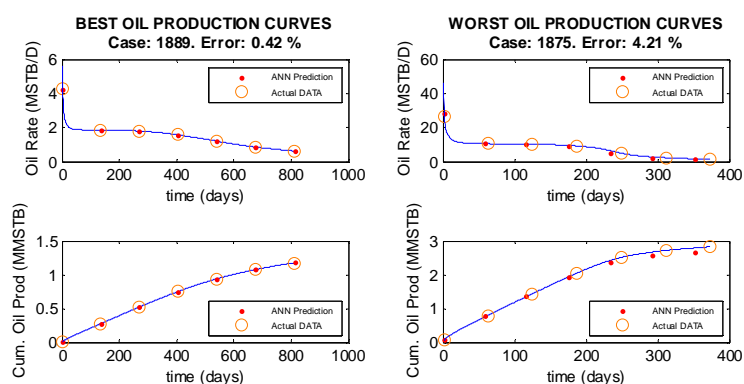
Figure **C-45**: Best and Worst Production Profiles Built using Stage-2 Network: N$_2$ Injection, PVT#3, 4-Spot. Batch 2 (Large Areas)
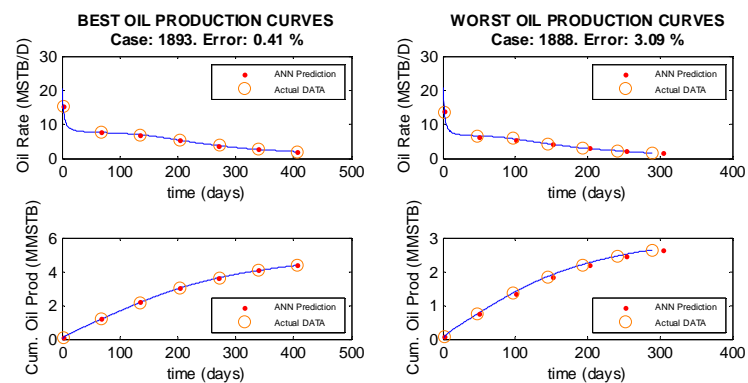

Figure **C-46**: Best and Worst Production Profiles Built using Stage-2 Network: N$_2$ Injection, PVT#3, 5-Spot. Batch 2 (Large Areas)

Figure **C-47**: Best and Worst Production Profiles Built using Stage-2 Network: N$_2$ Injection, PVT#3, 7-Spot. Batch 2 (Large Areas)

Figure **C-48**: Best and Worst Production Profiles Built using Stage-2 Network: N$_2$ Injection, PVT#3, 9-Spot. Batch 2 (Large Areas)
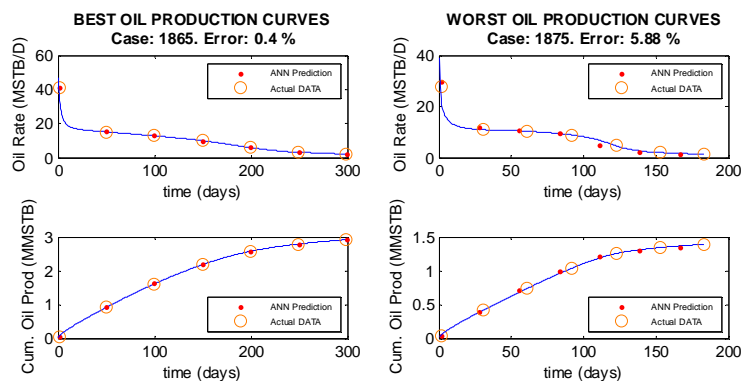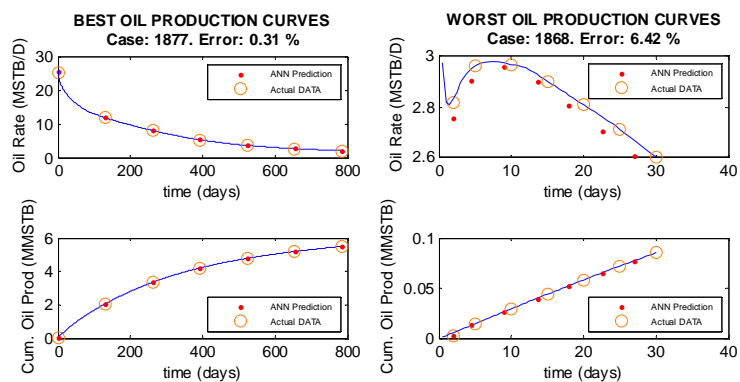
C.1.3 Water Injection

Figure **C-49**: Best and Worst Production Profiles Built using Stage-2 Network: Water Injection, PVT#1, 4-Spot. Batch 1 (Small Areas)

Figure **C-50**: Best and Worst Production Profiles Built using Stage-2 Network: Water Injection, PVT#1, 5-Spot. Batch 1 (Small Areas)

Figure **C-51**: Best and Worst Production Profiles Built using Stage-2 Network: Water Injection, PVT#1, 7-Spot. Batch 1 (Small Areas)

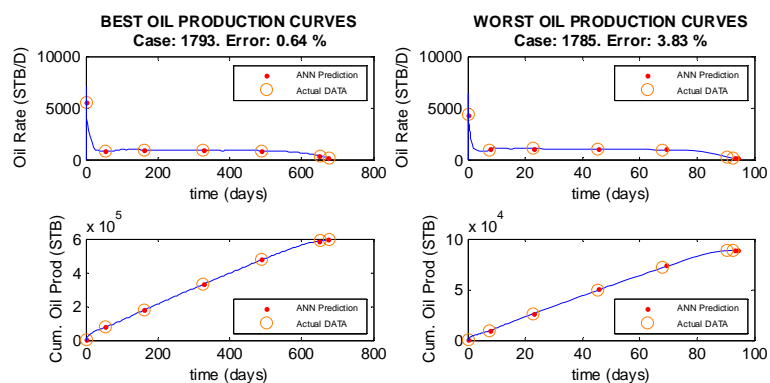Figure **C-52**: Best and Worst Production Profiles Built using Stage-2 Network: Water Injection, PVT#1, 9-Spot. Batch 1 (Small Areas)

Figure **C-53**: Best and Worst Production Profiles Built using Stage-2 Network: Water Injection, PVT#1, 4-Spot. Batch 2 (Large Areas)
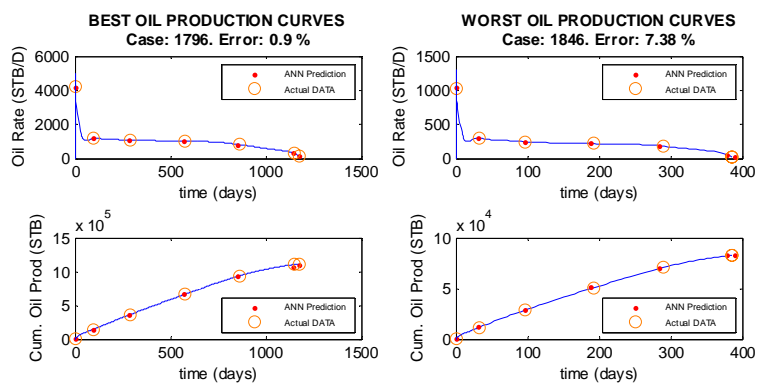

Figure **C-54**: Best and Worst Production Profiles Built using Stage-2 Network: Water Injection, PVT#1, 5-Spot. Batch 2 (Large Areas)

Figure **C-55**: Best and Worst Production Profiles Built using Stage-2 Network: Water Injection, PVT#1, 7-Spot. Batch 2 (Large Areas)

Figure **C-56**: Best and Worst Production Profiles Built using Stage-2 Network: Water Injection, PVT#1, 9-Spot. Batch 2 (Large Areas)

Figure **C-57**: Best and Worst Production Profiles Built using Stage-2 Network: Water Injection, PVT#2, 4-Spot. Batch 1 (Small Areas)

Figure **C-58**: Best and Worst Production Profiles Built using Stage-2 Network: Water Injection, PVT#2, 5-Spot. Batch 1 (Small Areas)
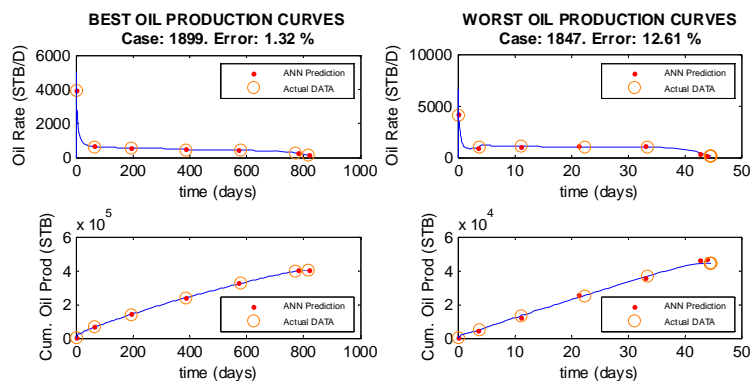
Figure **C-59**: Best and Worst Production Profiles Built using Stage-2 Network: Water Injection, PVT#2, 7-Spot. Batch 1 (Small Areas)
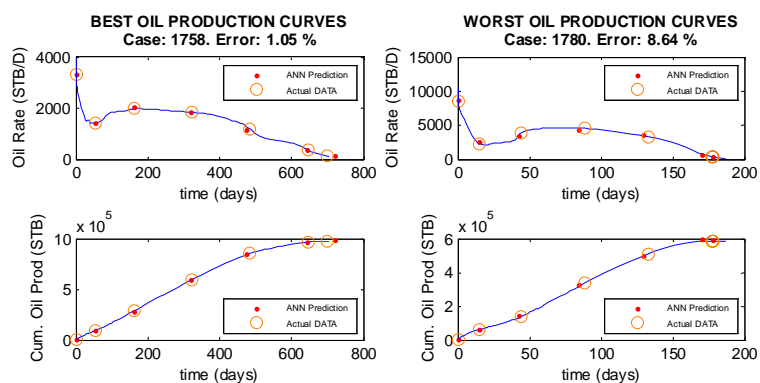

Figure **C-60**: Best and Worst Production Profiles Built using Stage-2 Network: Water Injection, PVT#2, 9-Spot. Batch 1 (Small Areas)
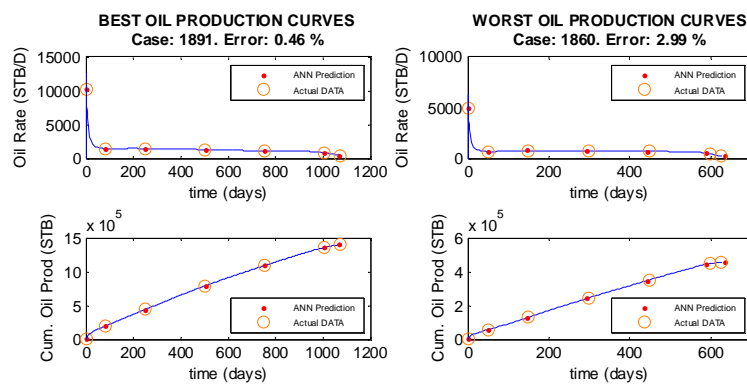

Figure **C-61**: Best and Worst Production Profiles Built using Stage-2 Network: Water Injection, PVT#2, 4-Spot. Batch 2 (Large Areas)

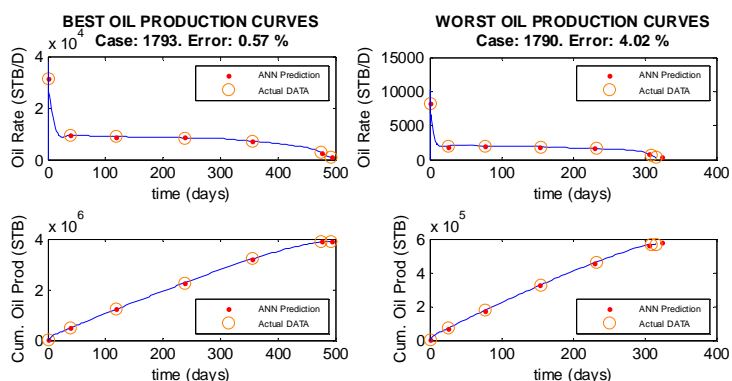Figure **C-62**: Best and Worst Production Profiles Built using Stage-2 Network: Water Injection, PVT#2, 5-Spot. Batch 2 (Large Areas)

Figure **C-63**: Best and Worst Production Profiles Built using Stage-2 Network: Water Injection, PVT#2, 7-Spot. Batch 2 (Large Areas)

Figure **C-64**: Best and Worst Production Profiles Built using Stage-2 Network: Water Injection, PVT#2, 9-Spot. Batch 2 (Large Areas)
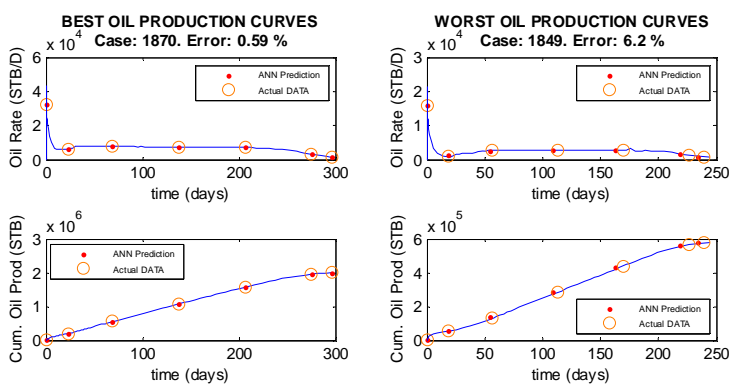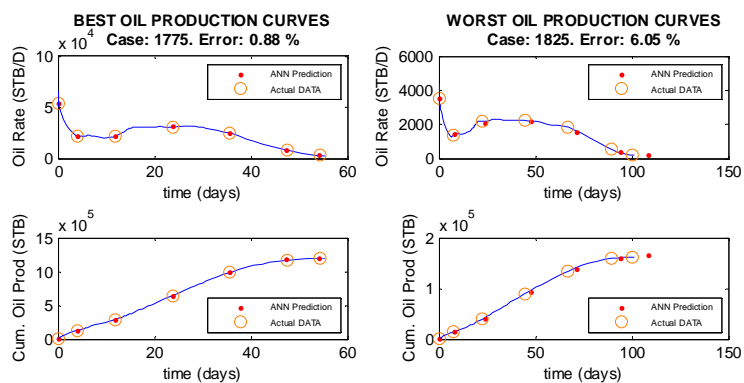
Figure **C-65**: Best and Worst Production Profiles Built using Stage-2 Network: Water Injection, PVT#3, 4-Spot. Batch 1 (Small Areas)

Figure **C-66**: Best and Worst Production Profiles Built using Stage-2 Network: Water Injection, PVT#3, 5-Spot. Batch 1 (Small Areas)

Figure **C-67**: Best and Worst Production Profiles Built using Stage-2 Network: Water Injection, PVT#3, 7-Spot. Batch 1 (Small Areas)

Figure **C-68**: Best and Worst Production Profiles Built using Stage-2 Network: Water Injection, PVT#3, 9-Spot. Batch 1 (Small Areas)

Figure **C-69**: Best and Worst Production Profiles Built using Stage-2 Network: Water Injection, PVT#3, 4-Spot. Batch 2 (Large Areas)

Figure **C-70**: Best and Worst Production Profiles Built using Stage-2 Network: Water Injection, PVT#3, 5-Spot. Batch 2 (Large Areas)
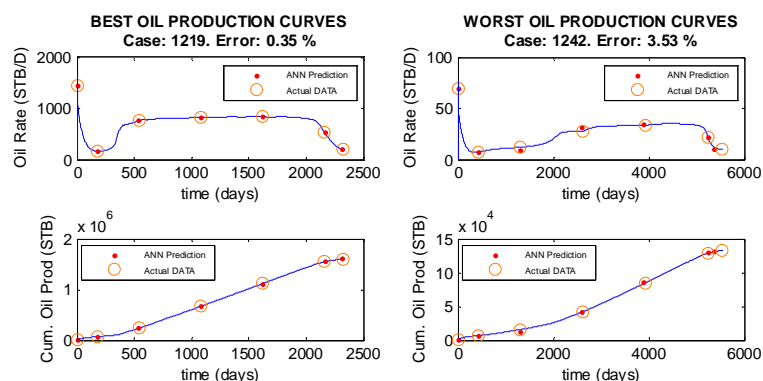
Figure **C-71**: Best and Worst Production Profiles Built using Stage-2 Network: Water Injection, PVT#3, 7-Spot. Batch 2 (Large Areas)
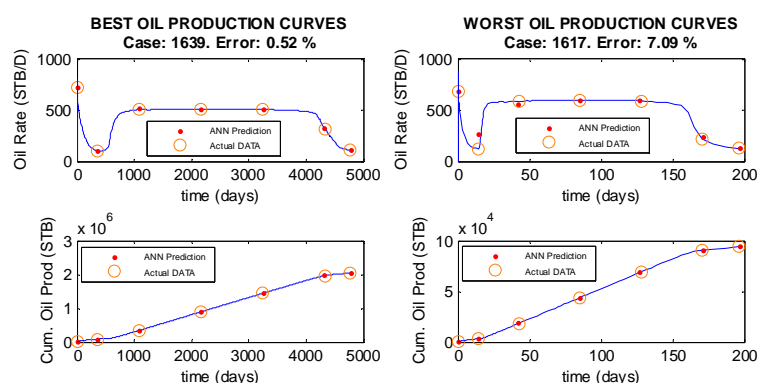

Figure **C-72**: Best and Worst Production Profiles Built using Stage-2 Network: Water Injection, PVT#3, 9-Spot. Batch 2 (Large Areas)

C.1.4 Steam Injection

Figure **C-73**: Best and Worst Production Profiles Built using Stage-2 Network: Steam Injection, PVT#2, 4-Spot. Batch 1 (Small Areas)

Figure **C-74**: Best and Worst Production Profiles Built using Stage-2 Network: Steam Injection, PVT#2, 5-Spot. Batch 1 (Small Areas)
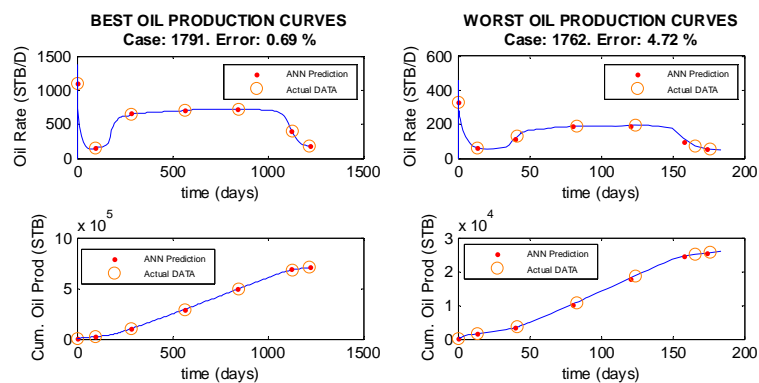
Figure **C-75**: Best and Worst Production Profiles Built using Stage-2 Network: Steam Injection, PVT#2, 7-Spot. Batch 1 (Small Areas)
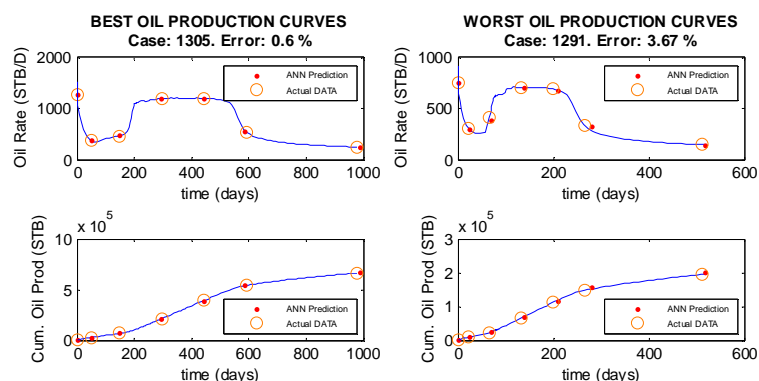

Figure **C-76**: Best and Worst Production Profiles Built using Stage-2 Network: Steam Injection, PVT#2, 9-Spot. Batch 1 (Small Areas)
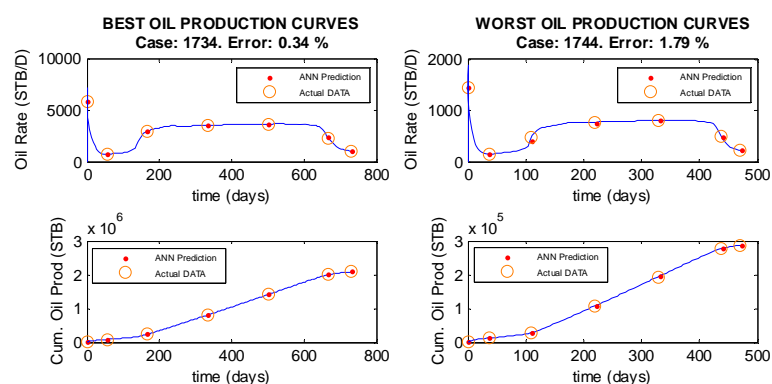

Figure **C-77**: Best and Worst Production Profiles Built using Stage-2 Network: Steam Injection, PVT#2, 4-Spot. Batch 2 (Large Areas)
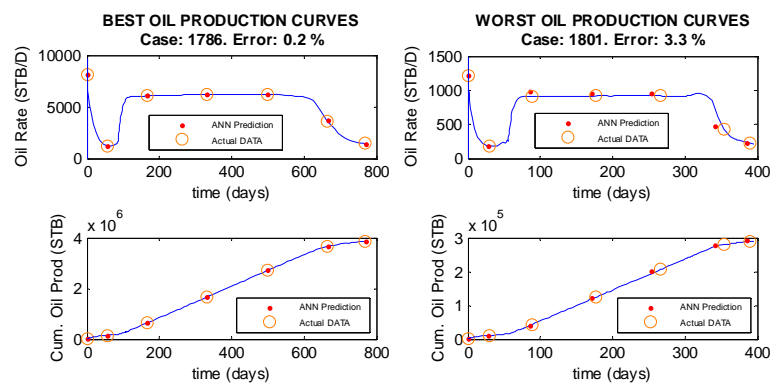
Figure **C-78**: Best and Worst Production Profiles Built using Stage-2 Network: Steam Injection, PVT#2, 5-Spot. Batch 2 (Large Areas)

Figure **C-79**: Best and Worst Production Profiles Built using Stage-2 Network: Steam Injection, PVT#2, 7-Spot. Batch 2 (Large Areas)

Figure **C-80**: Best and Worst Production Profiles Built using Stage-2 Network: Steam Injection, PVT#2, 9-Spot. Batch 2 (Large Areas)
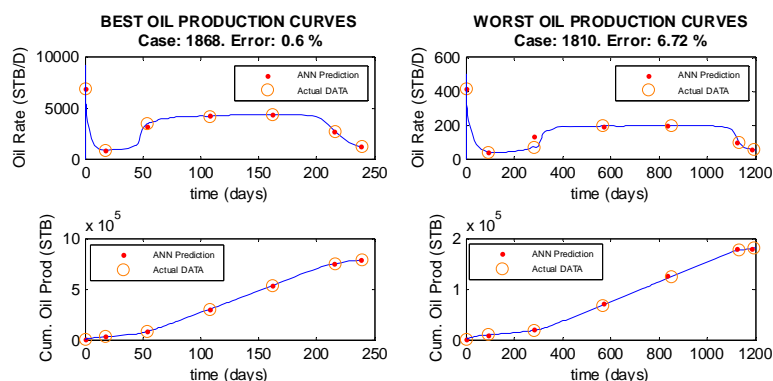
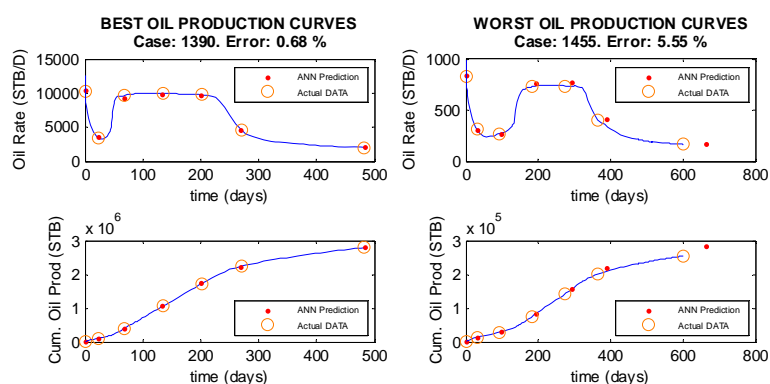Figure **C-81**: Best and Worst Production Profiles Built using Stage-2 Network: Steam Injection, PVT#3, 4-Spot. Batch 1 (Small Areas)

Figure **C-82**: Best and Worst Production Profiles Built using Stage-2 Network: Steam Injection, PVT#3, 5-Spot. Batch 1 (Small Areas)

Figure **C-83**: Best and Worst Production Profiles Built using Stage-2 Network: Steam Injection, PVT#3, 7-Spot. Batch 1 (Small Areas)

Figure **C-84**: Best and Worst Production Profiles Built using Stage-2 Network: Steam Injection, PVT#3, 9-Spot. Batch 1 (Small Areas)

Figure **C-85**: Best and Worst Production Profiles Built using Stage-2 Network: Steam Injection, PVT#3, 4-Spot. Batch 2 (Large Areas)

Figure **C-86**: Best and Worst Production Profiles Built using Stage-2 Network: Steam Injection, PVT#3, 5-Spot. Batch 2 (Large Areas)
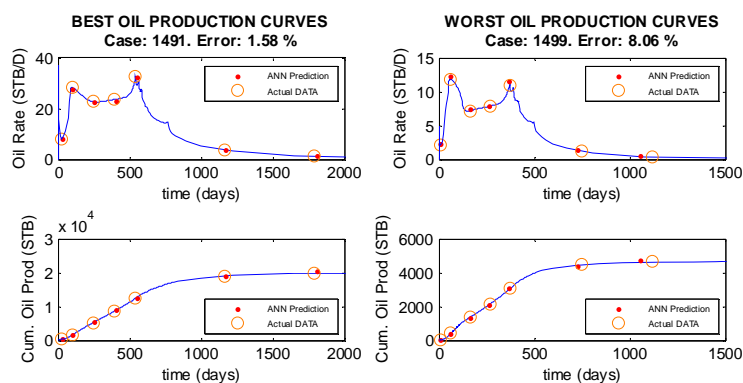
Figure **C-87**: Best and Worst Production Profiles Built using Stage-2 Network: Steam Injection, PVT#3, 7-Spot. Batch 2 (Large Areas)

Figure **C-88**: Best and Worst Production Profiles Built using Stage-2 Network: Steam Injection, PVT#3, 9-Spot. Batch 2 (Large Areas)

Figure **C-89**: Best and Worst Production Profiles Built using Stage-2 Network: Steam Injection, PVT#4, 4-Spot. Batch 1 (Small Areas)
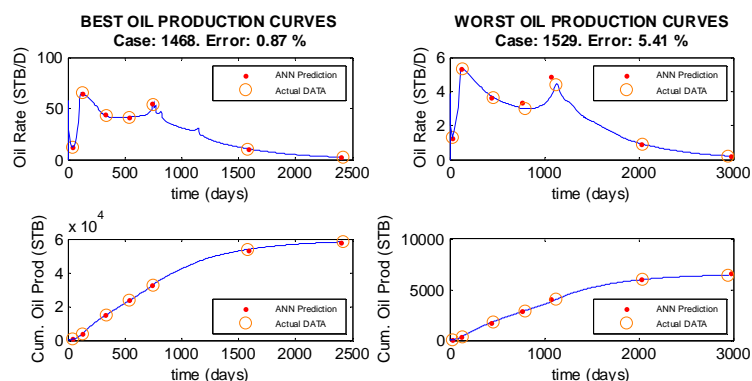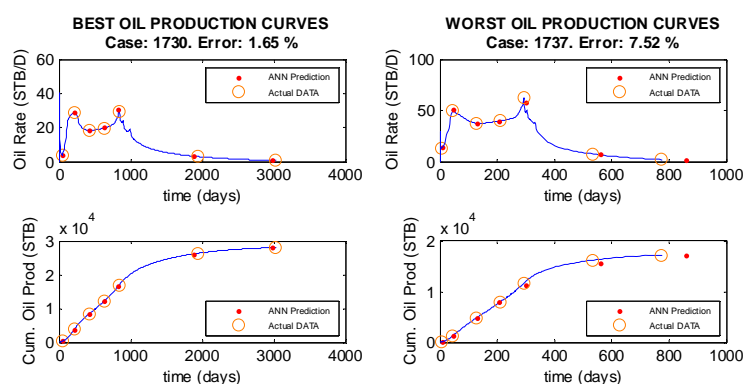
Figure **C-90**: Best and Worst Production Profiles Built using Stage-2 Network: Steam Injection, PVT#4, 5-Spot. Batch 1 (Small Areas)

Figure **C-91**: Best and Worst Production Profiles Built using Stage-2 Network: Steam Injection, PVT#4, 7-Spot. Batch 1 (Small Areas)
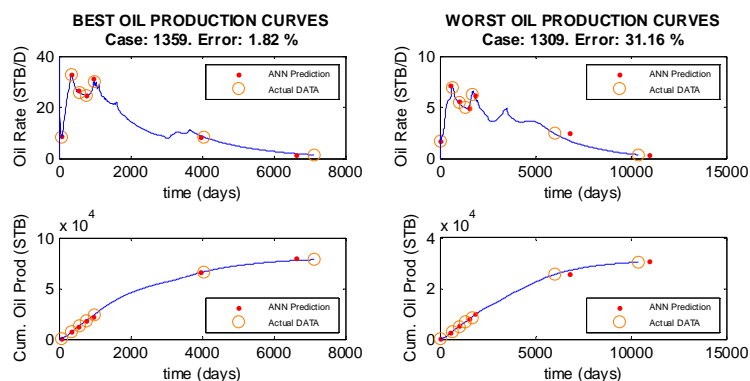

Figure **C-92**: Best and Worst Production Profiles Built using Stage-2 Network: Steam Injection, PVT#4, 9-Spot. Batch 1 (Small Areas)
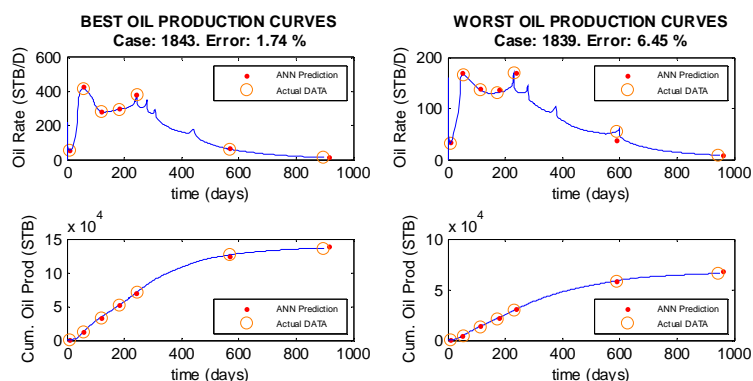
Figure **C-93**: Best and Worst Production Profiles Built using Stage-2 Network: Steam Injection, PVT#4, 4-Spot. Batch 2 (Large Areas)
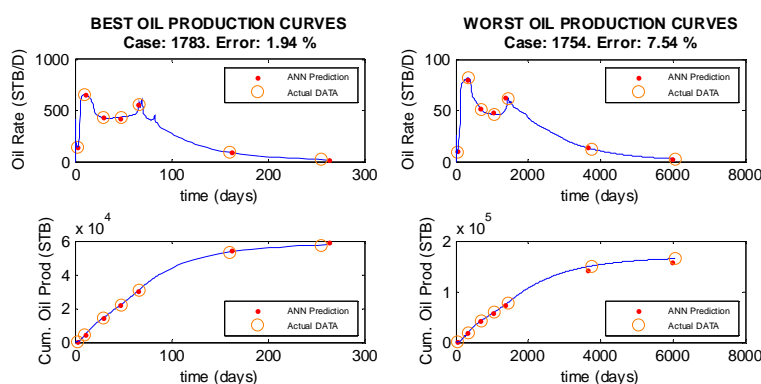

Figure **C-94**: Best and Worst Production Profiles Built using Stage-2 Network: Steam Injection, PVT#4, 5-Spot. Batch 2 (Large Areas)
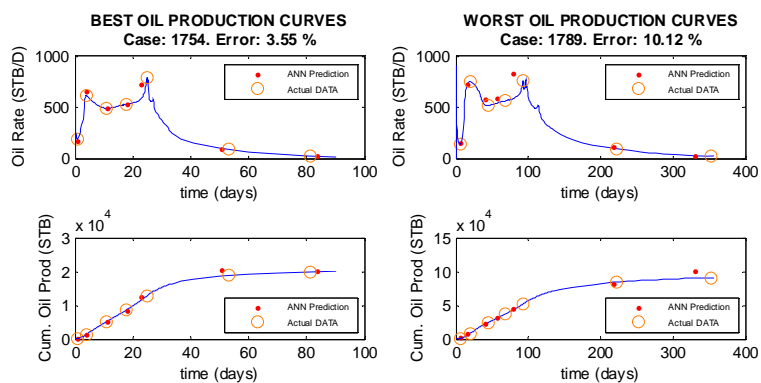

Figure **C-95**: Best and Worst Production Profiles Built using Stage-2 Network: Steam Injection, PVT#4, 7-Spot. Batch 2 (Large Areas)
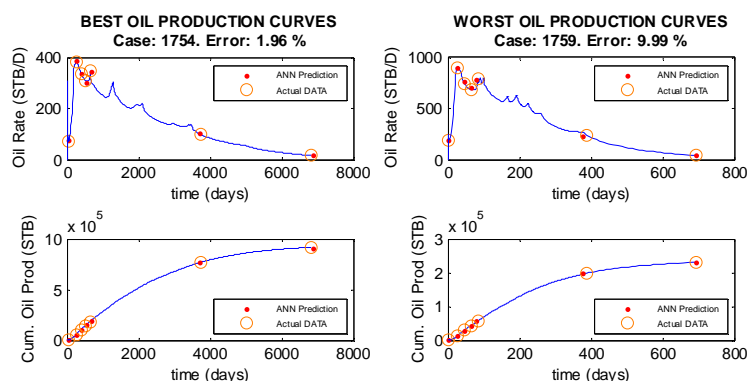
Figure **C-96**: Best and Worst Production Profiles Built using Stage-2 Network: Steam Injection, PVT#4, 9-Spot. Batch 2 (Large Areas)

C.2 Networks in the IOR Project Design Tool-box
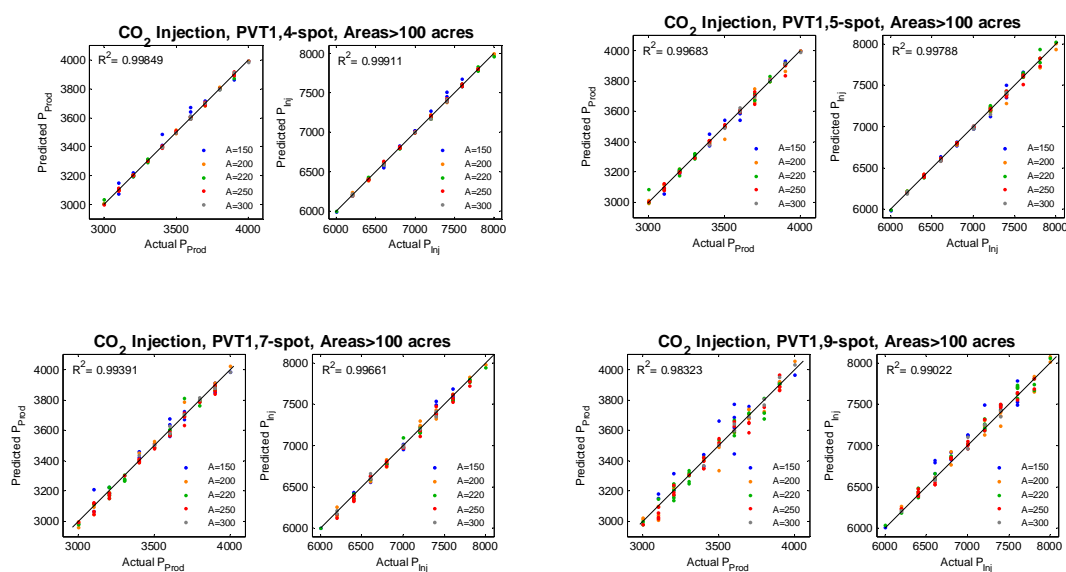
C.2.1 CO_2 Miscible Injection

Figure **C-97**: Correlation Between Actual and Predicted Pressures. CO_2 Injection, PVT#1, Step-2 Network
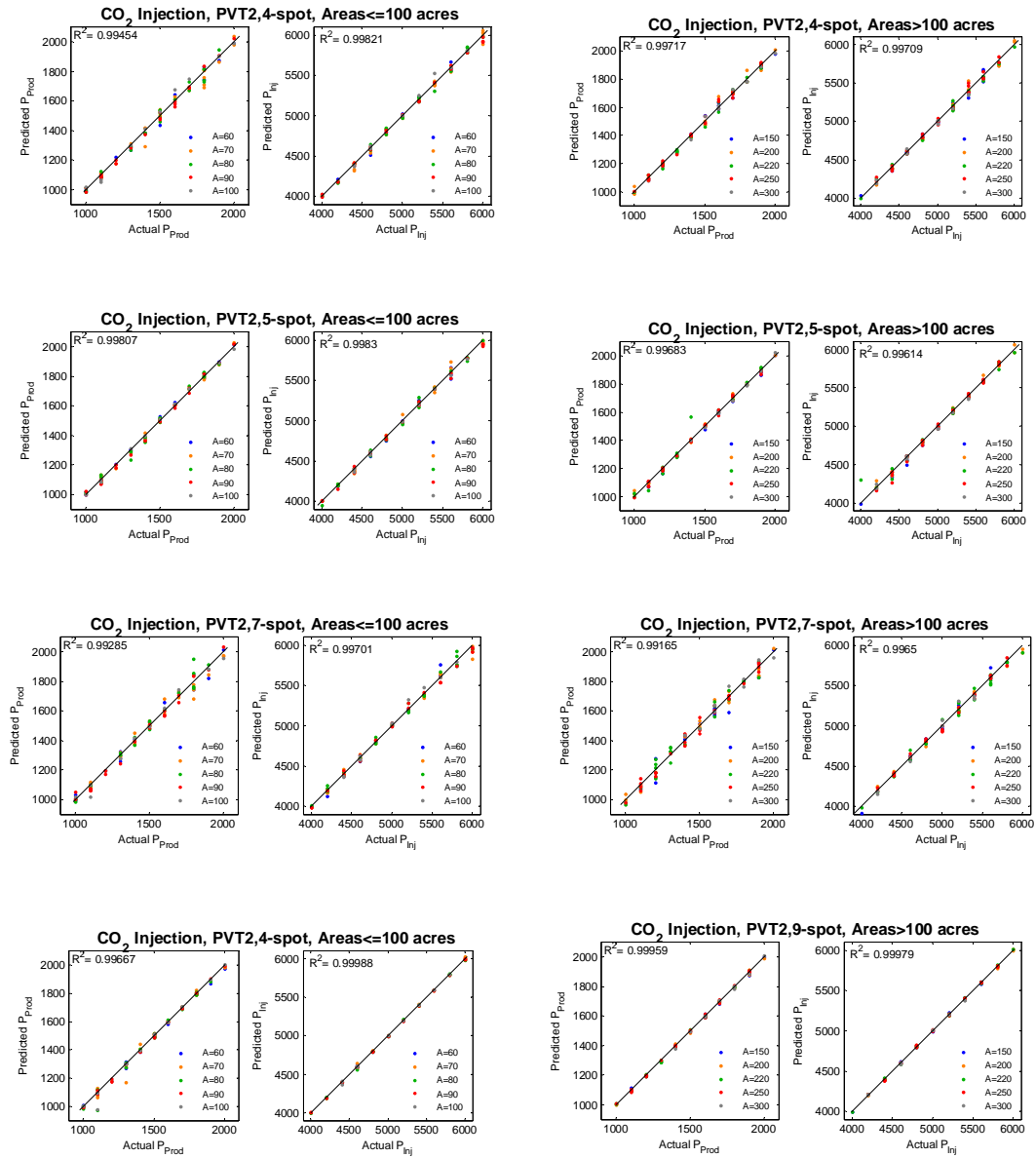
Figure **C-98**: Correlation Between Actual and Predicted Pressures. CO_2 Injection, PVT#2, Step-2 Network
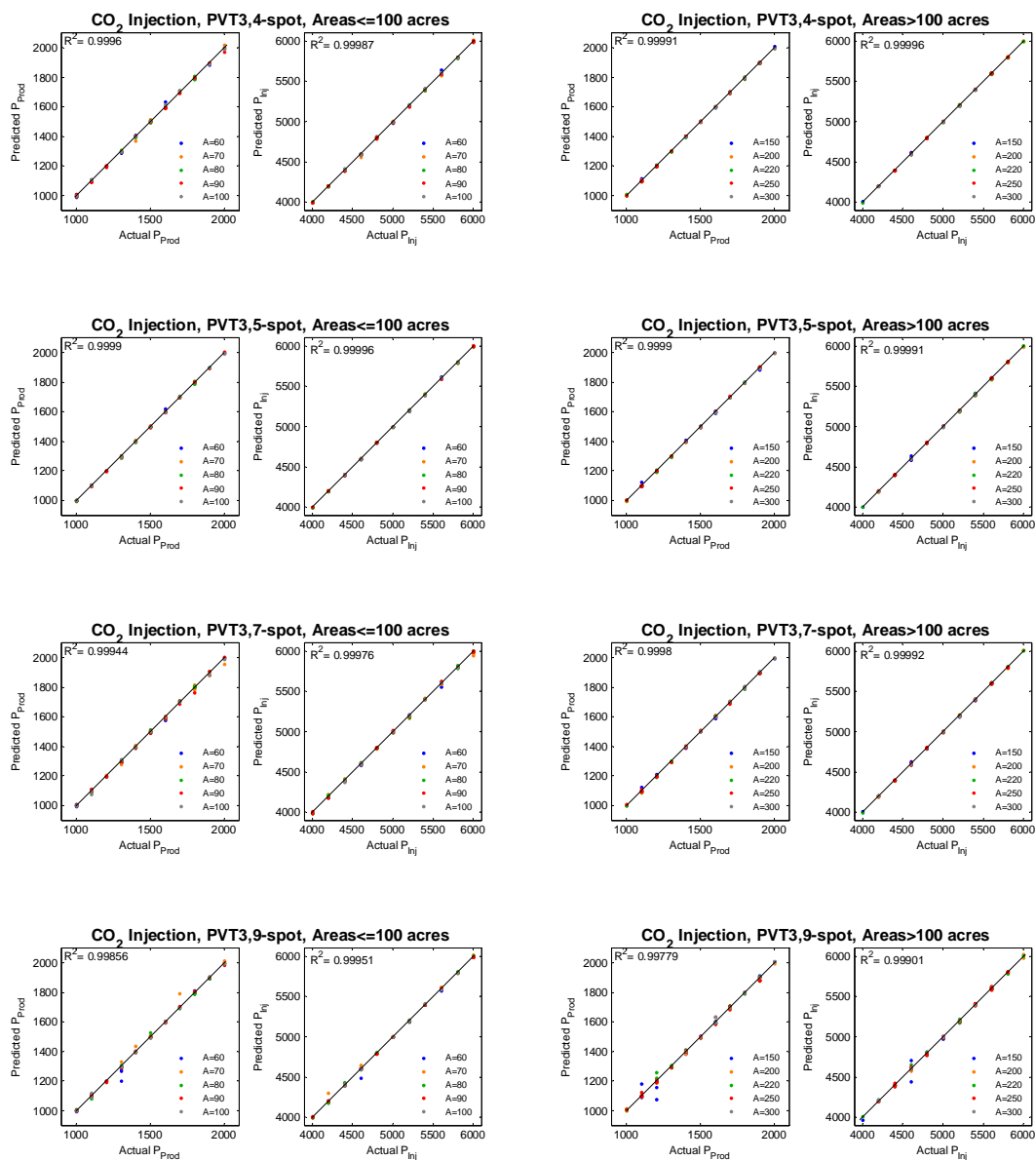
Figure **C-99**: Correlation Between Actual and Predicted Pressures. CO₂ Injection, PVT#3, Step-2 Network

C.2.2 N$_2$ Miscible Injection

Figure **C-100**: Correlation Between Actual and Predicted Pressures. N$_2$ Injection, PVT#1, Step-2 Network
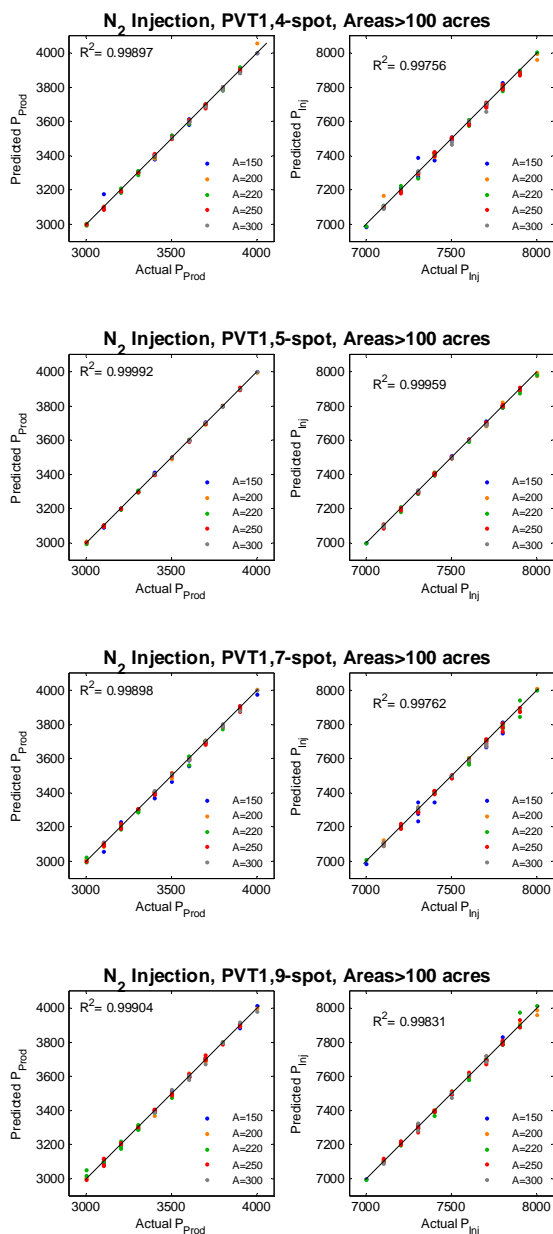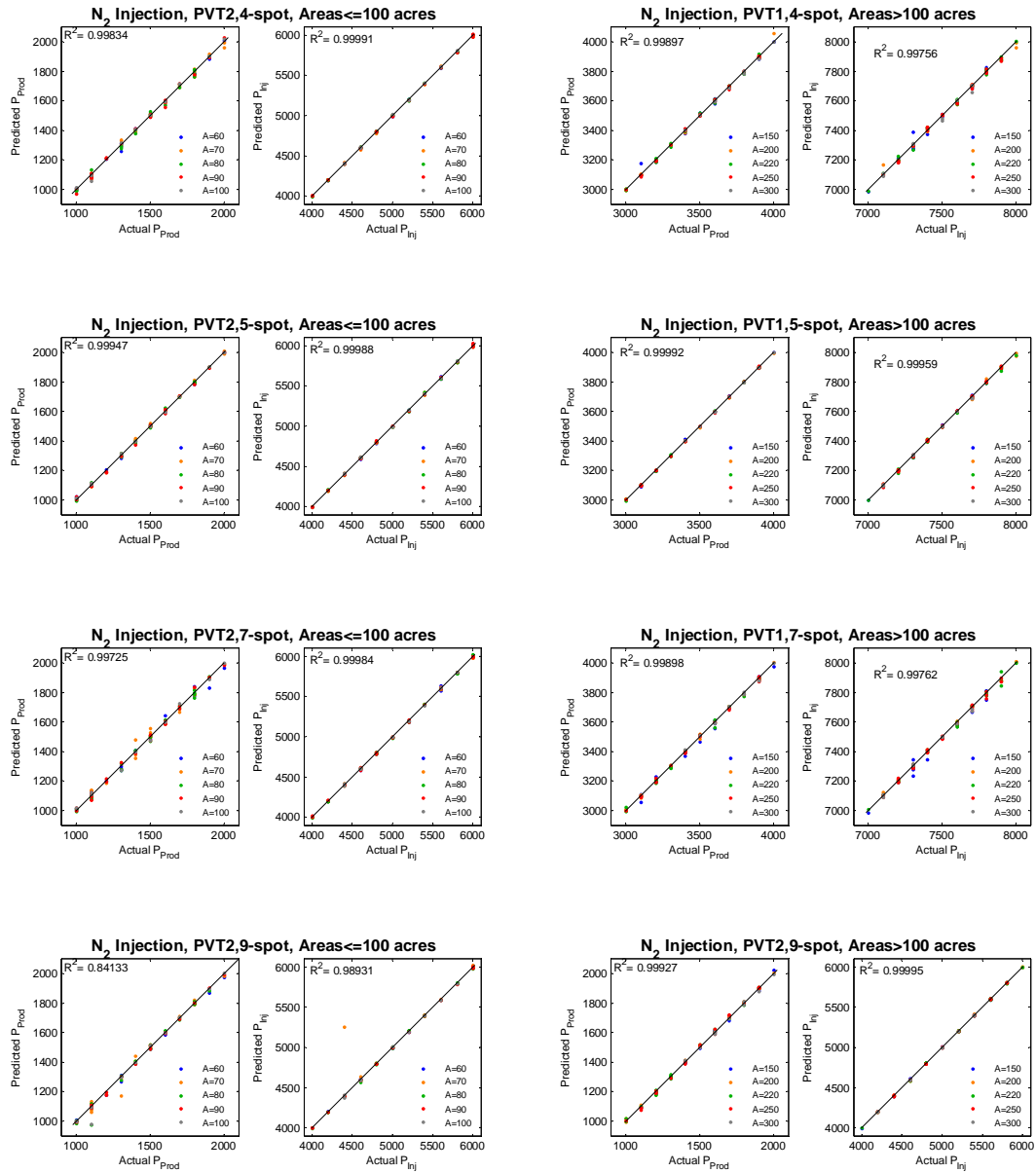
Figure **C-101**: Correlation Between Actual and Predicted Pressures. N_2 Injection, PVT#2, Step-2 Network
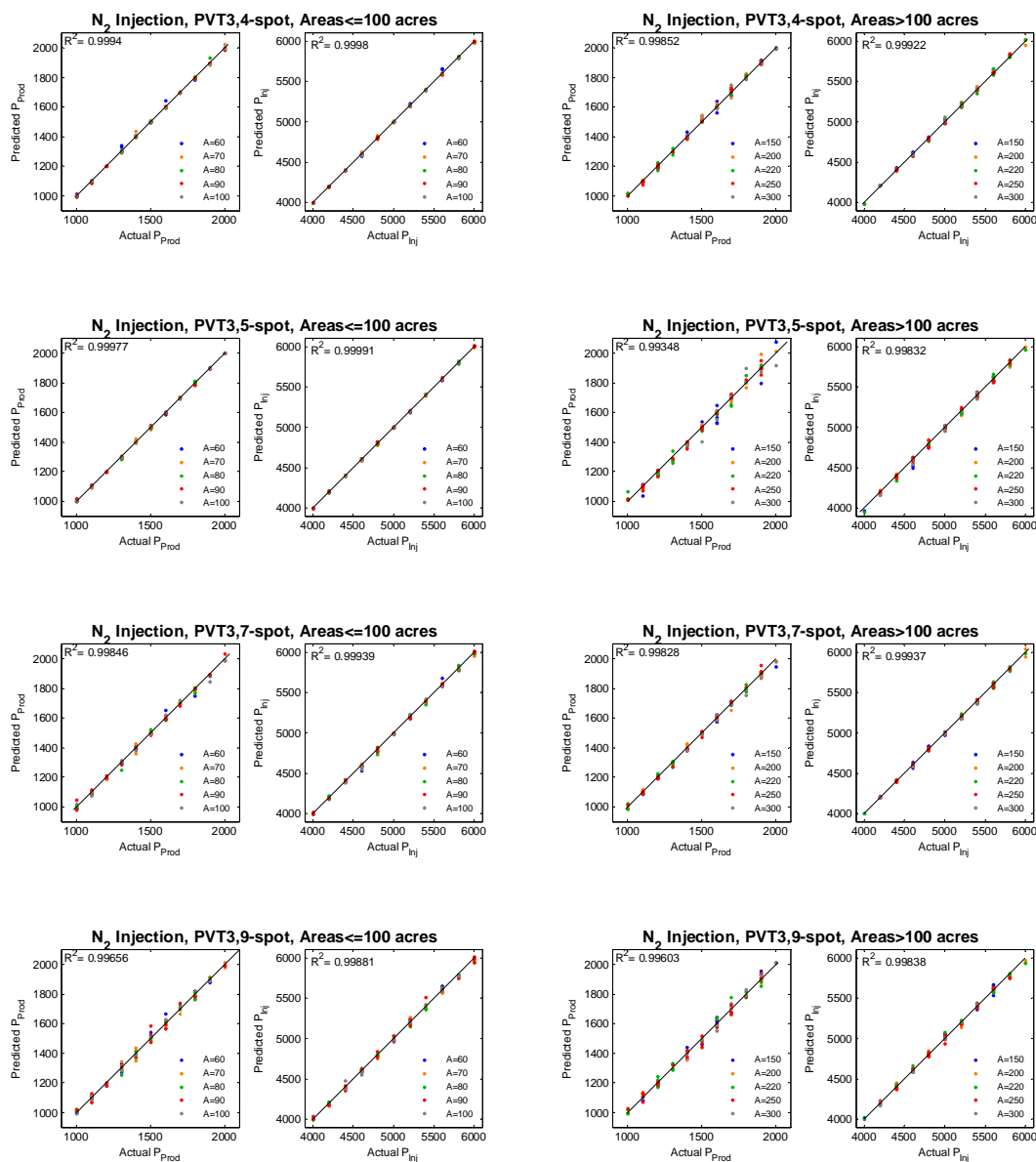
Figure **C-102**: Correlation Between Actual and Predicted Pressures. N_2 Injection, PVT#2, Step-2 Network

C.2.3 Water Injection

Figure **C-103**: Correlation Between Actual and Predicted Pressures (Testing). Waterflooding, PVT#2, Batch 1&2, Step-2 Network.

Figure **C-104**: Correlation Between Actual and Predicted Pressures (Testing). Waterflooding, PVT#3, Batch 1&2, Step-2 Network .

C.2.4 Steam Injection

Figure **C-105**: Correlation Between Actual and Predicted Pressures (Testing). Steam Injection, PVT#3, Batch 1&2, Step-2 Network .
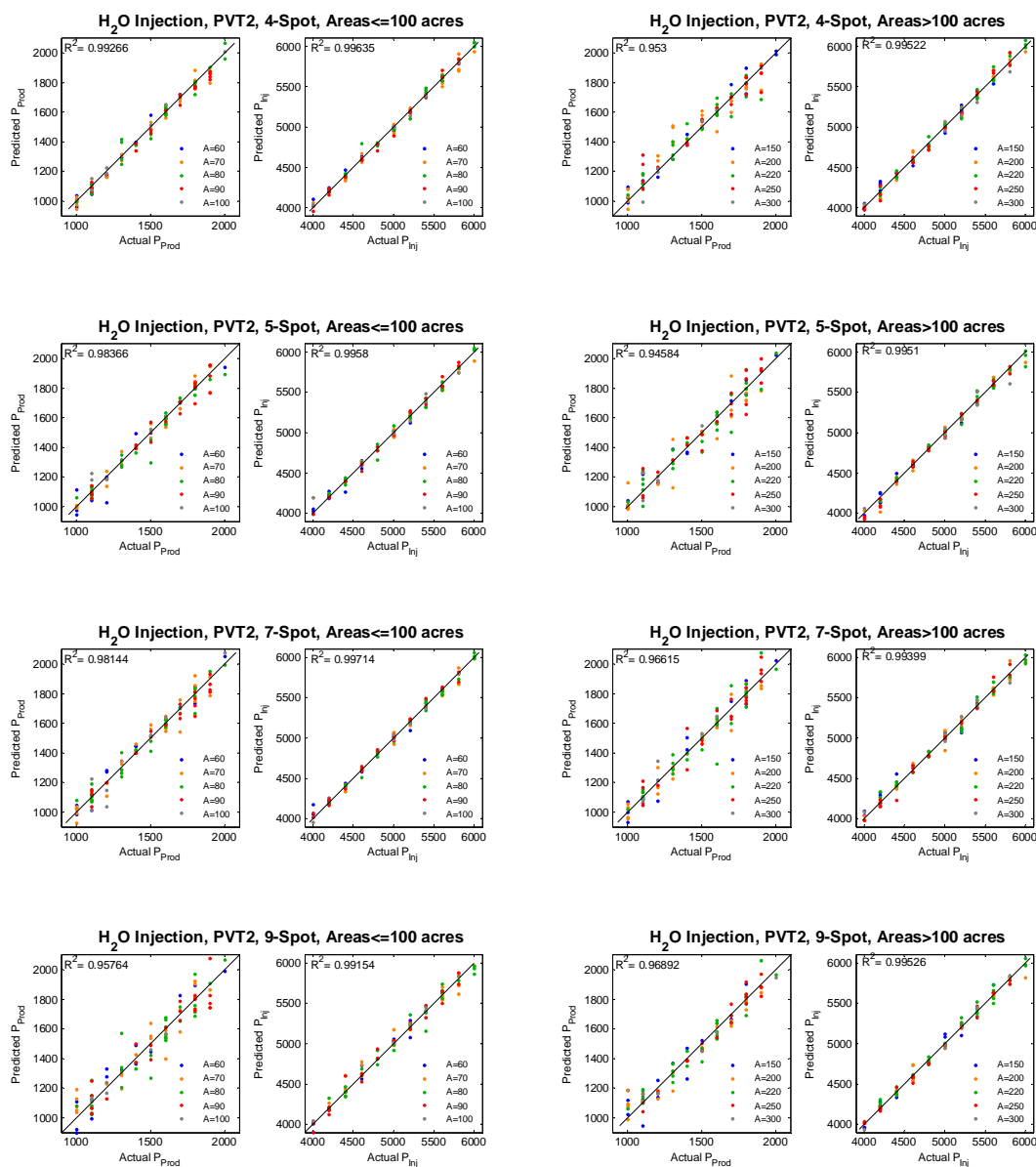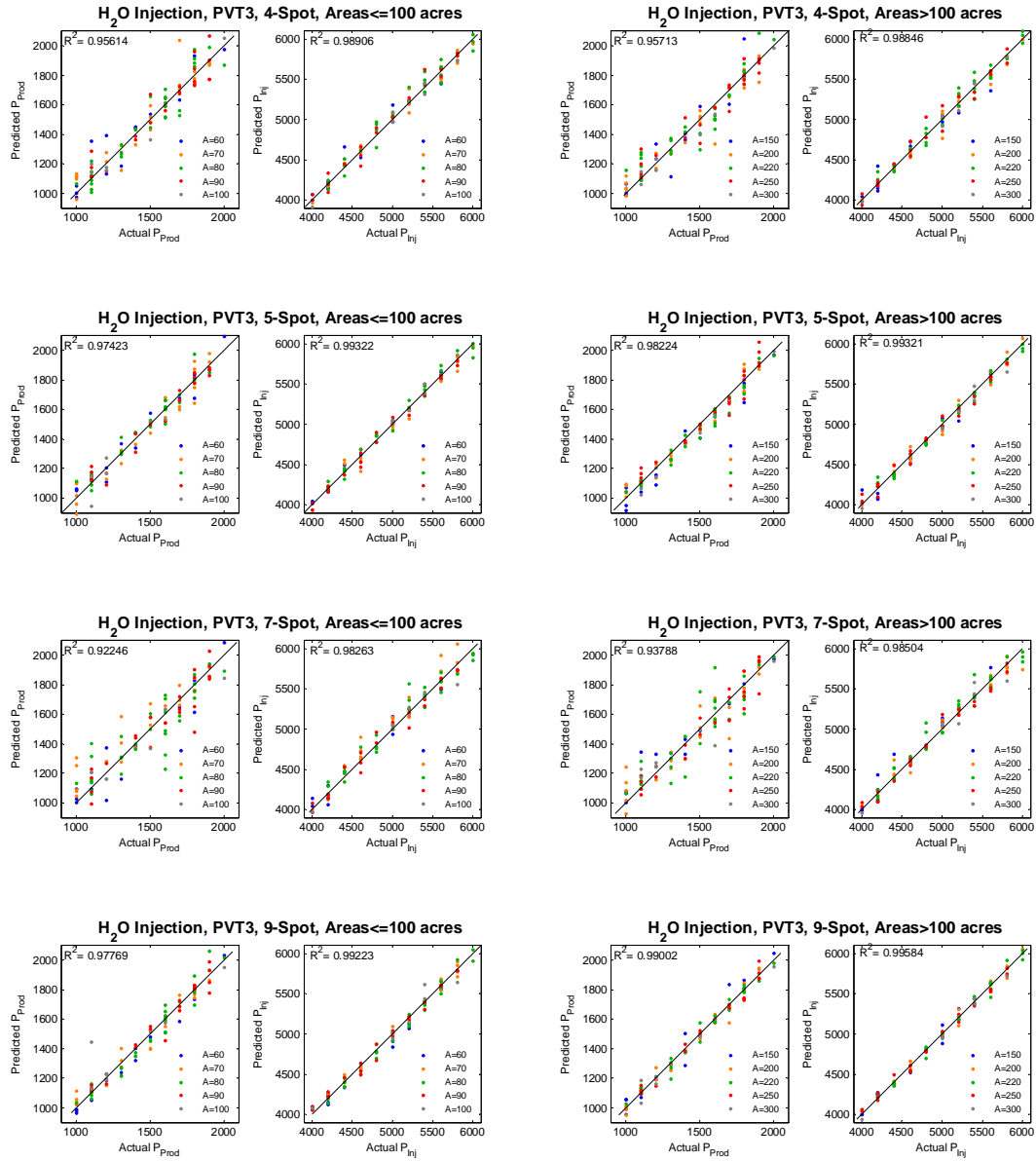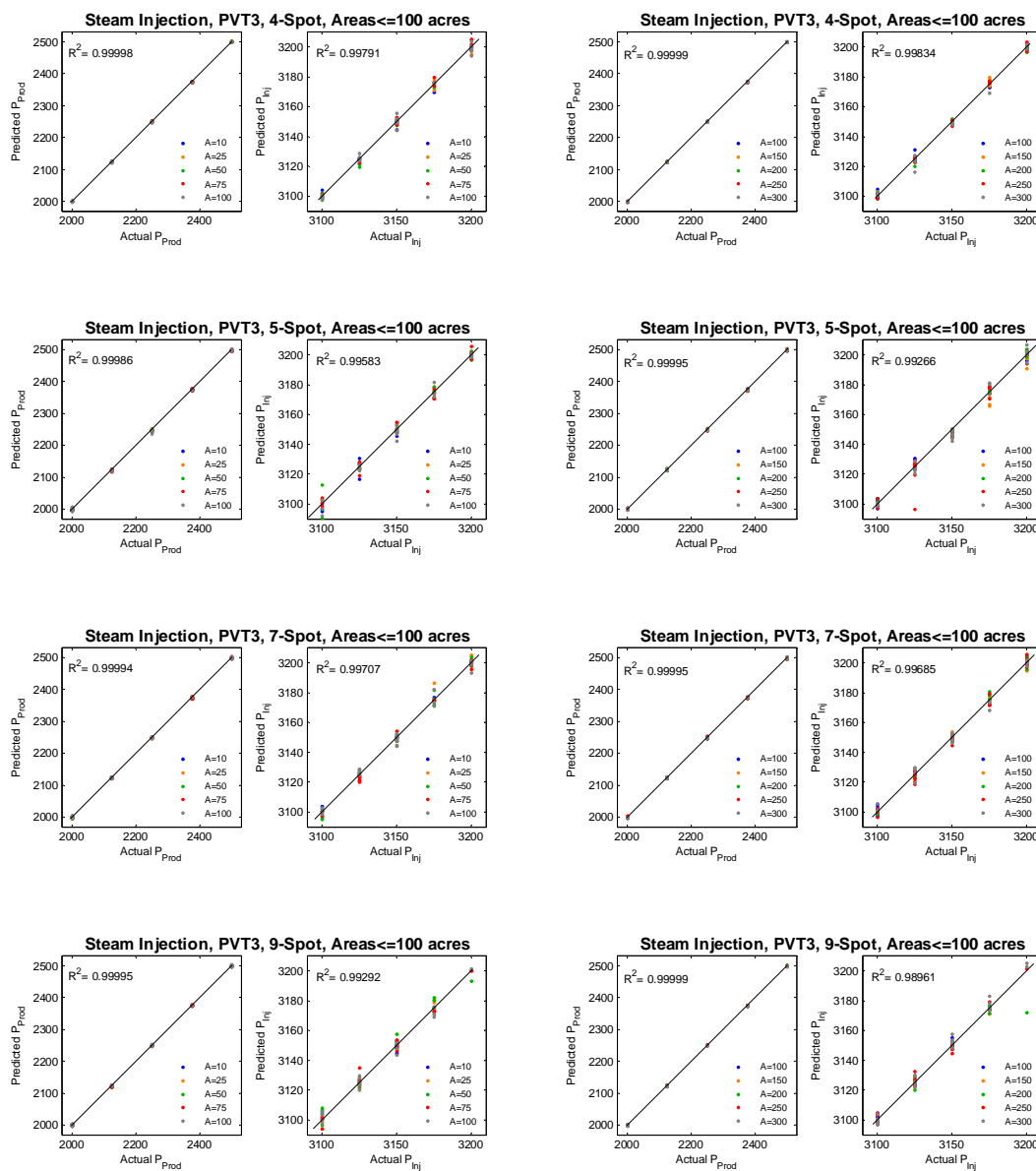
Appendix D

Matlab Code for Screening Network

```matlab
%%%%%%%%%%%%%%%%%%%%%%%%%%%%%%%%%%%%%%%%%%%%%%%%%%%%
%% Screening IOR Criteria Network
%% 4-Spot, PVT2, CO2 Injection, Small Areas
%% Developed by C. Parada
%%%%%%%%%%%%%%%%%%%%%%%%%%%%%%%%%%%%%%%%%%%%%%%%%%%%
format compact
clear
clc
close all
%set random to zero for initialization purposes
rand('state', 0);

%INPUT DATA SET FOR TRAINING
load 'CO2_PVT2_KHP_1000_100.txt'

%INPUT TARGETS FOR TRAINING
load 'CO2_PVT2_KHP_OUTPUT_ANN_4SPOT_1000_100.txt'

P(1,:)=CO2_PVT2_KHP_1000_100(:,1)'; %AREA
P(2,:)=CO2_PVT2_KHP_1000_100(:,2)'; %Pprod
P(3,:)=CO2_PVT2_KHP_1000_100(:,3)'; %Pinj
P(4,:)=CO2_PVT2_KHP_1000_100(:,4)'; %K
P(5,:)=CO2_PVT2_KHP_1000_100(:,5)'; %h
P(6,:)=CO2_PVT2_KHP_1000_100(:,6)'; %poro
%Pressure gradient calculation
P(7,:)= (2*sqrt(CO2_PVT2_KHP_1000_100(:,1).*43560./sqrt(3)))';
%distance btw injectors, "l"
P(8,:)=((2*sqrt(CO2_PVT2_KHP_1000_100(:,1).*43560./sqrt(3)))./sqrt(3))'
; %distance btw inj and prod
P(9,:)=((CO2_PVT2_KHP_1000_100(:,3)-CO2_PVT2_KHP_1000_100(:,2))./...
    (2*sqrt(CO2_PVT2_KHP_1000_100(:,1).*43560./sqrt(3)))./sqrt(3))';
%Pgrad
P(10,:)=(CO2_PVT2_KHP_1000_100(:,4).*CO2_PVT2_KHP_1000_100(:,5))'; %K*h

t(1,:)=(CO2_PVT2_KHP_OUTPUT_ANN_4SPOT_1000_100(:,1))'; %BT
t(2,:)=(CO2_PVT2_KHP_OUTPUT_ANN_4SPOT_1000_100(:,2))'; %t1
t(3,:)=(CO2_PVT2_KHP_OUTPUT_ANN_4SPOT_1000_100(:,3))'; %t2
t(4,:)=(CO2_PVT2_KHP_OUTPUT_ANN_4SPOT_1000_100(:,4))'; %t3
t(5,:)=(CO2_PVT2_KHP_OUTPUT_ANN_4SPOT_1000_100(:,5))'; %t4
t(6,:)=(CO2_PVT2_KHP_OUTPUT_ANN_4SPOT_1000_100(:,6))'; %t5
t(7,:)=(CO2_PVT2_KHP_OUTPUT_ANN_4SPOT_1000_100(:,7))'; %AT
t(8,:)=(CO2_PVT2_KHP_OUTPUT_ANN_4SPOT_1000_100(:,8))'; %q_2day  cum
t(9,:)=(CO2_PVT2_KHP_OUTPUT_ANN_4SPOT_1000_100(:,9))'; %q BT  cum
t(10,:)=(CO2_PVT2_KHP_OUTPUT_ANN_4SPOT_1000_100(:,10))'; %q_1 cum
t(11,:)=(CO2_PVT2_KHP_OUTPUT_ANN_4SPOT_1000_100(:,11))'; %q_2 cum
```

```matlab
t(12,:)=(CO2_PVT2_KHP_OUTPUT_ANN_4SPOT_1000_100(:,12))';  %q_3 cum
t(13,:)=(CO2_PVT2_KHP_OUTPUT_ANN_4SPOT_1000_100(:,13))';  %q_4 cum
t(14,:)=(CO2_PVT2_KHP_OUTPUT_ANN_4SPOT_1000_100(:,14))';  %q_5 cum
t(15,:)=(CO2_PVT2_KHP_OUTPUT_ANN_4SPOT_1000_100(:,15))';  %q_AT cum
t(16,:)=(CO2_PVT2_KHP_OUTPUT_ANN_4SPOT_1000_100(:,16))';  %q_2day rate
t(17,:)=(CO2_PVT2_KHP_OUTPUT_ANN_4SPOT_1000_100(:,17))';  %q BT rate
t(18,:)=(CO2_PVT2_KHP_OUTPUT_ANN_4SPOT_1000_100(:,18))';  %q_1 rate
t(19,:)=(CO2_PVT2_KHP_OUTPUT_ANN_4SPOT_1000_100(:,19))';  %q_2 rate
t(20,:)=(CO2_PVT2_KHP_OUTPUT_ANN_4SPOT_1000_100(:,20))';  %q_3 rate
t(21,:)=(CO2_PVT2_KHP_OUTPUT_ANN_4SPOT_1000_100(:,21))';  %q_4 rate
t(22,:)=(CO2_PVT2_KHP_OUTPUT_ANN_4SPOT_1000_100(:,22))';  %q_5 rate
t(23,:)=(CO2_PVT2_KHP_OUTPUT_ANN_4SPOT_1000_100(:,23))';  %q_AT rate


t=log(t); %functional link
[NPLin,NP] = size(P); %size of input
[NPLout,Nt] = size(t); %size of output layer
%NORMALIZATION OF DATA
[Pn,minp,maxp]=premnmx(P);  % normalization btw [-1 1]
[tn,mint,maxt] = premnmx(t); % normalization btw [-1 1]
%SEPARATE TRAINING, TESTING AND VALIDATION
[nxP,nyP]=size(Pn);
val_num=100;
test_num=100;
%TRAINING SETS
for i=1:nyP-val_num-test_num;
    Pn_train(:,i)=Pn(:,i);
    tn_train(:,i)=tn(:,i);
    t_train(:,i)=t(:,i);
end
%VALIDATION
for i=1:val_num;
    Pn_val(:,i)=Pn(:,i+nyP-val_num);
    tn_val(:,i)=tn(:,i+nyP-val_num);
    t_val(:,i)=t(:,i+nyP-val_num);
end

%TESTING SETS
for i=1:test_num;
    Pn_test(:,i)=Pn(:,i+nyP-test_num-val_num);
    tn_test(:,i)=tn(:,i+nyP-test_num-val_num);
    t_test(:,i)=t(:,i+nyP-test_num-val_num);
end

clear CO2_PVT2_KHP_1000_100
clear CO2_PVT2_KHP_OUTPUT_ANN_4SPOT_1000_100
clear P t

val.T=tn_val;
val.P=Pn_val;
test.T=tn_test;
test.P=Pn_test;

NPL1=60; %60
NPL2=30; %30
```

```
NPL3=NPLout;

%BACKPROPAGATION ALGORITHM - CREATING THE NETWORK
net = newcf(minmax(Pn_train), [NPL1,NPL2,NPL3],...
    {'tansig','tansig','purelin'}, 'trainlm','learngdm','mse');

%INITIALIZATION OF WEIGHTS AND BIAS
w1=zeros(NPL1,NPLin);
w2=zeros(NPL2,NPL1);
w3=zeros(NPL3,NPL2);
w1(:,:)=0.1;
w2(:,:)=0.1;
w3(:,:)=0.1;
net.IW{1,1}=w1;
net.LW{2,1}=w2;
net.LW{3,2}=w3;
net.b{1}=zeros(NPL1,1);
net.b{2}=zeros(NPL2,1);
net.b{3}=zeros(NPL3,1);

%ADJUST TRAINING PARAMETERS
net.trainParam.goal=1e-5; %1e-5;
net.trainParam.max_fail=5; %20
net.trainParam.epochs = 100000; %200000;
net.trainParam.min_grad = 10e-15;
net.trainParam.mem_reduc=80; %to reduce memory requirements
net.trainParam.mu=0.001; %0.001 Initial Mu
net.trainParam.mu_dec=0.1; %0.1 Mu decrease factor
net.trainParam.mu_inc=5; %10 Mu increase factor
net.trainParam.mu_max=100; %1e10 Maximum Mu
net.trainParam.show = 1; %20;

%TRAINING THE NETWORK
[net,tr_AT,Y_AT,E_AT] = train(net,Pn_train,tn_train,[],[],val,test);
%Weights and Bias
net_b1= net.b{1};
net_w1= net.IW{1,1};
net_b2= net.b{2};
net_w2= net.LW{2,1};
net_b3= net.b{3};
net_w3= net.LW{3,2};

%SIMULATION OF THE NETWORK WITH THE TRAINING DATA
tn_train_ann = sim(net,Pn_train);
%SIMULATION OF THE NETWORK WITH THE VALIDATION DATA
% tn_val_ann = sim(net,Pn_val);
%PREDICTIONS-NEW DATA-SETS THE NETWORK HAS NOT SEEN BEFORE
tn_test_ann = sim(net, Pn_test);
%DENORMALIZATION OF THE SIMULATION
t_train_ann = postmnmx(tn_train_ann, mint, maxt);
t_test_ann = postmnmx(tn_test_ann, mint, maxt);
%UNDO FUNCTIONAL LINK
t_train_ann = exp(t_train_ann); %tBT
t_test_ann = exp(t_test_ann); %tBT
```

```matlab
t_train = exp(t_train); %tbt
t_test = exp(t_test); %tBT

%ERROR TRAINING-STAGE (%)
[Nt_train,Nd_train]=size(t_train); %Nt = number of target per data-set,
Nd = number of data-set
NP_train = 1:Nd_train;
error_train = ((t_train-t_train_ann)./t_train).*100;
error_train_std=std(error_train');
error_train_mean=mean(error_train');
error_train_ave=sum(abs(error_train'))/Nd_train;

%ERROR PREDICTION-STAGE (%)
[Nt_test,Nd_test]=size(t_test);
NP_test = 1:Nd_test;
error_test = ((t_test-t_test_ann)./t_test).*100;
error_test_std=std(error_test');
error_test_mean=mean(error_test');
error_test_ave=sum(abs(error_test'))/Nd_test;


%%-----------------------------------------------------------------
%%                              PLOTS
%%-----------------------------------------------------------------

saveas(gcf,'CO2_CO2_PVT24S_train_100.fig');
figure; hintonwb(net_w1,net_b1);

for i=1:NPLout

    if i==1;  name='BT Time'; end
    if i==2;  name='Time1'; end
    if i==3;  name='Time2'; end
    if i==4;  name='Time3'; end
    if i==5;  name='Time4'; end
    if i==6;  name='Time5'; end
    if i==7;  name='Abdon Time'; end
    if i==8;  name='Cum Oil 2days'; end
    if i==9;  name='Cum Oil BT'; end
    if i==10; name='Cum Oil t1'; end
    if i==11; name='Cum Oil t2'; end
    if i==12; name='Cum Oil t3'; end
    if i==13; name='Cum Oil t4'; end
    if i==14; name='Cum Oil t5'; end
    if i==15; name='Cum Oil AT'; end
    if i==16; name='Oil Rate 2days'; end
    if i==17; name='Oil Rate BT'; end
    if i==18; name='Oil Rate t1'; end
    if i==19; name='Oil Rate t2'; end
    if i==20; name='Oil Rate t3'; end
    if i==21; name='Oil Rate t4'; end
    if i==22; name='Oil Rate t5'; end
    if i==23; name='Oil Rate AT'; end
```

```matlab
%TRAINING
figure ('Position',[10 40 1000 600]);
subplot(2,3,1),plot(NP_train,t_train_ann(i,:),'b*-
',NP_train,t_train(i,:),'ro--');
xlabel('Data-Set Number')
ylabel('Training Target')
h = legend('ANN','Data',2);

subplot(2,3,2),plot(NP_train,error_train(i,:),'b*-');
xlabel('Data-Set Number')
ylabel('Training error')
title([name,' - Training'])

subplot(2,3,3)
[m,b,r] = postreg(t_train_ann(i,:),t_train(i,:));
axis square
xlabel('Prediction Values')
ylabel('Input Values')
title(['Training, R^2= ', num2str(r)])
legend('off');

%PREDICTION
subplot(2,3,4),plot(NP_test,t_test_ann(i,:),'b*-
',NP_test,t_test(i,:),'ro--');
xlabel('Data-Set Number')
ylabel('Testing Target')
h = legend('ANN','Data',2);

subplot(2,3,5),plot(NP_test,error_test(i,:),'b*-');
xlabel('Data-Set Number')
ylabel('Testing Error')
title([name,' - Testing'])
grid on;

subplot(2,3,6)
[m,b,r] = postreg(t_test_ann(i,:),t_test(i,:));
axis square
xlabel('Prediction Values')
ylabel('Input Values')
title(['Testing, R^2= ', num2str(r)])
legend('off');

end
%% save workspace
save CO2_PVT2_ANN_4SPOT_1000_100.mat
```

VITA

Claudia Helena Parada Minakowski

Claudia Parada was born in Caracas, Venezuela, on May 7th, 1974. She attended the Colegio Santa Teresa del Niño Jesus High School. She graduated in July 1991, being ranked 2nd in her class. She earned a B.Sc. degree in Chemical Engineering from the Universidad Central de Venezuela in 1997. During her undergraduate studies, she received the OBE-UCV Fellowship from 1992 to 1996 and was appointed as a teaching assistant between 1995 and 1996. She started working as a process engineer for a local consulting company in Caracas during her last year of undergraduate studies. In her professional career, she was exposed to diverse projects where she designed upstream facilities for the Venezuela's state oil company PDVSA. She earned a scholarship from the Venezuelan "Gran Mariscal de Ayacucho" Foundation to pursue graduate studies. She joined Penn State University in 2000 and obtained a M.S. degree in Petroleum and Natural Gas Engineering in 2001. After graduation, Claudia worked for Schlumberger-GeoQuest for three years as a Reservoir Engineer. During this time, she focused her professional career in reservoir simulation. Claudia returned to Penn State University to pursue doctoral studies in Petroleum and Natural Gas Engineering in 2005. Claudia was awarded with several recognitions during her graduate studies at Penn State. She received the 2005-2006 Graduate Merit Award from Petroleum and Natural Gas Engineering Program, the Joseph and Anna Rubash Graduate Fellowship for two consecutive years in 2005 and 2006 and the Outstanding Graduate Teaching Assistant Award in PNGE in 2006. She participated in the poster competition at the 2007 Penn State Graduate Exhibition, where she won the third place award in the engineering division. Claudia is a member of the Society of Petroleum Engineers and a member of Colegio de Ingenieros de Venezuela